DISSERTATION

LOSS ANALYSIS AND LOSS BASED SEISMIC DESIGN FOR WOODFRAME STRUCTURES

Submitted by

Shiling Pei

Department of Civil and Environmental Engineering

In partial fulfillment of the requirements

For the Degree of Doctor of Philosophy

Colorado State University

Fort Collins, Colorado

Fall 2007

COLORADO STATE UNIVERSITY

November 5, 2007

WE HEREBY RECOMMEND THAT THE DISSERTATION PREPARED UNDER OUR SUPERVISION BY SHILING PEI ENTITLED LOSS ANALYSIS AND LOSS BASED DESIGN FOR WOODFRAME STRUCTURES BE ACCEPTED AS FULFILLING IN PART REQUIREMENTS FOR THE DEGREE OF DOCTOR OF PHILOSOPHY.

Committee on Graduate Work

Marvin E. Criswell

Paul R. Heyliger

Jennifer A. Hoeting

Adviser: John W. van de Lindt

Department Head: Luis Garcia

ABSTRACT OF DISSERTATION

LOSS ANALYSIS AND LOSS BASED SEISMIC DESIGN FOR WOODFRAME STRUCTURES

Light frame wood structures serve as the vast majority of construction type for residential structures throughout North America. This type of structure utilizes mainly wood shearwalls and a joist-sheathing floor system to resist the live and dead loads. Compared to concrete and steel structures, light frame wood structures typically have a relatively low construction cost, i.e. overall value. However, recent earthquake surveys and studies revealed that the costs involved in repairing these structures after earthquakes can be quite significant even when the structure survives the event without collapse. As a result of the large stock of residential construction in the U.S., earthquake-induced losses for this type of structure could have a detrimental financial impact on both the building owner and the community as a whole. During the 1994 Northridge earthquake in California, the economic loss directly connected with residential wood structures was more than $20 billion, and provides the impetus for this study. The limitation of current woodframe structural design philosophy is that it focuses only on life safety and does not address providing damage-limitations. The idea that financial losses for a structure during an earthquake should be addressed during the design stage leads to loss-based seismic design, which falls under a more comprehensive framework, performance-based seismic design (PBSD).

The objective of this study is twofold. The first objective is to develop a method to establish a probabilistic model for earthquake-induced loss of existing or newly designed wood frame structures for a given period of time into the future; then this method is to be incorporated into a performance-based seismic design framework to conduct loss-based design/optimization for wood frame structures. The first objective involves the modeling of the structural behavior during earthquake loading, financial loss estimation of the structures, and probabilistic modeling/simulation of the seismic hazard. An improved non-linear structural model for light frame wood structures was proposed and used in the structural analysis. A vulnerability based loss estimation framework was developed to incorporate multiple uncertainty sources which contribute to financial losses. Bayesian techniques were used in the modeling of the framework elements in order to include as much usable information as possible. An alternative loss estimation procedure based on Monte-Carlo simulation was also proposed with the ability to consider more realistic situations such as damage accumulation and structural degradation. The results of the long-term earthquake-induced loss were obtained in the form of simulated sample pools conditional on time span. Based on the results from the first objective, simplified loss estimation in the design stage was introduced in order to obtain the vulnerability target for loss based optimization. This optimization procedure was later used to implement loss-based design in the numerical examples.

The most significant anticipated contribution of this study to the woodframe design and research communities will be the development of a long-term seismic-

induced loss estimation framework/procedure for woodframe structures that enables loss-based design and evaluations. Although this procedure will only be applied to woodframe structures in this dissertation, the general solution can also be used to analyze other structure types provided the necessary details are addressed. The automated analysis package developed in this study will essentially be a practical implementation of the performance-based seismic design (PBSD) concept for most commonly constructed residential structures (in North America). Other contributions will include a new formulation for the hysteretic models for wood shearwalls, a performance-based seismic design procedure for woodframe residential buildings, and a generalized user-friendly woodframe building seismic analysis tool package for the research community.

Shiling Pei

Department of Civil and Environmental Engineering

Colorado State University

Fort Collins CO 80523

Fall 2007

Dedication

To the one I loved

"There is nothing new under the sun."

-Ecclesiastes

Acknowledgements

I would like to acknowledge the assistance, support and advice of many people without whom this work would not have been possible. Dr. John W. van de Lindt, my advisor, provided support, assistance, advice and helped me through the 4 years of my study in the United States. Dr. van de Lindt always encouraged me to pursue new ideas and extend my horizon. My appreciation is beyond words. I would also like to thank the other members of my graduate committee, Dr. Marvin Criswell, Dr. Paul Heyliger and Dr. Jennifer Hoeting. Their guidance and assistance is deeply appreciated. I would also like to thank my fellow graduate students at Colorado State University for their support, encouragement, assistance, and friendship.

I would like to thank the people that encouraged me to pursue my dreams and goals. Dr. William M. Bulleit provided advices and assistance during my study at the Michigan Technological University. Dr. Jack Cermak provided encouragement and financial support during my study at Colorado State University. Dr. Shizhong Qiang provided guidance during my graduate studies at Southwest Jiaotong University back in China and helped me to pursue the degree at oversea institutions. I would have not begun this long journey without his encouragement. I would also like to thank Jonathan Goode, CJ Riley, Matthew Walz, Saharat Buddhawanna, Dao Nguyen Thang, and Rebecca Atadero for their friendship, help, and support during my studies. In particular, I would like to thank my wife Hongyan Liu for her patience, support, friendship, and love.

I would like to extend many thanks to my parents and the rest of my family for their guidance, sacrifices, support, love, and advice. Anything that I have ever or will ever accomplish is due to them.

Table of Contents

List of Figures

List of Tables

Chapter One

Introduction

1.1 Background and Problem Definition

The objective of engineering is to apply principles and methodologies in science to the design, manufacture, and optimization of products; or simply, turning ideas to reality. The field of civil engineering benefits society by providing ways to build and maintain reliable structures that satisfy different aspects of human needs; one of them being to provide shelter against the environment. The importance of providing safety against natural hazards has been well addressed and considered in the design and construction methods developed by generations of civil engineers and researchers. Such considerations are well reflected in current design codes and for the most part construction practices. However, other aspects of human need (other than life-safety) had not been addressed until the late 1980's when the concept of performance-based design was first proposed. It was not until the late 1990's, that the financial losses due to natural hazards, another important aspect of performance associated with civil engineering structures, was recognized by the profession as a research area which

warrants significant effort in future civil engineering. The term financial integrity could be used to describe the ability of a structure to keep itself and its contents from losing financial value or incurring repair costs because of the hazard loading events. Extreme hazard events such as earthquakes and hurricanes can result in severe financial losses for civil engineering structures. Accurate estimation and assessment of the structural performance and subsequent losses under such hazards are beyond the capability of the traditional design and analysis methods.

Wood frame (light-frame wood) construction is used extensively for residential buildings throughout North America, and although these buildings typically provide life safety, they are particularly vulnerable to earthquake loading. Different from steel and concrete structures which exhibit nonlinear behavior only after the displacement/stress exceeded certain limit point, wood frame structures are nonlinear virtually immediately upon loading. This is primarily caused by the nonlinear load resisting properties of the sub-assemblies (shearwalls) the system is built from. In the U.S., current design codes for such structures are the National Design Specification for wood construction 2001 edition implementing allowable stress design (ASD) and the 2005 edition for load and resistance factor design (LRFD). The majority of current residential buildings are specification-based and even conventionally built, i.e. based on engineering experience. Following the 1994 Northridge earthquake, the community suffered nearly $40 billion in losses, in addition to casualty and other damage. More than $20 billion in losses was directly associated with the damage and repair cost for wood frame residential buildings. From the experience of similar hazardous events, it

is quite clear that although a woodframe house might not collapse during an earthquake, the cost involved in the repair following the event may still be considered unacceptable from the owner's point of view. This observation drew great attention to the performance of wood frame residential buildings during earthquakes, particularly the losses incurred as a result of an earthquake. Research projects on these types of structures have been conducted to investigate their seismic behavior and potential losses, essentially attempting to address these important topics. The results from these studies (described later) provide the starting point for the methods and procedures developed in this dissertation work.

Obviously, the structural configuration and design of sub-assemblies and components will significantly affect the losses for a structure during an earthquake. One of the most important tasks for civil engineering, particularly seismic structural engineering, is to predict the behavior of a structure with a given configuration during a pre-defined earthquake. This task has been investigated by a number of researchers in the past. However, it is noted here that it is even more important to investigate how the structure will perform under multiple earthquake events that may occur over a given period of time since this influences design decisions early in the design process. Specifically, it would be useful to find a way to optimize the structure so that the annualized losses are kept under an acceptable level. Such topics lead to the concept of loss-based seismic design in which the uncertainty of future seismic, as well as the variation in the interaction of design configuration and economical performance must be incorporated. This study is based on the idea that the financial losses due to future

earthquakes can be used as a performance target for loss-based seismic design (LBSD), falling under the paradigm of performance-based seismic design (PBSD).

Loss estimation (prediction) is the first step towards LBSD. In order to accurately estimate earthquake-induced losses, which directly relate to the structural responses (displacement and acceleration) under earthquake loading, an accurate structural model must be used to predict the dynamic response of the structure. Hysteretic modeling of the shearwall system and other components in a wood frame structure is the key to high quality (accurate) predictions. A new family of hysteretic models was developed in this study for dynamic analysis based on existing models. The new model can track the damage induced by the loading process to the structural components and adjust the shape of the hysteresis loop for the nonlinear "spring" element accordingly. The prediction accuracy is improved at a variety of hazard levels by using this new model, particularly at higher intensity levels.

After obtaining an accurate prediction of structural dynamic behavior, the methodological link between the structural responses and financial loss must be modeled properly to perform loss estimation based on the dynamic response. A categorized fragility system was proposed and used for the loss estimation in this study. This method, based on conditional distributions of responses and cost given pre-defined damage levels, provides a way to generate loss information given the structural response from dynamic analyses. Firstly the vulnerability model for single earthquake loss was constructed based on time history analysis results. Then this

model was combined with Monte-Carlo simulation procedure to generate samples for total loss in a given future period of time. Since the single earthquake loss has been represented by the vulnerability model, there is no need to perform time domain analysis in the long term loss simulation. This procedure is called the vulnerability based loss simulation.

Vulnerability based long term loss simulation make the assumption of a fully intact (i.e. undamaged) structure upon each simulation (if a Monte-Carlo simulation technique is used), which means the structure model is damage-free upon any earthquake events that happen in the given period. However, this is not quite realistic for wood frame structures subjected to earthquake hazards. In the regions where minor earthquakes occur very frequently, the structure could experience multiple small earthquakes and accumulate some level of damage (unseen from normal inspection, thus would not be repaired) before the larger earthquakes come. The loss of a damaged structure in an earthquake will be different from the loss of the undamaged (or new) structure in the same earthquake since the dynamic response will be different due to stiffness and strength degradation of the structural components. An alternative method, termed herein as Virtual Hazard simulation, is proposed in this study to account for such types of effects. By using the structural model that reflects the damage accumulation and probabilistically generated virtual hazard loading events over the future exposure period, a more realistic/accurate estimate of losses can be made. The drawback of this method would be computational expenses, since the

loading history of the structure during the entire exposure period must be reflected by time domain analyses using a single damage accumulating model.

Long term loss estimation results could be used directly in the decision making processes during either design or retrofit. Thus, the ultimate purpose of performing loss estimation in civil engineering (and this study) is the loss-based design/optimization. A simplified relationship between expected long term losses and vulnerability target was established and an incremental optimization procedure was adopted to find the optimal design given the long term financial target, e.g. annualized loss. This dissertation represents the first attempt to design a woodframe building based on long term losses to earthquakes.

1.2 Current State of Art/Practice

In order to obtain an accurate prediction for financial loss during earthquakes, the response and damage of the structure during the earthquake must be properly modeled. The first task of this dissertation work is to develop or improve dynamic analysis models for light frame wood structures. Since the lateral displacement and acceleration responses produce most of the damage during earthquake events, the modeling of shearwall assemblies, which are the main lateral resisting elements in a wood frame building, are very important to an accurate time domain analysis model. Numerous analytical models and tests for wood shearwalls have been developed and performed over the last three decades (see e.g. van de Lindt, 2004 for a comprehensive

list). These models vary from empirical drift formulae to nonlinear finite element models at the individual fastener level.

In the early 1980's, Easley et al. (1982) studied the monotonic transverse load resisting mechanism of wood shearwalls beginning at the fastener level and derived formulae for fastener forces and wall stiffness. The results from these formulae were shown to be in agreement with test results and detailed finite element simulation. In 1995, White and Dolan developed a finite element program, WALSEIZ, to perform nonlinear time history analysis on wood shearwalls. Nonlinear hysteresis model for connectors were used in this model and the bearing effect was also included. Filiatrault (1990) used a displacement-based energy formulation with the nonlinear load-slip characteristics of connectors in order to develop a two-dimensional shearwall model. His model used a discrete matrix formulation and was implemented into a program (SWAP) capable of both static and earthquake excitation (dynamic) analysis. By introducing nonlinear connector behavior into the finite element analysis, the general finite element formulation became a useful tool in wood shearwall analysis.

In order to include the nonlinear behavior of individual shear walls in a system level model to perform time domain analysis, nonlinear hysteretic models were usually used to represent the wall with a nonlinear spring element. These hysteretic models could be directly obtained from cyclic wall tests or from a wall level models that includes fastener behavior. Hysteretic elements have been used extensively in current applications of wood frame structural analysis. Baber and Wen (1981) proposed a

general modeling approach for hysteretic degrading systems that related the degradation of the system to hysteretic energy dissipation. The development of this model was not focused on any specific physical system but rather a generalized single degree-of-freedom (SDOF) hysteretic system. Later, Baber and Noori (1985) added quantitative measurement of pinching into their energy-based degrading model (BWBN model), making it more applicable to wood shearwall modeling. Foliente (1995) then proposed a SDOF degrading model for wood joints and structural systems based on the BWBN model and compared it to cyclic loading test results. Folz and Filiatrault (2001) constructed a wood shearwall analysis package (including two programs, CASHEW and SAWS) that is capable of developing SDOF assembly-level hysteresis models from hysteresis properties of the fasteners and a given wall configuration (CASHEW). Then, this SDOF wall model was assembled into the whole woodframe structural model to perform dynamic analysis (the program SAWS). This set of programs has been proven to be very convenient and provides considerable accuracy in the prediction. A study by van de Lindt and Walz (2003) used a polynomial backbone hysteresis model based on cyclic loading test data to examine the reliability levels for allowable drifts for a basic wood shear wall.

Earthquake related loss estimation has been studied on a regional scale by many researches (e.g. Crowley et al. 2006). Detailed loss estimation for individual structures remains a new topic and only a limited number of studies could be found for wood frame structures. Loss estimation for wood frame structures is quite complicated due to the fact that the structural response is highly nonlinear and, perhaps more

influential, that nonstructural component damage contributes a larger percentage of the total repair costs compared to structures built with heavier materials such as concrete and steel. In the CUREE Caltech woodframe research project (see Porter, 2001), studies on the damage-loss relationships for several typical woodframe building components were conducted, including stucco, gypsum wall board (GWB drywall), oriented strand board (OSB), shearwalls, windows, and water heater, etc . Estimates for financial losses of wood frame structures due to a given earthquake were performed using an assembly-based vulnerability (ABV) framework (Porter, 2000), which calculates a structures' losses as the summation of assembly level component losses.

Loss estimation for an individual structure could be incorporated into regional loss prediction models, but another realistically more important application is loss-based design for individual structures. Although the current practice in wood frame structural design is still focused on strength-based seismic design approaches (*National Design Specification for Wood Construction*, AF&PA, 2005), performance-based seismic design has been a focus of woodframe research community for well over a decade due to its ability to incorporate a variety of performance objectives into an analysis or design (see e.g. Ellingwood, 1998). The loss-based optimization concept had been considered by researchers in the seismic design problems since the early 1970's (e.g. Liu et al., 1972). A group of researchers have looked into lifecycle losses for different types of structures in recent years. Liu et al. (2005) proposed optimizing a seismic design procedure for steel moment frames towards lifecycle loss

minimization. Similar research on reinforced concrete structures can be found in Ang et al. (2001). But life cycle loss-based design, or optimization, for wood frame structures has not been addressed to date.

1.3 Concepts and Procedures

Long term earthquake induced loss to wood frame structures will be the focus of this study. This financial loss, characterized by dollar amount, was modeled as a random variable depending on exposure duration. The method introduced in this dissertation work is essentially a method to generate samples from this long term loss distribution. Statistical models for each source of uncertainty that has contribution to the total loss were established based on available information. Monte-Carlo simulation was used to "assemble" these uncertainty contributions together. In order to find the relationship between the seismic hazard and financial loss, structural models for light frame wood structures were established to perform time domain analysis for structures subjected to earthquake ground motion realizations. The responses from these analyses were used as input to a damage-loss fragility system to generate the economical losses as the output. This simulation procedure was adopted in this study in order to determine the loss characteristics of a specific design against an individual earthquake event in the form of vulnerability models. By incorporating earthquake occurrence and intensity distributions with the vulnerability model, the long term loss corresponding to the structural design for any exposure period can be simulated using Monte-Carlo simulation. Monte-Carlo simulation was also used in the alternative loss estimation

procedure which makes it possible to consider damage accumulation and other time-dependent effects. This method simulates the whole exposure duration continuously without decoupling the individual earthquake event with the vulnerability model.

After simulation of the long term loss, one can use the samples directly in the comparison of alternative design options. On the other hand, loss distribution models can be established based on the samples and used in the loss-based design process. In this study, the loss based design problem was defined as the constraint for the loss probability curves. Incremental optimization procedures, together with assumptions to help simplify the computational efforts were used to obtain design configurations given performance requirements on both the long term loss and single earthquake loss.

This study emphasizes the application of proposed loss estimation procedures within the context of performance based seismic design. Thus, the focus will be the economical performance of an individual structure rather than structures in a region. Regional loss estimation, which considers spatial correlation of ground motion pattern and attenuation (e.g. Crowley et.al. 2006.), was not the subject of this research but can surely benefit from the results of this dissertation work.

1.4 Software Development

One important objective of engineering is to produce a useable product based on science and technology. Without appropriate tools to test hypotheses and implement

subsequent results, the benefit of abstract theory and methodology would be limited to only the research community. This is the main motivation for developing a user-friendly software package based on the results of this dissertation work. SAPWood (Seismic Analysis Package for Woodframe structures) was developed as part of the NEESWood project and can be regarded as a practical implementation tool of the methodology in this dissertation work.

The loss estimation methodology proposed in this study is a simulation based procedure, thus most tasks involved are computationally intensive and repetitive. General research tools such as Matlab have the ability to carry out the analysis but the efficiency of the computation is not suitable for simulation purposes (a single time domain analysis with an average size model in Matlab could take several minutes). Furthermore, the structural model used in this study relies on a new hysteretic model developed for wood frame assemblies which is not available in any existing structural analysis package. Based on these considerations, a standalone software package which includes different modules to perform the tasks covered in this study was developed with a user-friendly graphical interface. This program, SAPWood, incorporates all the models discussed in this dissertation work and was used to perform all the numerical analysis discussed in Chapter 8. It enables a design engineer to perform the tasks covered in this dissertation work (quasi-static analysis of light frame components, nonlinear time domain analysis of the entire structure, and loss analysis, etc.) on any newly designed or existing woodframe building without specialty in dynamics and simulation.

1.5 Expected Results and Contributions

The hysteretic model proposed in this study is expected to improve the accuracy in the modeling of seismic behavior of wood frame structures. The comparison between the model prediction and shake table test results will be used to verify the numerical models. The model developed in order to perform assembly level analysis is expected to produce results that are consistent with shear wall test results. The expected results from this study include the comprehensive loss analysis on the index buildings of this study, including three typical single family style structures and a three story office building. The financial impact of earthquakes in both the short (1~5 years) and long exposure period will be examined. By performing a sensitivity analysis on possible influential factors on the predicted loss behavior, an effective strategy to gather input data and apply an even more robust loss estimation framework will be developed.

This dissertation work will benefit the wood frame seismic analysis and design profession in four aspects. Firstly, the general formulation for more accurate hysteresis models was proposed and could be used to account for complicated hysteretic behavior of light frame assemblies. This model is a step forward from the existing models and will improve the accuracy and robustness of the time domain analysis of such structures. Secondly, the method to assess long term loss of the structure within a statistical framework which comprehensively includes the most influential sources of uncertainty will be developed in this dissertation. This procedure will be applied to the

loss-based optimization of woodframe structures for the first time. If one chooses to exchange the woodframe analysis modules with analysis tools for other types of structures within the procedure, it can be applied to a general seismic hazard evaluation for virtually any type of structure. Thirdly, the effort to implement loss-based design and optimization involved in this study will be the first time this has been done within a PBSD context. Finally, the software package SAPWood will be developed to perform loss analysis and a variety of other commonly used seismic engineering analyses types for wood frame structures. Currently, there is no user-friendly seismic analysis stand-alone package that has all the features proposed herein.

1.6 Overview

The remaining chapters of this dissertation lead the reader through the theoretical development of the numerical hysteretic models for wood shearwall assemblies, dynamic analysis of light frame wood structures, construction of the long term loss estimation framework through the introduction of probabilistic uncertainty, simulation of long term loss with traditional and alternative assumptions, and finally, loss-based design of wood frame structures. Subsequent chapters also provide the results and discussion of the numerical examples conducted for this research on the estimation and design methodology based on loss. Finally, conclusions and recommendations resulting from this study are collectively offered for the reader and for potential future research avenues.

The following chapter summaries provide a brief overview of the remaining sections in this study:

Chapter 2: Light Frame Wood Structure Modeling

Chapter 2 mainly discusses the structural models developed and used in this dissertation. Firstly, it covers the development of the theory and application for the Evolutionary Parameter Hysteretic Models (EPHM), which will be used throughout this dissertation for a better estimate of the wood frame structural dynamic behavior. The EPHM was first applied to wood shearwall connectors (nails and screws) in an assembly level model to investigate the hysteretic behavior of wood shearwall assemblies. A quasi-static assembly model was established in Section 2.2 based on the principal of virtual work in order to accomplish this task. Once the hysteretic behavior of shearwall assemblies was obtained, they were incorporated into an existing system level model which is discussed in Section 2.3 and is used for all the structural analysis in this study. The accuracy of the system level model was verified by comparing the model prediction with shake table test results in Section 2.4.

Chapter 3: Long Term Loss Estimation Framework

Chapter 3 presents the elements that contribute to uncertainty in the long term loss estimation and the details and formulation of the estimation framework. Three main sources of uncertainty are explained and addressed: structural uncertainty, loss-

damage relationship, and seismic uncertainty, are discussed in this chapter. Appropriate use of subjective information/experience in these models was investigated. How the estimation framework can benefit from additional data/information and how to incorporate this data into Bayesian models when they became available are also discussed. By the end, the vulnerability based simulation procedure using the assumption of an undamaged structure for each event was proposed to obtain long term loss given exposure duration.

Chapter 4: Alternative Loss Estimation

Chapter 4 discusses an alternative loss estimation procedure based on the framework introduced in Chapter 3 but adopting what is felt to be a more realistic assumption. Instead of developing decoupled single earthquake loss fragilities using vulnerability models, the procedure focuses on simulating the loss during the entire design life span (or any time frame of interest) as a whole, tracking the cumulative damage induced by all earthquake events and the influence of repair/retrofits. The concept of Virtual Hazard simulation was proposed and the possibility of applying this idea to a combination of hazard types was discussed.

Chapter 5: Loss-Based Design and Optimization

Chapter 5 utilizes the methods and models developed in Chapters 2 through 4 to construct a loss-based seismic design method. Firstly the concepts of performance-

based seismic design were reviewed and the definition of a loss-based design problem was proposed. Then a simplified long term loss estimation procedure was developed to calculate expected long term loss associated with a single earthquake loss probability curve. Finally an incremental optimization approach was used to identify the design configuration that satisfies the loss requirement.

Chapter 6: Software Development

Chapter 6 presents the software package developed to perform the structural dynamic analysis and loss estimation tasks covered in this dissertation work. This Windows based program, Seismic Analysis Package for Wood frame structures (SAPWood), provides the wood frame research and design community with a powerful yet user-friendly tool to perform non-linear structural analysis and loss estimation of wood frame structures during earthquakes. The details on how the models and framework developed in earlier chapters were built into different modules in this package are discussed in this chapter.

Chapter 7: Index Building Analysis

Chapter 7 present in detail the procedures and results of the loss estimation and design optimization of 3 index buildings selected for this dissertation work. The buildings represent the main stream construction style of the residential structures in North America. These numerical examples verified the viability of the approach proposed in

this dissertation work, with the incorporation of currently available data related to the economical behavior of wood frame structures.

Chapter 8: Sensitivity analysis

Chapter 8 investigates sensitivity analysis on the loss distribution against variations in the framework input information. The impacts of seismic hazard, structural configuration and strength, and the accumulation of damage were evaluated through sensitivity analysis. The results from the sensitivity analysis provided preliminary insight into the behavior of the loss estimation framework. It also served as an example of how the results in this study can be used to benefit research in related fields.

Chapter 9: Summary, Conclusions, and Recommendations

Chapter 9 provides the overall summary of the conclusions and recommendations as a result of this study. These are based on the loss estimation and loss-based design methods for light frame wood structures and their application to the index buildings conducted in this study. There are also further comments on the behavior of the index structures based on the studies of Chapter 7 and 8.

Chapter Two

Woodframe Structure Modeling

2.1 Evolutionary Parameter Hysteretic Models

In order to build accurate structural models, one needs to investigate the most fundamental load resisting mechanism that controls the behavior for the structure of interest, such as Hook's law for steel, post-cracking load transfer for reinforced concrete. Lateral strength/stiffness of woodframe structures is mainly provided by wood shearwalls. The wood shearwalls are built from framing members and sheathing panels connected by hundreds of connectors usually nails and sometimes screws. As the shearwall undergoes deformation, each of these connectors behaves as nonlinear springs trying to hold the structure in the initial position. The actual physical behavior involved in this process is very complex because the deformation of the material, nail-wood interface friction, and geometrical nonlinearity of the nail will all contribute as the nail deforms. A simplified model for such a mechanism, given one is interested only in the load-displacement relationship, is a hysteretic model which defines the shape of the force-deformation loops with a set of empirical rules. Since these models

are not fundamentally associated with any physical system, they can be used both for the fasteners and shearwalls which have been shown to have hysteresis of similar shapes (White and Dolan, 1995).

Existing models

An existing hysteretic model used by a number of studies is the CUREE model (Folz and Filiatrault, 2002) which is based on a hysteresis model first developed by Foschi (1974). The CUREE model is a single degree-of-freedom (SDOF) hysteretic model that defines the resisting force response of a wood shearwall under reversed cyclic loading by using exponential backbone curves and linear loading and unloading paths. It can also be implemented into connector modeling as in the program CASHEW, in order to perform cyclic loading analysis of shearwalls numerically (Folz and Filiatrault, 2004a; 2004b). Ten hysteresis parameters are used to define the loading paths in the CUREE model, which is illustrated in Figure 2-1.

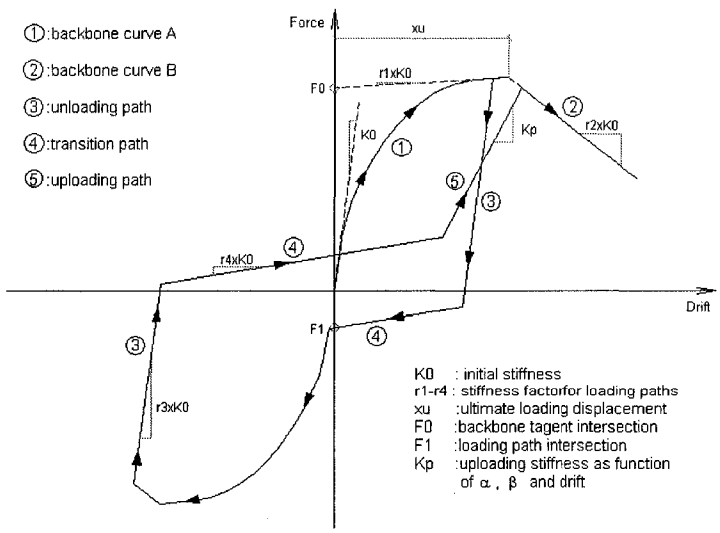

Figure 2-1: Loading paths and parameters in CUREE model

The CUREE model has been shown to be accurate for nail and shearwall behavior when the damage (directly related to displacement or drift) to the system is limited. However, as the woodframe/seismic research/design community moves toward PBSD for woodframe structures, it will be necessary to accurately model woodframe dynamic response in large drift regions particularly when these components have been subjected to a significant amount of damage, i.e. as the wall approaches the collapse-prevention and life-safety levels (as defined in FEMA 356 pre-standard). Static-parameter models have limited accuracy mainly because the strength and stiffness degradation of the physical system become so significant in these cases that their behavior become difficult to model using loading paths with constant (static) parameter sets. Figure 2-2 shows a hysteresis loop from a cyclic load test where large displacements are observed and stiffness degradation becomes significant. A fitted static-parameter model is also shown in Figure 2-2. Inspecting figure, one can see that the accuracy of the model is good up to a displacement of approximately 38 mm (1.5 inches) and acceptable up to about 50 mm (2 inches). However, as the stiffness degrades significantly, it can be observed from the hysteresis that the model is not able to flatten the hysteresis loops enough and may overestimate the energy dissipation. This could result in an under-prediction for the deformation at high displacement levels in time domain analysis.

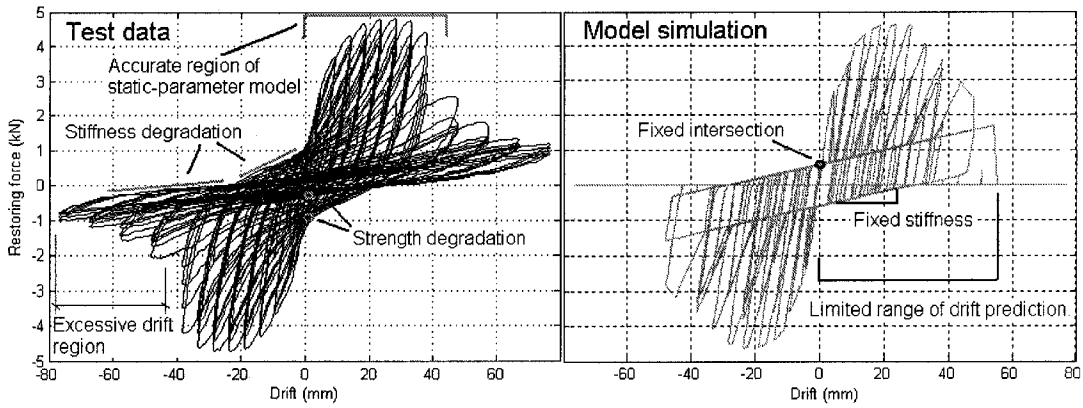

Figure 2-2: Comparison between test data and static-parameter model simulation

Evolutionary formulation for wood shearwall hysteresis

By introducing degradation rules into the hysteretic parameters themselves, a new family of models can be developed which are capable of tracking the degradation, and thus the dynamic response, of the system better than static-parameter models. These evolutionary models are believed to be more robust within a wide range of dynamic load cases than existing hysteretic models. The evolutionary formulation for wood shearwall hysteresis can be expressed functionally as

$$F = f(x, \vec{p}, g_1(\vec{D}, \vec{p}_1), ...g_k(\vec{D}, \vec{p}_k)) \tag{2-1}$$

where F is the restoring force of the SDOF system, x is the displacement of the SDOF system, $f(\cdot)$ is the function defining the loading paths that govern the behavior of the SDOF model, $\vec{p}$ is the ***static hysteretic parameter*** vector (constant vector) that represents the load-independent parameters of the system (e.g. initial stiffness), and

$g_{1,\ldots,k}(\cdot)$ is a series of functions that define the degradation rules of the system, termed here as ***degradation functions,*** each representing one ***evolutionary parameter*** that continues to change with damage/displacement level of the system. Vector $\vec{D}$ is the tracking index vector consisting of several tracking indices which are themselves functions of the loading history. Finally, $\vec{p}_{1,\ldots,k}$ is the ***local degradation parameter*** vector which defines the functional relation between the tracking index vector, $\vec{D}$, and the evolutionary parameter, g_i. A simple flowchart showing the structure of the evolutionary formulation is shown in Figure 2-3 for clarification.

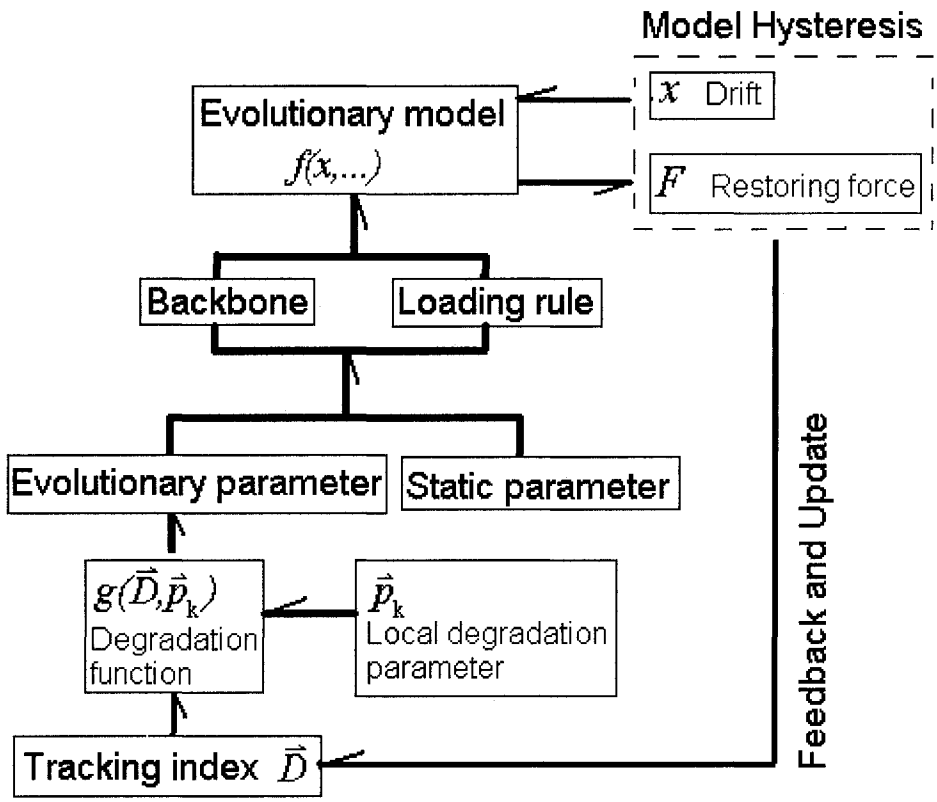

Figure 2-3: Structure of the evolutionary parameter formulation

Modeling approach

Following the formulation given by equation 2-1, there are numerous ways to construct evolutionary models depending on the tracking indices, degradation functions, and evolutionary parameters. Four major components exist in the construction process of an evolutionary-parameter hysteretic model. Namely (1) *tracking indices*, (2) the *backbone curve* (envelope curve for hysteresis) modeling, (3) the *loading paths* (rules) and (4) *evolutionary parameters* (degradation functions/rules).

The *tracking index*, as indicated by the name, is the index in a hysteretic model that keeps track of the damage accumulated in the physical system. One may include as many tracking indices as necessary to ensure the complete of the damage information. But a simple damage tracking index vector, D, constructed with two drift levels will serve the purpose of this study,

$$\vec{D} = \begin{Bmatrix} d_p \\ d_n \end{Bmatrix} \tag{2-2}$$

where d_p and d_n are the maximum absolute drift levels in the positive and negative directions for the loading history, respectively. Later in the discussion, it will be shown that the evolutionary-parameter formulation with such a simplified tracking mechanism can provide considerable improvement on the behavior of the simulated loading paths over static-parameter model.

The *backbone curve* confines the hysteresis loops, essentially defining the ultimate load resisting capacity of the system at different levels of drift. Typically, the backbone curve of a wood shearwall or wood frame connector should at least consist of a 'strain hardening' (characterized by decreasing but always positive stiffness) curve and a 'decaying' (negative stiffness) curve. The backbone curves in most existing assembly-level models (e.g. Folz and Filiatrault, 2001; van de Lindt and Walz, 2003) are assumed to be constant during loading. However, they could also have evolutionary parameters that include some adjustment related to the influence of the loading history (damage). Then the backbone curve can be functionally expressed as

$$F_b = f_b(x, \vec{p}_b, g_{b1}(\vec{D}, \vec{p}_{b1}),..., g_{bk}(\vec{D}, \vec{p}_{bk})) \tag{2-3}$$

where $\vec{p}_b$ is the static parameter vector for the backbone, which will typically include parameters independent of the loading history/protocol (e.g. initial stiffness). The term $g_{b1...k}(\vec{D}, \vec{p}_{b1...k})$ denotes the *evolutionary parameters* for backbone as functions of the *tracking indices* and local degradation parameters. However, accurate modeling of the backbone evolutionary parameters requires a systematic series of tests performed in order to gather information on how the backbone is influenced by different loading histories, which is not possible for current study. So, a backbone curve with no evolutionary parameters is shown in Figure 2-4 was used throughout this dissertation work. Also shown in Figure 2-4 are the seven static parameters used in the backbone

curve functions in equation (2-4). The curves are similar to the backbone used in the CUREE model except for a modification in the decaying region:

$$F_b(x) = \begin{cases} \text{sgn}(x)(F_0 + r_1 K_0|x|)[1-\exp(-K_0|x|/F_0)] & |x| < x_u \\ \text{sgn}(x)F_u + r_2 K_0[x - \text{sgn}(x)x_u] & x_u \le |x| \le x_{u1} \\ \text{sgn}(x)(F_{u1} - F_{ur})\exp[\lambda_b(|x| - x_{u1})] + \text{sgn}(x)F_{ur} & |x| > x_{u1} \end{cases} \quad (2\text{-}4)$$

where K_0 is the initial stiffness, F_0 and r_1 are the shape parameters of the backbone curve 1, r_2 is the slope ratio of backbone curve 2 to the initial stiffness, x is the displacement/drift of the nonlinear element, x_u is the drift corresponding to the maximum restoring force, x_{u1} is the drift corresponding to the end of backbone curve 2, λ_b is the exponential degradation rate for the backbone curve 3, F_u is the maximum restoring force, F_{ur} is the residual restoring force before collapse of the wall, F_{u1} is the restoring force at the end of backbone curve 2, and F_b is the restoring force as function of drift x.

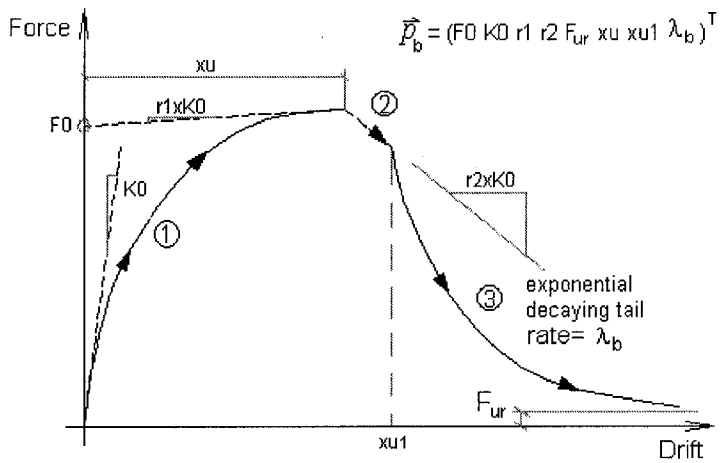

Figure 2-4: Backbone curve for illustrative model

The *loading path* is defined as those portions of the hysteresis that do not belong explicitly to the *backbone curve*. A variety of continuous functions in the drift-restoring force coordinates can be used to model the loading paths. In order to implement the evolutionary formulation, *evolutionary parameters* were incorporated as boundary conditions for these loading paths. And the function that represents the *loading path* can be written functionally as

$$y = \phi(x, x_1, y_1, y_1', x_2, y_2, y_2') \qquad |x_1| < |x| < |x_2| \tag{2-5}$$

where (x, y) is a point on the loading path in general x-y coordinates (x should be drift and y should be restoring force for the physical system). Parameters (x_1, y_1), y_1', (x_2, y_2) and y_2', or some of them, will be *evolutionary parameters* defining the boundary conditions of the *loading path* by specifying the location and slope at ends. In this study, a forth-order polynomial was used and the parametric function for loading path would be

$$y = ax^4 + bx + c \tag{2-6}$$

where

$$a = \frac{y_2 - y_1 - y_1'(x_2 - x_1)}{x_2^4 - x_1^4 - 4x_1^3(x_2 - x_1)} \tag{2-7}$$

$$b = \frac{y_2 - y_1 - a(x_2^4 - x_1^4)}{x_2 - x_1} \tag{2-8}$$

$$c = y_1 - ax_1^4 - bx_1 \tag{2-9}$$

Further more, in order to apply the loading path and backbone functions within the model, a set of *loading rules* were used to describe the response of the model under an arbitrary displacement loading history. The *loading rules* for the fourth order polynomial loading curves were listed as the following:

Loading Rule #1: If $x \cdot \frac{dx}{dt} > 0$ and $|x| > |x_t|$, $y = F_b(x)$.

Loading Rule #2: If $x \cdot \frac{dx}{dt} > 0$ and $|x| \le |x_t|$, $y = \phi(x, 0, \text{sgn}(x) \cdot F_1, K_I, x_t, F_b(x_t))$.

Here F_I, K_I and x_t are evolutionary parameters that will be discussed in next section.

Loading Rule #3: If $x \cdot \frac{dx}{dt} < 0$, $y = \phi(x, 0, -\text{sgn}(x) \cdot F_1, K_I, x_{un}, y_{un})$. Here x_{un} and y_{un} is the previous drift and force level at which the quantity $x \cdot \frac{dx}{dt}$ changes its sign (nearest unloading point).

Figure 2-5 presents an illustrative hysteresis model that shows how the three loading rules described above and the forth-order polynomial loading path work together at different drift levels.

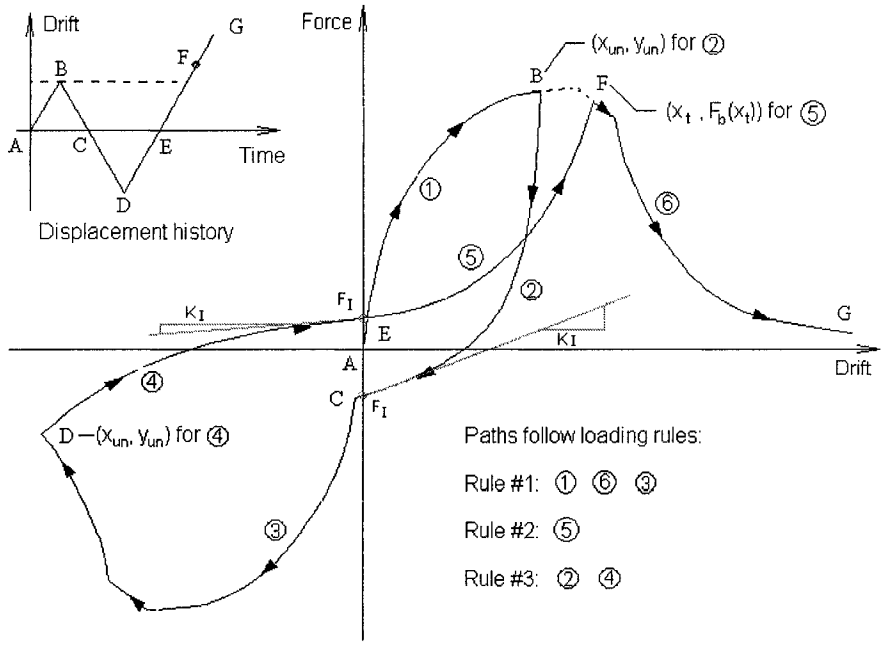

Figure 2-5 Loading paths in illustrative model

The most essential step in the evolutionary modeling of wood shearwall behavior is choosing and modeling the *evolutionary parameters*. *Evolutionary parameters* cannot be visualized as model parameters explicitly but must be modeled as functions (specifically, degradation functions) of *tracking indices*. The parameters in these functions, which were referred to earlier as "*local degrading parameters*", can be evaluated from regression analysis on the reversed-cyclic test results of the physical system.

Three *evolutionary parameters* were used in this study for the *loading path*. The *evolutionary parameters* used here are F_I (restoring force level passing the neutral position), K_I (stiffness at the neutral position) and x_t (target drift level where the

loading path intersects with backbone curve). First, it is assumed that x_t is a linear function of the *tracking indices*, namely

$$x_t = \begin{cases} \beta \cdot d_p & x_t > 0 \\ -\beta \cdot d_n & x_t < 0 \end{cases} \tag{2-10}$$

where β is the *local degradation parameter* for x_t. The assumption for x_t is similar to the CUREE model in which the next target drift level on the backbone is proportional to the previous unloading drift level from the backbone.

For F_I and K_I, their functional form with respect to *tracking indices* should be assumed based on observation of the physical system hysteresis. For example, one can record/calculate F_I and K_I for each applicable data point, i.e. every time the test hysteresis passes the neutral position. At the same time, the corresponding values of the *tracking indices* can also be determined and recorded. Then, these records can be plotted against one another to observe the trend and appropriate functions can be chosen to model these *evolutionary parameters*. Finally, regression analysis can be performed to yield the local parameters for these degradation functions. For this particular illustrative example, a scalar value termed simply as *average drift* D_a (defined in equation (2-11)) which comes from the tracking index vector is used in the regression analysis.

$$D_a = \begin{pmatrix} 0.5 & 0.5 \end{pmatrix} \times \vec{D} \tag{2-11}$$

Figure 2-6 presents the example of *evolutionary parameters* versus average drift from cyclic test data of a 2.44m x 2.44m (8x8 ft) wood shearwall and the local parameters from regression analysis. It can be seen from the trend in Figure 2-6 that an option for the degradation function for F_I might be

$$F_I = \begin{cases} F_C D_a / x_{F1} & D_a < x_{F1} \\ F_C & x_{F1} \le D_a \le x_{F2} \\ (F_C - F_R)\exp(\lambda_F (D_a - x_{F2})) + F_R & D_a > x_{F2} \end{cases} \quad (2\text{-}12)$$

where F_1 is the intersection of loading path and force axis, F_C is the maximum value of F_1, F_R is the residual value of F_1 in the severe damage region, λ_F is the decay factor for F_1, x_{F1} is the displacement corresponding for the beginning of the maximum F_1 value, x_{F2} is the displacement corresponding to the exponential decaying region for the F_1 value.

The evolutionary behavior of K_I, was also modeled with a degradation function, for example

$$K_I = (K_0 - K_R)\exp(\lambda_k D_a) + K_R \quad (2\text{-}13)$$

where K_R is the residual value of K_I in the severe damage region and λ_k is the decay factor for K_I. This is also presented in the lower plot of Figure 2-6.

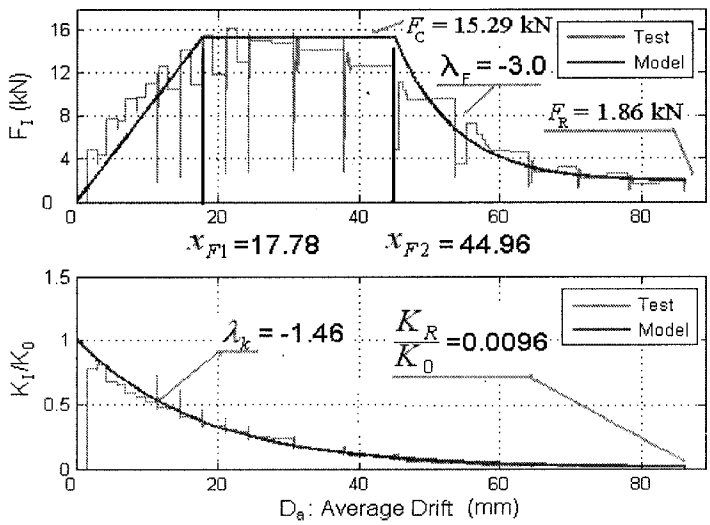

Figure 2-6: Evolutionary parameter modeling

Figure 2-7 presents the evolutionary-parameter concept and shows how these varying evolutionary parameters affect the hysteresis at different drift (or damage) levels based on the degradation functions in equation (2-12) and (2-13).

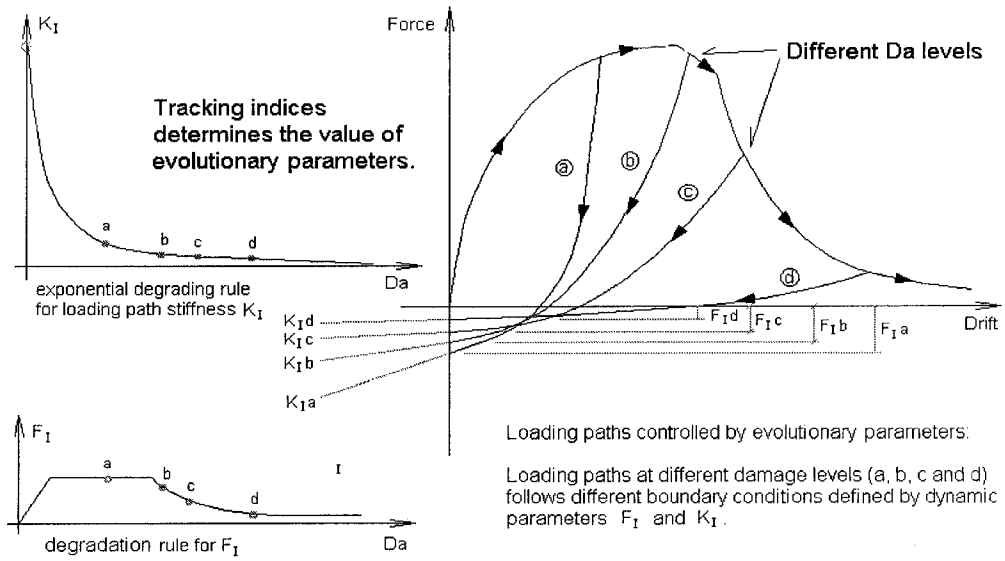

Figure 2-7 Degradation of loading paths

The framework of EPHM is completed after all evolutionary parameters are defined with a degradation function. Thus, the behavior approximated by the degradation functions discussed above is essential to the construction of EPHM. However, depending on the particular functions in a particular EPHM, there may be additional important phenomena observed during the cyclic response of physical system that significantly influence the system response but not included in the degradation function. For example, one hysteresis loop characteristic observed in most reversed-cyclic wood shearwall tests, termed herein as the ***inner loop scaling effect***, is illustrated in Figure 2-8. Assuming one uses the polynomial-based EPHM discussed here to model these hysteresis loops, it is apparent that during the loops 'inside' the first larger loop, the average drift, D_a, remains constant because loading during those inner loops did not push the system any further (the tracking index vector remains the same as in the previous loop). According to the degradation function in equation (2-12) and loading rules 2 and 3, these loops should have the same value for the evolutionary parameter F_1. However, this contradicts the actual behavior observed in the system (F_1 for these 'inner loops' is much smaller than the 'outer' loops). This discrepancy can also be seen in Figure 2-6, in which the F_1 versus D_a curve from the test data is not smooth and has sudden drops. And this behavior is not included in the aforementioned degradation functions. So the degradation function should be modified to account for it. The value of F_1 can be scaled according to the previous unloading event to yield this behavior in the model. In the revised model, the scaling factor is

taken as the ratio of the previous unloading drift level x_{un} to d_p or d_n (depending on the sign of x_{un}). So, for $x_{un} > 0$, equation (2-12) can be modified as

$$F_I = \begin{cases} (x_{un}/d_p)\times F_C D_a / x_{F1} & D_a < x_{F1} \\ (x_{un}/d_p)\times F_C & x_{F1} \le D_a \le x_{F2} \\ (x_{un}/d_p)\times((F_C - F_R)\exp(\lambda_F(D_a - x_{F2})) + F_R) & D_a > x_{F2} \end{cases} \quad (2\text{-}14)$$

If $x_{un} < 0$, d_p in equation (2-14) should be replaced by $-d_n$. The loading loops generated with this modified evolutionary parameter are shown in Figure 2-8 and compared with test data. One can see the effectiveness and accuracy of this empirical and straightforward approach. It is worth pointing out that this kind of modification can be avoided or done in another way if the degradation functions were constructed in a different form. But checking the behavior of the model and test data is always recommended for any EPHM.

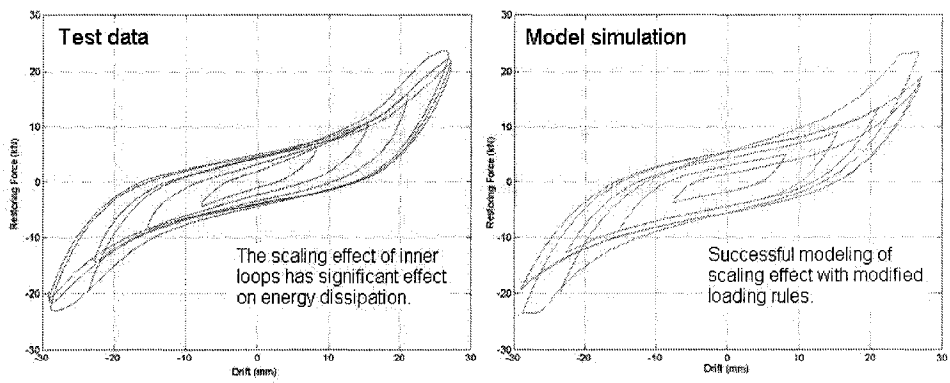

Figure 2-8: Inner loop scaling effect

As mentioned earlier in this section, EPHM is an empirical model which can be used to represent different physical systems. In this study, the model was applied to both the load-slip relationship of the nails on a shearwall assembly and the lateral force-drift relation of the shearwall segments. The parameters for the EPHM of the nails came from reversed cyclic loading tests conducted on different nail types (10d, 8d, 4d, etc.) conducted at Colorado State University. The parameters for the EPHM wall segments can also be obtained from cyclic loading tests. However, it is not realistic to test all walls in a building prior to the construction mainly due to the variation of possible wall configurations in a design. A connector level assembly model was developed to solve this problem by allowing the designer to build the wall segments using the EPHM of each nail, screw, or other connectors and numerically load the wall model under cyclic protocols. This model is discussed in detail in next section.

The EPHM has been programmed into the program package SAPWood as an element module. The element allows the user to "push" the element incrementally with a loading protocol and returns the tangent stiffness and restoring force at every load step based on user inputted EPHM parameters. This set up is very useful in updating the stiffness of the system in a Newmark-Beta algorithm and quasi static displacement loading analyses. In summary, the EPHM developed in this dissertation work can be defined with 16 parameters. The description of each of these parameters is listed in Table 2-1.

Table 2-1: Parameters in EPHM

Parameter	Description
K_0	Initial stiffness
F_0	Force parameter of the backbone curve, very close to ultimate capacity
r_1	Stiffness parameter of the backbone curve, typically a very small value
x_u	Displacement value corresponding to ultimate capacity
r_2	Stiffness ratio for the linear descending backbone between x_u and x_{u1}
x_{u1}	Displacement value corresponding to the start point of exponential decaying portion of the backbone curve
λ_b	Exponential decaying rate parameter of the backbone curve
F_c	Maximum pinching force at x=0
F_r	Residual pinching force at x=0
x_{F1}	Displacement value corresponding to the start point of maximum pinching plateau
x_{F2}	Displacement value corresponding to the end point of maximum pinching plateau
λ_F	Exponential decaying rate parameter of the pinching force
λ_k	Exponential decaying rate parameter of the pinching stiffness
K_r	Residual pinching stiffness
β	Stiffness degrading parameter
F_{ur}	Residual force of the backbone

2.2 Wood Frame Assembly Modeling

As discussed earlier, cyclic test data of the physical system (connectors and shearwalls in this case) will be needed to calibrate the parameters used in EPHM. Although a standard cyclic test database for a limited number of nail types and panel arrangements can be constructed, it is not practical to have every shearwall tested before using them in the design. A numerical model for shearwall assemblies was developed in this section based on the principal of virtual work to estimate the cyclic response of the shearwalls given EPHM for nails. The model for any shearwall segment can be constructed and forced through a cyclic load protocol numerically to get the hysteresis. Then this hysteresis was used to calibrate EPHM for the wall assembly which will be included in the dynamic analysis of the whole structure.

Existing model and limitations

An existing model for wall assemblies was previously developed by Filiatrault et. al. and incorporated into a software package CASHEW (2001). In the CASHEW model, the frame behind the sheathing panels was assumed to undergo a uniform shear deformation such that a rectangular frame can only deform into a parallelogram. The sheathing panels were allowed to develop uniform shear deformation and in-plane rigid body motion (see Figure 2-9). The nails connecting the sheathing panel and framing members were modeled with ten-parameter CUREE hysteretic model discussed in Section 2.1. The CASHEW model has been used to predict cyclic behavior of wood shearwalls and proven to yield accurate results for regular wall configurations based on the comparison of numerical force to standard cyclic tests. However, there are some limitations for this model which lie in the fundamental kinematics assumptions. The pure shear deformation assumption for the frame will not be valid for irregular wall framing schedules (e.g. walls with big openings) or shearwalls with framing connection damage (such as separation between the vertical stud and sill plate). Furthermore, the use of static parameter hysteretic nail models limits the model's ability to predict wall behavior exceeding a certain level of damage. In order to circumvent these limitations, a more robust wall assembly model based on new kinematics assumptions was developed for this dissertation work. This new model, termed here as a Nail Pattern (NP) model, was also incorporated into the SAPWood software program for the ease of use.

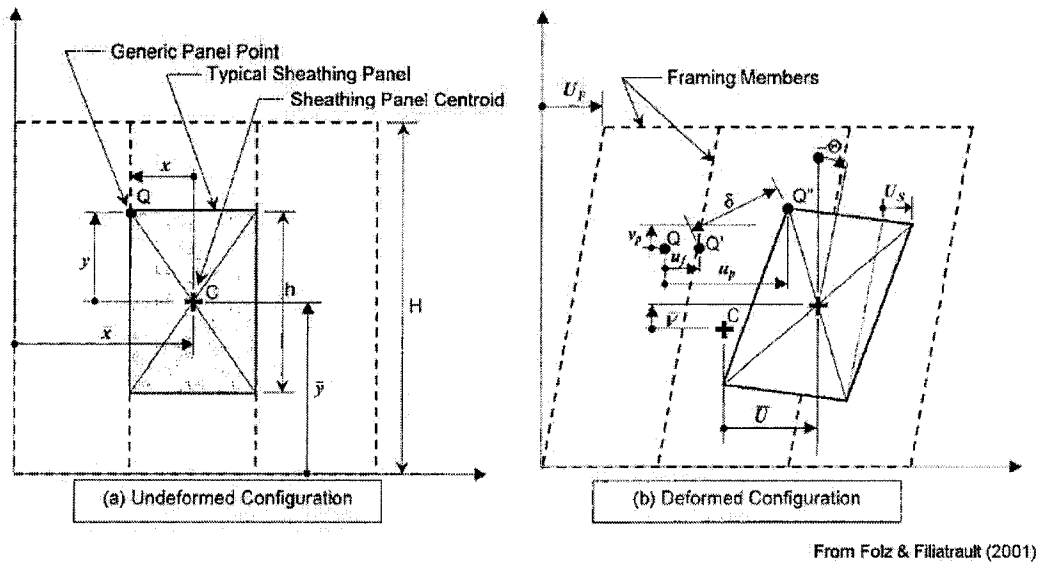

Figure 2-9: CASHEW model kinematics

SAPWood-Nail Pattern (SAPWood-NP) model

In the newly developed NP model, every framing member and sheathing panel is considered as a component of the assembly system. Each component is assumed to be a rigid body which has three in-plane degrees of freedom. The kinematics assumptions for the NP model can be illustrated in Figure 2-10. These components were connected with nails that were modeled with EPHM calibrated from the nail test data. This model was for use in quasi static analysis with a reversed cyclic loading protocol (displacement control), resulting in a global force resistance based on the equilibrium of the forces in the nail elements.

Consider the diagram illustrated in Figure 2-10. The Global coordinates (X, Y) can be defined anywhere in the wall plane. The local coordinates were defined at the center of each components and the local axis will be parallel to the global axis (θ=0) in the initial configuration. Local coordinates will undergo rigid body movement with the components on two transitional degrees-of-freedom (DOF) and one rotational DOF Thus a wall model with N components (studs and panels) will have 3N DOF's total. The purpose of this derivation is to develop the 3N x 3N stiffness matrix for the components' DOF based on the nail connector stiffness through the principal of virtual work.

Assume in the initial configuration, a nail connects component *i* and *j* at point P, as it is shown in Figure 2-10 (the components has been blown apart for illustration). We assume the nail head is on component *i* and the other end of nail is on component *j*. These two points, although physically on different components, coincide with each other at P before the deformation. After deformation, components *i* and *j* both moved and the original P will move to P*i* for component *i* and P*j* for component *j*. We are interested in how to calculate the distance between P*i* and P*j* from the rigid body deformation of component *i* and *j*, which is also the slip distance of the nail. And the calculation can be performed following these steps:

Firstly, calculate the global coordinates for P*i* based on the deformed configuration of component *i*, which is also the deformed configuration for the local coordinate system on component *i*.

$$\begin{Bmatrix} x_i \\ y_i \end{Bmatrix} = \begin{bmatrix} 1 & 0 & \xi_i & -\eta_i \\ 0 & 1 & \eta_i & \xi_i \end{bmatrix} \times \begin{Bmatrix} X_i \\ Y_i \\ \cos\theta_i \\ \sin\theta_i \end{Bmatrix} \tag{2-15}$$

Then obtain the linearized incremental relationship by taking derivatives

$$\begin{Bmatrix} \Delta x_i \\ \Delta y_i \end{Bmatrix} = \begin{bmatrix} 1 & 0 & -\xi_i \sin\theta_i - \eta_i \cos\theta_i \\ 0 & 1 & -\eta_i \sin\theta_i + \xi_i \cos\theta_i \end{bmatrix} \times \begin{Bmatrix} \Delta X_i \\ \Delta Y_i \\ \Delta\theta_i \end{Bmatrix} \tag{2-16}$$

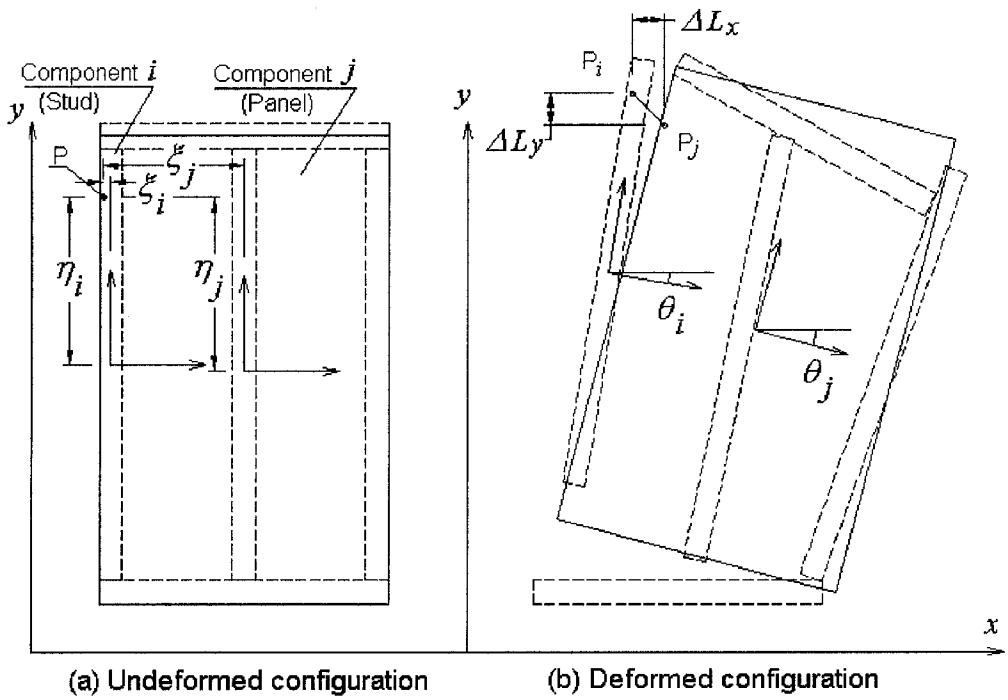

Figure 2-10: Nail-Pattern (NP) model kinematics

Similar results can be easily derived for component *j*. Now, we can write out the global locations for both end of the nails based on their initial location (P) and incremental. So the incremental distance between P*i* and P*j* is calculated as

$$\begin{Bmatrix}\Delta L_x\\ \Delta L_y\end{Bmatrix}=\begin{Bmatrix}x_P+\Delta x_i\\ y_P+\Delta y_i\end{Bmatrix}-\begin{Bmatrix}x_P+\Delta x_j\\ y_P+\Delta y_j\end{Bmatrix}=\begin{Bmatrix}\Delta x_i-\Delta x_j\\ \Delta y_i-\Delta y_j\end{Bmatrix} \tag{2-17}$$

If one arranges the components' incremental DOF one by one into a global vector then

$$\Delta D=\{\Delta X_1 \quad \Delta Y_1 \quad \Delta\theta_1 \quad \ldots \quad \Delta X_N \quad \Delta Y_N \quad \Delta\theta_N\}^T \tag{2-18}$$

The incremental distance (nail slipping) can be written as:

$$\begin{Bmatrix}\Delta L_x\\ \Delta L_y\end{Bmatrix}=\begin{Bmatrix}\ldots & 1 & 0 & -\xi_i\sin\theta_i-\eta_i\cos\theta_i & \ldots & -1 & 0 & \xi_j\sin\theta_j+\eta_j\cos\theta_j & \ldots\\ \ldots & 0 & 1 & -\eta_i\sin\theta_i+\xi_i\cos\theta_i & \ldots & 0 & -1 & \eta_j\sin\theta_j-\xi_j\cos\theta_j & \ldots\end{Bmatrix}\times\Delta D$$

$$=B\times\Delta D \tag{2-19}$$

Where B is the geometric matrix for this nail connection component *i* and *j*; all other terms in B are 0.

The principal of virtual work states that the amount of work done by the internal forces and external forces through a virtual displacement is zero on a balanced system. The only internal force considered in this model is the force of nails. The external

force on the wall is limited to the in plane forces applied to the components of the wall. Then the virtual work statement for this problem is

$$\sum F_n \delta L_n - F \delta D = 0 \tag{2-20}$$

Where F_n is the force in the nail connection, δL_n is the virtual nail slip displacement; F is the force vector acting on the global DOF's; and δD is the virtual displacement on the global DOF

Since the behavior of the nail is highly non-linear, we need to use the virtual work statement in an incremental form

$$\sum \Delta F_n^T \times \delta L_n - \Delta F^T \times \delta D = 0 \tag{2-21}$$

Where

$$\Delta F_n = \begin{Bmatrix} F_x \\ F_y \end{Bmatrix} \text{ and } \delta L_n = \begin{Bmatrix} \delta L_x \\ \delta L_y \end{Bmatrix} \tag{2-22}$$

Notice that the force and displacement of the nail in the X and Y direction are treated separately. This is mainly to represent each nail with two EPHM for numerical stability. The incremental forces in equation 2-22 can be calculated as

$$\Delta F_n = \begin{bmatrix} K_x & 0 \\ 0 & K_y \end{bmatrix} \times \Delta L_n = K_n \times \Delta L_n \quad \text{for nail and} \quad \Delta F = K \times \Delta D \text{ for wall} \qquad (2\text{-}23)$$

Where K_x and K_y are the tangent stiffness of the EPHM models for the nail; K is the tangent stiffness matrix of the wall system (which we are looking for).Then the virtual work statement can be further rewritten as

$$\Delta D^T \times (\sum B^T K_n B - K) \times \delta D = 0 \qquad (2\text{-}24)$$

In order to satisfy the principle of virtual work at all possible virtual displacement, the matrix in the parenthesis must be a zero matrix. Therefore the stiffness of the wall assembly can be calculated from the sum of all the nail contributions as

$$K = \sum B^T K_n B \qquad (2\text{-}25)$$

Notice that this system stiffness matrix is derived in an incremental configuration. So it will keep changing at every load step. And it is only valid when the incremental displacement is small since the geometric matrix is obtained through a linearized approximation.

Once the stiffness matrix of the system is obtained, arbitrary cyclic displacement protocols can be applied incrementally to the transverse DOF of the top plate while the bottom plate is set to be fixed. The displacement of other DOF's are solved at every

load step. The resulting force on the top plate undergoing forced deformation is easily obtained once the displacement vector is known. Then this resulting force will be plotted against the displacement protocol to yield the hysteresis of the model. This is the procedure to perform numerical cyclic loading tests.

Due to the configuration of the model, the length of wall segment that can be appropriately (and accurately) represented by the NP model is limited. The top plate of the wall segment must behave close to a single rigid plate under the deformation, as it is shown in Figure 2-11(a). The wall segment illustrated in Figure 2-11(b) cannot be accurately represented by a single NP model due to the flexibility of the top plate. Wall strength/stiffness will be overestimated if wall b is modeled with a single NP model. A solution to such long wall segments is to divide them up into several smaller segments and use multiple NP models to represent them.

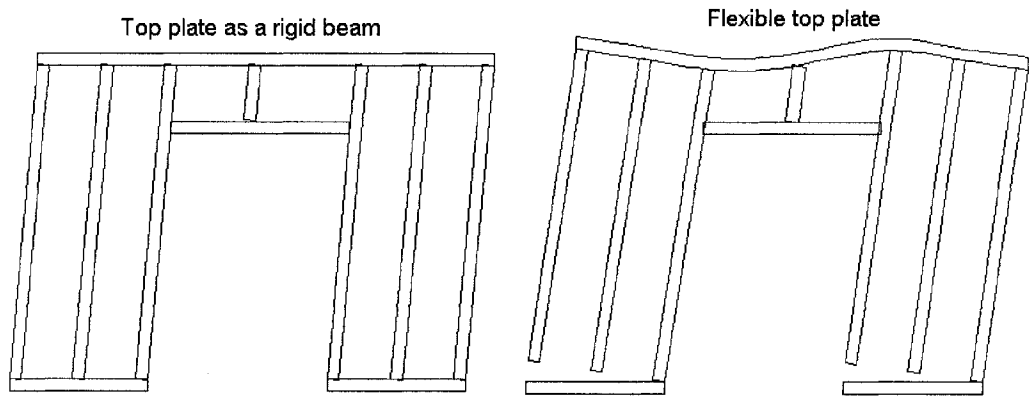

Figure 2-11: NP model applicability

With the flexibility provided through NP model kinematics, a variety of wall configurations and behavior can be modeled, such as the separation of framing members, implementation of hold down devices, rocking behavior of shearwalls, etc. The model allows the user to use any kind of nonlinear element as connectors. Compared to the existing CASHEW model, the only drawback for the NP model will be that the shear deformation of the panel is neglected. This will make the model response slightly stiffer compared to reality. However, the deformation of the panel itself is very limited during the deformation of the shearwall and the influence of neglecting this deformation will not be significant considering the desired accuracy level in the model application. This assembly model has been implemented into the software package SAPWood as an analysis module. Detailed information on the software development can be found in Chapter 6 of this dissertation.

2.3 System Level Structural Modeling

Once the EPHM for each shearwall segment in a structure has been obtained through the model described above, a structural model at the system level is needed to assemble these individual wall models into a system-level structural model to perform dynamic time domain analysis. Under earthquake loading, woodframe structures can experience very large lateral deformation which is the main cause of global instability, or total collapse. In order to seek a balance between the model accuracy, modeling efforts, and computational expense, a simplified bi-axial lumped mass/stiffness model was used for this study. The model chosen was the pan-cake style biaxial model (Folz

& Filiatrault, 2004) which has two translational degrees-of-freedom (DOF) and one rotational DOF at each story level. The shearwalls are modeled with EPHM as nonlinear springs connecting these rigid body story diaphragms together. The conceptual structure of this model is shown in Figure 2-12.

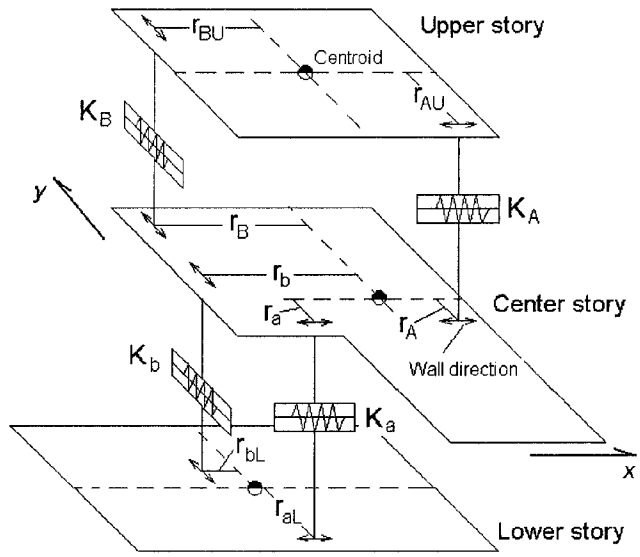

Figure 2-12: Biaxial system level model

The development of the model stiffness matrix is quite straight forward, since the stiffness terms related to a single story diaphragm would only be affected by the nonlinear springs connected directly to this story. All of the elements in the stiffness matrix will be zero except elements in a narrow diagonal band. Each wall element in the model is either in the x direction or in y direction, depending on the physical direction of the walls. For some special design configuration where walls were not orthogonally oriented, two elements could be used to represent the stiffness contribution of such walls.

Consider the story diaphragm in Figure 2-12 which is connected with the upper and lower story by 4 wall elements (A, B and a, b), each represented by its own EPHM. The modeling task is focused on how to lump the stiffness of these for wall elements into the global stiffness matrix. Consider only the DOF's associated with the center story diaphragm, the non-zero term of the stiffness matrix can be written in equation 2-26

$$\begin{bmatrix} -K_{xL} & 0 & -K_{xRL} & K_x & 0 & K_{xR} & -K_{xU} & 0 & -K_{xRU} \\ 0 & -K_{yL} & -K_{yRL} & 0 & K_y & K_{yR} & 0 & -K_{yU} & -K_{yRU} \\ -K_{xRL} & -K_{yRL} & -K_{RRL} & K_{xR} & K_{yR} & K_{RR} & -K_{xRU} & -K_{yRU} & -K_{RRU} \end{bmatrix} \times D = F \quad (2\text{-}26)$$

$$D = \{X_L \quad Y_L \quad \theta_L \quad X \quad Y \quad \theta \quad X_U \quad Y_U \quad \theta_U\}^T \quad (2\text{-}27)$$

$$F = \{F_X \quad F_Y \quad M\}^T \quad (2\text{-}28)$$

The terms in equation 2-26 can be calculated as follows

$$K_x = K_{xL} + K_{xU} \quad (2\text{-}29)$$

$$K_y = K_{yL} + K_{yU} \quad (2\text{-}30)$$

$$K_{xR} = K_{xRL} + K_{xRU} \quad (2\text{-}31)$$

$$K_{yR} = K_{yRL} + K_{yRU} \quad (2\text{-}32)$$

$$K_{RR} = k_a r_a^2 + k_A r_A^2 + k_b r_b^2 + k_B r_B^2 \quad (2\text{-}33)$$

$$K_{RRL} = k_a r_a r_{aL} + k_b r_b r_{bL} \quad (2\text{-}34)$$

$$K_{RRU} = k_A r_A r_{AU} + k_B r_B r_{BU} \quad (2\text{-}35)$$

where

$$K_{xL} = k_a \qquad K_{xU} = k_A \tag{2-36}$$

$$K_{yL} = k_b \qquad K_{yU} = k_B \tag{2-37}$$

$$K_{xRL} = r_a k_a \qquad K_{xRU} = r_A k_A \tag{2-38}$$

$$K_{yRL} = r_b k_b \qquad K_{yRU} = r_B k_B \tag{2-39}$$

If there are more walls in the structure, a similar procedure and assembly method could be used to form the global stiffness matrix of the system. This assembly procedure is repeated at every time step in the Newmark-Beta integration, since the wall stiffness will keep changing based on EPHM parameters.

This structural model, together with the time domain analysis sub-routine, has been integrated into the SAPWood program, where a mixture of spring elements in addition to the EPHM can be used in the same system model.

2.4 Model Verification

The numerical models described above can be verified by comparing the numerical results to cyclic shearwall test hysteresis (for NP model) and shake table test responses (for system level model). Shear wall cyclic test data from different research facilities throughout the U.S. was collected as part of this study to provide a basis for the modeling of the hysteretic behavior for different wall configurations. Due to the difference in the test setup and randomness in the specimen themselves, the responses of the walls with even nominally identical configurations differ from test to test. So there is essentially no "right" answer for the wall responses, although there are

certainly incorrect responses. Thus the results from NP model were verified in a lease restrictive sense in that they are comparable to the existing test data group with similar configurations. The system level model was verified using the shake table test data from the full scaled tests conducted by Filiatrault and colleagues as part of the NEESWood benchmark structure testing (Christovasilis et al., 2007) at University at Buffalo NEES facility.

NP model Verification

The shearwall cyclic test data used in this study came from four research facilities, namely the APA – The Engineered Wood Association (APA), University of California, Irvine (UCI) structural lab as part of the City of Los Angeles tests (CoLA), Michigan Technological University, and Virginia Polytechnic Institute. The data base consists of cyclic loading hysteretic curves for wood shearwalls with varying nail patterns, stud spacing, panel type, and panel thickness. A brief description of the data base was shown in Table 2-2.

Table 2-2: Test data in the shearwall data base

Data Source	Wall dimension	Nail Type*	Nail spacing	Stud spacing	Number of specimen
APA	2x8	8d common	3/3	24	4
	4x8	8d & 10d common	3/6, 3/12, 2/12	24	11
	8x8	8d box, 8d & 10d common	2/6, 3/6, 4/6, 2/12, 3/12, 4/12	24	49
CoLA	8x8	Various	2/12, 4/12, 6/12, 4/6, 6/6	16	108
MTU	8x8	8d box	3/12, 4/12, 6/12	16	3
V tech	2x8	8d common	6/12	16	7
	4x8	8d common	6/12	16	8
	8x8	8d common	6/12	16	7

* The diameter of the nail types: 8d-box (0.113 in); 8d-common (0.131 in); 10d-common (0.148 in).

As it was shown in the table, shearwalls tested were grouped together according to their length (2 ft, 4 ft, and 8 ft) and nail patterns. By using the EPHM parameter extracting program developed with Matlab, the parameters of EPHM that will represent the recorded hysteretic data can be determined. There is considerable variation (uncertainty) in these test results even for the same wall configuration, which results in different EPHM parameters. As an example, the cyclic test data for two identical 4 ft wall specimen tested at Virginia Tech lab are shown in Figure 2-13. Even though the specimen were constructed and tested by the same facility, the hysteretic behavior can be very different.

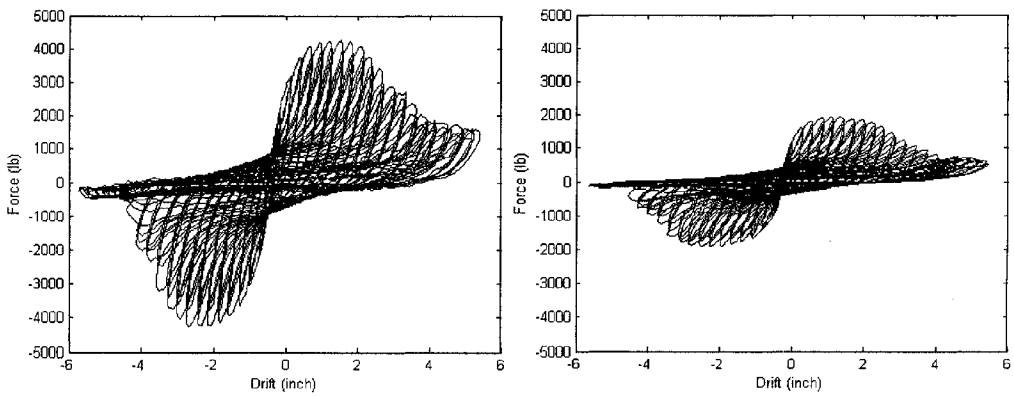

Figure 2-13: Variation in cyclic test results

Different NP models were setup according to the configuration of the shearwalls in the database. The connector (nail) parameter for these NP model came from the cyclic nail tests conducted at CSU. Figure 2-14 shows one of the test hysteresis curves for a single 8d common nail and the EPHM simulation using the model parameters obtained from the test data.

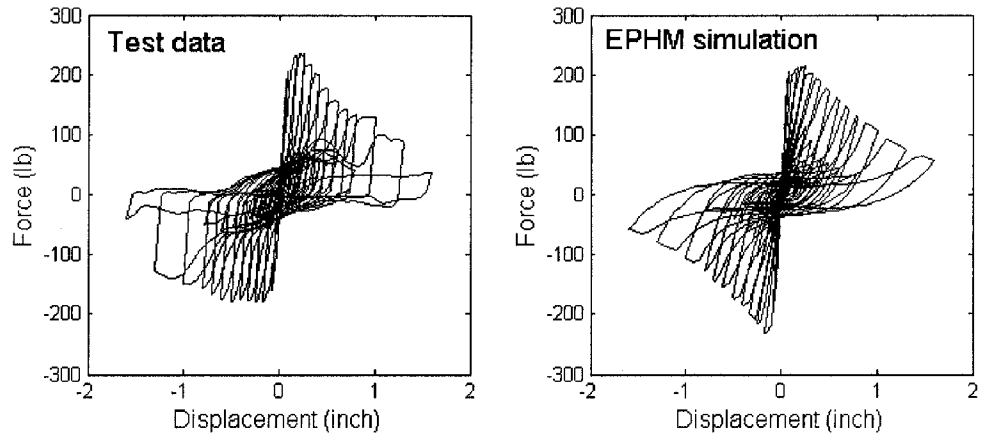

Figure 2-14: Test hysteresis for single 8d common nail (tested at CSU)

The EPHM parameters were obtained through NP model analysis and compared with the parameters obtained from the test data. Figure 2-15, 2-16, and 2-17 illustrated the comparison of the hysteresis from NP model simulation and wall test data. It can be seen from the comparison that the NP model can provide a reasonable estimation of the resistance of wood shearwall assemblies. The prediction is not (and will never be) perfect since the complicated details in the deformation of shearwalls can not be fully accounted for.

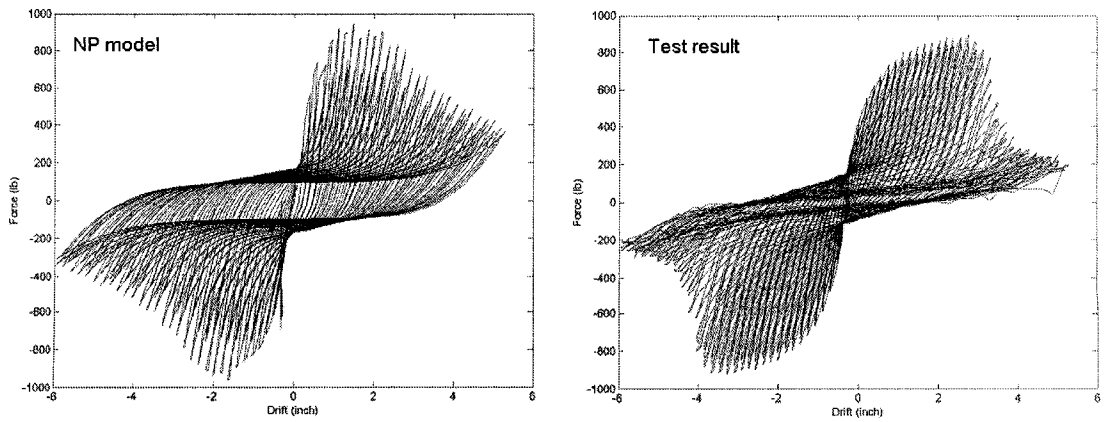

Figure 2-15: Comparison between NP model and test data (2 ft wall segment)

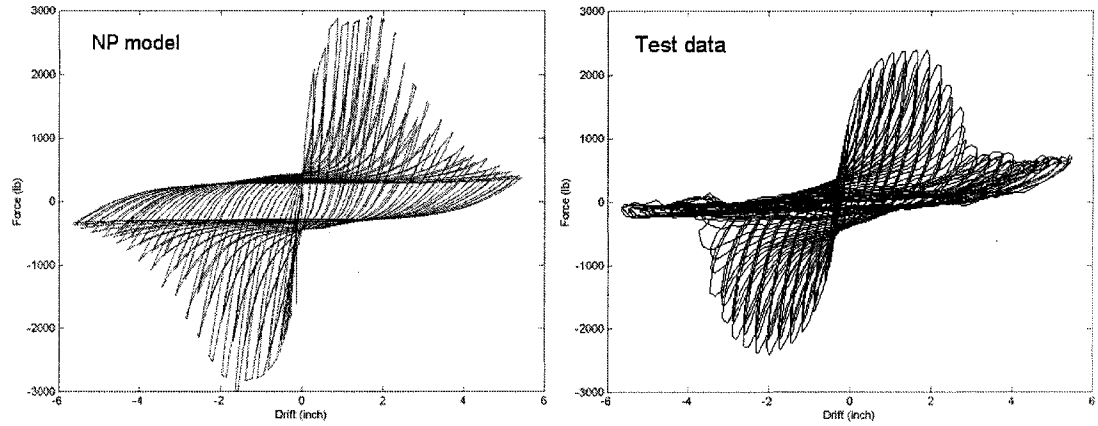

Figure 2-16: Comparison between NP model and test data (4 ft wall segment)

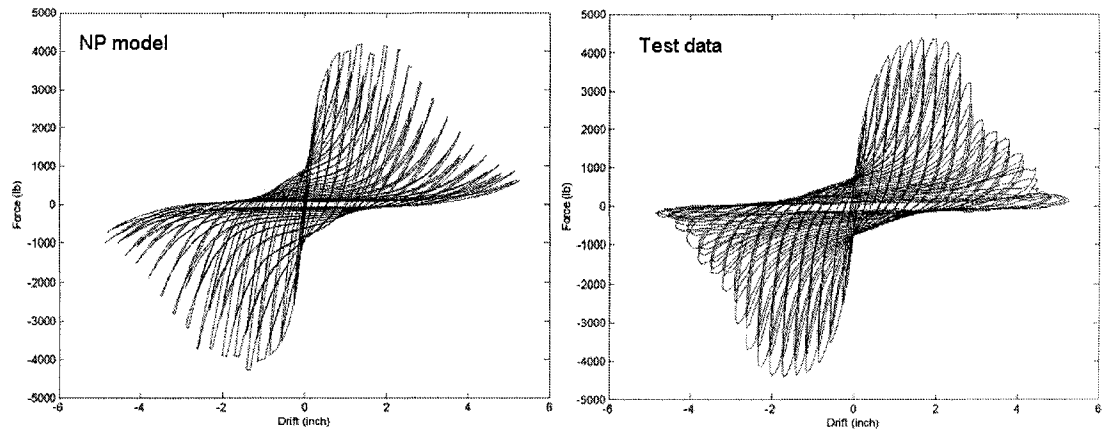

Figure 2-17: Comparison between NP model and test data (8 ft wall segment)

System model verification

The accurate modeling of the individual shearwall component is only an intermediate step towards time domain analysis of wood frame buildings. The accurate prediction of the dynamic responses of the structural system cannot be guaranteed by the accuracy in component modeling alone. Verification of the system level model must be conducted before applying this model to the loss estimation framework. The structure used to verify the time domain analysis model at the system level was the benchmark house structure from the NEESWood project (report forthcoming by

Christovasilis et al. 2007). This structure is a 1,800 square ft two story townhouse segment with the floor plan illustrated in Figure 2-18.

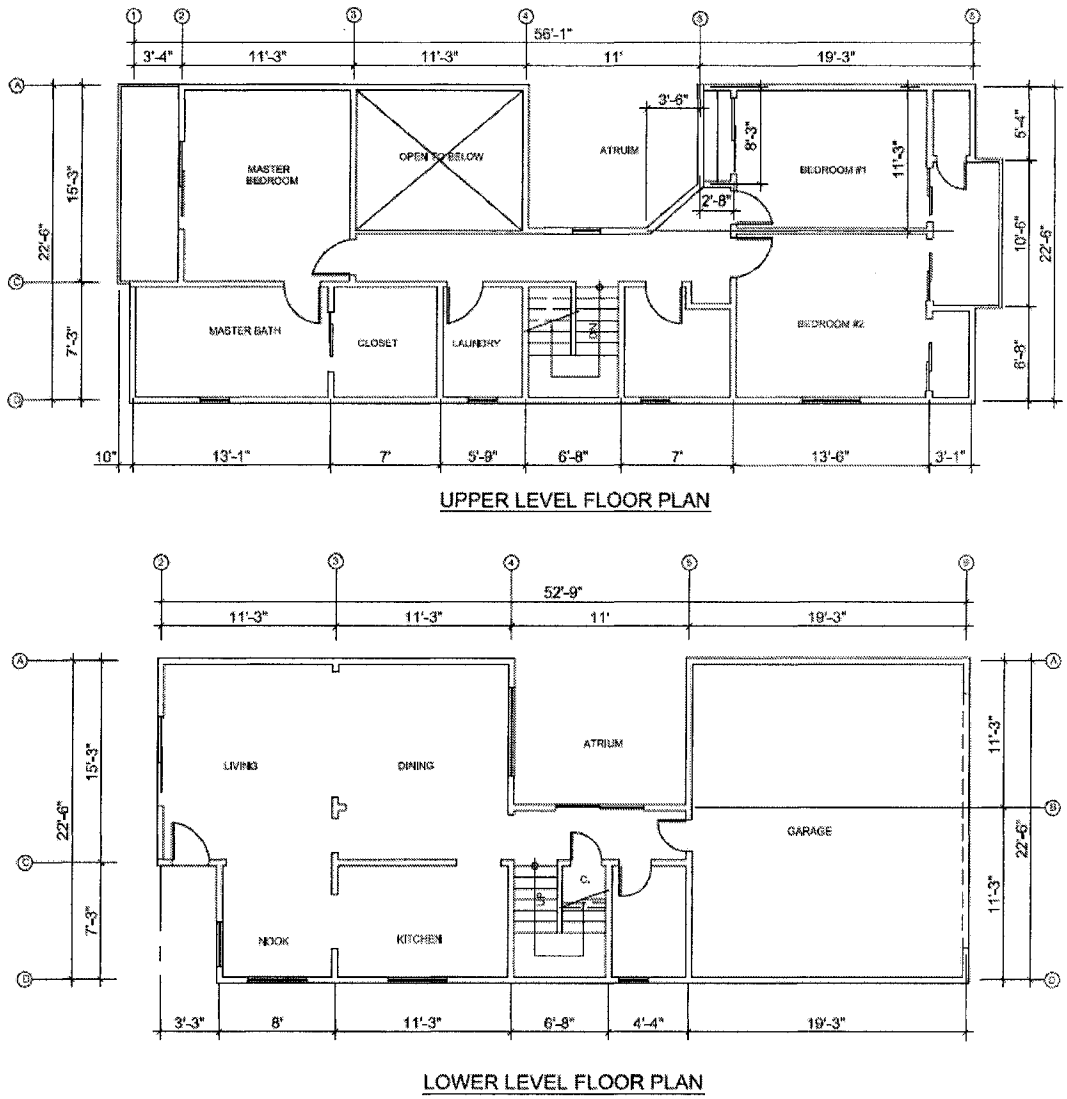

Figure 2-18: Floor plans for the benchmark structure

The structure was tested on the shake table at University at Buffalo in the summer of 2006 as part of NEESWood project. A series of earthquakes with increasing intensity level were used as the shake table excitation input. Table 2-3 lists all the ground motion records used and their peak ground acceleration (PGA) in the test. The test was

divided into several phases to investigate the contribution of different structural and non-structural components to the structural resistance. The test data used in the verification process came from the phase 1 and phase 3 tests, representing "wood shearwall only" and "wood walls plus drywall" structure configurations, respectively. Only level 1 and level 2 tests were conducted for these phases. Test ID S01~S04 in Phase 1 are all level 1 tests; test ID S06, S07, and S17 are level 2 tests. Test ID S05 was stopped and aborted during test due to mechanical problem of the equipment. But the acceleration record from the table is still included in the analysis to estimate the damage accumulation. There are 4 tests in Phase 3. The first two (S01 and S02) are level 1 tests and the others are level 2.

The system model for this structure was built and the recorded shake table motion from the test was used as the ground motion input in time domain analysis. The displacement at the centroid point of each floor level was compared between the simulated model response and the recorded test results. Since the maximum responses (displacement and acceleration) of the structure during earthquakes are closely related to structural damage, the ability of the model to accurately predict the maximum responses is of significant importance. Table 2-4 and 2-5 show the comparison of the maximum displacements at both directions during a series of earthquakes. The locations at which the maximum values occurred in time were also compared in order to illustrate the similarity between the simulated and test time history. Part of the time history plots were selected to illustrate the comparison between model prediction and test. The response under low intensity ground motion excitation was plotted in Figure

2-19. It can be seen from the comparison that the prediction is quite different from the actual behavior, probably due to the lack of engagement in the structural components at such a small drift level. However, this will not affect the damage assessment and loss estimation because the damage is negligible for these small responses. Then, the response and prediction for moderate excitation were compared for both the wood-only structure (Phase 1) and structure with dry-wall installed (Phase 3). The comparison in both the strong and weak direction of the building (see Figure 2-20 ~ 23) indicated that the numerical model is capable of matching the test results in both the pattern and magnitude once the earthquake intensity increases and the shearwalls become fully engaged. Figure 2-24 further showed the superimposed plots of the response time history in one of the Phase 3 tests. From the comparison of the time history, it can be observed that although the system model prediction does not match the test result perfectly, it provided a relatively accurate estimation considering all the simplification involved in the modeling process. The agreement between the analysis and test in both the Phase 1 and Phase 3 data verifies the model accuracy with and without non-structural components (dry-wall board). Although loss estimation could benefit from a more accurate model, this model is the state-of-art for seismic analysis of light frame wood structures.

Table 2-3: Shake table test earthquakes at UB (All records from 1994 Northridge earthquake)

Test Level	Direction	Record station	Scaling Factor	PGA (g)		
				X Longitudinal	Y Transverse	Z Vertical
1	3D	Canoga Park	0.12	0.04	0.05	0.06
2	3D	Canoga Park	0.53	0.19	0.22	0.26
3	3D	Canoga Park	0.86	0.31	0.36	0.42
4	3D	Canoga Park	1.2	0.43	0.5	0.59
5	3D	Rinaldi	1	0.47	0.84	0.85

Table 2-4: Comparison of the maximum drift with Phase 1 test data (Wood-only structure)

Response	Test ID		NWP1S01	NWP1S02	NWP1S03	NWP1S04
	Test setup		3D	X-Y	X only	
Story 1:X	test	Maximum	0.04	0.04	0.04	Y only
		time	15.6	55.4	95.6	
	SAPWood	Maximum	0.08	0.07	0.09	
		time	18.4	58.2	114.7	
Story 1:Y	test	Maximum	0.12	0.12	X only	0.09
		time	17.3	57		137.7
	SAPWood	Maximum	0.2	0.2		0.19
		time	17.3	57		137.7
Story 2:X	test	Maximum	0.05	0.06	0.06	Y only
		time	15.1	57.7	98.4	
	SAPWood	Maximum	0.1	0.09	0.18	
		time	18.4	58.2	114.6	
Story 2:Y	test	Maximum	0.29	0.26	X only	0.23
		time	17.3	57		137.7
	SAPWood	Maximum	0.29	0.28		0.29
		time	17.3	57		137.7

Response	Test ID		NWP1S05	NWP1S17	NWP1S07	NWP1S06
	Test setup		ABORTED*	3D	X only	X-Y
Story 1:X	test	Maximum		0.24	0.22	0.29
		time		217.8	257	297.4
	SAPWood	Maximum		0.29	0.32	0.32
		time		219	253.5	293.9
Story 1:Y	test	Maximum	ABORTED	1.46	X only	1.36
		time		217.9		297.5
	SAPWood	Maximum		1.17		1.48
		time		217.8		297.4
Story 2:X	test	Maximum	ABORTED	0.38	0.29	0.37
		time		219	258.2	298.6
	SAPWood	Maximum		0.37	0.39	0.42
		time		219	257.1	298.6
Story 2:Y	test	Maximum	ABORTED	2.73	X only	2.42
		time		217.9		297.5
	SAPWood	Maximum		1.45		1.78
		time		217.8		297.4

* Test S05 was aborted due to mechanical problem of the shake table. Since the actual acceleration of the shake table in this test is not available, the error in the numerical prediction is not controllable.

Table 2-5: Comparison of the maximum drift with Phase 3 data (Wood-drywall structure)

Comparison Item	Test ID		NWP3S01	NWP3S02	NWP3S03	NWP3S04
	Test setup		3D	X-Y	3D	X-Y
Story 1:X	test	Maximum	0.04	0.05	0.22	0.24
		time	14.9	57.1	98.6	137.4
	SAPWood	Maximum	0.03	0.04	0.20	0.26
		time	15.5	54.9	97.4	138.4
Story 1:Y	test	Maximum	0.12	0.12	0.79	1.03
		time	17.2	57.0	98.6	137.4
	SAPWood	Maximum	0.07	0.07	0.66	1.21
		time	17.1	57.0	97.4	137.4
Story 2:X	test	Maximum	0.06	0.09	0.33	0.33
		time	17.2	57.0	98.6	137.4
	SAPWood	Maximum	0.04	0.06	0.24	0.31
		time	15.0	54.9	98.5	138.4
Story 2:Y	test	Maximum	0.28	0.28	1.70	2.20
		time	17.2	57.0	98.9	137.4
	SAPWood	Maximum	0.10	0.10	0.78	1.32
		time	17.1	56.9	97.4	137.4

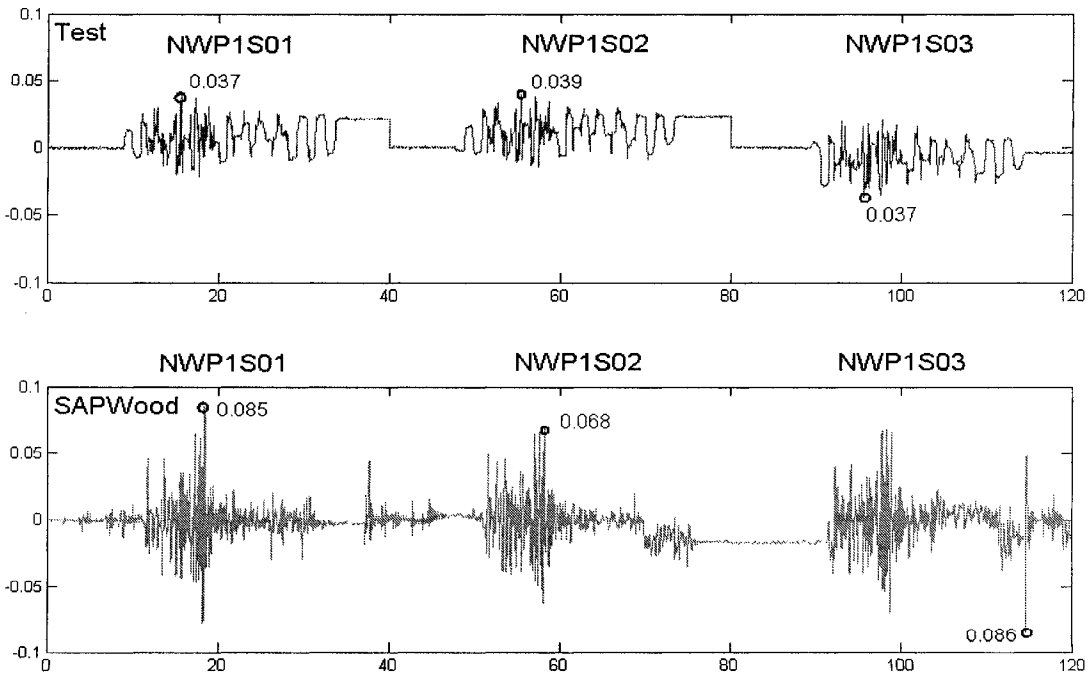

Figure 2-19: Drift comparison under low intensity earthquake (Phase 1)

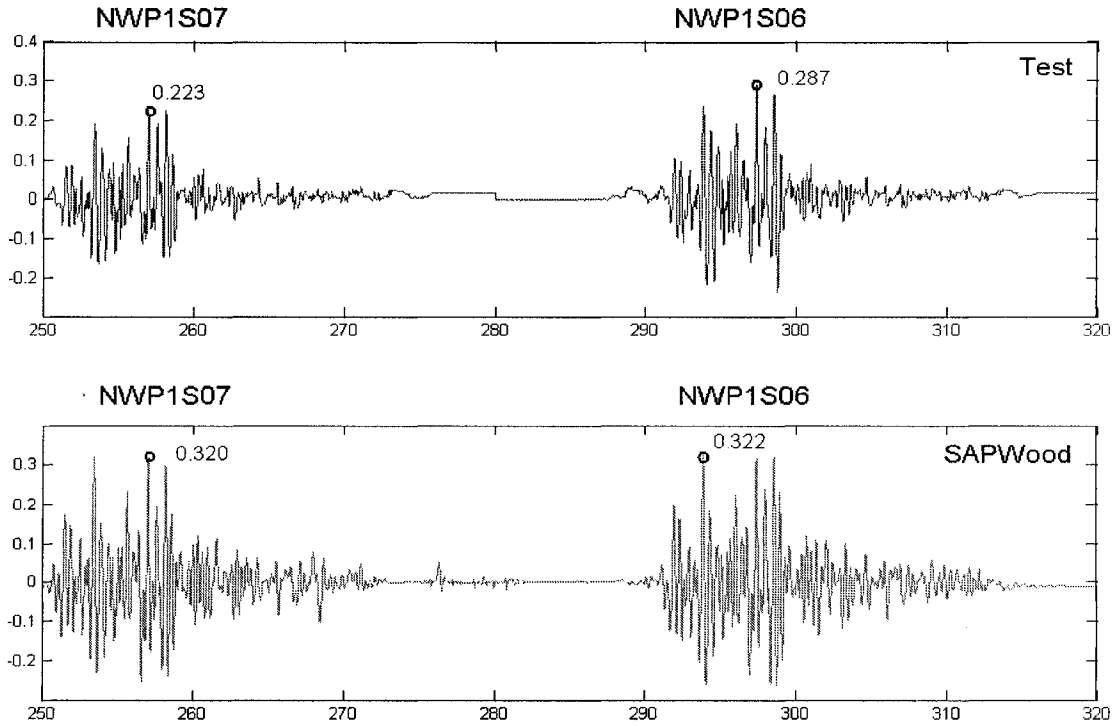

Figure 2-20: Drift comparison under moderate intensity earthquake (Phase 1 strong direction)

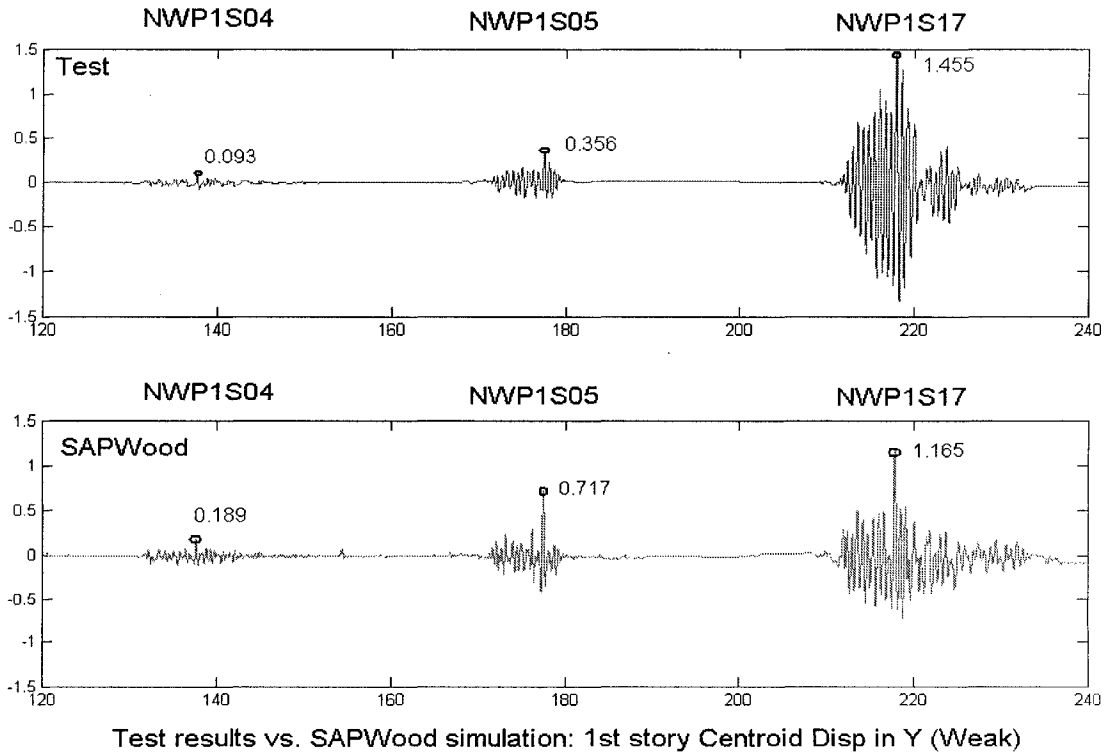

Figure 2-21: Drift comparison moderate intensity earthquake (Phase 1 weak direction)

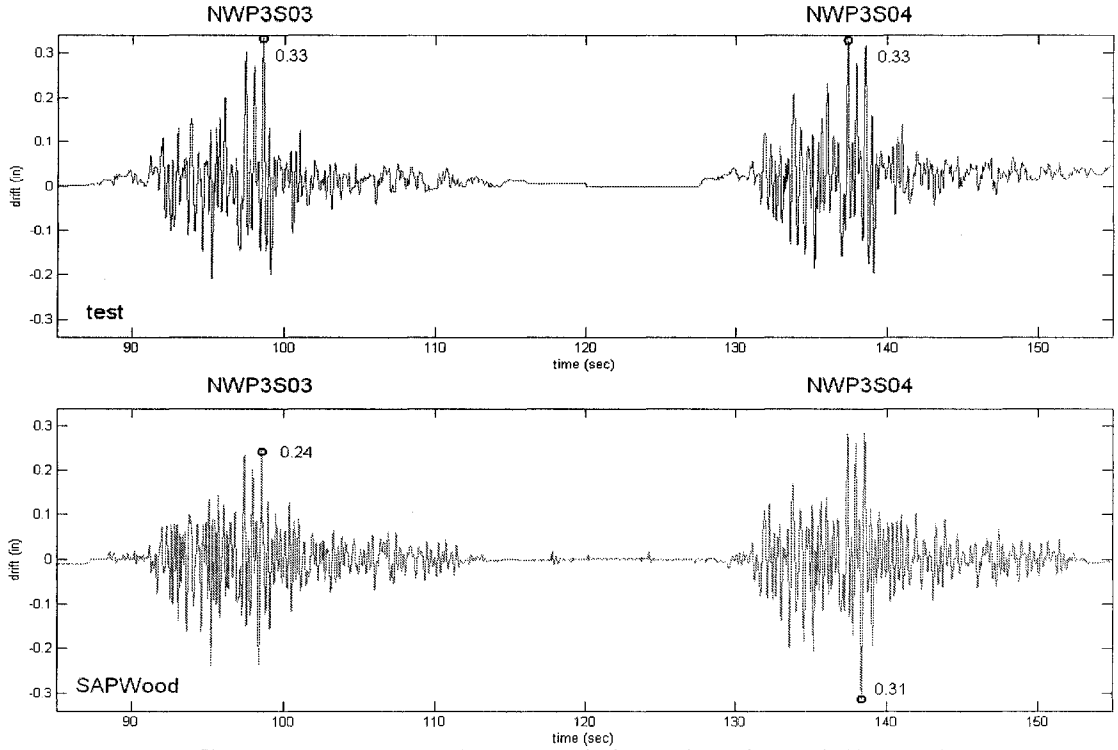

Test results vs. SAPWood simulation: 2nd story Centroid Disp in X (Strong)

Figure 2-22: Drift comparison moderate intensity earthquake (Phase 3 strong direction)

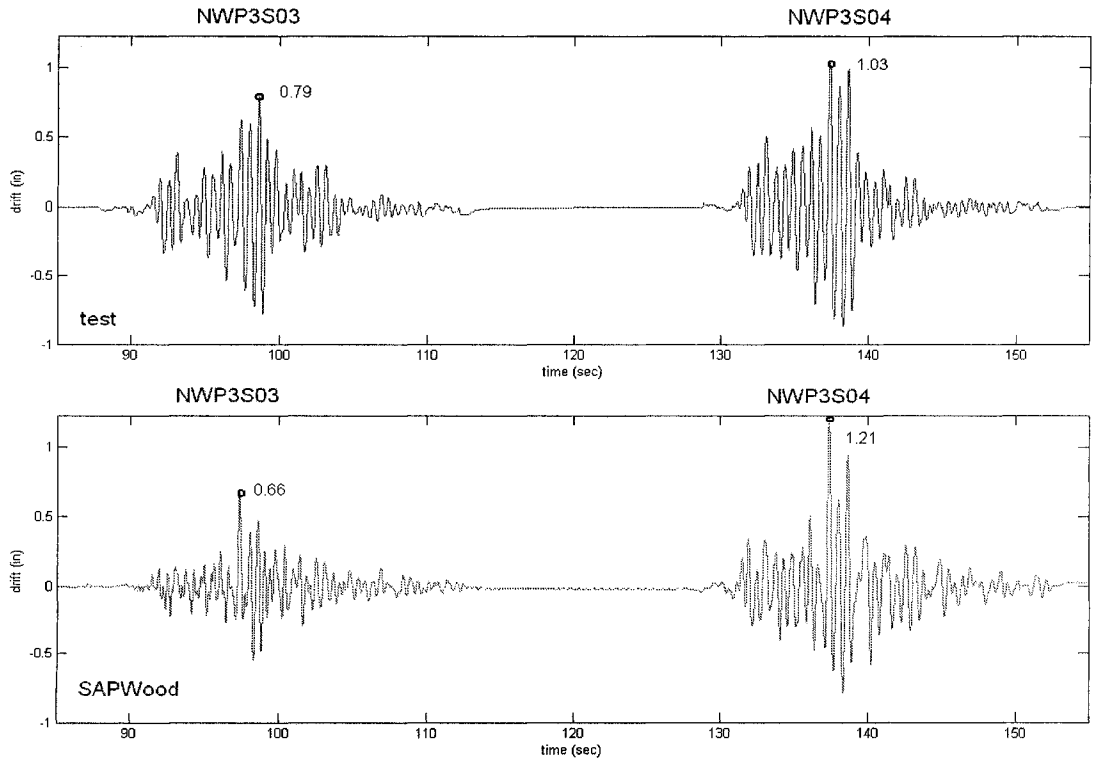

Test results vs. SAPWood simulation: 1st story Centroid Disp in Y (Weak)

Figure 2-23: Drift comparison moderate intensity earthquake (Phase 3 weak direction)

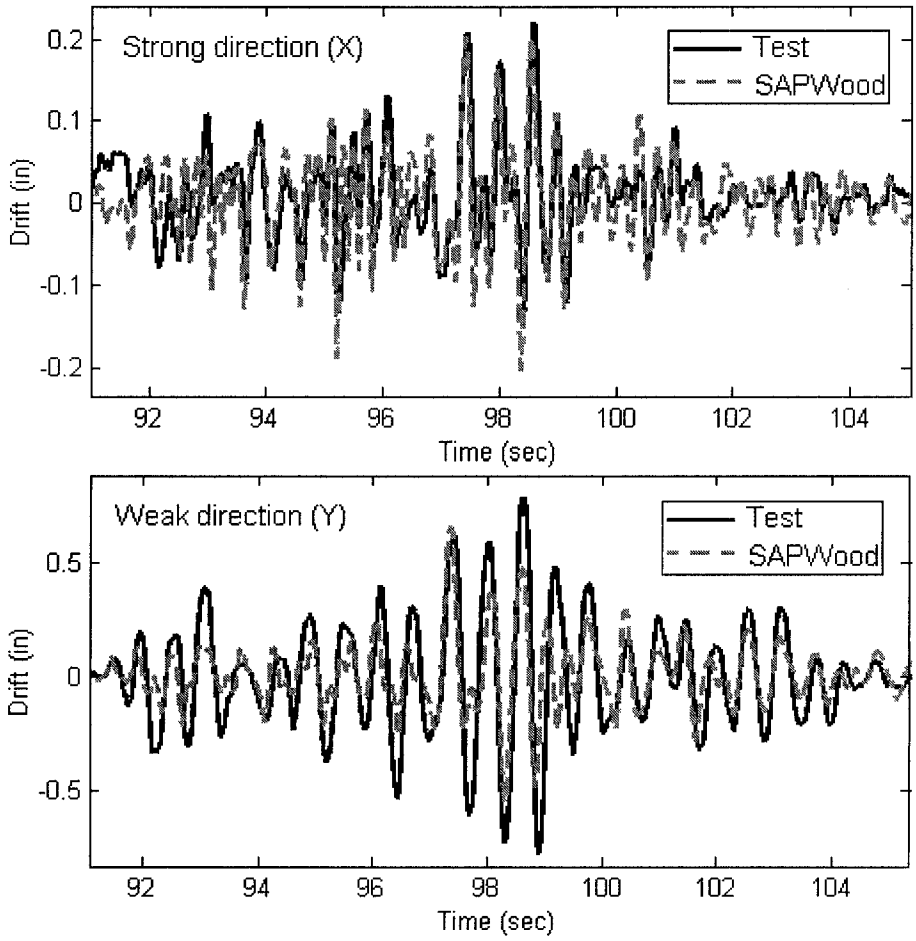

Figure 2-24: Similarity between responses from simulation and test (Phase 3, level 2 test)

Chapter Three

Long Term Loss Estimation Framework

3.1 Framework Elements and Assumptions

The long term loss estimation framework developed in this study is for a single structure at a given location. It is not a regional loss estimation model which accounts for spatial correlation and attenuation of the earthquake events. The main purpose of developing such a model is to provide viable and accurate loss estimation procedures for the development of PBSD. Generally speaking, earthquake-induced economic loss for woodframe structures is determined by the interaction between the structural and economical properties of building components and seismic events. As one considers the expected economic loss over some period of time in the future for a new/existing design, a significant amount of uncertainty is introduced into the assessment. These include, but are not limited to, the uncertainty in the construction, building materials, repair costs, future earthquake intensity, and the number of earthquake events in the estimation period. These elements need to be modeled separately according to their individual uncertainty characteristics and built into the estimation framework to reflect their contributions to the cumulative financial loss.

Given a time period beginning at the completion of a buildings construction, t, the earthquake induced ground motion event in this period can be assumed as a random event following a Poisson process. If the repair of the structure is assumed to be performed immediately following every earthquake, the total economic loss, $L(t)$, can be modeled as a random variable following the compound Poisson distribution, defined as follows,

$$L_c(t) = \sum_{i=1}^{N} C_s(i) \tag{3-1}$$

$$N \sim Poisson(\lambda t) \tag{3-2}$$

where $C_s(i)$ is a random variable representing the loss due to the i^{th} earthquake that happens in t, and these values for different earthquakes are assumed to be independent of one another; N is a random variable that follows the Poisson distribution, representing the total number of earthquakes in t; λ is the rate parameter of the Poisson distribution, which can be interpreted as the average number of earthquakes in a unit of time.

The rate parameter in equation 3-2 denotes the frequency of earthquake occurrence at the site/location of interest, which is available from past earthquake records in the region of interest. However, the modeling of $C_s(i)$ in equation 3-1, namely the loss from a single earthquake event, is more complicated due to the many sources of

uncertainty contributing to it variation. Firstly, the most important factor is the intensity of the earthquake, which is not predetermined but will definitely affect the damage and subsequent loss for a structure. Secondly, the ground motion specifics of the specific earthquake will vary significantly affect the response of the structure, even with a fixed intensity value. For example, two earthquakes having similar intensities but different response spectra can induce significantly different damage on the same structure depending on its natural period and other details. Furthermore, the structural uncertainty, such as construction quality, building materials, component and sub-assembly connections, etc., will affect the strength and stiffness of the structure and its seismic response, damage, losses, etc. Finally, the replace/repair process, i.e. the relationship between structural responses and repair cost, is non-deterministic in nature because even the same structural component with identical damage will have significant cost variation to repair/replace in different cases.

One viable way to implement this procedure is to separate the uncertainty in the calculation of $C_s(i)$ by first considering the cost of an earthquake with a fixed intensity on a pre-determined nominal structural design; and then combine this intensity based cost with the statistical models that characterize earthquake events in the duration of interest to calculate the long term loss. With numerical models of the structure established based on the nominal design, dynamic analysis can be performed to obtain the response of the structure (and subsequently the response of each component and sub-assembly in the structure) during any given earthquake. Monte-Carlo simulation can be used to incorporate structural uncertainty and ground motion

uncertainty (once their samples were generated from their models) into the structural response output. Then a response-cost relationship model for every component that might induce loss because of the excessive response will be applied to the response output and transforms it into a loss output. This procedure will be repeated for a group of earthquake intensity values. The model (termed *vulnerability model* which will be discussed in detail later) to construct single earthquake cost distribution given intensity can be established based on the simulation results.

Then, earthquakes as well as their intensities will be generated from their statistical models based on the time span, and for each of the earthquakes, a single earthquake fragility model will be applied to generate a loss value. Finally, these generated losses will be added together to obtain the long term loss of the design. This process is illustrated with the flowchart shown in Figure 3-1.

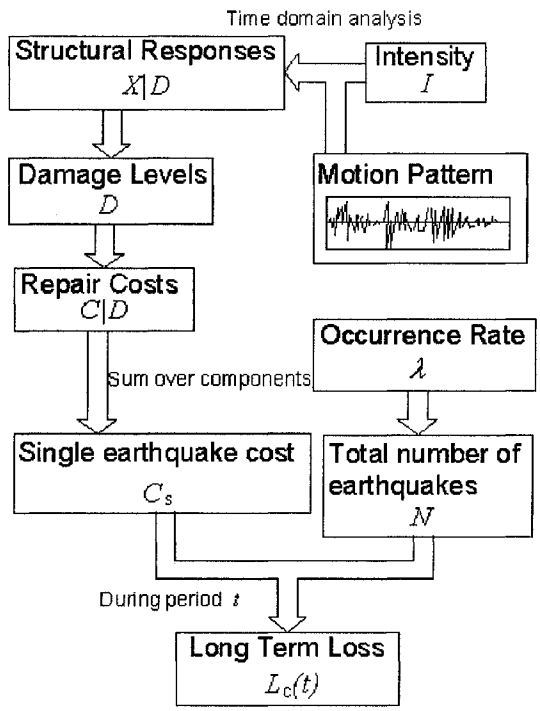

Figure 3-1 Uncertainty sources in the long-term loss estimation

Long term loss estimation can also be obtained analytically through numerical integration once the single earthquake loss vulnerability models are in place. But the only way to estimate vulnerability model is Monte-Carlo simulation, since the structural responses of wood frame structures are highly nonlinear and cannot be derived in closed form.

The following sections will address in detail the methods used in this study to model the framework elements mentioned above including structural uncertainty, seismic hazard, and damage-cost relationship.

3.2 Structural Uncertainties

Structural uncertainties exist mainly due to the variation in material properties and construction quality. In current construction practice, wood frame structures are typically constructed on site with standard pre-manufactured components (dimension lumbers, standard panels, nail, and floor joist systems). Although the nailing schedule was specified in the design, it might not be followed very strictly in practice. For example, the nails might miss the stud behind the panel; the hold down devices might not be properly installed; or the sill plate might have cracks at the anchor bolt location during the installation. This type of uncertainty will always exist but can be reduced by stricter on site quality control or providing pre-manufactured assembly components such as segments of shear wall.

Structural uncertainty will affect the loss estimation through its influence on the structural dynamic responses during earthquakes. Typically, a poorly constructed structure will have a lower ultimate strength and initial stiffness in its components, which will lead to larger displacements or even total collapse during moderate earthquakes. In this study, the quality of construction was modeled with a simplified random capacity reduction factor. Three categories, namely superior, average, and poor, were defined by applying different levels of reduction factor on the strength and stiffness parameters in the EPHM.

The most influential parameters in the EPHM to structural responses are the initial stiffness (K_0) and the ultimate strength parameter (F_0). These two parameters can be obtained (together with other parameters) from SAPWood NP analysis for any newly designed wall configurations, or from the results of a cyclic loading test, i.e. hysteresis fitting. The ideal results yielded from the analysis were used as the upper limit of the parameter value. The parameters used in the model are generated based on the following equation:

$$p = p_a - \varepsilon \tag{3-3}$$

Where p is the parameter (K_0 or F_0) used in the model; p_a is the ideal value or upper limit obtained from the NP model; and ε is a uniformly distributed random variable representing the reduction factor (non-negative) related to construction quality. A

uniform distribution was used in this study solely based on the subjective estimate of the author; it could be improved through a Bayesian updating process if appropriate data can be obtained testing. Such tests could be performed by testing the sample wall segments constructed by the contractors from a certain region of interest and compare the parameters from test results to the ideal analyzed values.

Since the higher construction quality normally results in higher stiffness and strength, the parameters used for superior construction quality model with a deduction term uniformly distributed between 0 to 5% of the ideal value. Average quality models will use a deduction value within 2 to 10% of the ideal value, while the parameters of poorly constructed model were deducted by 5 to 20%. It is worth pointing out that the quality categories used in this dissertation work were not required by the estimation framework but only designed to investigate the impact of construction quality on loss. However, they provided a ready-to-use evaluation system to categorize the building quality when more detailed construction information is not available. The impact of construction quality on the seismic induced loss will be further investigated with numerical examples using sensitivity analysis in later chapters.

3.3 Response-Loss Modeling (Damage Fragility)

The calculation of cost based on structural loading responses is a key step in any kind of structure loss estimation. This calculation, of course, requires a response-cost relationship for every component which in turn provides their damage or deformation.

This relationship is not deterministic because of the uncertainties involved, including but not limited to, the variability in the cost of repairing material, workmanship, repair method, and influence of repair to adjacent undamaged components, etc. A fragility-based categorization system termed *damage fragility* is proposed in this study to incorporate these uncertainties. The concept of this method is shown in Figure 3-2.

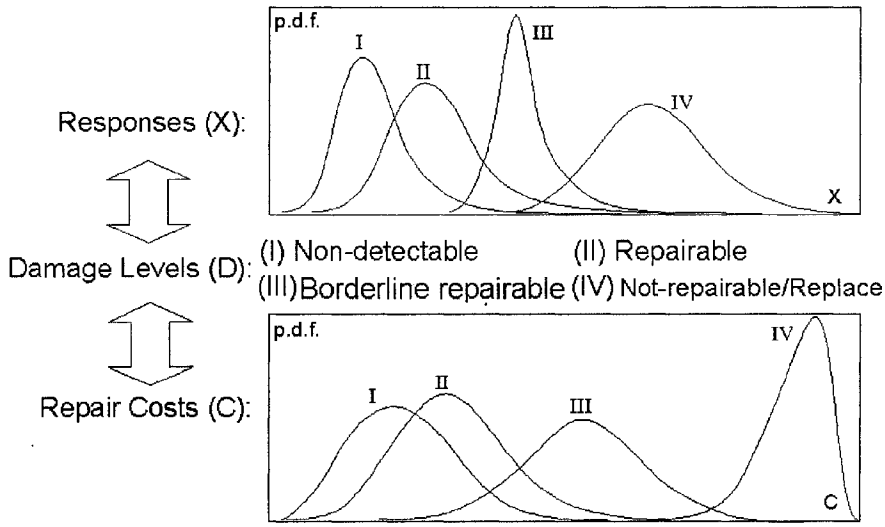

Figure 3-2: Damage fragility system

As shown in Figure 3-2, four damage categories/levels are defined as (I) non-detectable, (II) repairable, (III) borderline repairable, and (IV) not repairable-replace to capture the components' damage status. Note that it is not believed to be reasonable to assume a clear cut-off point between these categories since the judgment can be quite subjective. Damage fragilities (probability distributions conditional on the damage level) of the structural responses (inter-story drift in the case of wood shearwalls) and repair cost (economical loss) are then assigned for each damage category based on the available information. These fragilities characterize the amount

of damage sustained by components and the resulting financial implications. For example, given a level (I) damaged shearwall, whose damage is assumed to be directly related to drift, the drift of the wall might be a random variable with a mean value of 25 mm (1 inch) and a standard deviation (Std) of 12.5 mm (0.5 inch). The cost to repair a shearwall with level (I) damage might be uniformly distributed between $12 and $100. Later in the simulation framework, these distributions will be the basis to generate samples for repair cost given a fixed structural response from the numerical analysis. This step requires the information on the probability of a component belonging to each damage level given component response. Based on a known damage fragility (the conditional distribution of response given damage), this damage probability can be found as follows,

$$\Pr(D \mid X < x < X + \Delta X) = \frac{\frac{\Pr(X < x < X + \Delta X \mid D)}{\Delta X}\Pr(D)}{\sum \frac{\Pr(X < x < X + \Delta X \mid D)}{\Delta X}\Pr(D)} \tag{3-4}$$

where D denotes the damage level of the component; X is the response value; x is the given response from structural analysis; and ΔX is an increment of X. As ΔX approaches 0, equation 3-4 becomes

$$\Pr(D \mid x = X) = \frac{f(X \mid D)\Pr(D)}{\sum f(X \mid D)\Pr(D)} \tag{3-5}$$

where $f(X \mid D)$ is the probability density function (PDF) of response given damage level (assigned damage fragility). Without any other information, the probability of a component belonging to any one of the damage level can be assumed to be the same, so

$$\Pr(D) = \text{constant} \tag{3-6}$$

So finally,

$$\Pr(D \mid X) = \frac{f(X \mid D)}{\sum f(X \mid D)} \tag{3-7}$$

With the probability of each damage level known, damage level data can be generated based on response samples. Once the damage level of the component was determined, the loss caused by that component was generated from the loss distribution corresponding to that damage level. Although it seems to be easier to directly establish conditional loss distribution from response, the method of using damage level as an intermediate step makes it possible to treat uncertainty in damage estimation and repair cost separately. Another important reason for using this procedure is that the available data from a damage survey following a test are/were often grouped or organized into descriptive damage levels.

In addition to structural damage-induced cost, this fragility system could work for virtually any sub-assembly for which a reasonable relationship can be developed with various structural response quantities. For example, it might be important to include in the analysis the cost of finding a temporary residence (e.g. hotel) while the damaged

structure is being repaired following an earthquake. Determination of whether or not to include costs associated with displaced residents might be associated with residual inter-story drift or the percentage of heavily damaged components and subassemblies. One can then define the resulting damage level as (I) No evacuation; (II) Short term evacuation (several days); (III) long-term evacuation (couple of weeks) and establish corresponding conditional distributions (fragilities) for each. However, only repair/replacement related costs/fragilities are considered in this study, with displacement costs to be considered in a forthcoming effort.

The information to construct these fragilities can be obtained from damage-repair tests of the component of interest. For example, to construct the drift-driven damage fragility for a certain type of door assembly, samples of the door can be pushed at the top to achieve a certain damage level, say level (II) for example. Then the drift values of the samples as they reach level (II) damage can be recorded to find the drift distribution given damage level equal to II. Similarly, the damaged samples can be repaired and the repair costs can be recorded to yield cost distributions. For fragilities related to costs other than repair, past data from earthquake surveys can be used. For example, one can collect the residual inter-story drift data for all the short-term evacuated buildings after an earthquake and develop conditional drift distribution for evacuation level II; then the cost data of these evacuated activities could also be collected through a survey to yield a distribution of evacuation loss conditional on short term evacuation.

In the present study the effort did not include component fragility testing, thus damage fragilities for the numerical examples in Chapter 7 were constructed based on component test results from earlier research, rather than from the tests described above. A comprehensive summary of these results can be found in the report "improved loss estimation for wood frame structures" from CUREE Caltech woodframe research project (Porter et al., 2004), with the data included in the appendix. The damage-cost relationship of a number of commonly used structural and non-structural components for light frame construction was covered in this report, including OSB sheathing shearwalls, stucco, Gypsum wall board, door and window, and water heater etc. The damage descriptions (e.g. damage levels) for that project were not the same as they are in this study. Practical assumptions to incorporate these data into the damage level system used here will be discussed in Chapter 7. Costs to repair these components at different damage levels were also estimated in this report.

In summary, the damage fragility system is composed of three components. The first one is the damage categories defined by the user. The second part is the conditional response distribution for each damage category. The last one is the conditional cost distribution for each damage category. The purpose of developing such a system is to make it possible to reflect the uncertainty in the simulation process from structural responses to cost. The simulation of cost given response is quite straight forward based on this system. First the likelihood of each damage level could be obtained directly from the PDF values of conditional response distributions at the given response value. Then the relative likelihood of this response belonging to each damage

level can be used in combination of a random number generator to generate a damage level sample for the response value. Finally, the cost sample can be generated from the conditional distribution of cost once the damage level is known.

3.4 Seismic Uncertainties

Aside from the structural and damage-cost uncertainties, seismic uncertainty will inevitably affect the long term loss of the structure. Since the future earthquakes are still not predictable based on current technologies, some assumptions were used in this study to establish the models to characterize the uncertainties in earthquake events.

An earthquake can be characterized (described) in many ways depending on the user's interest. For loss estimation and structural engineering purposes, the most important concerns were: how often will the earthquake occur, what is its intensity and what will the ground motion look like. Based on these influential factors, the basic assumption of seismic uncertainty was made in this study that any earthquake event can be treated as the realization of three independent random events: the occurrence, intensity, and ground motion time history. By using this assumption, future earthquakes can be simulated using independent models for occurrence rate, intensity, and ground motion wave form. Another reason to adopt this simplification is the unknown correlation structure between these elements.

The occurrence of an earthquake, decoupled from the intensity or magnitude, deliberately means the occurrence of any ground motion occurrence. It can be modeled as a random arrival event with an annual occurrence rate λ. This annual rate parameter denotes the average number of earthquakes (no matter how large or how small they were) that occurred in one year and can change among different regions. For example, the annual rate in many California areas will be much higher than the rate in Texas, which is essentially zero. This concept is slightly different from current design practices where the focus is on one (or several) particular events having certain intensities corresponding to a particular return period. However, the approach herein provides a way to model a continuous spectrum of possible earthquake events rather than only the worst case scenario. By using this occurrence model together with the intensity model (which will be discussed next), probability information for any intensity levels for any return period can be derived through standard statistical computation. The information on the earthquake occurrence rate, λ, can also be estimated from the recorded earthquakes in the past or are available through entities such as the United States Geological Survey (USGS).

Seismic intensity is often quantified in different ways in different disciplines. For structural engineering purposes, the most commonly used indicators include response spectrum (S_a) and peak ground acceleration (PGA). The choice on the intensity indicator will not influence the implementation of the loss estimation framework. The results from different choice should remain certain level of consistency. In order to ease the effort of earthquake scaling in numerical simulation, spectral acceleration (S_a)

at 0.2 seconds and 5% damping is used in this study as the intensity indicator. The uncertainty in the seismic intensity (denoted here as I) is considered by modeling the S_a of an earthquake as a random variable based on available information. An estimation of the earthquake intensity distribution was obtained from the earthquake hazard curves published by USGS, which indicates the value of S_a for a given location in the United States with the corresponding annual probability of exceedance (PE). Specifically, this hazard curve represents the distribution of the annual maximum intensity. The intensity distribution must be derived from the annual exceedance probability data in order to generate intensity samples during the simulation. Given the hazard curve, the probability of exceedance corresponding to a certain spectra acceleration value $S_a = x$ is known to be $PE(x)$. Firstly one can assume the cumulative density function (CDF) value corresponding to x equals to $F_I(x)$; if the rate of earthquake occurrence per-year is equal to λ, the annual probability of exceedance for x can be calculated as

$$PE(x) = 1 - \sum_{i=0}^{\infty} \Pr(N = i) \cdot F_I(x)^i \tag{3-8}$$

$$\Pr(N = i) = Poisson(i \mid \lambda) = \frac{e^{-\lambda}(\lambda)^i}{i!} \tag{3-9}$$

The $PE(x)$ is known from the hazard curve, and $F_I(x)$ can be calculated from equation 3-8. In the numerical examples, the value of λ in equation 3-9 is taken as the sample generated from the occurrence rate probability density function. Thus the intensity distribution was calculated for every simulation. Similarly one can obtain

CDF values for any other S_a values along the curve. Then data points on the hazard curve can be transferred into the data points on the CDF curve of the intensity distribution. With the CDF curve known numerically, samples for the ground motion intensity can be generated. Notice that the distribution obtained based on USGS hazard map can be used as a prior in a Bayesian updating process (which will be discussed later) if localized intensity data (S_a in this case) is available.

The ground motion time series characterizes the "pattern" of the earthquake excitation. It is directly related to many important characteristics of earthquakes such as the shape of the response spectra and the power spectral density. The structural responses to earthquakes with the same intensity with different ground motion time series are usually not the same except for some special cases (linear SDOF system under same S_a intensity). Since realizations of ground motion time histories will be needed for the simulation procedure, it would be necessary to develop a method to generate ground motion time series based on the seismologic characteristics of the building site. This task is extremely difficult for several reasons. Firstly, the non-stationary property of earthquakes makes it hard to represent or model them with a random process model. Secondly, too many uncertain factors such as fault type, distance, fault mechanism, and soil type contribute to the ground motion series and cannot easily be quantified into a model. This problem was addressed in this study with an empirical approach. The uncertainty of the ground motion itself can be built into the simulation by repeating the simulation with a suite of earthquake records. These records are selected (possibly from the historical monitored database of nearby areas) and scaled to the

appropriate hazard level. Based on this assumption, rather than finding a theoretical model for ground motion series, a data base of regional earthquake ground motion can be established based on historical earthquake records. As the size of this data base grows larger, the simulation can be performed using the ground motions randomly drawn from it. The historical ground motion data is relatively easy to obtain through research and monitoring programs throughout the U.S.

It should be emphasized that the fundamental assumption used in the simulation procedure is the independence of earthquake occurrence, intensity, and ground motion. On the other hand, the actual models used to represent these independent events are not intrinsically related to the loss estimation framework. So these models can be improved or replaced by more accurate models when needed. For example, the earthquake data base discussed above could be replaced by a random field model which is capable of generating ground motion time series.

3.5 Bayesian Model for Uncertainty Elements

As discussed in previous sections, there are a number of sources of uncertainty that control the distribution of long term loss. In this study, these sources of uncertainty were considered as elements of the loss estimation framework. Bayesian statistical models were used to represent these elements mainly for two reasons. The first is the flexibility in incorporating subjective information, objective test data, and historical information into the model. The second reason is the form of presentation, where the

abstract statistical model can be represented in a way that can be understood and constructed (via the help of the software) by a person without a strong statistics background.

Bayesian models have been adopted in many engineering applications due to their ability to incorporate subjective knowledge/experience and the ability to update the model with additional data. Information of the basic techniques and methods used in Bayesian statistics can be found in classical textbooks (Gelman et.al. 2004). In this study, uncertainty elements that can be updated directly with data, such as earthquake intensity, structural uncertainty, and damage fragilities, etc., are modeled with Bayesian predictive distributions, whose parameters follow the posterior distribution constructed based on data and priors. The structure of a Bayesian predictive function is illustrated in Figure 3-3. One can see the improvement of the PDF of predictive distribution in the lower right corner (from the dashed line to the solid line) with the application of Bayesian updating. Since most of the variables can only take positive values, a lognormal likelihood function is very useful in deriving the posterior, which is the joint distribution of mean and standard deviation of the random variable. The rate parameter for earthquake occurrence is modeled slightly differently using an exponential likelihood function, due to the assumption that the earthquake occurrence follows a Poisson distribution. Priors in this study are set to be uniform over certain ranges. The reason for using this prior type is that subjective experience can be easily implemented, even by someone without formal statistics training. An alternative method to incorporate a more complicated prior distribution will be discussed later.

Development of the Bayesian predictive model for lognormal likelihood variables is explained in detail as follows. This calculation was implemented numerically (in the software package) since closed-form results are hard to obtain.

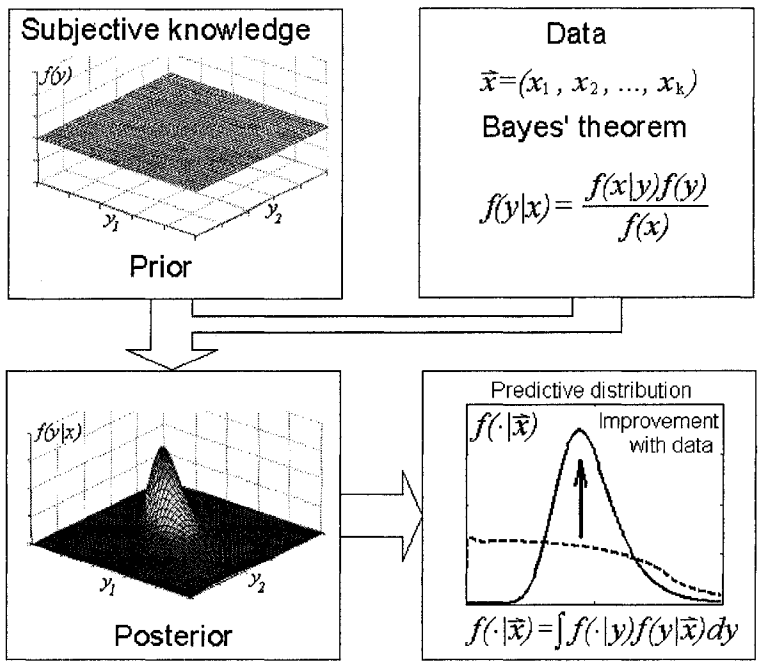

Figure 3-3: Bayesian model for frame work components

As discussed earlier, the subjective initial knowledge/belief for the random variable can be constructed in the uniform priors as,

$$f(\mu)=\frac{1}{\mu 2-\mu 1} \quad \mu 1<\mu<\mu 2 \text{ and } f(\sigma)=\frac{1}{\sigma 2-\sigma 1} \quad \sigma 1<\sigma<\sigma 2 \qquad (3\text{-}10)$$

where $\mu 1, \mu 2, \sigma 1$, and $\sigma 2$ are the boundaries for the random variable mean and standard deviation selected subjectively. For example, it would be reasonable to say

that for damage level (I), the inter story drift for a wood shearwall should have a mean value lying within [0% 2%] inter-story drift. Further, for example, for earthquake intensity, it is with almost near certainty that one can state that the mean value of S_a for future earthquakes will lie between 0.01 and 5 times gravity (g). Note that by assuming μ and σ to be independent, the probability density function (PDF) of their joint distribution is simply the product of the individual PDF's, and is also uniformly distributed over the predefined region.

For the lognormal distribution, the likelihood function given data $\bar{x}$ as a $1\times k$ vector can be calculated as

$$L(\bar{x}) = \prod_{i=1}^{k} \frac{1}{\sqrt{2\pi} x_i \sigma_{\ln}} \exp\left(-\frac{(\ln x_i - \mu_{\ln})^2}{2\sigma_{\ln}^2} \right) \tag{3-11}$$

where

$$\sigma_{\ln} = \sqrt{\ln\left(1 + \left(\frac{\sigma}{\mu} \right)^2 \right)} \tag{3-12}$$

$$\mu_{\ln} = \ln \mu - \frac{\sigma_{\ln}^2}{2} \tag{3-13}$$

Then the posterior will be

$$f(\mu, \sigma \mid \bar{x}) \propto L(\bar{x}) f(\mu) f(\sigma) \tag{3-14}$$

The predictive distribution will be

$$f(\cdot \mid \bar{x}) = \int_{\mu 1}^{\mu 2} \int_{\sigma 1}^{\sigma 2} f(\cdot \mid \mu, \sigma) f(\mu, \sigma \mid \bar{x}) d\sigma \, d\mu \tag{3-15}$$

If there is no data available at the time of estimation, the estimation of the predicative distribution can still be made with only the prior, which is constructed based on initial belief/experience as

$$f(\cdot \mid \bar{x}) = \int_{\mu 1}^{\mu 2} \int_{\sigma 1}^{\sigma 2} f(\cdot \mid \mu, \sigma) f(\mu) f(\sigma) d\sigma \, d\mu \tag{3-16}$$

The resulting distribution without data would have a larger dispersion and probably some level of shift in the mean value. The integration might not be easy to evaluate in closed form but can be evaluated numerically. Once the PDF for the predictive distribution is obtained, it can be used to generate element samples in the simulation.

Priors and updating process

Almost all decision making processes in practical civil engineering involve a certain level of subjectivity. Although the physical system will behave regardless of people's opinion, useful information from past experiences and expertise can still help increase the accuracy of predictive models for the system behavior. The loss estimation framework, which is designed to find a predictive model for the seismically-induced loss, could also benefit from justifiable opinions and experience. The key to incorporate this type of information is the priors in Bayesian statistical models. Uniform priors are used as the default prior type for most of the elements in this framework for two reasons. Firstly, it is possible to express subjective opinion related to damage, cost, or earthquake intensity with upper and lower bounds. The detailed

distribution information inside those bounds is typically unknown or unjustifiable. Secondly, the uniform distribution could serve as either an informative or non-informative prior depending on the situation. Consider earthquake intensity as an example, a uniform prior within 0 g to 10 g for the mean of peak ground acceleration practically provides no subjective information to the analysis, since the PGA could never exceed 10 g for real earthquakes. But a uniform prior between 0.5 g to 2 g will definitely be considered as an informative prior in this case.

There are occasions where the subjective belief or experiences from the past contains details that could not be represented fully with just two boundaries and a uniform distribution. For example, based on past earthquake records, it is strongly suggested that the intensity of the earthquake follows a distribution characterized by an empirical frequency curve. Detailed subjective belief such as this could be built into the Bayesian model by "pre-updating" a non-informative prior using artificial data points. Different from the actual test or field survey data, artificial data points are samples generated from the distribution which represent the experience or belief. With enough artificial samples, the non-informative prior could be updated to match the desired distribution closely.

If the model for earthquake uncertainties (rate of occurrence, intensity, and ground motion) was pre-updated based on available seismological research results (e.g. USGS seismic intensity maps), it might be an option to apply additional earthquake activity data to increase the accuracy of the model since these readily available references are

supposed to provide a readily objective representative for earthquake uncertainties. However, the Bayesian model still provides the opportunity to use local seismic data from earthquake monitoring stations near the building site of interest. The intensity data can be used directly in the Bayesian model of the intensity; the rate parameter for the earthquake occurrence can be estimated through the interval of the data; and the ground motion records themselves can be used to construct the localized earthquake suite for the building site area.

For structural resistance uncertainties, the data should come from comprehensive structural component tests and/or existing statistics for certain components and sub-assemblies. However, consideration of structural uncertainty will not change the concept of the simulation procedure but only add computational expense (simulation must be performed for multiple cases), thus only very limited structural samples were included in the numerical examples later. Similarly, in order to obtain reliable data to evaluate the loss for the structure, all components that result in losses induced by an earthquake, including the non-structural losses such as the water heater, plumbing, and personal contents, should be analyzed individually to obtain damage fragilities. Some of the components are displacement-sensitive, such as shearwalls, drywall panels, tiles for the bathroom, plumbing, etc. Others might be acceleration sensitive, such as the water heater, furniture, computers, televisions, etc.

This framework is proposed so that uncertainties in the long term loss are categorized and can be updated individually if there is historical or test data. For the uncertainty

source whose data is not available, the ability to represent the subjective experiences in priors still makes it possible to systematically estimate the loss, albeit with some subjectivity. In the extreme condition where there is no data at all, the estimation reduces to a systematic guess which is completely subjective. Each data point (seismic or structural) will help to reduce the subjectivity of the estimation and, hopefully, the uncertainty/variance in the final result.

3.6 Vulnerability Based Loss Estimation

The loss estimation framework discussed here was based on single earthquake cost, which was assumed to follow independent single earthquake loss distributions conditional on seismic intensity. This is a direct result of the adoption of the assumption that the structure is always "new" (newly constructed with no damage accumulation) prior to the occurrence of each earthquake. Although not very realistic, this assumption is widely used in existing loss estimation procedures. Thus the method developed in this chapter could also be viewed as a traditional loss estimation method. An alternative procedure which considers more realistic situations will be discussed in Chapter 4.

Vulnerability model is defined as the model which relates (functionally or empirically) the parameters that characterize the single earthquake loss distribution and earthquake intensity. The purpose of developing such a model is to obtain single earthquake loss based on any given intensity value. Then Monte-Carlo simulation could be used to

generate loss samples from the resulting single earthquake cost distribution. Vulnerability model is an overall representation of the loss behavior of the structure against a single earthquake. It serves as the connection between seismic intensity and loss, representing all the uncertainties from vulnerability analysis including the uncertainty associated with the structure, ground motion pattern, and component cost-response relationship. This vulnerability model made it possible to treat the uncertainty in structural response/cost and earthquake intensity separately.

In order to obtain single earthquake data to construct vulnerability model, the structural model samples were generated based on the nominal design and construction quality first, with components parameters being randomly generated (as was discussed earlier). Then earthquake ground motion records will be selected from the ground motion data base. These earthquakes will be scaled to a particular intensity level and applied to the structural model. After dynamic analysis, the response of all damageable components will be obtained and the cost determined from these responses using the damage fragility system. Finally these costs will be summed together to obtain one sample of single earthquake cost. Keeping the intensity unchanged and repeating these steps multiple times (with different earthquake records and structural model samples) will yield a pool of single earthquake cost samples at this intensity level. Then the vulnerability model can be established by representing the simulated sample with distributions controlled by parameters depending on intensity. However, the characteristics of the simulated loss data differ from most commonly used distribution types in the way that it is truncated on both ends. When

the intensity is relatively low, a big portion of simulations will result in zero loss samples. On the other hand, the single earthquake loss has an upper boundary termed here in as collapse loss, which is the sum of all the cost of the damageable components in the structure. Majority of the samples will be in a very close vicinity of the collapse loss when the intensity is high or equal to 0 when the intensity is low. So it will be inadequate to simply represent single loss samples with traditional continuous distributions. In this study, the distribution model for single earthquake loss was consisted of three parts: the first one is zero loss probability, indicating the probability of the zero loss result given an intensity; the second one is collapse probability, indicating the probability of total collapse given intensity level; the third part is a lognormal distribution model fitted using the simulated data points exclude the ones corresponding to zero loss and collapse loss. Lognormal distribution was used because the loss can only be positive. Thus the vulnerability model is the relationship between 4 parameters: zero loss probability ($\Pr_0$), collapse probability ($\Pr_c$), and two parameters for the lognormal distribution ($\mu_{\ln}$ and $\sigma_{\ln}$), and seismic intensity. All of these parameters could be easily found with the simulated sample pool. Figure 3-4 illustrated the concept of single earthquake loss model and vulnerability model discussed above. The plot on the bottom is the CDF curve for the single earthquake loss with four controlling parameters illustrated. The two plots on the top are the curves of these parameters against earthquake intensity. In the examples in Chapter 7 and 8, an empirical linear interpolation between the intensity values included in the simulation was used somewhat arbitrarily to avoid the need to justify a regression model.

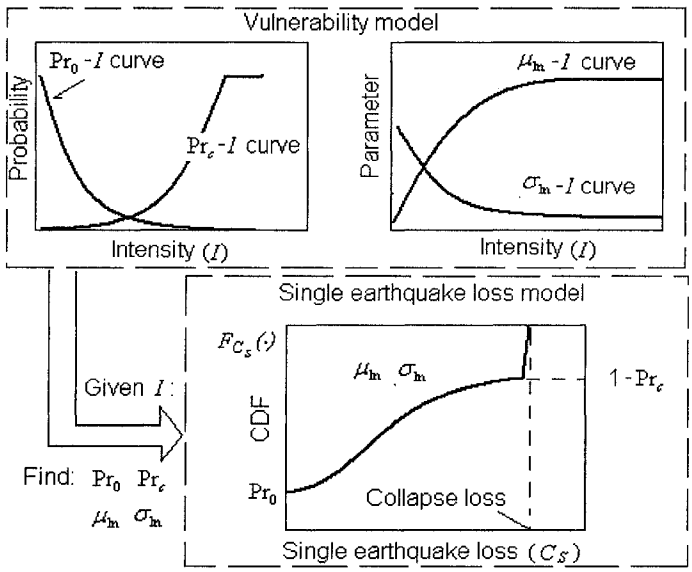

Figure 3-4: Vulnerability model and single earthquake loss model concept

There are two ways to obtain the distribution for long term loss once the vulnerability model is in place: numerical integration and simulation. The numerical integration approach follows the steps in the analytical derivation for a compound Poisson distribution, integrating the probability density functions numerically since the closed form solution is hard or not possible to obtain. The simulation approach simply generates samples for each element in the framework and determines the resulting long term loss. The ultimate goals of both approaches are identical, that is to obtain accurate estimation of the long term loss distribution conditional on time. In order to make the notation in the following derivation clear, a list of random variables and their corresponding notation for PDF are listed in Table 3-1.

Table 3-1 Components of the loss estimation framework

Element	Corresponding Statistical Model	Description
Earthquake counts (N)	Poisson model: $f(N \mid \lambda t) = \frac{e^{-\lambda t}(\lambda t)^N}{N!}$	Number of earthquakes occur in time period t.
Average occurrence rate (λ)	Bayesian posterior model $f_\lambda(\cdot)$	Rate parameter for earthquake occurrence as a Poisson process
Earthquake intensity (I)	Bayesian predictive model $f_I(\cdot)$	Intensity of an earthquake modeled based on historical data.
Single earthquake loss given intensity (Cs|I)	Distribution of single earthquake loss conditional on intensity: $f_c(\cdot \mid I)$	This distribution can be obtained for any intensity value after the vulnerability model is in place.
Component response given damage (X|D)	Bayesian predictive model $f_{x\|D}(\cdot)$	The distribution of structural response (inter-story drift) given damage level. Part of component damage fragility.
Repair cost given damage (C|D)	Bayesian predictive model $f_{c\|D}(\cdot)$	The distribution of repair cost given damage level. Part of component damage fragility.
Ground motion	Realization of random process that represents the earthquake ground motions at the site of interest.	A suite of recorded ground motions will be used.

As the first step in the numerical integration, the distribution of the ground motion intensity (obtained from USGS maps and/or historical data, please see earlier discussion) is combined with the single earthquake loss model to calculate the marginal distribution (in terms of the PDF) for the loss as the result of a single earthquake as shown in equation 3-17. This step might need to be performed numerically since the vulnerability model might not be available in functional form.

$$f_{cm}(x) = \int_0^\infty f_I(t) f_c(x \mid t) dt \tag{3-17}$$

Then from the marginal distribution of loss due to a single earthquake one can derive the cumulative distribution function loss from multiple earthquakes using a convolution integration scheme. Let $F_{Li}(\cdot)$ be the CDF for the summation of loss in i earthquakes.

$$F_{L1}(x) = \int_0^x f_{cm}(t)dt \tag{3-18}$$

$$F_{L2}(x) = \int_0^x F_{L1}(t) f_{cm}(x-t)dt \tag{3-19}$$

...

$$F_{Li}(x) = \int_0^x F_{L(i-1)}(t) f_{cm}(x-t)dt \tag{3-20}$$

Finally, the CDF for the long term loss can be calculated as

$$F_{Lt}(x) = \sum_{i=1}^{\infty} \Pr(N=i) F_{Li}(x) \qquad \text{for} \quad L(t) \neq 0 \tag{3-21}$$

$$\Pr(L=0) = \Pr(N=0) \qquad \text{for} \quad L(t) = 0 \tag{3-22}$$

where

$$\Pr(N=i) = \int_0^{\infty} \frac{e^{-\lambda t}(\lambda t)^i}{i!} f_{\lambda}(\lambda)d\lambda \tag{3-23}$$

if the posterior distribution of earthquake occurrence rate is to be used.

Another way to obtain estimation for the long term loss is simulation. Once the statistical distribution of each element within the framework is obtained, samples from each of these, e.g. earthquake intensity, single earthquake loss, number of earthquake events in time t, etc., can be easily generated via Monte Carlo simulation and the long term loss can be calculated following the framework structure. Firstly the user will provide a time period t. Then the earthquake occurrence rate will be generated from rate distribution and the total number of earthquakes in this period will be generated from a Poisson distribution. For every earthquake, an intensity value will be generated and used to obtain a single earthquake loss sample from the vulnerability model. Finally all the single earthquake loss samples will be added together to yield a long term loss sample. Then this process can be repeated for desired amount of samples needed, as it is summarized in Figure 3-5.

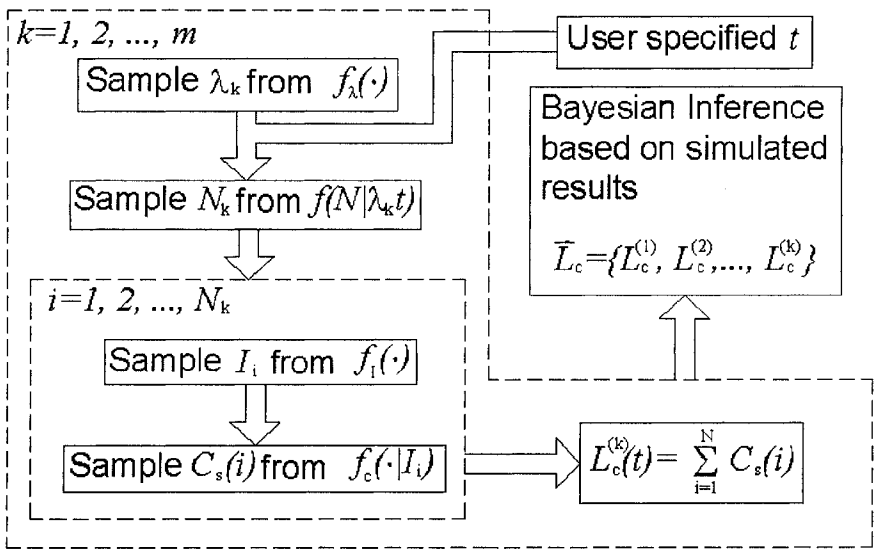

Figure 3-5: Simulation scheme for long-term seismic loss evaluation

In order to obtain multiple samples for the evaluation of long term loss, the simulation over the time period of interest, i.e. design life of the building, must be performed numerous times. In reality, the future period of interest will never repeat. So the simulated data can only be treated as theoretical trials that provide information on the final loss distribution. Thus it is recommended that a Bayesian model based on the simulation data (rather than commonly used parametric models such as lognormal or normal model) be constructed as the final output result of the framework if such a model is needed.

Chapter Four

Alternative Loss Estimation

4.1 Improved Assumption

The long term loss model discussed in Chapter 3 was based on the assumption that the structure will behave as a newly constructed structure upon the occurrence of each earthquake during the simulated period. This assumption has been used in the vast majority of simulation-based loss estimation studies related to wood frame and other type structures. It requires detection of all the damaged components after each earthquake and immediate restoration of these damaged components before the next earthquake occurs. This may be difficult to achieve, especially for wood frame structures, due to following reasons. Firstly, the structural damage to wood frame structures is hard to detect until certain damage level is reached. The loosening of sheathing nails will occur even under minor earthquakes and often remain un-detected and un-repaired with repairs only made to the drywall surface cracking. Degradation of stiffness will accumulate after a series of small earthquakes and change the natural period of the structure. For residential structures in seismically active regions, this damage accumulation process is always under progress beginning with construction.

Secondly, even in the cases where damage can be detected right after an earthquake, it is not possible to have them fixed before the next ground motion excitation. Since most major earthquakes will be followed very closely (from several minutes to days or weeks) by after-shocks, the repair of the damage in the first earthquake in such a limited time may be practically impossible. Actually, some post earthquake surveys indicated that some of structural collapse happens during the after-shocks rather than the major ground motion. This important characteristic of earthquake events cannot be reflected in the simulation procedure proposed in Chapter 3. Although the procedure does provided the user with a relative measure of the loss potential for the structure against earthquakes, a more accurate set of assumptions should be developed if more realistic loss estimation is to be obtained.

An alternative simulation procedure was developed in this study to reflect the earthquake induced loss more realistically. Firstly, the structural model was altered so that it became a repairable damage-accumulation model. Since each element in the system model was represented through EPHM, they could have the option to be fully restored (repaired) or left un-repaired after each earthquake by assigning the damage tracking index to initial values or keep it at the damaged stage after the earthquake, respectively. In the new simulation procedure, only the components whose damage is beyond a certain level (the non-detectable level was used in the numerical examples in this study) will be repaired after the earthquake. Even the repair strategy could be incorporated into the simulation. For example, one could assume that as the damage level becomes higher, the probability of it getting repaired will be higher. The

simulation could be configured so that damage level I component will not be repaired and damage level IV component will always get repaired; 75% of the components with damage level II and 95% of the level III components will be repaired. However, these detailed simulation configurations will not change the concept and procedure of the simulation (but will affect the results).

With this repairable model in place, the impact of unseen damage accumulation could be transferred between earthquakes. The repair action is implemented in the simulation by assigning a new set of EPHM parameters to the repaired components depending on the quality of repair. This repairable damage-accumulation model was programmed within the program SAPWood and could be found within the module SAPWood-Loss Analysis.

For the earthquake hazard, it is assumed that each strong earthquake (upon a magnitude threshold) will possibly have after-shocks following it. The number and the intensity of after-shocks should be related to the major earthquake intensity. The ground motion of the after-shock is independent of the major earthquake. And there will not be enough time to conduct any repair on the structure before all the after-shocks occur. This situation can be easily simulated using the same earthquake model discussed in Chapter 3 combined with an independent after-shock generator based on above assumptions.

Notice that although the assumptions discussed above have been improved from the vulnerability based loss estimation assumption, there are still space for improvement as the user discovers more crucial details that will affect the loss estimation. Clearly there is a great amount of subjectivity in the assumptions set forward. However, the purpose of this study is to propose this new simulation scheme rather than putting out a standard for earthquake hazard simulation.

4.2 Virtual Hazard Simulation

Based on the assumption discussed above, the concept of Virtual hazard simulation was developed. The key to this simulation process is the repairable damage-accumulation model. Since the difference between this method and the standard method is that the influence of previous earthquakes on the outcome of the future earthquake can be simulated. Through this coupling of the earthquake hazard simulation and structural loss simulation in the given period, the actual hazard-response-loss interaction was able to be investigated more thoroughly. In addition, this procedure allows a better representation of the earthquake hazard characteristics, such as the after-shock characteristics. Rather than give a conceptual estimation on the possible loss that might occur in the future through simplified (decoupled) statistical models, this method can virtually "act out" the time period of interest and the loading-structure interaction thus yielding more realistic estimation of loss related events. Whereas one simulation represents one possible time history outcome for the future, a large number of such simulations can reveal the statistical characteristics of any

hazard related values, especially when the simulated data was integrated into a Bayesian model with the historical data available.

Extended a little further, this virtual hazard simulation could be easily applied to multiple hazards situation. Different kinds of hazard loadings, e.g. earthquakes, hurricanes, heavy snow storm, might be uncoupled in nature but represent a phenomenon in structural reliability known as competing hazards. The probability of two types of disastrous loading event happening at the same time will be practically negligible, but their effects on a structure will definitely interact due to damage accumulation in the structure. For example, the damage of the same earthquake upon a new building and a building that has survived 20 years of hazard loading history will be different. Although taking into account an average degradation rate (strength and stiffness) might be a viable way to consider the impact of loading history, virtual hazard simulation with a repairable damage accumulation model is believed to be more accurate for this purpose. The concept of virtual hazard simulation can be illustrated in Figure 4-1.

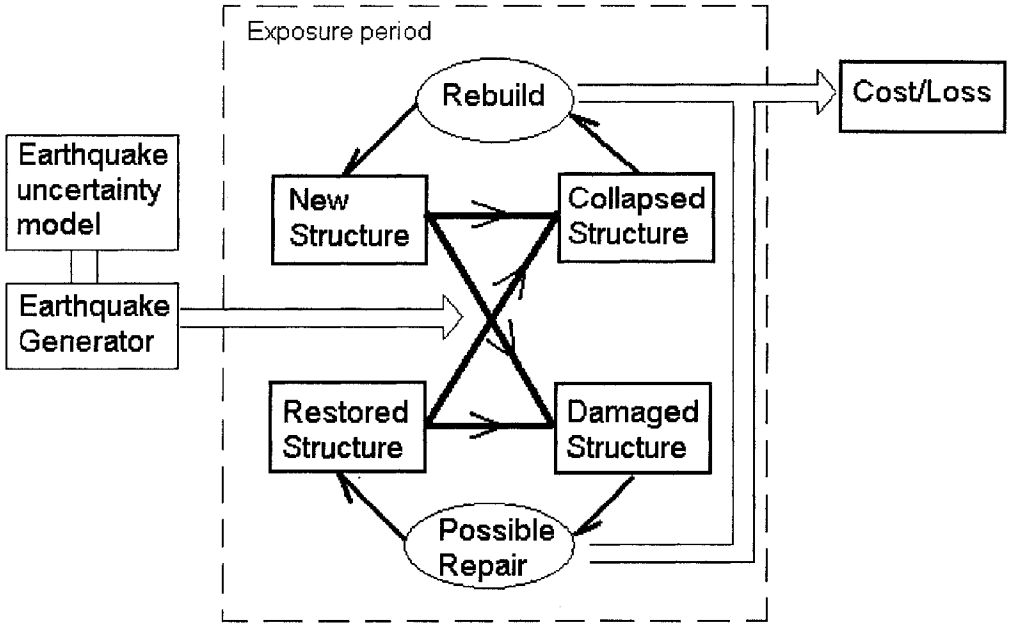

Figure 4-1: Concept of Virtual Hazard simulation

The procedure to perform virtual hazard simulation in this study is as follows:

Step 1: A structural model will be generated based on initial construction quality as the new structure.

Step 2: The time interval of the earthquake will be generated from an exponential distribution whose rate parameter is the average rate of earthquake occurrence. Upon the end of each time interval, an earthquake ground motion will be randomly selected from the suite of earthquakes obtained for the specified location. An intensity value will be generated from the intensity distribution discussed in Chapter 3.

Step 3: This earthquake will be applied to the structural model in the time domain analysis to obtain the structural responses.

Step 4: Then, a model for the occurrence and intensity of the after-shock should be used to generate after-shock events (possibly) based on the main earthquake. In this study, a simplified model was used for illustration in which the occurrence of after-shocks was determined from a Bernoulli trial whose success probability is related to the intensity level of the major earthquake (the earthquake just analyzed). If there is an after-shock, it will be picked randomly from the same ground motion suite with an intensity randomly generated from a uniform distribution within the range of a fraction of the major intensity. This after-shock ground motion will be applied to the damaged structure from the simulation of the major earthquake without any repair.

Step 5: After the after-shock simulation, the repair will be made based on the assumptions discussed in section 4.1. A predefined repair quality factor different from construction quality will influence the repaired EPHM parameters, since the construction team might be different from the repair contractor. The earthquake cost will be evaluated for each component based on the damage fragility relationship (see Chapter 3) and added up to determine a single earthquake loss. This procedure will be repeated by beginning to generate another earthquake occurrence interval until the sum of intervals exceeds the period of investigation. This procedure has been automated and built into SAPWood for analysis conducted in this study.

Chapter Five

Loss-Based Design and Optimization

5.1 Concepts and Procedure

Performance based seismic design is ideally a concept aimed at satisfaction of the end-user and can account for multiple performance objectives during the design process, rather than just life safety as with force-based seismic design methods such as allowable stress design or load and resistance factor design. Currently, the development of this concept for light frame wood structures has been characterized by the effort to shift the design focus from load based design to displacement based design. Newly developed design procedures such as direct displacement design (Priestly, 2002; Pang et.al. 2007) enable the designer to use inter-story drift of the building as the target for the design. This is a significant step forward since displacement is a better descriptive measure related to structural performance during moderate to strong ground motion. While the life safety issues have been well addressed through existing code documents such as ASCE 7-05 (2005), a design procedure focusing on the economic performance of light frame wood structures has not been developed up to date. Advanced, but expensive, seismic protective systems

such as base isolation can be used in woodframe structures, but the benefit of using these new techniques/devices may not justify their initial cost if lifetime economic loss considerations are not taken into account. Using the loss estimation framework developed in this study, a loss-based design concept for light frame wood structures is proposed and implemented in a simplified fashion. Firstly, the general loss-based design problem was defined in terms of a probabilistic design target statements. Then, the target statements were represented with target *loss probability curves* (will be discussed later) using a simplified long term loss estimation process so that a generalized binary search could be performed to locate the range of suitable design configurations. Finally, a detailed search with iterative incremental optimizations near the binary search result will be carried out with incremental strengthen (or weaken) guidelines to approach the target system behavior. The (economic) performance expectations (targets) will be used directly as boundary conditions during incremental optimization. Similar to the loss estimation framework, the loss-based design concept discussed here only applies to a single structure, not structures in a region. Some of the tools used to implement the loss based design procedure, such as the simulation procedure used to obtain vulnerability curves and long term loss, has been built into the software package associated with this dissertation work (SAPWood). However, the loss based design method discussed in this chapter is not programmed as a standard module because it requires owner/user feedback and is only an experimental first trial in loss-based woodframe structure design.

5.2 Loss-based Design Statements

Two Types of Statements

Loss based design is a new concept based on which a variety of specific design problems can be defined. In this study, the loss based design was confined to two types of problems. The Type I problem, termed as a *single earthquake design problem*, is focused on finding an owner/engineer acceptable structural configuration which keeps the financial loss under a predefined value with a given confidence level for a single earthquake with a given magnitude (usually corresponds to a particular return period). This is similar to the "scenario" approach used to understand the effects of natural and human-induced disasters. The Type II problem, termed herein as a *lifetime loss design problem*, involves finding an owner/engineer acceptable structural configuration which keeps the cumulative financial losses under a predefined value with a given confidence level for a fixed exposure period at the design location. If the required loss limit is considered the demand and the actual loss estimation results from the designed structure are viewed as the resistance against "loss", the concept of loss based design problem here is the same as that of traditional force/strength based design problems and a margin or safety factor against the losses could even be computed. The definition of both problems can be expressed as an inequality relating the demand and resistance. However, as a PBSD procedure, the design objective in loss based design is always associated explicitly with a probability measure. While the probabilistic features behind the traditional design statement are implicit within safety factors and design value tables.

Based on the two basic types, the requirement for a loose based design problem can be phrased as "the total loss in 75 years should not exceed $100,000 with 95% confidence" or "there is a 95% chance that the damage to the house will not exceed a quarter of the property value if an earthquake like Northridge occurs again". Obviously, the design requirements in loss based design can be easily understood and accepted by the actual users of the final product (the home owners), which is another important feature of PBSD.

The Loss Probability Curve Representation

The *Loss probability curve* for a structure is defined as a curve composed of points on a single earthquake loss vs. intensity plot corresponding to a given probability of exceedance (PE). The procedure used to develop loss probability curves for a structure is essentially the same as the procedure used in Chapter 3, i.e. in the development of the single earthquake loss vulnerability model. With the vulnerability parameters ready, single earthquake loss distribution corresponding to any intensity level could be found. Thus the single earthquake loss value corresponding to any given probability of exceedance could be calculated and plotted against intensity. However, a predefined confidence level (can be calculated as 1-PE) must be set before the loss probability curve can be plotted. As was discussed in Chapter 3, the vulnerability model can include the randomness in the ground motion, structures quality, and the component loss fragilities if the simulation is performed with these included. So the loss

probability curve, being essentially another way to present the information included in the vulnerability model, also reflects all of the uncertainty information included in single earthquake loss simulation. As a result, the accuracy of the vulnerability curve depends on the accuracy of the given information and the number of samples in the simulation.

The two basic types of problems/requirements discussed previously can be expressed as target performance points that the vulnerability curve is required to meet or exceed. The *Type I* problem essentially states that the loss probability curve of the structure corresponding to given confidence level must be "lower" than the point denoted by the requirement. As shown in Figure 5-1, the *Type I* problem appears as a boundary condition imposed by a single point (design point in Figure 5-1) on the loss probability curve, which requires the acceptable loss probability curve to pass the intensity level indicated below the design point. On the other hand, the *Type II* problem directly confines the long-term loss which is based on both the vulnerability curve (single earthquake loss) and cumulative effect of loss over time, which must be represented by a boundary condition over the entire vulnerability curve rather than just a single point. In order to find a direct relationship (other than simulation) between the vulnerability curve and the long term loss, a new concept termed the *annual frequency function* is introduced in this study. An annual frequency function is defined as

$$f_F(I) = \lambda f(I) \tag{5-1}$$

where *f(I)* is the PDF of the seismic intensity; λ is the annual frequency of earthquake events. This function has the same shape as intensity PDF, only the integral of this function in all range of possible intensities will be λ instead of 1. By introducing such a function, the annual frequency of earthquakes lies in a specific range of intensity can be easily found by calculating the integral of this function within the interested range.

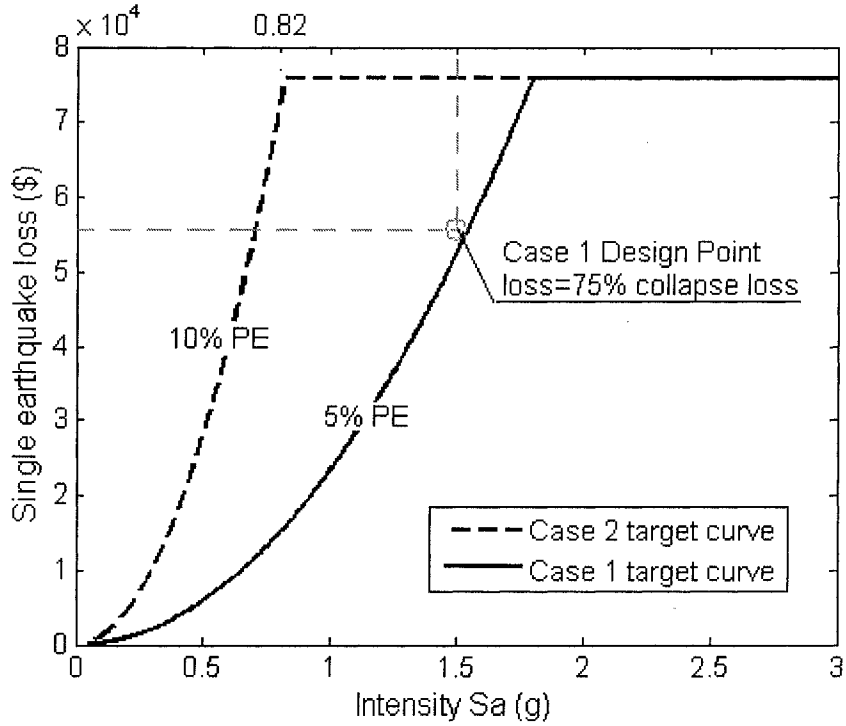

Figure 5-1: Type I statement presented as design point

If the loss probability curve corresponding to the desired confidence level can be expressed as a function of intensity, *C(I)*, the annual cost function can then be defined as

$$f_C(I) = C(I)\lambda f(I) \tag{5-2}$$

The annual loss of earthquakes corresponding to this confidence level in the long run can be calculated by integrating $f_C(I)$ over all possible range of intensity. With this function developed, the cumulative loss of the structure in N years can be calculated as

$$L = N\int_0^{+\infty} f_C(I)dI \tag{5-3}$$

Then the long term loss based design problem (the *Type II* problem) can be formulated as

$$\text{Target } L < N\int_0^{+\infty} f_C(I)dI \tag{5-4}$$

This transformation does not take into account the short term fluctuation of the earthquake occurrence by only considering the average rate of occurrence rather than the contribution from the Poisson process itself. So the representation in equation (5-4) weakens the performance requirement in an average sense. However, this discrepancy is assumed to be acceptable for the design stage estimation in this study, since point fluctuations would introduce error.

Once the location of the building is decided, the intensity distribution and average occurrence rate can be found through available data using the procedure described in Chapter 3. Then the long term loss for a given confidence level is controlled by the

period of exposure (N years) and the loss probability curve with that confidence level. On the other hand, a "target" vulnerability curve could be back-calculated based on a given long term loss value. Thus, the long term loss based design requirement could be expressed as a target loss probability curve which may be obtained from equation 5-2 and 5-3 based on given conditions. Similar to the *Type I* problem seeking to constrain the vulnerability curve at one point, the *Type II* problem is aimed at obtaining a realistic loss probability curve $C(I)$ which satisfies equation 5-4. Since this equation is to be satisfied in an integral sense, the theoretical solution will contain a group of functions (curves). Seeking a general solution to this equation can be hard and of very little practical significance, since the realistic vulnerability curves only consist of a limited subset of this general solution. A simplification of the possible shapes for realistic vulnerability curves was introduced in this study. Based on the observations of the vulnerability data generated from the index buildings used in this study (which will be presented later in Chapter 7), a realistic loss probability curve is assumed to have the shape illustrated in Figure 5-2. This simplified loss probability curve was assumed to be a parabolic curve passing through (0, 0) and the point corresponding to the maximum single earthquake loss, which is taken as the collapse loss. The loss was assumed to be constant after that point, equal to the maximum single earthquake loss (total collapse). Curves for a single structure with different confidence levels can all use this configuration since the maximum single earthquake loss does not depend on the confidence level. The only parameter that will change is the intensity level at which the curve reaches collapse loss. This intensity (I_c in Figure 5-2), termed *collapse intensity*, is the key parameter that controls the shape of this

simplified curve. During the design stage, it is relatively straightforward to estimate an approximate maximum loss for the structure. By using the equation related to long term loss and the frequency density function, the average annual loss can be calculated given I_c (numerically in this case) and compared with the *Type II* loss based design requirements. The annual loss will be different with different I_c values. So it is useful to plot the average annual loss against I_c so that the appropriate value of I_c which could result in the desired target loss performance can be easily identified. Figure 5-3 shows the relationship between I_c and resulting long term loss normalized by the *Type II* loss target. The I_c corresponding to the unit normalized loss is the I_c that could yield the target annual loss. The curves in Figure 5-3 were derived using earthquake hazard data from the San Francisco area with an average annual occurrence rate of 2.2 occurrences per year. Three *Type II* requirements were investigated in this figure. They are: "loss does not exceed half of the collapse cost over 50 years (0.5/50)", "loss does not exceed the cost of collapse over 50 years (1/50)", and "loss does not exceed twice the cost of collapse over 20 years (2/20)". Notice the requirements were all given in term of collapse loss. So they could be applied to all types of structures with different construction values. The target loss probability curves for each requirement can be obtained once the collapse intensity is found. The influence of the loss requirement on the shape of the target loss probability curve can be clearly seen from the figure.

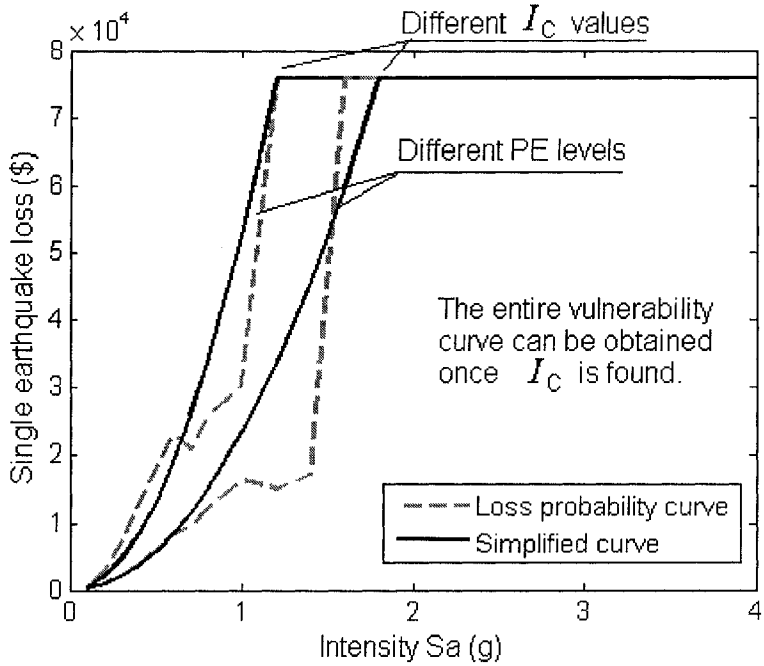

Figure 5-2: Type II statement presented as simplified vulnerability curves

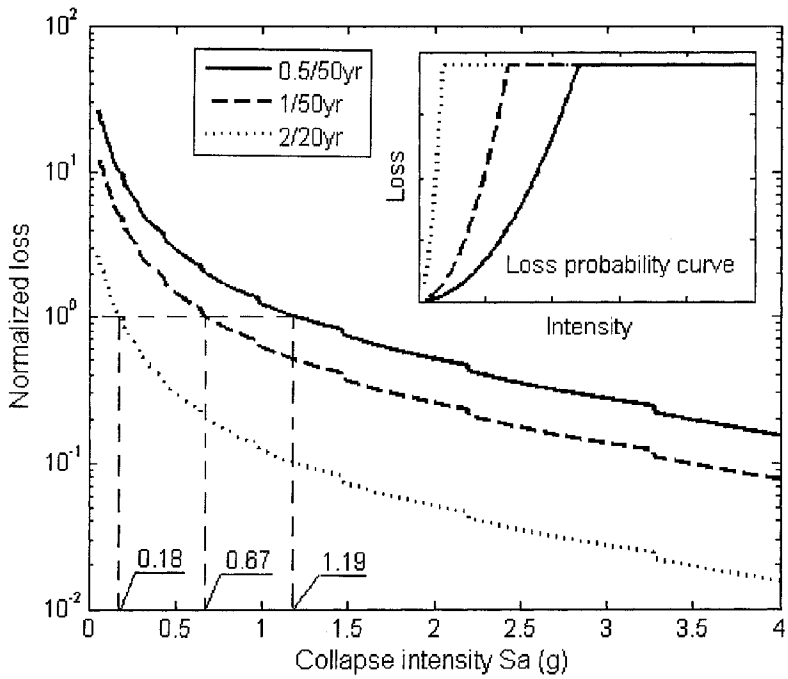

Figure 5-3: Collapse intensity-loss curve and simplified target vulnerability

In summary, the objective of both types of loss based design problem reduces to finding a realistic structural configuration whose loss probability curve corresponding to the desired confidence level matches a "target" vulnerability curve obtained based on the performance requirements. In other words, the *Type I* and *Type II* loss based design statements can be presented as a target loss probability curve with a predefined confidence level.

System Identification

Once the target vulnerability curve is obtained based on the desired performance, the loss based design procedure is then applied to find the structural system whose loss analysis output matches the target curve. This is essentially a system identification problem since the input (hazard environments) and output (target loss probability curve) are given while the system is sought. Traditional system identification procedures in structural dynamic analysis concentrate on seeking a group of structural modeling parameters that yields the known output. Although similar procedure might be applied to pursue a drift target in displacement based design, it is hard to implement into loss based design due to the flexibility in the design and complexity in loss-response relationship. An alternative procedure similar to the traditional trial and error method was used in this study to match the target vulnerability curve. This method is term here as *incremental optimization* and will be discussed in detail in the next section.

When a structure is designed to meet a wide range of performance requirements such as strength, safety, livability, and loss resistance, a requirement that controls the design must be found. It is hard to predict which performance requirement will control the design until each of the requirements has been designed for. With the new concept of loss based design, the question arises as to how this new performance requirement compares with the current force based design requirements which concerns more about life-safety issues. Theoretically, loss based design will not be of any use if the loss requirement is already satisfied by a structure designed based on strength requirements, which can in some cases occur. On the other hand, an unrealistically tight loss requirement might never be able to be achieved or be so expensive in initial cost that it is not realistic. This situation actually narrows the range of meaningful (or realistic) loss performance targets making the identification of an acceptable design more straightforward. The process of identifying a reasonable range for the loss based design target is an important problem in PBSD that must be addressed before the concept can be accepted by the engineering community. However, this problem is not the focus of current dissertation work and the loss targets used in the examples later had been carefully chosen so that they lead to realistic designs and optimizations for, primarily, illustrative purposes.

5.3 Incremental optimization

The concept of incremental optimization comes from the traditional trial and error design method and the tools enabled by time domain analysis to identify and improve

the relative weak points. The traditional trial and error procedure has been widely used in the design of many structural components, commonly seen in the design of reinforced concrete members. This procedure is especially useful for the situation in which the general configuration of the design has been determined but some details are still need to be sought. The effects imposed on the performance through the change of these details are usually hard to express in an inversed functional form. So the logical (and efficient) way to find out the appropriate design is to propose and improve trail designs with similar configurations and small changes until the design requirement is met. The loss base design of woodframe structures is a suitable case for applying this procedure due to several reasons. Firstly, the architectural floor plan of a woodframe house is usually pre-determined and will remain the same unless there is significant benefit in changing it. This provides a basis to propose similar design configurations. Secondly, the structural components that can be used in the woodframe house are limited to several standard configurations. For example, a nail spacing of 3.7 inches for wood shearwalls might meet the requirement of the design, but it is not practical and will not be used in practice. This situation further narrows the range of adjustment that can be imposed on the trial designs.

The implementation of incremental optimization consists of two iterative steps: trial and optimization. Trail is the step where the designer proposes a design setup based on the architectural floor plan given and previous optimization (if any). Optimization is the step where the trail design is used to estimate the performance and modified based

on the comparison with the target. In order to make the design converge faster, a strategy to modify the structure based on the comparison must be developed.

From the previous discussion, it can be concluded that loss-based design can be represented by matching points on the vulnerability curve. Then it is quite clear that between each trail and optimization, a vulnerability analysis corresponding to that target point is required. Although this task seems to be unrealistic for practitioners at this stage, the method will become practically viable when there is an automated loss analysis tool (such as SAPWood) available. The procedure for incremental optimization could be summarized in the flowchart in Figure 5-4.

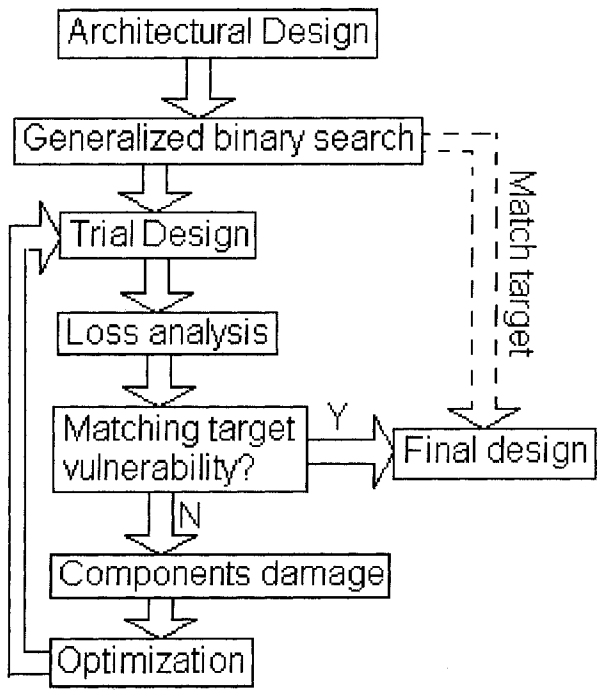

Figure 5-4: Flowchart for incremental optimization

Firstly, a generalized binary search should be carried out to narrow the design to a vicinity of a conventional design based on the comparison of the target point on the

vulnerability curve. This procedure was based on the assumption that the loss resistance of the structure is positively correlated with structural strength on a large scale, which means given strength difference significantly enough between two alternative designs; the stronger one will have a superior loss performance than the weaker one. As a result, the alternative design configurations proposed in the binary search should be significantly different from one another. The search starts from vulnerability analysis of a pair of significantly over-designed and under-designed structures based on the predefined architectural floor plan. If the resulted performance boundary does not include the target, the target might be unrealistic without advanced techniques such as base isolation, or the target will be automatically satisfied with conventional construction. If the target lies within the boundaries, the designer can choose to propose a design in the middle of previous designs to narrow the boundary, or proceed with the design which produces closer performance compared to the target curve in the next step. In order to choose a design "in the middle" requires some level of engineering insight and experience. But it is not unrealistic to assume that the person using loss based design procedure will very likely have such experience. The narrowing of the range should stop when the structural configuration "in the middle" becomes hard to identify. Then the configuration which produces closer performance to the target point (curve) will be used as the first trial case in the detailed incremental optimization. It is also possible that the target loss probability curve was matched through this searching process. If that happens, a detailed loss simulation should be conducted to calculate the loss target value and compare it with the requirement. There will be no need to perform detailed incremental optimization of individual components

if the results satisfy the requirement. Notice that target loss probability curve is used in this search as the reference, rather than the actual percentile value of the long term loss.

After the designer identifies the trial design from binary search, a more in-depth look into the loss structure should be carried out to identify the weak points (in case the trial design is under performing) or over designed points (in case the trial design is over performing) in the structure. At this point, it is important to identify what aspect of structural response induces the most severe damage and loss. Recall in the loss estimation procedure the damageable components were the causes of financial loss. They could be divided into displacement sensitive components and acceleration sensitive components. Each type of component can be optimized following guidelines to reduce the excessive loss to bring the overall performance closer to the target. The SAPWood loss analysis module provides the information on both the total loss and individual component damage during earthquake simulations. By comparing the damage of each component, the severely damaged components can be identified (e.g. the components that exhibit a level III or higher damage level). Then the optimization should follow the descriptive guidelines listed below:

Table 5-1 Incremental optimization guidelines

Type	Components	Optimization measures
Displacement sensitive	Shearwall	Strengthen the structural component attached
	GWB drywall	Improve symmetric condition if torsion controls
	Door and window	increase length if possible
	Stucco, Paint	use double sided sheathing
	Plumbing system	use special strong wall products
	...	...
Acceleration sensitive	Furniture	relocate if possible
	Electronics	add fixture to increase overturning resistance
	Water heater	use advanced acceleration reduction device such as base
	General contents	isolation to reduce floor acceleration
	...	...

It is necessary to point out that table 5-1 is not a complete list of the guidelines that can be used in the incremental performance optimization procedure. It is the freedom of the designer to decide which damage reduction measure should be adopted in the optimization; this freedom provided to the designers is a key characteristic of PBSD. As a result, a more experienced designer will have a distinct advantage over less experienced designers through the more efficient optimization thus reducing the effort of the iterations. However, since the designer can assess the effect of optimization and propose alternative optimization strategies based on the vulnerability analysis and loss simulation results from his/her trial design, the performance of the final design output could be well controlled close to the target regardless of the level of experience. Theoretically, the design towards the performance (loss) target should also include the case in which the structure has to be "weakened" to approach the target loss amount. But this is typically not very realistic in real design. When the performance target was set to be weaker than current performance, the guidelines could be reversely applied (such as shorten the wall length, remove the base isolation system, etc.) to serve the purpose. In Chapter 7, the incremental optimization procedure will be applied to the design of a two story single family house for both *Type I* and *Type II* loss requirements.

Chapter Six

Software Development

6.1 Necessity for a New Program Package

In the 2001 CUREE-Caltech wood frame research project, seismic analysis programs were developed for light frame wood structures based on similar models discussed in Chapter 2. These programs, namely Cyclic Analysis program for wood SHEar Walls (CASHEW) and Seismic Analysis program for Wood Structures (SAWS), are the basis for the development of the program package (SAPWood) developed in this dissertation work. The reasons for developing a new software package rather than using the existing ones are as follows. Firstly, the newly developed EPHM element could not be easily incorporated into any of the existing programs. Secondly, the stability of CASHEW and SAWS program is relatively good, but could stand for improvement when subjected to large displacements and high earthquake intensities, mainly due to the use of the static parameter hysteretic model for shearwalls and connectors. The third, it is more efficient to have the huge amount of simulations run by an automatic tool rather than to do each of them by hand. Furthermore, loss estimation with damage accumulation could not be performed by any existing

programs and needed to be programmed. The most advantageous aspect of this new program is that it enables the engineers without the background in time domain analysis and loss estimation to apply the methods developed in this dissertation work to any existing or newly designed structures.

With the aforementioned concerns, SAPWood was developed with a graphical user interface using Visual Basic (see Figure 6-1). It is part of the NEESWood project and had been made available to the public free of charge through the NEESWood website (www.engr.colostate.edu/NEESWood/). Other than the EPHM element discussed earlier, commonly used linear, bilinear, and ten-parameter CUREE hysteretic elements can also be used in the structural models in SAPWood. All analysis procedures discussed in this dissertation can be easily carried out using different modules in the software package except for the loss-based design procedure.

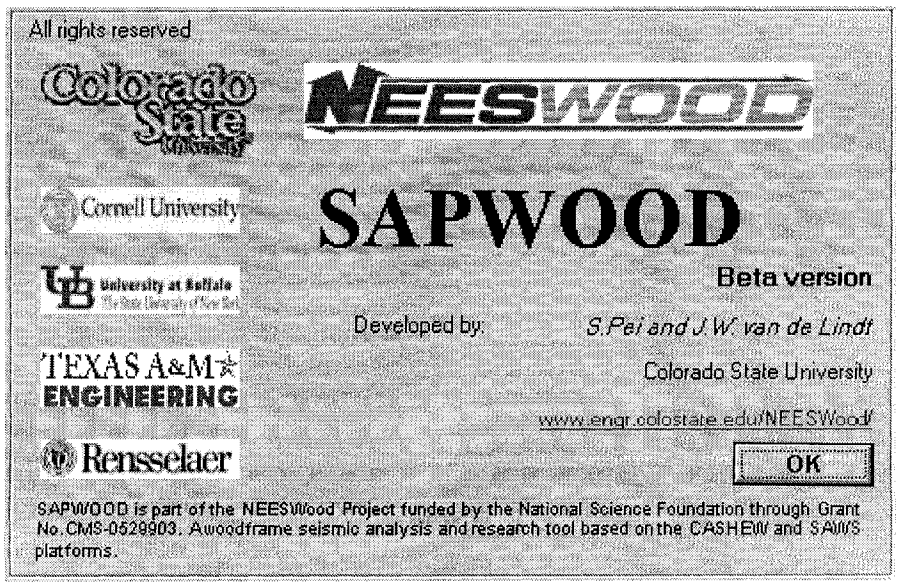

Figure 6-1: SAPWood software package

6.2 SAPWood Components and Applications

SAPWood includes all of the models discussed in Chapter 2 and a lumped mass uni-axial shear building model for simplified analysis purposes. It is not a finite element program and can only be used to analyze seismic loading or other lateral force dominated loading cases for light frame wood structures.

Building Models

All the nonlinear (and linear) elements in SAPWood have only one degree of freedom. So they were coded as a general "spring" element. A mixture of different spring types are allowed in all of the system models in SAPWood (biaxial structural model, NP model, and shear building model), which is an improvement compared to the original SAWS and CASHEW models which use only the CUREE hysteretic model. The user has the capability of constructing the model file using a text editor or the interactive model builder provided in SAPWood. The GUI of the model building module is illustrated in Figure 6-2 and 6-3.

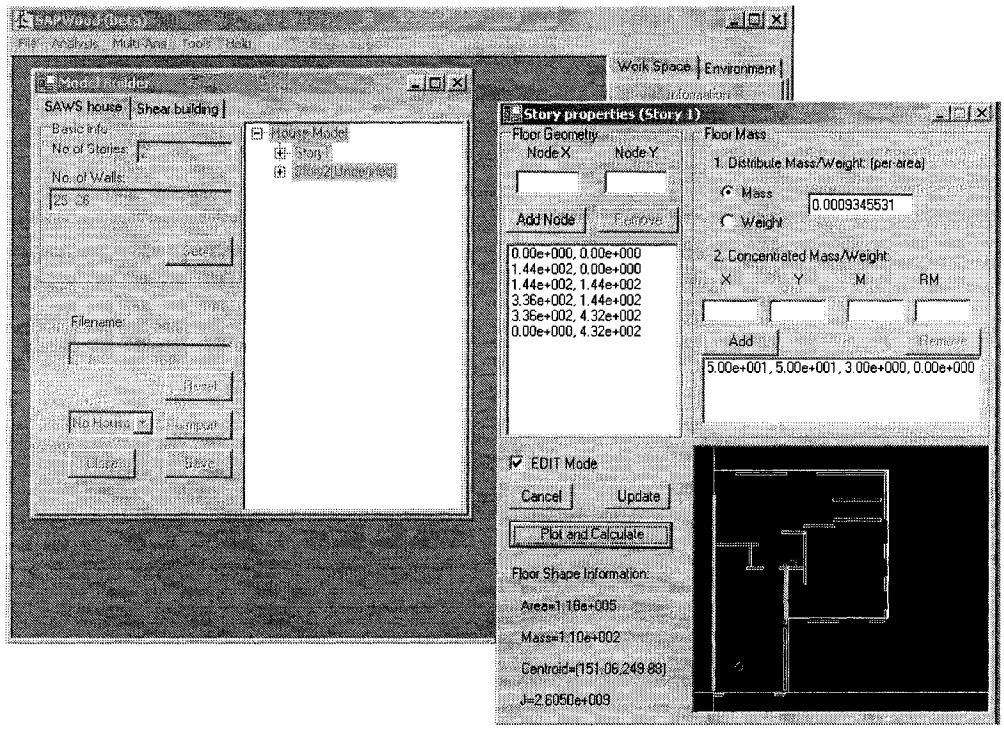

Figure 6-2: Biaxial system model builder

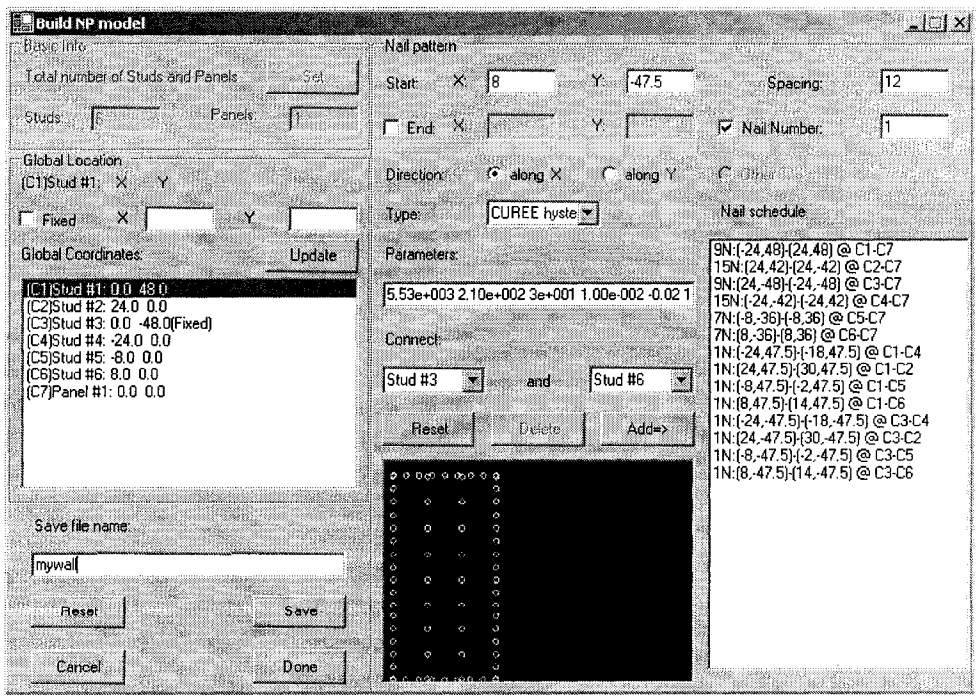

Figure 6-3: NP model builder

Time domain analysis

SAPWood is capable of performing one dimensional and biaxial time domain analysis on a shear building model and biaxial model, respectively. The inertial vertical degree of freedom is not included in current version. The user is allowed to scale the earthquake record to a specific peak ground acceleration (PGA) or spectra acceleration (S_a) in both directions. The analysis time step is controllable. A simplified constant damping matrix is used in the Newmark Beta procedure since the majority of damping effect comes from the energy dissipation of the hysteretic elements for this type of structure. From the model verification experience, the analysis with viscous damping ratio assigned to a very small number (usually 0.01) yields good results that agrees with the shake table tests. The earthquake analysis module (see Figure 6-4 and 6-5) also provides an easy tool to obtain preview of the results before save them into a file. The results include story drifts and rotation, maximum displacement, and hysteresis loops of each wall.

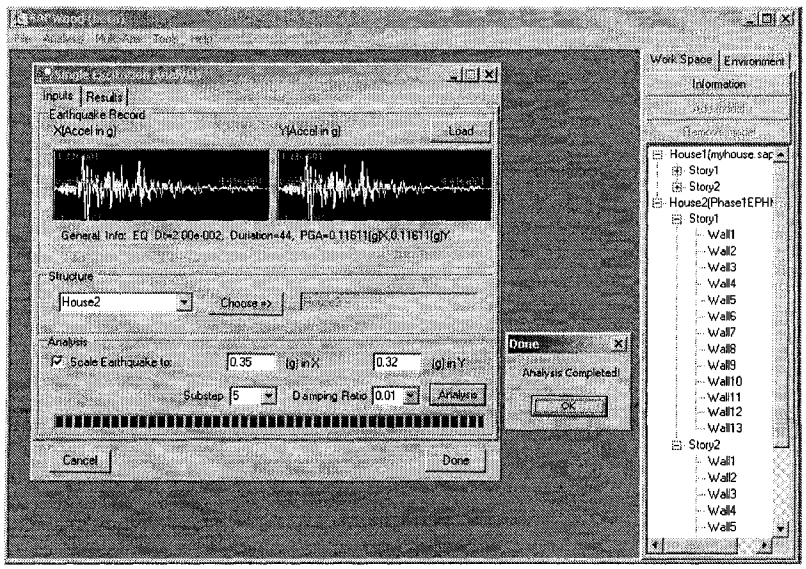

Figure 6-4: Biaxial time domain analysis inputs

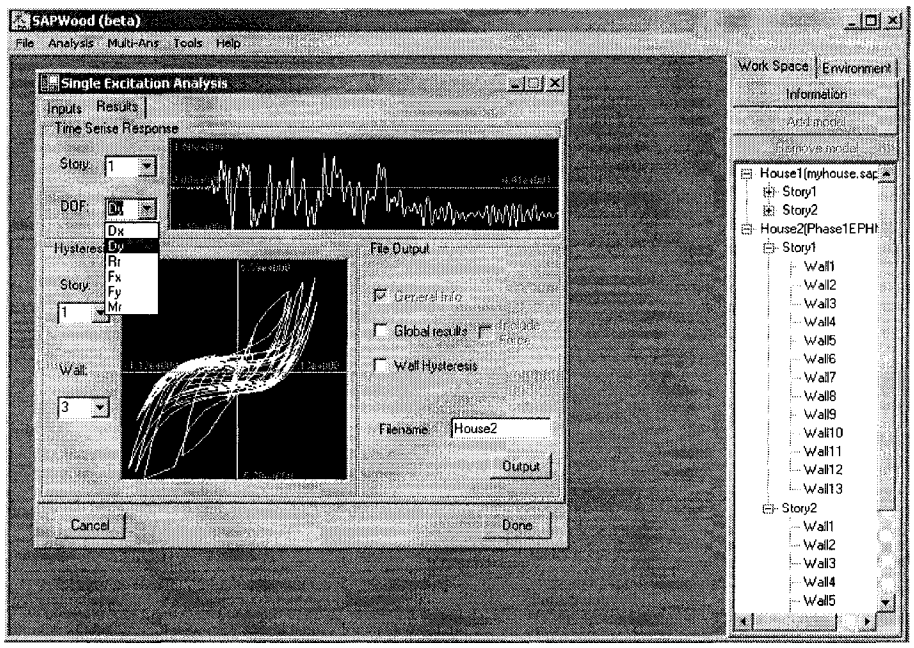

Figure 6-5: Biaxial time domain analysis results

Also included in SAPWood are the tools to automate commonly performed tasks in seismic engineering research. Incremental dynamic analysis (IDA) is a widely used method to study the seismic behavior of nonlinear structures by performing a series of time domain analysis with incrementally increasing ground motion intensity. It has been proven to be useful and become a standard analysis procedure in the earthquake research community yet not practical enough for design yet. With the IDA module (Figure 6-6 and 6-7) available in SAPWood, it is very straightforward to perform IDA and investigate the behavior of the structure at different hazard levels.

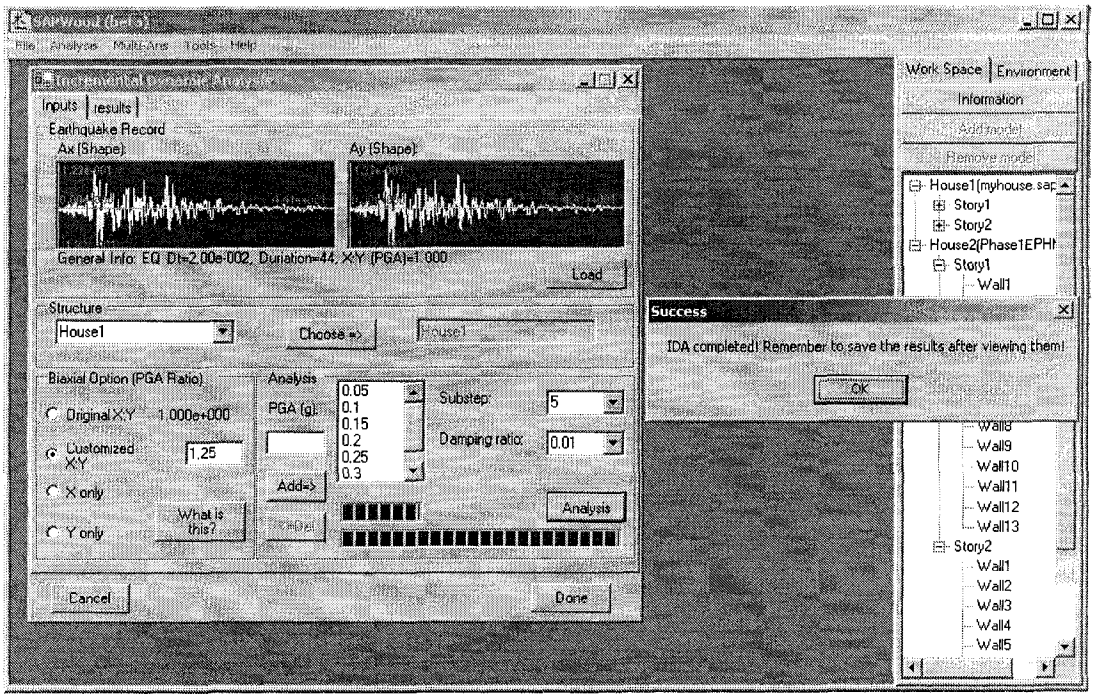

Figure 6-6: Incremental dynamic analysis inputs

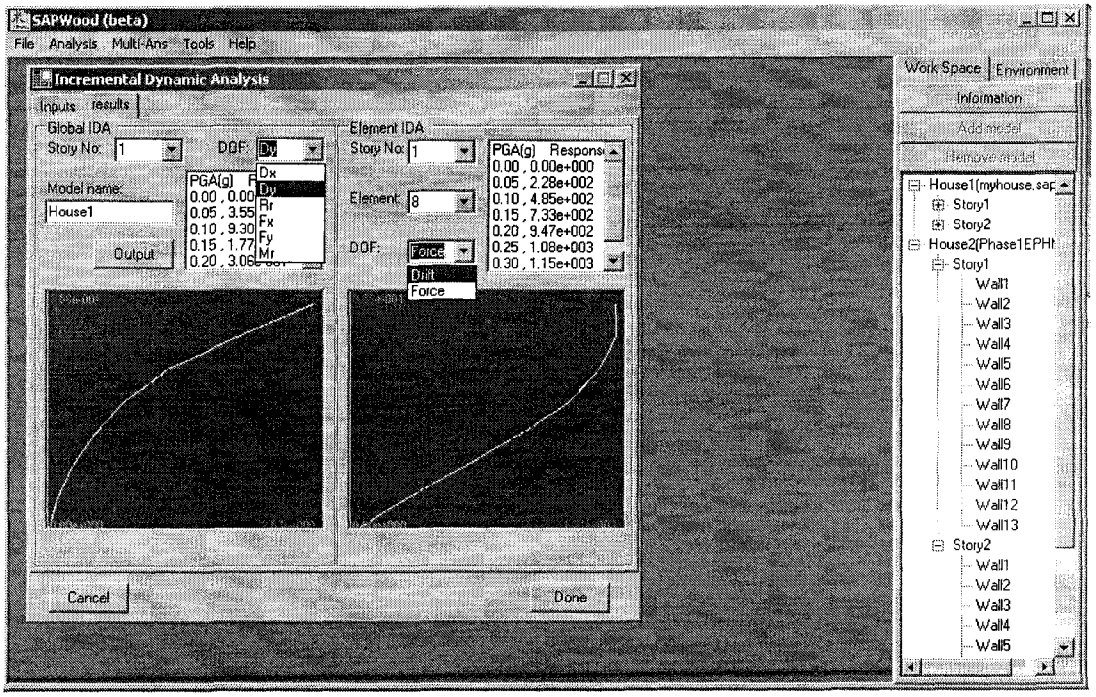

Figure 6-7: Incremental dynamic analysis results

An extension of IDA concept leads to the Multi-case IDA, which is virtually the IDA procedure performed on different design options/variations with a suite of earthquake records. Similar to the IDA module, the analysis is automated and preliminary results can be viewed after analysis for both the story and individual wall responses (see Figure 6-8 and 6-9). This procedure is not novel and might have already been used within seismic research community to achieve purposes such as model comparison and design optimization. The integration of this procedure to an easy-to-use module enables the users to benefit from this advanced analysis tool without the need to have a full understanding of all the underlying assumptions. This procedure was used in the present study to develop the single earthquake cost models.

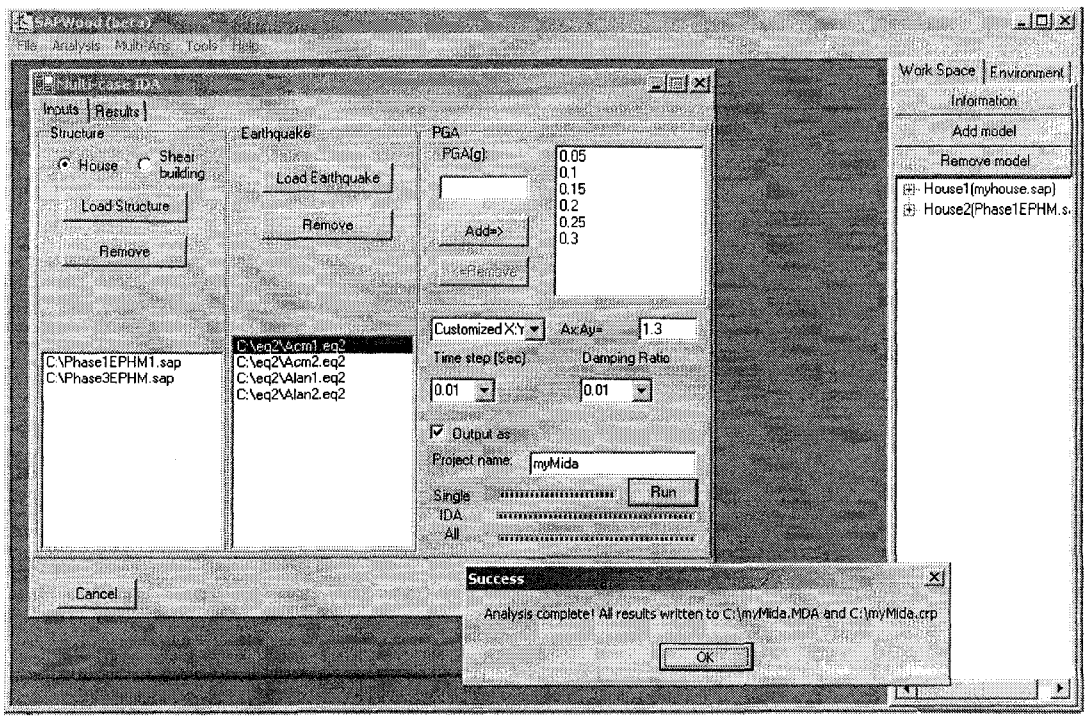

Figure 6-8: Multi-case IDA inputs

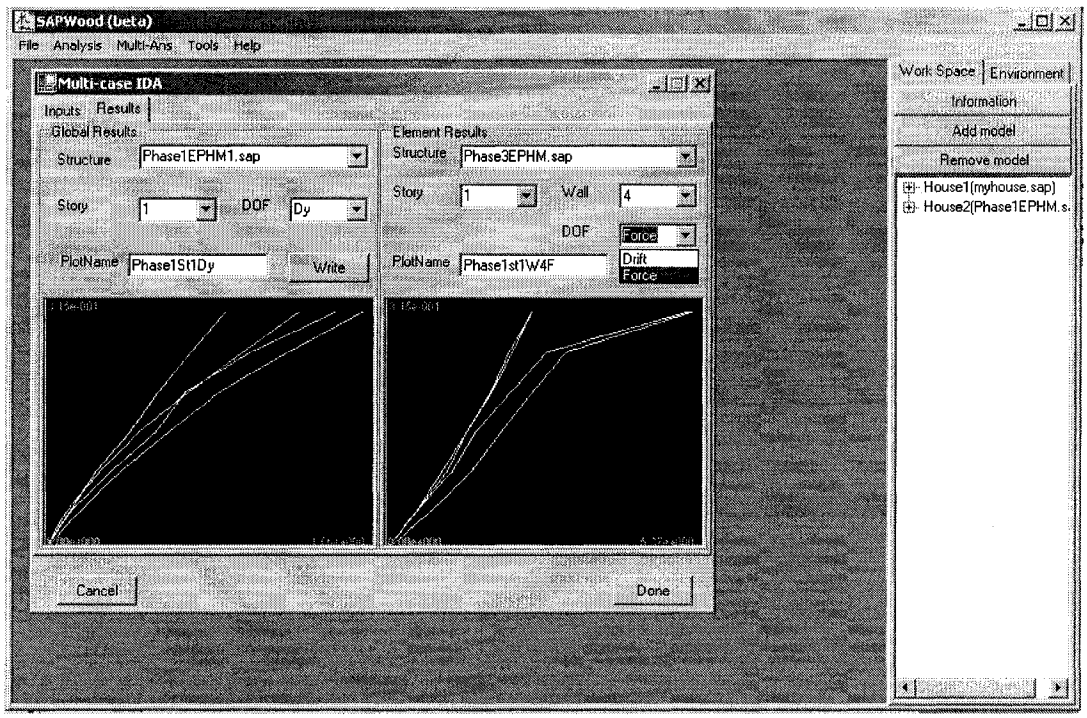

Figure 6-9: Multi-case IDA results

Quasi static analysis

The quasi static analysis tools were designed mainly to investigate the nonlinear load-resisting behavior of light frame assemblies and systems. The steps to obtain the result for quasi static analysis include the assembling of the stiffness matrix, applying incremental displacement at a given degree of freedom, and solving for resistance at every load step. The results from the analysis could be used to construct a simpler model for dynamic analysis or within a system identification procedure.

NP analysis

The Nail Pattern model of wall assemblies was discussed in detail in Chapter 2. In the analysis, the bottom plates of the wall will usually be fixed and the displacement protocol will be applied to the top plate in the horizontal direction. Different from the CASHEW model in which only the panel to stud nails were specified, both the panel nails and framing connectors need to be specified by the user. If the framing nails were represented by linear springs with very large stiffness, the NP result resembles the results from its predecessor, CASHEW. Because of the flexibility provided by NP model kinematics, customized boundary conditions could be modeled with SAPWood. For example, if the shear wall is restrained by the story diaphragm above, the rotational degree of freedom for the top plate can be restrained accordingly. Special elements such as hold down devices and diagonal damping devices could also be built into the wall model using different spring elements.

After the analysis, the hysteresis loop of the system will be plotted and the user can obtain hysteretic model parameters immediately. If the "check nail" option was checked before the analysis, the load-slip hysteresis of every nail (or other connector) in the model could also be available after the analysis, as shown in Figure 6-10. This option is very useful in discovering the damage pattern of the wall, i.e. where is the most damaged region.

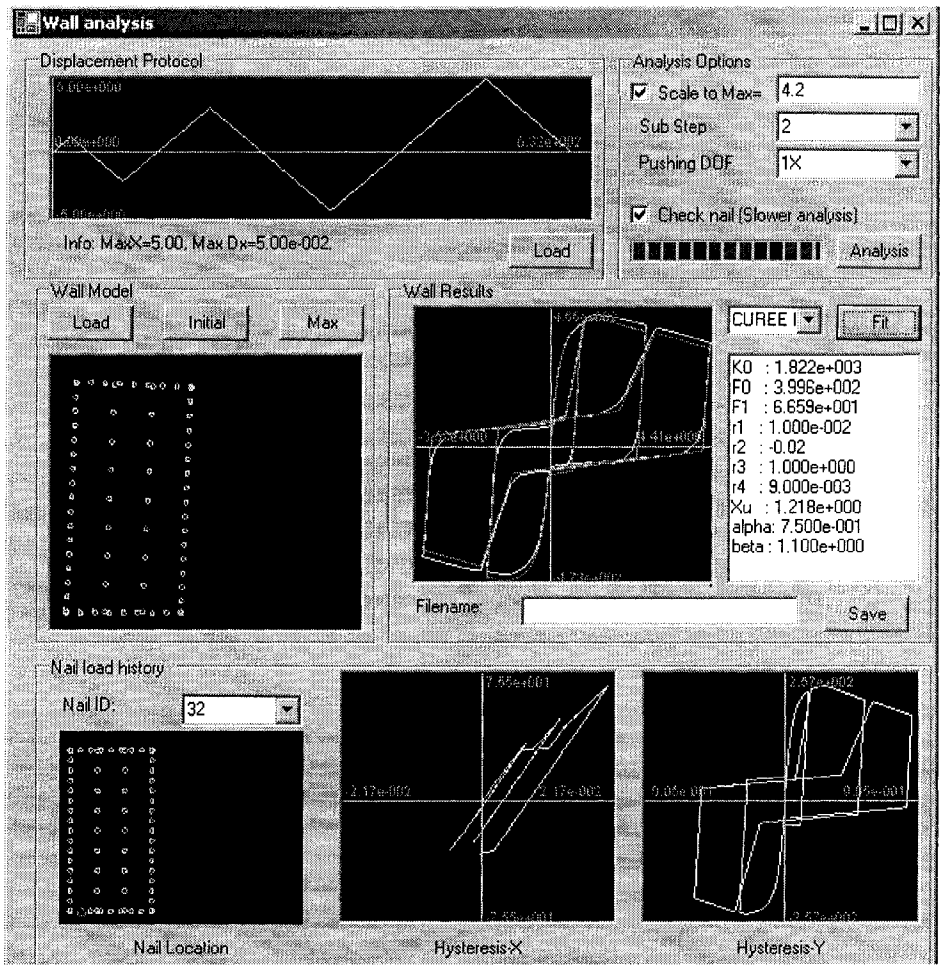

Figure 6-10: Cyclic NP model analysis

SDOF identification analysis

SDOF identification analysis provides the user with a tool to artificially apply a predetermined displacement history to any degree of freedom for the bi-axial model to investigate the load-resistance behavior of the structure, e.g. shear resistance of the entire story. It may be used in simplified analysis procedures, such as representing a biaxial model with a shear building model. The user needs to specify the degree of

freedom on which the displacement protocol is applied. The displacement protocol is arbitrary and can be scaled. Figure 6-11 shows the graphical interface of this module.

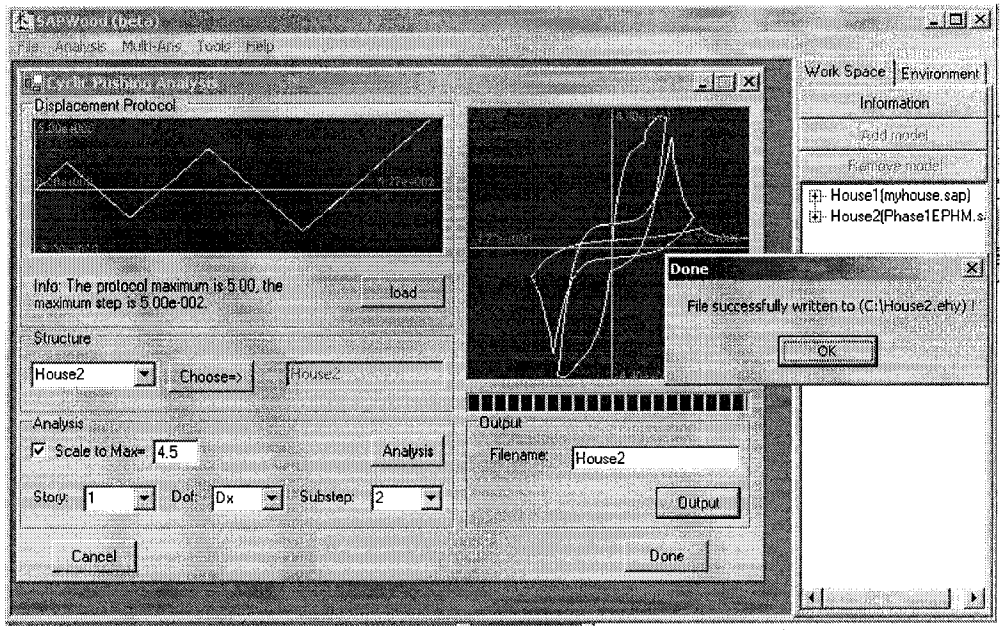

Figure 6-11: SDOF identification analysis

Loss analysis

Loss estimation methods included in this study have all been programmed into the SAPWood loss analysis modules. There are two types of loss analysis that can be performed using sapwood, the first one is the traditional loss estimation based on the single earthquake cost and vulnerability; the second one is the virtual hazard simulation. The user needs to provide input information such as the nominal model of the structure, fragility information on the financially crucial elements related to the structural response, earthquake hazard, and long term simulation parameters, etc. The

final output of the loss analysis was the sample for the long term loss. Without including any model for the long term loss distribution in the program, the user is encouraged to establish various types of models for long term loss based on this sample pool to serve their specific needs.

Vulnerability based simulation

Due to the amount of information needed for loss estimation, the input section for the loss estimation module was divided into 3 parts: the structure, damage fragility, and seismic uncertainty. In the structure information section, the user can load and choose the nominal model in the workspace, specify the construction quality, and define the type and cost for each cost sensitive element through the damageable element input file. Then the damage fragilities for each cost type can be defined in the damage fragility input section, where the user will load the fragility model file. The user could assign priors (uniform priors are most commonly used) for fragility functions and input available data points in fragility model files. For seismic uncertainty information, an earthquake hazard input file is used where the user could define their own earthquake hazard model by specifying occurrence rate, provide ground motion records, and assign intensity distribution (or Hazard curve data from USGS). The input files used in the numerical examples containing seismic and fragility information have been built into the distribution package of SAPWood for users to use or study as an example.

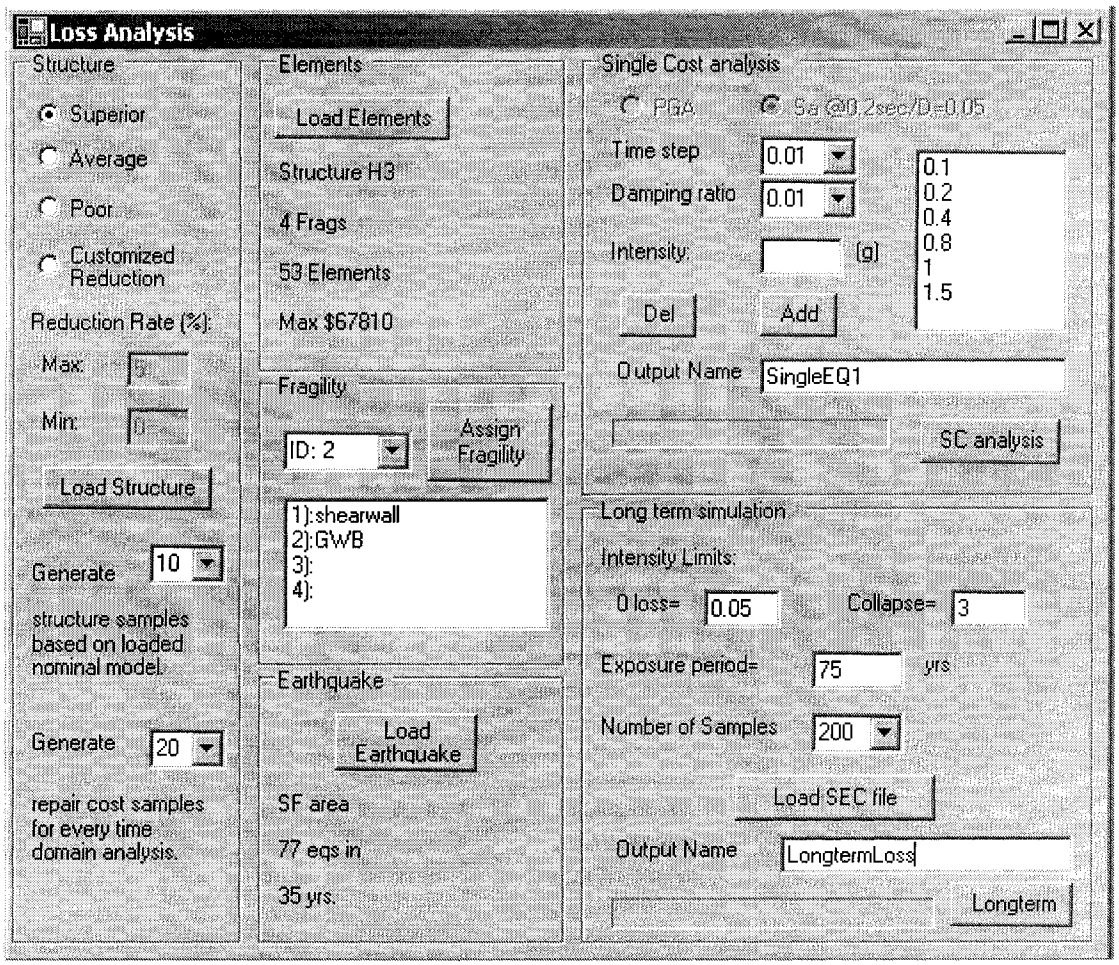

Figure 6-12: Inputs for loss estimation

Since the single earthquake cost distribution characterizes the financial robustness of the structure, the comparison between different design options can be made without doing further analysis. The program can give single earthquake cost simulation data as an intermediate analysis output. Both the vulnerability model parameters introduced in Chapter 3 and the simulated single earthquake samples will be given in the output file. So the user can use the vulnerability model established in this study directly or use these single earthquake cost data to develop their own vulnerability models (model that relates single earthquake cost to seismic intensity). These vulnerability models

could be combined with long term seismic hazard models to simulate the long term loss. Once the vulnerability model is established, only the seismic uncertainty information is needed in the long term loss simulation. Although the user may use more advanced vulnerability models depending on their needs, the linear interpolation model proposed in Chapter 3 is built in SAPWood long term simulation so that someone without much background in vulnerability analysis can generate long term loss samples by simply loading the single earthquake loss simulation output file and specifying the exposure period.

Virtual hazard simulation

As has been discussed in Chapter 4, virtual hazard simulates the entire exposure period multiple times, using a more realistic set of assumptions. The draw-back of this simulation method is the computational expense and the lack of intermediate results such as vulnerability data. The input information for virtual hazard simulation is similar to that for traditional loss simulation. However, there is some additional information that needs to be specified. The first will be the repair quality, which can be different from the construction quality. However, it is assumed in SAPWood that the effect of repair quality contributes more to the long term loss than initial construction quality. The construction quality is set by default to be the same as repair quality. The repair strategy embedded in the current version of the SAPWood program is a relatively simplified one under which every component having a damage level greater than level I (non-detectible) will be repaired when the earthquake and after-shock excitations are complete. The input information for after-shocks used in the

program include the lower limit intensity of the major earthquake that may produce an after-shock, probability of after-shock occurrence, and a range of after-shock intensities. More advanced after-shock prediction/statistical models may be incorporated into the program later, but this is not a focus of the current study. Another feature of the Virtual Hazard simulation tool in SAPWood is the option to create a hazard log file for every single simulation of the exposure period. A hazard log is a time history of simulated seismic events and corresponding financial losses. The final output from virtual hazard simulation is a sample pool of long term losses, similar to that from traditional loss analysis.

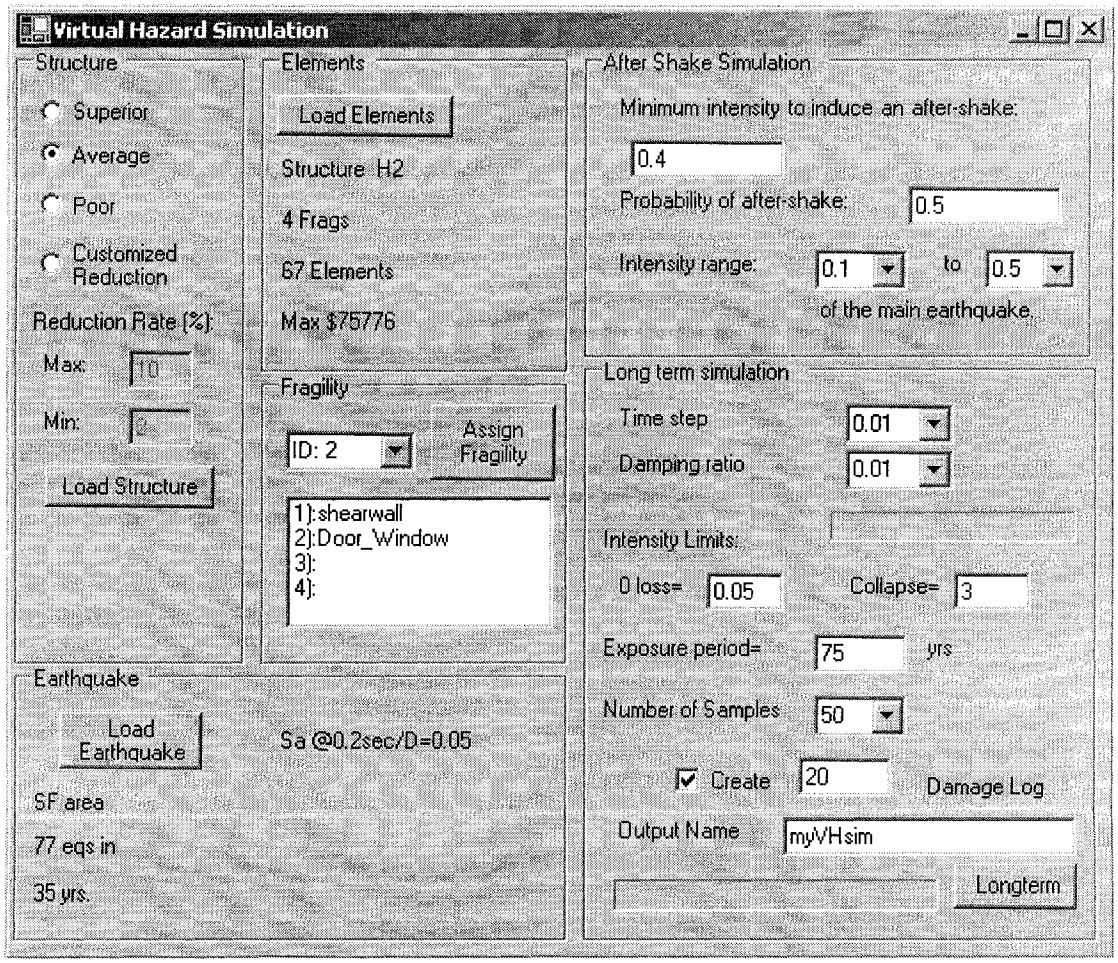

Figure 6-13: Virtual Hazard simulation inputs

All of the analyses in this dissertation work are performed using automated tools in SAPWood. The only exception is the incremental optimization procedure in loss-based design which requires subjective input and control.

Chapter Seven

Index Building Analysis

7.1 Index Building Configuration

The methodology and concepts developed in this dissertation work are to be applied to loss-based evaluation and performance based design of wood frame structures. The procedures and results from the loss analysis and loss based design were illustrated in this chapter with realistic woodframe structural configurations. Through these examples, the concepts introduced in earlier chapters are illustrated with specific procedures applied to realistic woodframe structures; the loss behavior of typical woodframe construction styles was studied; and the loss-based design of a two-story single family house was performed. Although it is impossible to incorporate all types of woodframe construction style in these examples, the validity of the loss estimation framework and loss-based design concept is believed to be well illustrated through the analysis and results presented herein.

Three index buildings were used in this study, including two single family homes and a four story office building. The single family houses were of conventional light frame

wood construction, i.e. using only wood shearwalls (and GWB partition walls, to some extent) as the lateral force resisting components. The office building had some steel and concrete columns on the bottom and first floor to help resist the vertical and lateral load from above. Architectural floor plans for the index buildings are presented in the following figures. The exterior walls for the single family houses were assumed to be structural shearwalls while the interior walls were assumed to be partition walls sheathed using GWB. For the office building, the structural design plan of an existing building in Davis, CA. was used in the loss analysis. The model parameters for shearwalls were obtained using the SAPWood-NP tool based on the nail schedule indicated by the design.

Index Building A: One story single family home

This building is a ranch style 2 bedroom house with a two car attached garage. The total area of the house is approximately 1440 sq. ft. The cost of constructing this type of building is relatively low, thus this model represents the low-end construction style among these examples. The architectural floor plan is shown in Figure 7-1.

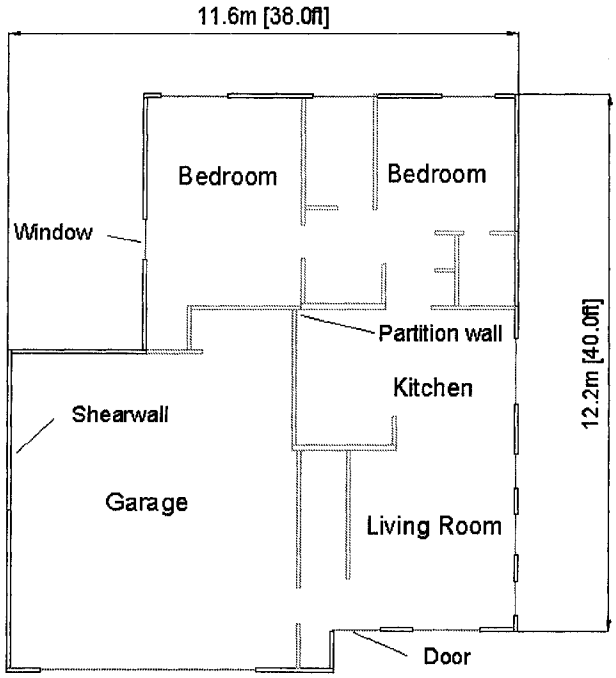

Figure 7-1: Index building A floor plan

Index Building B: Two story single family home

This building is a typical two story single home with 2 bedrooms and a one car garage. The total usable area is about 2400 sq. ft. In this study, this building represents the main stream construction style. The high-end homes which often have customized designs were not included in this study, but the methodology is applicable. The architectural floor plan of building B is shown in Figure 7-2

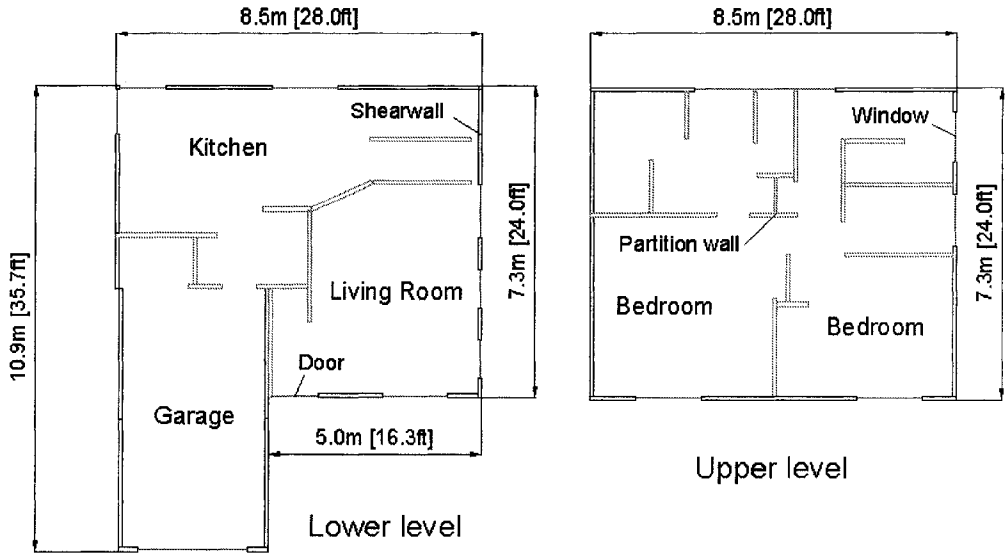

Figure 7-2: Index building B floor plan

Index Building C: Commercial Mid-Rise Office Building

This building floor plan was obtained from the actual design of the McCormick building in Davis CA, USA. It is a three-story wood frame office building with an additional mezzanine floor on top, so effectively four stories for the structural model. The use of steel and concrete columns enables a large open space on the bottom floor as a garage area. The model was constructed based on the structural floor plan which contains the location and length of structural shearwalls and columns. The floor plan layout with the structural component locations is shown in Figure 7-3.

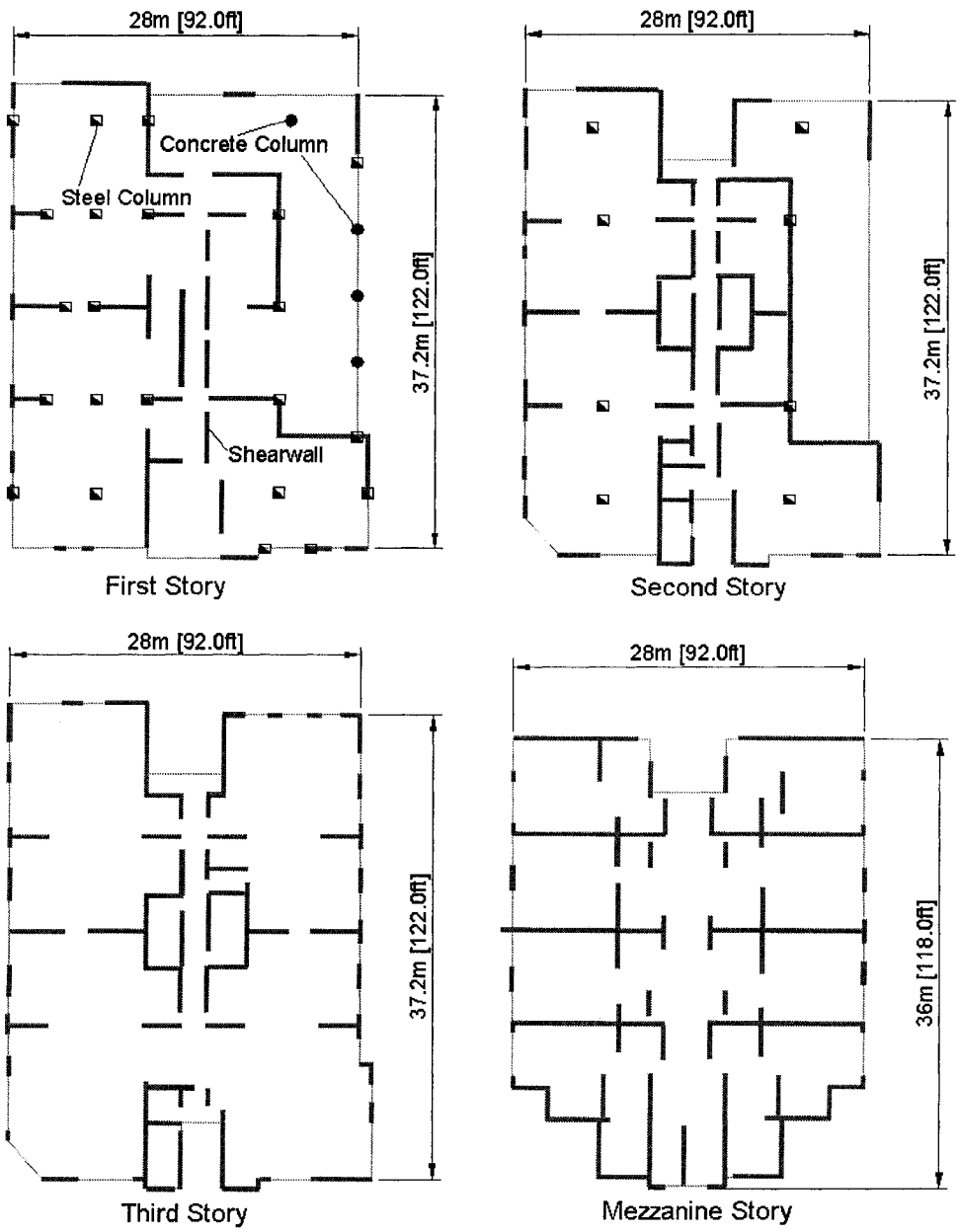

Figure 7-3: Index building C floor plan

Vulnerability analysis and long term loss simulation were performed on all of the index buildings using the loss estimation procedures outlined in Chapter 3. While index building B was used as an example of loss based design for illustration for residential woodframe structures, index building C was not included in the discussion

of loss based design because the design of such a complex, multi-resistance-system-supported structure is much more complicated than conventional wood frame structures and was beyond the scope of this study. Although the loss analysis methodology developed in this study can be applied to such structures, the loss based design study was confined to traditional wood frame structures.

7.2 Available Information and Analysis assumptions

As was mentioned in Chapter 3, the information on the structures properties (both structural and financial) and seismic hazard are required to perform loss analysis. For the structural properties, the structural model must be built based on the configuration of the structural components of the design and damage fragilities must be updated (calibrated) using damage-loss data for the damageable components. For seismic hazard, the randomness in ground motion, intensity level, and occurrence rate should be estimated from site-related data and represented properly with statistical models. The available historical and test data for part of this information were gathered and processed for this study. However, it should be mentioned that a considerable number of assumptions were made when the needed information was not available. Although the accuracy in the input information will have some impact on the results, the methodology illustrated in these index building examples will not be affected by these assumptions.

Structural modeling

In strength based design (see e.g. IBC, 2006), wood shearwalls are the only lateral force resisting component considered for light frame wood buildings. Recent experimental studies have shown that gypsum wall board (GWB) panels applied to the framing members provided a considerable influence on the seismic behavior of the structures (van de Lindt et al., 2006). Thus, both the OSB/GWB sheathed shearwalls and GWB sheathed partition walls are considered as components that provide lateral resistance during an earthquake (in the case of index building C, steel and concrete columns were also included). Although recent research showed that other non-structural components, such as stucco, did provide additional resistance against earthquake, they are not included in this study since not all buildings, residential or otherwise, have stucco exteriors.

Shearwalls

All of the wood shearwall parameters in the index building model were estimated based on the sub-assembly (connector) level model analysis using the SAPWood-NP program. Cyclic loading tests of 8d common and 10d common nails were conducted at CSU to obtain accurate connector hysteresis data. Three different displacement protocols were used in the test to fit the resulting hysteresis in order to try to reduce the test protocol-dependent effects of the nail response. Selected test results are shown in Figure 7-4, 7-5, and 7-6. The nail hysteresis was imported into the SAPWood fitting module in order to obtain the parameters of the evolutionary-parameter hysteretic model (EPHM) which can be used to represent the test responses. Finally, the average parameters from all the tests performed using the same nail types were used in the sub-

assembly NP model. The hysteresis parameters for 8d-common and 10d-common nails are listed in Table 7-1.

Table 7-1: Nail parameters used in the NP analysis

Nail	K_0	F_0	r_1	x_u	r_2	x_{u1}	λ_b	F_c
10d	9180	265	0.01	0.165	-0.03	0.25	-3.65	70
8d	7730	234	0.01	0.167	-0.021	0.451	-1.43	61.7
Nail	F_r	x_{F1}	x_{F2}	λ_F	λ_k	K_r	β	F_{ur}
10d	2.28	0.0826	0.198	-2.5	-12	0.0001	1.1	3.03
8d	5.73	0.0832	0.2	-1.17	-7.67	0.0001	1.1	2.6

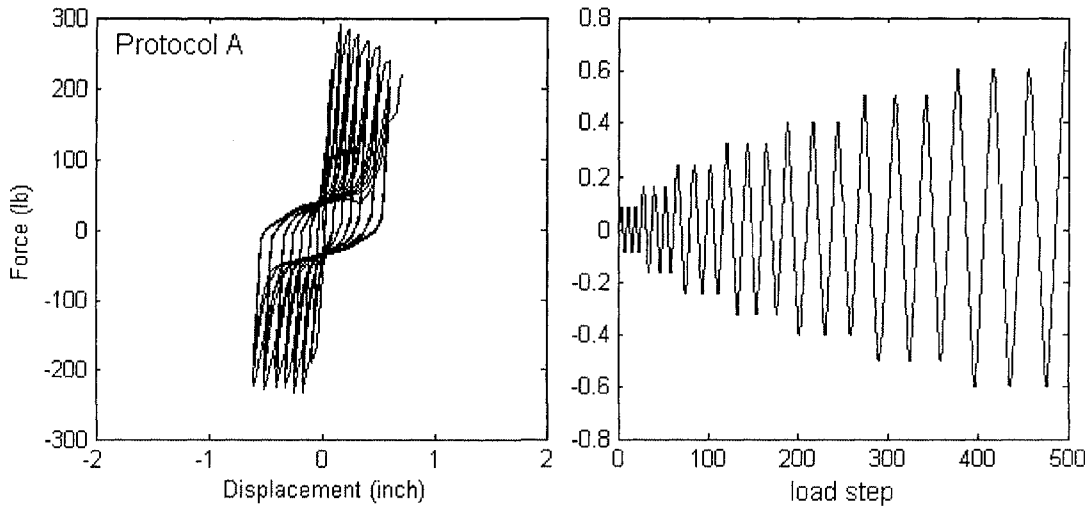

Figure 7-4: Nail test hysteresis result using protocol A (8d common)

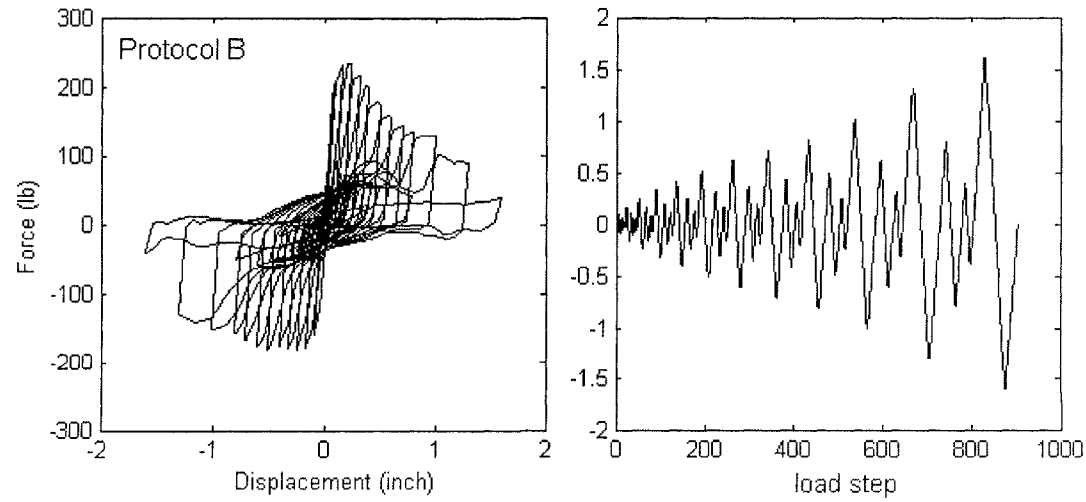

Figure 7-5: Nail test hysteresis result using protocol B (8d common)

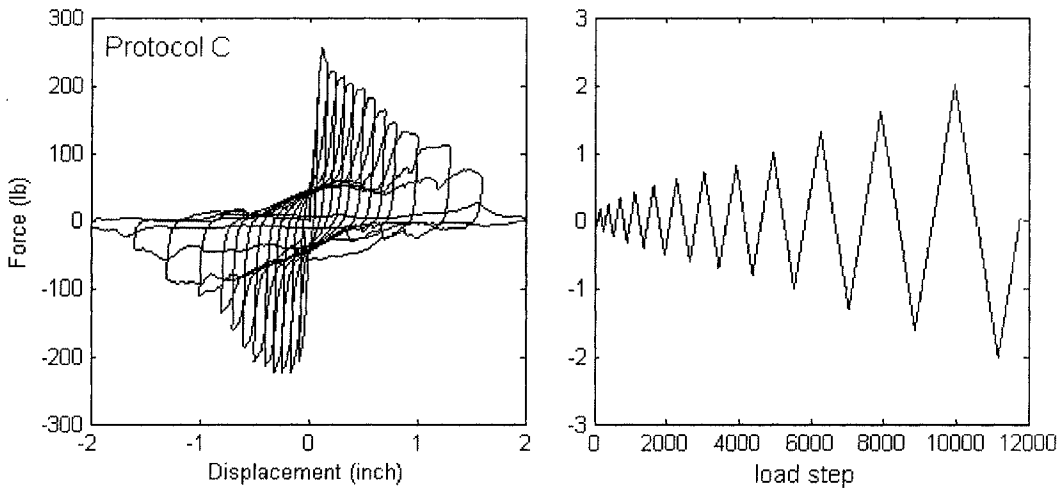

Figure 7-6: Nail test hysteresis result using protocol C (8d common)

For a traditional wood shearwall, the framing members will be setup first with the openings, i.e. windows and doors. Then the sheathing panels, either OSB or GWB, will be cut around the opening and attached to the frame using nails and screws. The position and size of openings on the wall will affect the behavior of the walls. Although the SAPWood-NP model has the ability to construct and analyze detailed wall models with openings and irregular nail schedules, detailed modeling for every wall components in the index buildings was not necessary because such a level of details in the structural model is not compatible with the accuracy of other information (fragility and seismic information) used in simulations. Furthermore, most of the details in woodframe structures are not likely to be decided at the time of loss analysis, especially during loss based design. An alternative way to obtain wall parameters is to consider only the solid shearwall and partition wall segments and use a standard wall parameter database developed using the test nail parameters and NP model. The length of these solid wall segments could be used to perform interpolation between the

standard length wall parameters readily calculated in a parameter database. This was the procedure used in the examples in this study.

To establish the wall parameter database, the shearwall models were built for nail schedules including 2/12, 3/12, 4/12, 6/12, and 12/12. The notation 2/12 stands for 2 inch nail spacing along the edges and 12 inch spacing for field (interior stud) nails, and was similar for other patterns. This list of combinations covered most of the commonly used nailing patterns in residential wood frame construction. Each schedule was repeated for 8d common and 10d common nails. For each combination of nail type and schedule, 5 types of wall length were analyzed, including 1 ft, 2 ft, 4 ft, 8 ft, and 12 ft. All of these standard wall models were solid walls using a 16 inch stud spacing. Figure 7-7 shows the layout of the panels for some of the wall segments of different lengths. A portion of the parameters for the walls in the database are listed in Table 7-2 (The complete parameter database used in this analysis could be found in the distribution package of SAPWood program).

Table 7-2: Shearwall parameters in the wall parameter database

Nail	Pattern	K_0	F_0	r_1	x_u	r_2	x_{u1}	λ_b	F_c
8d	2/12	56870	15890	0.01	1.32	-0.08	1.84	-0.7	2648
	6/12	20840	5000	0.01	1.4	-0.02	1.8	-1	875.5
10d	2/12	66490	15280	0.01	1.11	-0.15	1.532	-2	2547
	6/12	32210	5218	0.01	0.9	-0.08	1.58	-1.4	769.6
Nail	Pattern	F_r	x_{F1}	x_{F2}	λ_F	λ_k	K_r	β	F_{ur}
8d	2/12	132.4	0.66	2.584	-0.5	-1.6	0.0001	1.1	176.5
	6/12	50	0.7	1.68	-0.3	-1.5	0.0001	1.1	58.36
10d	2/12	127.4	0.555	1.232	-0.5	-2.5	0.0001	1.1	169.8
	6/12	43.48	0.45	1.8	-0.5	-2	0.0001	1.1	57.97

* The units for parameters: K_0 (lb/inch), F_0 , F_c , F_r, and F_{ur} (lb), x_u , x_{u1} , x_{F1} , and x_{F2} (inch), all other parameters are dimensionless

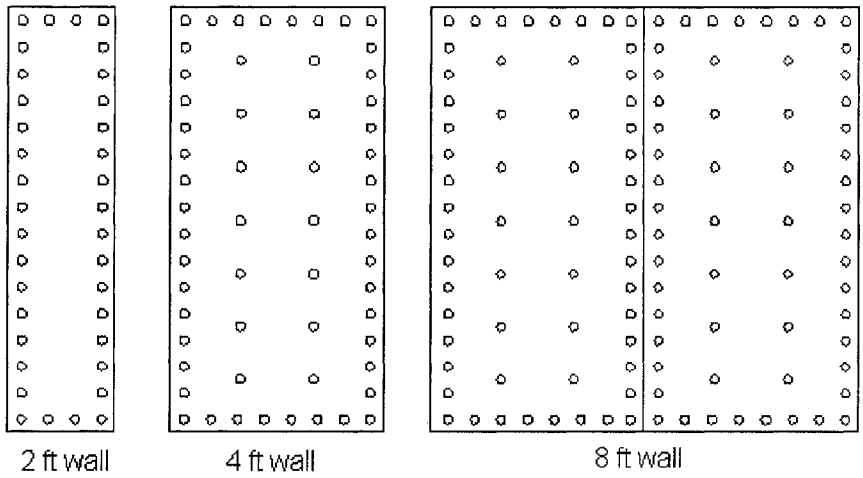

Figure 7-7: Standard wall nailing pattern used in wall parameter database

With this parameter database ready, the parameters for walls with the same schedule and nail type can be estimated based on the length of wall segments. It was assumed in this study that the wall parameters could be linearly interpolated based on wall length for walls less than 12 ft. The parameters for wall longer than 12 ft were obtained by superposition of wall segments under 12 ft. When superimposing wall parameters, the stiffness and strength related parameters (such as K_0 and F_0) were added together, while the ductility related parameters (such as X_u) were taken as the minimum value among the walls to be imposed. This assumption sacrifices some level of accuracy in exchange for a very substantial reduction of effort in finding the hysteretic wall parameters, but is felt to be consistent with or exceeding accuracy in practice. It was extremely useful during the design stage when the detailed schedule of walls remains unknown. A module in SAPWood was designed to perform the interpolation and superimposing of parameters given wall length. This automated tool makes it possible for practicing engineers to perform nonlinear hysteretic analysis without the need for

SAPWood-NP modeling of shearwalls. However, in the final design check prior to construction, a detailed model should be constructed to verify the structural performance predicted with the simplified procedure. The nailing patterns used for all shearwalls in index building A and B were assumed to be 6/12 in this study for illustrative purposes.

Partition walls (GWB sheathed walls)

In the modeling of index building A and B, the contribution of interior partition walls which were sheathed with GWB was considered. Due to the lack of test data on the dry wall screws, it is hard to construct a parameter database for dry wall component as was done for shearwalls. The parameter for drywall in the analysis were obtained through a linear model established based on a set of parameters for an 8 ft x 8 ft GWB wall obtained by Filiatrault et.al. (2001) (listed in Table 7-3) from a group of wall tests. The stiffness and strength of the drywall (GWB) were assumed to be proportional to the length of the wall segment. The CUREE ten parameter model was used because (1) the available parameters were in this format; and (2) the degradation of GWB is very sudden and the parameters do not necessarily evolve during the simulation, i.e. no need for the EPHM. It was assumed that the initial stiffness (K_0) and ultimate capacity (F_0) of the wall is proportional to the length of the wall; and the yielding drift (X_u) is proportional to the inverse of the length of the wall. This assumption limited the use of the parameters obtained to a limited range around the

tested wall specimen length. But this is assumed to be accurate enough for the purpose of this study.

Table 7-3: CUREE parameter for 8 ft by 8 ft GWB wall model

Parameter*	K_0	F_0	F_1	r_1	r_2	r_3	r_4	x_u	α	β
Value	14846	800	179.8	0.029	-0.017	1	0.005	0.9449	0.8	1.1

* The units for parameters: K_0 (lb/inch), F_0 and F_1 (lb), x_u (inch), all other parameters are dimensionless

Steel and concrete columns

Index building C contains steel and concrete columns in the first and second story. This mixture of different structural components is quite common in modern mid-rise woodframe construction due to the limitation in the compressive strength of woodframe dimension lumber, i.e. ability to carry gravity load and still leave ample space for plumbing and electrical throughout the walls. Since the spring elements in SAPWood are all one dimensional, each column was modeled using 2 bi-linear spring elements set perpendicular to one other. The parameters for the columns were estimated from the cross section and length of the column with the boundary condition at the ends of the column assumed to be "fixed-fixed". Although this assumption might overestimate the stiffness of the columns, the additional stiffness could partially make up the stiffness provided by the non-structural components in this building (due to the lack of information, the GWB partition walls in index building C were not included in the illustrative model). The parameters used for each type of steel column cross section were listed in Table 7-4.

Table 7-4: Steel column bilinear parameters in the model

Section	Length (ft)	K0 (lb/in)	Ky (lb/in)	Dy (in)
TS5x5x5/16	10.7	3080	308	1.38
TS6x6x5/16	10.7	5560	556	1.14
TS10x10x5/16	10.7	27883	2788	0.69

Seismic mass

Effective mass during seismic analysis of a structure typically consists of the dead load and part of the contents inside the building. It is important for woodframe buildings to take into account the additional mass from contents since the dead load of the structure itself is relatively low compared to the concrete and steel structures. In this study, calculation of the seismic mass for index building A and B considered the weight of roof, floor system, shearwalls, and contents. The weight calculation was based on the estimated material weight, total floor area, and shear wall length. The seismic masses for index building C were taken as the design seismic weight values used in the original design calculation of the building, which was 24 psf for roof and 45 psf for office floors. The summary of the weight (seismic mass) calculation was listed in Table 7-5.

Table 7-5: Seismic mass for index buildings

Building	Story	Weight/Area (lb/ft2)	Area (ft2)	Total Weight (kips)
A	1	43	1400	60
B	1	52	819	43
	2	48	672	33
C	1	45	11458	516
	2	45	10972	494
	3	45	10972	494
	4	24	9514	228

Response-loss modeling (Damage fragilities)

Only five types of damageable elements (component) were considered in this study. These components included shearwalls, partition walls, doors and windows, structural columns, and general contents. This is certainly not a comprehensive list of sources for seismic induced loss since other damageable components such as the floor system, paint, ceiling, sewer system, and electronic systems could also contribute to the financial loss during earthquakes. However, the number of components included in the analysis would not affect the procedures and methods used in these illustrative examples. Since loss-based design is a new concept that had only been studied since the 1990's, there has been no systematic experiment conducted on most of these components to address the relationship between their losses and seismic response to this point. Theoretically, a series of response-loss experiments could be conducted to obtain test data usable for the modeling of damage fragility. Firstly, the damage levels for components must be defined and the dynamic structural response (drift, acceleration, energy dissipation, twisting angle etc.) that directly lead to this damage must be identified. Then the specimen can be loaded with this type of response (dynamically or statically) until the desired damage level is observed. The response at this point can be recorded and the cost to restore this damage should be calculated. By repeating this procedure for a large amount of specimens, two sample pools can be established from the tests: the first one is the response samples given damage level; the second one is the cost samples given damage level. The conditional distribution models for the damage fragility can be established using these data points.

The damage fragility data used in this study came from a series of test performed during the CUREE-Caltech woodframe research project. The results from all these loss-related tests were summarized in Porter et al (2001). The damageable components covered in these tests include: stucco, drywall partition walls and ceiling, OSB sheathed shearwalls, windows, and water heaters. The test results used in this study include the partition wall test results from McMullin which was reorganized into 3 damage levels in the CUREE report; OSB sheathed shearwall test results from Pardoen, which was associated with 2 damage levels; and window damage tests by Pantelides et al. and Behr et al. The results from these tests were summarized in Table 7-6. Notice that the original data points in these tests are not available; the fitted distribution parameters from these tests were listed instead.

Table 7-6: Summary of damage-response available test data

Component	Response	damage stage		
sheawall	Drift (inch)	LS1	LS2	
	mean	1.49	2.39	
	std	0.24	0.48	
GWB	Drift (inch)	LS1	LS2	LS3
	mean	0.25	0.4	1.6
	std	0.13	0.21	0.32
Window	Drift (inch)	Break		
	mean	3		
	std	0.89		
Water Heater	PGA (g)	Overturn		
	mean	0.61		
	std	0.23		

Because these tests were conducted by different individuals and institutions, the definition of the damage levels used in these tests are, of course, not exactly the same with the four damage states used in this analysis. Subjective assumptions were made in order to use the information from these tests. For example, the two damage levels

used in the OSB shearwall test were assumed to be equivalent to the damage level (II) and (IV) in the loss analysis, the statistics for level (I) and (III) were then calculated from linear interpolation. The final fragility information used in the analysis was listed in Table 7-7. The information on acceleration-sensitive general contents was estimated based on the calculation for the water heater overturning study in the CUREE Caltech Woodframe Project.

Table 7-7: Damage-response information used in the examples

Component	Sensitive type	Response*	Damage level			
			I	II	III	IV
GWB	Displacement	Mean	0.1	0.25	0.4	1.6
		Std	0.05	0.13	0.21	0.32
shearwall		Mean	1.04	1.49	1.94	2.39
		Std	0.24	0.24	0.36	0.48
Door/window		Mean	1	2	2.5	3
		std	0.4	0.7	0.8	0.89
Contents	Acceleration	mean	0.1	0.35	0.61	1
		std	0.05	0.15	0.23	0.3

*The unit for responses for displacement sensitive components is inch; unit for acceleration is gravity.

In this study, Bayesian models were used for conditional distributions of responses given damage levels. a lognormal likelihood function was used with uniform priors for both the mean and standard deviation as was discussed in Chapter 3. The priors used for the response distributions were listed in Table 7-8.

Table 7-8: Uniform priors boundaries for structural response distribution given damage level

Component	Damage level	Non-detectable (I)	Repairable (II)	Borderline repairable (III)	Not-repairable /Replace (IV)
Shearwall (Displacement)	Mean	[0%, 2%]	[0.5%, 2.5%]	[1%, 3%]	[2%, 5%]
	Std	[0%, 2%]			
Drywall and Door/Window (Displacement)	Mean	[0%, 1%]	[0%, 2%]	[0.5%, 2.5%]	[1%, 3%]
	Std	[0%, 1%]			
Contents (Acceleration)	Mean	[0%, 20%]	[10%, 50%]	[20%, 80%]	[40%, 100%]
	Std	[10%, 30%]			

All conditional cost distributions were established using normalized cost, which is calculated by dividing the actual repair cost by the replacement cost of the component. So the normalized cost of a component is always a value between 0 and 1. This setup is based on the assumption that the cost of repair for a certain level of damage is smaller than the cost to demolish and replace the damaged component with a new one. The benefit of adopting such a configuration is that the distribution of cost conditional on damage can be treated independently from the actual cost of specific components. The priors for cost fragilities used in this study are listed in Table 7-9.

Table 7-9: Normalized cost priors

All Components	damage level	Non-detectable (I)	Repairable (II)	Borderline repairable (III)	Not-repairable /Replace (IV)
Normalized Cost	Mean	Const=0	(0.1, 0.5)	(0.2, 0.8)	(0.8, 1]
	Std	N/A		(0, 0.3)	

With the conditional distribution of normalized loss given the damage level, normalized loss can be generated for each component once the damage level of the component is assigned based on response. However, one still needs to know the actual cost of replacing the component to calculate the dollar loss from normalized loss. All of the replacement costs used in this study are approximate values based on assumptions and existing literature/studies. In the appendix of Porter et al (2001), estimation for the unit price for replacing and repairing shearwall, drywall, and window components was listed. These values were directly adopted in the estimation of corresponding components in the index buildings. The unit cost of doors, columns, and general contents were arbitrarily assigned based on experience. The final values adopted in the analysis are list in Table 7-10.

Table 7-10: Replacement cost data from CUREE report

Component	Shearwall	Drywall	Door	Window
Units	5.9 m^2 (64 ft^2)	5.9 m^2 (64 ft^2)	each	0.9 x 1.2 m (3 x 4 ft)
Replacement cost ($)*	742	445	190	149

* Cost data obtained from CUREE report: Improved loss estimation, Porter, 2001

Seismic uncertainty

It was assumed in this framework that seismic uncertainty is site-specific, which means the earthquake occurrence rate, ground motion, and intensity distribution should be modeled based on site information. For the loss analysis performed in this Chapter, the site of interest was chosen to be San Francisco and surrounding areas.

Firstly, an earthquake catalog search (Northern California Seismic Network database) was conducted for an approximately 50km x 50km rectangular region centered at San Francisco city in order to find out the total number of earthquakes experienced in this region from 1970 to 2005. Only earthquakes with magnitudes greater than 3 were counted towards the total number based on the assumption that the ground motion cause by an earthquake under magnitude 3 will not cause damage to structures. The result from the search was 77 earthquakes in 35 years. This search result provided information on the occurrence time of each earthquake and could be used to update the Bayesian model for earthquake occurrence rate λ, which was established based on an exponential likelihood function. The rate parameter, which represents the expected number of earthquakes in one year (given the unit of t is in years), has a uniform prior

between 0 and 50 (for California, may be different for other region). Given 77 earthquakes over 35 years, the posterior for λ could be derived in closed form as

$$f_{\lambda}(x) \propto \lambda^{77} e^{-35\lambda} \tag{7-1}$$

The PDF of the occurrence rate parameter was plotted in Figure 7-8.

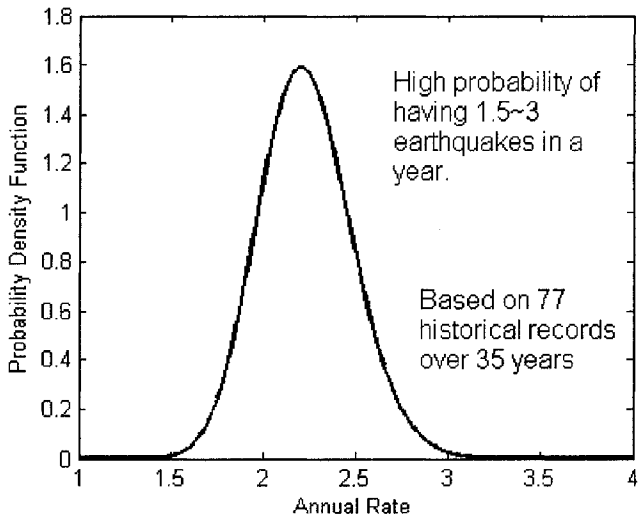

Figure 7-8: Annual earthquake occurrence rate distribution.

Using the procedure discussed in Chapter 3, the hazard curve data for the San Francisco, CA area from the USGS website is used to calculate the intensity distribution given occurrence rate. The spectral acceleration at 0.2 seconds and 5% damping was used as the intensity indicator. Figure 7-9 showed both the original hazard curve and the CDF curve derived from the intensity curve based on equations 3-8 and 3-9. Table 7-11 listed the CDF values for each data point on the hazard curve. The occurrence rate used in developing these curves is the median value of the occurrence rate distribution. One can see from the results that the hazard curve only

provides the information on earthquake intensities with a maximum annual PE of 0.553. As a result, the derived CDF curve is not completed, containing only the part of the CDF value greater than 0.6. However, this will not make too much difference in loss estimation since the known part of the curve already covers all the earthquake intensities that might cause damage to the structures.

Table 7-11: Hazard curve values for San Francisco

Intensity (g)	Annual PE	CDF value
5.00E-03	5.53E-01	6.3403E-01
7.50E-03	5.19E-01	6.6724E-01
1.13E-02	4.67E-01	7.1399E-01
1.69E-02	3.98E-01	7.6929E-01
2.53E-02	3.16E-01	8.2739E-01
3.80E-02	2.34E-01	8.7878E-01
5.70E-02	1.62E-01	9.1968E-01
8.54E-02	1.07E-01	9.4861E-01
1.28E-01	6.65E-02	9.6875E-01
1.92E-01	3.93E-02	9.8181E-01
2.88E-01	2.25E-02	9.8962E-01
4.32E-01	1.30E-02	9.9402E-01
6.49E-01	7.81E-03	9.9646E-01
9.73E-01	4.66E-03	9.9786E-01
1.46E+00	2.47E-03	9.9890E-01
2.19E+00	1.02E-03	9.9951E-01
3.28E+00	2.94E-04	9.9988E-01
4.92E+00	5.29E-05	9.9994E-01
7.38E+00	5.05E-06	9.9997E-01

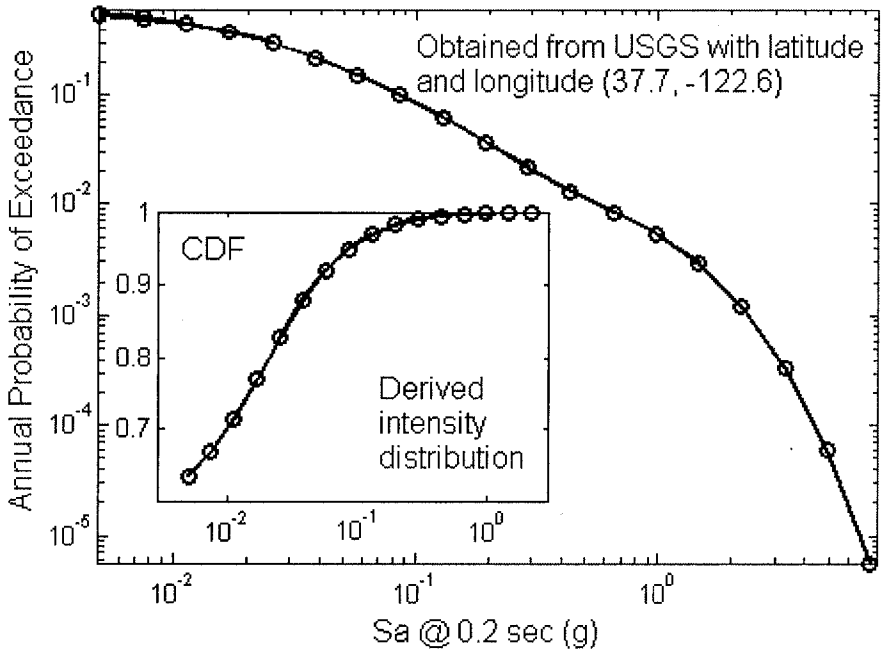

Figure 7-9. Hazard curve for S.F area and derived intensity CDF

As for ground motion records, a suite of 20 earthquake records was used for the loss analysis. These records were first collected and scaled by Krawinkler et al. (2000). Table 7-12 provides a list of the 20 earthquakes in the suite, with the scaled peak ground motion corresponding to the three hazard levels defined in FEMA356 (2000), namely the Immediate Occupancy (IO), Life Safety (LS), and Collapse Prevention (CP) levels. These records are only the ground motion in one direction. In order to perform bi-axial analysis in this study, the ground motions were applied in both directions of the models simultaneously.

Table 7-12: Suite of earthquake records used

Earthquake Event & Year	File	Station	Peak Ground Acceleration(g)		
			IO	LS	CP
Superstition Hills(1987)	SUP1	Brawley	0.264	0.604	0.985
	SUP2	El Centro Imperial County Center	0.255	0.584	0.973
	SUP3	Plaster City	0.174	0.398	0.643
Northridge (1994)	NOR2	Beverly Hills 14145 Mulhol	0.205	0.470	0.759
	NOR3	Canoga Park – Topanga Canyon	0.261	0.599	0.967
	NOR4	Glendale – Las Palmas	0.206	0.472	0.762
	NOR5	LA – Hollywood Storage	0.210	0.482	0.778
	NOR6	LA – (North) Faring Road	0.266	0.609	0.84
	NOR9	North Hollywood – Coldwater	0.212	0.485	0.783
	NOR10	Sunland – Mt Gleason Ave	0.206	0.472	0.762
Loma Prieta (1989)	LP1	Capitola	0.185	0.423	0.683
	LP2	Gilroy Array #3	0.206	0.473	0.764
	LP3	Gilroy Array #4	0.227	0.520	0.840
	LP4	Gilroy Array #7	0.179	0.410	0.662
	LP5	Hollister Differential Array	0.181	0.415	0.670
	LP6	Saratoga – West Valley	0.262	0.600	0.969
Cape Mendocino (1992)	CM1	Fortuna Boulevard	0.231	0.530	0.856
	CM2	Rio Dell Overpass	0.232	0.532	0.859
Landers (1992)	LAN1	Desert Hot Springs	0.237	0.542	0.875
	LAN2	Yermo Fire Station	0.174	0.399	0.644

7.3 Loss Analysis for Index Buildings

Before running the simulations to find loss fragilities with multiple earthquakes and randomized structural sample models, it is very helpful to first perform incremental dynamic analysis on the structural models. By increasing the seismic intensity gradually, the collapse intensity of the building can be identified when the model becomes unstable numerically (yielding unrealistic responses). This information will be useful in determining the upper bounds for the intensity levels used in the loss analysis by identifying the point at which numerical collapse of the building occurs, single the earthquake loss of any structure will converge to the collapse loss which is the loss caused by the collapse of the entire structure. This loss was taken as the

summation of the maximum losses for all damageable components in this study for illustration. It was determined from the analysis that all of the index building models will become unstable (collapse) after spectral acceleration exceeds 4g, which is quite logical as this is far beyond the maximum credible earthquake (MCE). Thus, the vulnerability analysis will be conducted within the range below 4 g.

Vulnerability analysis (Single earthquake loss simulation)

The index building vulnerability analyses were carried out with different construction qualities defined in Chapter 3 (this was also done for isolated shearwalls by Rosowsky and Kim, 2004), however only the superior quality results were presented in this section. The effects of different construction qualities will be discussed later in the sensitivity analysis of Chapter 8. In the vulnerability simulation, ten sample structures within the superior quality category (statistical distribution) are generated, then each of these models was subjected to a suite of 20 ground motions scaled to increasing intensity levels (from 0.05g to 4g). Following each nonlinear time domain analysis, the response of each damageable component was gathered and 50 repair cost samples were generated based on the fragility information for every component in the structure. Thus a total of 10,000 single earthquake loss samples were generated at each intensity level. This limited sample size may not be able to reflect all of the characteristics of the single earthquake loss distribution; it is assumed to be an accurate representation of the loss distribution for the illustrative purpose of this study. As was mentioned in Chapter 3, the single earthquake samples were characterized with a four parameter model. Zero loss probability, Pr_0, was obtained by calculating

the ratio of 0 value sample number to the total sample number. Collapse probability Pr_c was calculated based on the number of samples with values greater than 95% of the collapse loss. The other two parameters which control the lognormal distribution in between were obtained by fitting the rest of the samples to a lognormal distribution. The parameter and basic statistics of the simulated data are listed in Table 7-13, 7-14, and 7-15 for index building A, B, and C, respectively. The mean and standard deviation calculated from all of the samples (including 0 and collapse loss) were also listed in the tables.

Table 7-13: Vulnerability parameter and statistics for building A (collapse loss=$67,812)

Intensity	μ_{ln}	σ_{ln}	Pr_0	Pr_c	Mean	Std
0.05	4.82	1.06	0.871	0.000	$27	$165
0.10	5.08	1.26	0.217	0.000	$444	$2,389
0.20	6.58	1.37	0.007	0.000	$2,224	$5,095
0.30	7.54	1.42	0.001	0.000	$4,955	$7,644
0.40	8.26	1.31	0.000	0.000	$7,792	$8,777
0.50	8.66	1.17	0.000	0.050	$12,788	$15,424
0.60	9.00	1.04	0.000	0.050	$14,924	$15,238
0.70	9.24	0.94	0.000	0.100	$19,638	$18,528
0.80	9.40	0.89	0.000	0.185	$25,591	$21,938
0.90	9.58	0.82	0.000	0.215	$28,955	$22,170
1.00	9.68	0.82	0.000	0.325	$35,377	$23,753
1.10	9.79	0.78	0.000	0.400	$39,886	$23,792
1.20	9.87	0.77	0.000	0.475	$44,000	$23,306
1.30	9.97	0.66	0.000	0.531	$47,053	$22,352
1.40	10.06	0.68	0.000	0.512	$47,482	$21,604
1.50	10.08	0.64	0.000	0.616	$51,465	$20,556
1.60	10.12	0.61	0.000	0.650	$52,960	$19,607
1.80	10.27	0.52	0.000	0.745	$57,394	$16,336
2.00	10.34	0.44	0.000	0.800	$59,604	$14,121
2.20	10.41	0.44	0.000	0.850	$61,550	$11,927
2.60	10.61	0.36	0.000	0.850	$62,589	$9,566
3.00	10.63	0.38	0.000	0.900	$63,836	$7,865
3.50	10.68	0.28	0.000	0.950	$65,042	$5,234
4.00	10.68	0.33	0.000	0.950	$65,069	$5,308

Table 7-14: Vulnerability parameter and statistics for building B (collapse cost=$75,775)

Intensity	$\mu_{\ln}$	$\sigma_{\ln}$	$\Pr_0$	$\Pr_c$	Mean	Std
0.05	5.04	1.03	0.458	0.000	$146	$484
0.10	6.02	1.09	0.053	0.000	$777	$1,739
0.20	7.33	1.27	0.002	0.000	$3,298	$4,598
0.30	8.23	1.12	0.000	0.000	$6,458	$6,547
0.40	8.82	0.98	0.000	0.000	$9,791	$7,532
0.50	9.13	0.82	0.000	0.050	$15,048	$15,442
0.60	9.36	0.72	0.000	0.150	$23,094	$22,557
0.70	9.56	0.64	0.000	0.200	$28,138	$24,209
0.80	9.67	0.60	0.000	0.324	$36,505	$27,149
0.90	9.80	0.59	0.000	0.314	$37,631	$26,099
1.00	9.90	0.53	0.000	0.389	$42,432	$26,347
1.10	9.96	0.50	0.000	0.454	$46,456	$26,116
1.20	10.00	0.50	0.000	0.583	$53,327	$25,300
1.30	10.06	0.48	0.000	0.593	$54,415	$24,570
1.40	10.05	0.46	0.000	0.648	$56,916	$23,859
1.50	10.16	0.42	0.000	0.648	$57,766	$22,788
1.60	10.21	0.44	0.000	0.664	$59,004	$21,893
1.80	10.34	0.37	0.000	0.693	$61,346	$19,805
2.00	10.34	0.40	0.000	0.828	$66,952	$16,086
2.20	10.37	0.42	0.000	0.847	$67,870	$14,921
2.60	10.48	0.35	0.000	0.847	$68,413	$13,688
3.00	10.53	0.29	0.000	0.877	$69,689	$11,926
3.50	10.60	0.26	0.000	0.892	$70,452	$10,506
4.00	10.57	0.22	0.000	0.947	$72,158	$7,767

Table 7-15: Vulnerability parameter and statistics for building C (collapse cost=$1,413,543)

Intensity	$\mu_{\ln}$	$\sigma_{\ln}$	$\Pr_0$	$\Pr_c$	Mean	Std
0.05	10.59	0.77	0.934	0.000	$3,416	$16,805
0.10	10.79	0.82	0.674	0.000	$21,577	$44,826
0.20	11.16	0.89	0.273	0.000	$72,369	$83,811
0.30	11.47	0.92	0.095	0.000	$121,926	$108,602
0.40	11.68	0.87	0.044	0.050	$212,897	$289,647
0.50	11.92	0.85	0.016	0.050	$251,951	$287,902
0.60	12.19	0.79	0.007	0.100	$358,231	$369,635
0.70	12.34	0.67	0.003	0.200	$490,980	$460,692
0.80	12.49	0.70	0.001	0.300	$631,008	$504,551
0.90	12.47	0.59	0.000	0.550	$892,404	$546,022
1.00	12.54	0.54	0.000	0.600	$951,739	$529,682
1.10	12.73	0.59	0.000	0.600	$977,230	$500,321
1.20	12.83	0.67	0.000	0.750	$1,138,105	$424,280
1.30	13.18	0.58	0.000	0.750	$1,181,719	$359,610
1.40	13.26	0.55	0.000	0.750	$1,191,188	$345,128
1.50	12.94	0.49	0.000	0.900	$1,285,950	$282,903
1.60	13.11	0.39	0.000	0.850	$1,251,057	$311,493
1.80	13.15	0.32	0.000	0.900	$1,294,146	$258,212
2.00	13.22	0.28	0.000	0.900	$1,296,817	$246,964
2.20	13.34	0.27	0.000	0.900	$1,304,972	$226,591
2.60	13.42	0.22	0.000	0.950	$1,343,656	$155,339
3.00	13.51	0.20	0.000	0.950	$1,346,606	$142,185
3.50	13.53	0.20	0.000	0.950	$1,347,666	$138,164
4.00	13.63	0.17	0.000	0.950	$1,351,364	$121,308

From the tables one can see that the probability of zero loss is quickly reduced as the seismic intensity increases. The probability of collapse keeps increasing and approaches 0.95 (the threshold value used to define collapse) as the seismic intensity increases. The sample mean value keeps increasing towards the collapse loss and the sample standard deviation decreases as it approaches the upper and lower boundary

(collapse loss and zero loss). These trends can be also be seen in the vulnerability model curves shown below.

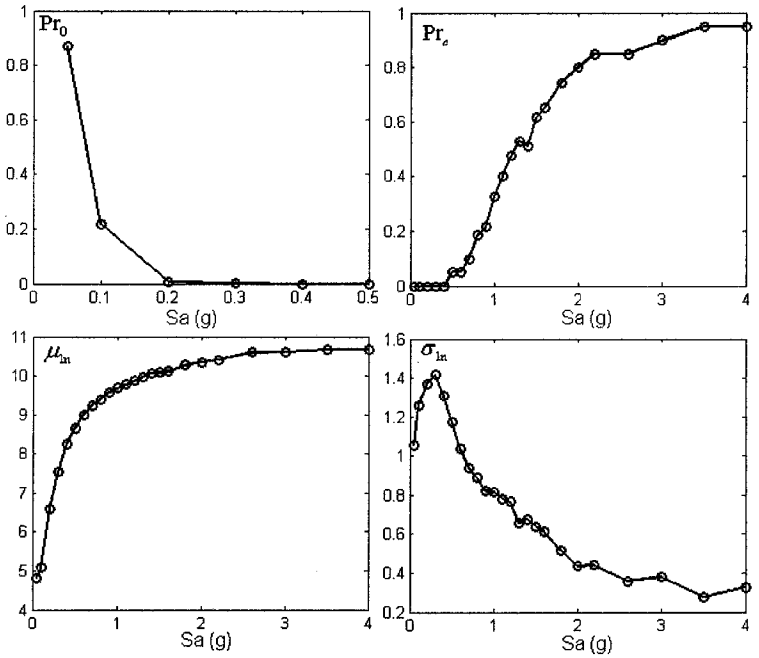

Figure 7-10: Vulnerability curves for index building A

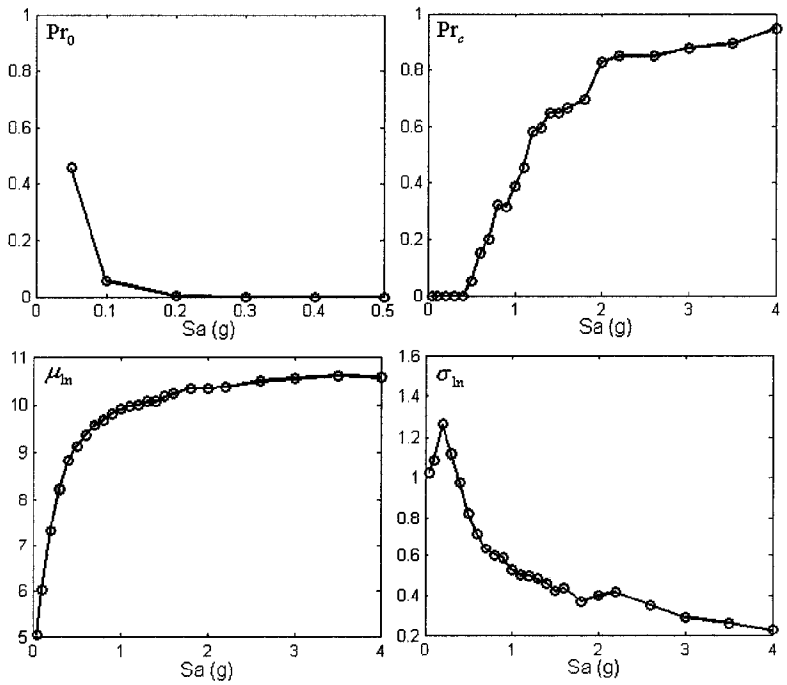

Figure 7-11: Vulnerability curves for index building B

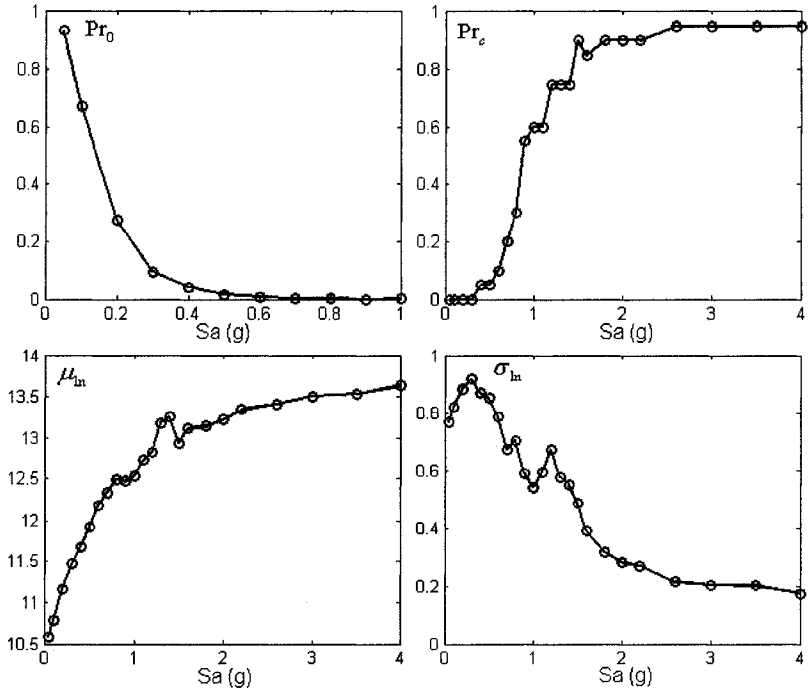

Figure 7-12: Vulnerability curves for index building C

The responses to earthquakes from different buildings are, of course, usually not the same. In order to allow a relative comparison between structures having different values, a comparison between the normalized mean losses, which are calculated by dividing the mean loss (with zero loss and collapse loss values included), by the collapse loss was conducted. Figure 7-13 shows the comparison among index buildings using the normalized mean single earthquake loss at different intensity levels. This comparison can be viewed as a preliminary representation of the building's relative loss potential against earthquakes. One can see that the single earthquake loss performance of building A and B is very close. The performance for buildings A and B were better than building C since both building A and B yield lower loss percentages at a wide range of intensity levels. A more detailed comparison on

loss behavior of different structural configurations will be conducted later in Chapter 8, as well as its impact on the long term loss.

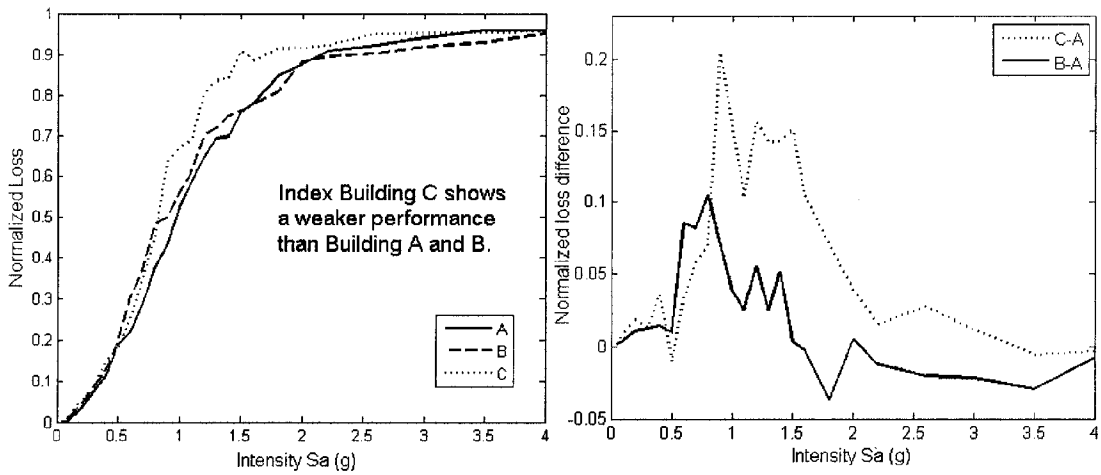

Figure 7-13: Single earthquake loss comparison for index buildings

Since the four parameters will be used later in the long term loss simulation to represent the distribution of all single earthquake loss samples at different intensity levels, it is important to confirm with simulated samples that the four parameter controlled single earthquake loss distribution model does capture the important distribution characters of the sample pool for all index buildings. A comparison between the empirical CDF curves of the data obtained through simulation and the vulnerability model curves was conducted and plotted in Figure 7-14, 7-15, and 7-16. All of the model curves were developed using vulnerability parameters listed in table 7-13, 7-14, and 7-15.

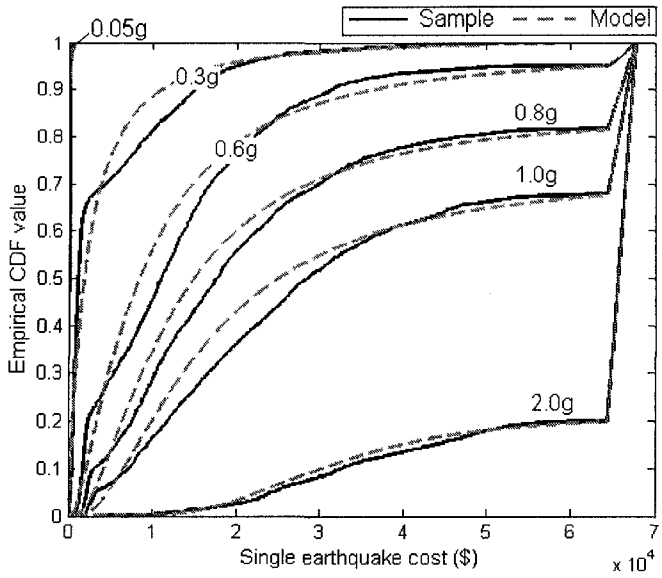

Figure 7-14: Single earthquake samples and vulnerability models for Building A

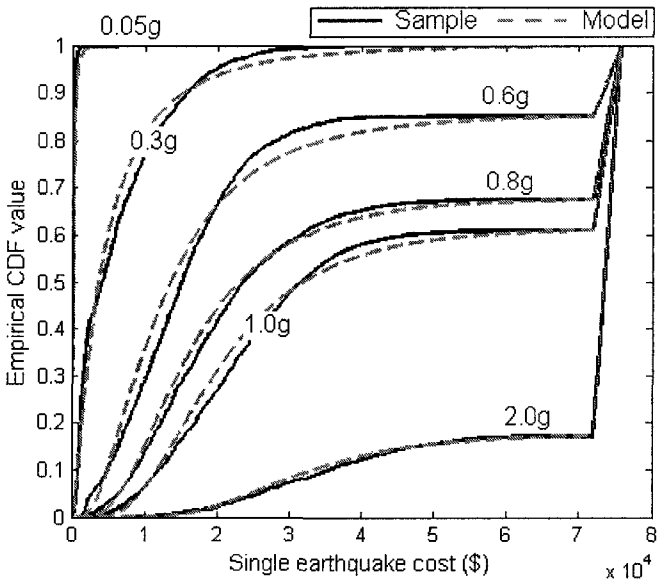

Figure 7-15: Single earthquake samples and vulnerability models for Building B

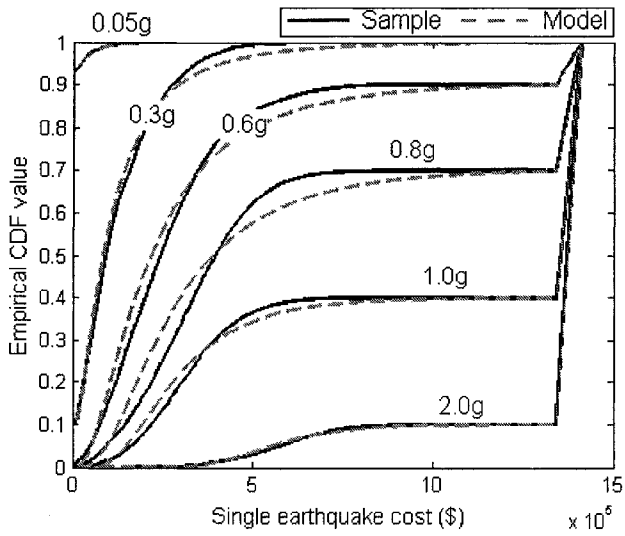

Figure 7-16: Single earthquake samples and vulnerability models for Building C

These figures showed that the single earthquake distribution model and vulnerability model used in this study accurately represented the behavior of the simulated single earthquake data. The collapse loss value can also be seen from the empirical CDF curves. However, this value is not a comprehensive representation of the total loss of the real structure after collapse because only certain types of damageable components were included in the analysis. Thus it will be more meaningful to investigate the normalized loss amount by dividing the loss value with the collapse loss in the long term loss estimation later.

Components loss behavior

SAPWood not only provides the overall loss during an earthquake simulation, it will also automatically provide the categorized total loss amount for each type of damageable component considered in the vulnerability analysis. This information can

be used to determine the "weak" components in a loss-resisting sense and develop a loss reduction strategy accordingly. Different analysis techniques could be used to study the behavior of each type of component using these categorized data. A simple indicator termed as *average loss ratio* was used in this study to compare the economical performance of these components. The *average loss ratio* of a component is calculated by dividing the average value of component loss samples by the total replacement value of that type of component. Using this indicator, components with different values can be compared directly, similar to the comparison conducted with normalized loss on buildings with different collapse loss values. The *average loss ratio* for damageable components at different intensity levels is listed in Table 7-16. This ratio was also plotted against intensity in Figure 7-17. It can be seen from the table and figure that the most vulnerable component to earthquake loading is the drywall, which accumulates damage at very low seismic intensities (Sa=0.1~0.5). This is the range of seismic intensities for the most frequently occurring earthquakes. Thus the dry wall damage is the most commonly seen damage in minor earthquakes. This conclusion agrees with the observation in post earthquake surveys and following the NEESWood benchmark experiments.

Table 7-16: Average loss ratio for different types of components

Intensity	Shearwall	GWB	Door/Window	Column	Contents
0.050	0.000	0.010	0.000	0.000	0.001
0.100	0.000	0.045	0.000	0.000	0.010
0.200	0.001	0.123	0.004	0.000	0.047
0.300	0.005	0.194	0.015	0.000	0.093
0.400	0.027	0.264	0.051	0.049	0.148
0.500	0.062	0.349	0.097	0.049	0.209
0.600	0.124	0.432	0.169	0.097	0.281
0.700	0.203	0.499	0.255	0.195	0.357
0.800	0.313	0.580	0.366	0.292	0.455
0.900	0.411	0.619	0.475	0.536	0.532
1.000	0.490	0.678	0.547	0.585	0.598
1.100	0.545	0.720	0.594	0.585	0.642
1.200	0.649	0.771	0.691	0.731	0.730
1.300	0.682	0.792	0.724	0.732	0.760
1.400	0.699	0.809	0.748	0.733	0.775
1.500	0.758	0.825	0.798	0.878	0.818
1.600	0.760	0.836	0.802	0.829	0.824
1.800	0.814	0.868	0.844	0.878	0.865
2.000	0.855	0.907	0.878	0.877	0.901
2.200	0.874	0.920	0.890	0.878	0.917
2.600	0.898	0.929	0.911	0.926	0.932
3.000	0.912	0.941	0.925	0.926	0.944
3.500	0.927	0.949	0.934	0.926	0.953
4.000	0.941	0.962	0.944	0.926	0.960

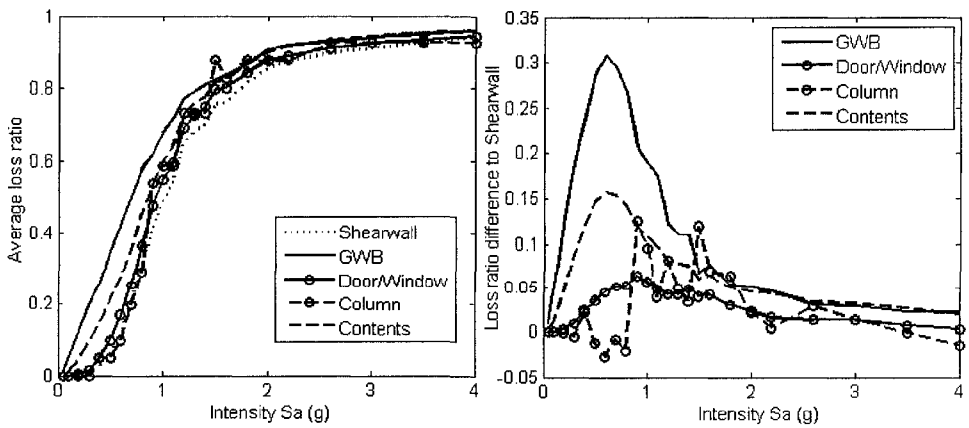

Figure 7-17: Average damage ratio for different types of components.

Long term loss analysis

Long term loss analysis on index buildings was performed once the vulnerability model was established. SAPWood will first generate the earthquake occurrence rate sample based on historical earthquake data. Then the total number of earthquakes over the given exposure period is generated from a Poisson distribution with the rate parameter just obtained. For each earthquake in the exposure period, a random intensity value is generated from the intensity distribution. This intensity value was then used to determine the four parameters that control the single earthquake loss distribution using interpolation between existing intensity values. For every intensity sample generated, a random number between 0 and 1 was used to determine the state of the structure. If the random number is smaller than Pr_0 corresponding to that intensity level indicating no damage occurred, the simulation will result in 0 loss. If the number is greater than $1-Pr_c$, the structure is assumed to have collapsed, which will yield a loss value lies between 95% and 100% of collapse loss. For other cases, the corresponding parameters for the lognormal distribution will be used to generate a loss value for that earthquake. After all earthquake in the exposure period have been considered, the loss from each of these earthquake will be added together to produce one sample of long term loss. The entire procedure will then be repeated for the desired number of long term loss samples needed, which is input by the user at the beginning of the simulation. This simulation procedure has been programmed into SAPWood to be performed automatically. The user also needs to indicate a zero-loss intensity and a collapse intensity boundary, which can usually be set as the upper and lower boundary of the intensity levels used in the vulnerability analysis. All simulated

intensities less than the zero-loss intensity will be assigned zero loss. The intensities over the collapse intensity will be assigned the collapse loss. This rule is introduced because the vulnerability model cannot provide information on the loss behavior outside the intensity range of the vulnerability analysis. Thus it is recommended for SAPWood users to extend the intensity range of the vulnerability analysis to the intensity level at which the structure will definitely fail. The time spans investigated here for long term loss include relatively short term periods (less than 10 years) and long term periods (greater than 10 years). Such data can be directly used by homeowners or management agencies in developing insurance or maintenance strategies. It also has the potential to justify the use of expensive high-end damage reduction products such as base isolation and supplemental damping systems in residential structures. The simulated long term loss data for each index building was plotted in the following figures immediately following the statistics listed in the tables. The long term loss values normalized by the collapse loss are also listed in the table.

Table 7-17: Statistics of building A long term loss samples

Time duration (year)	Zero loss probability	Probability of exceedance					
		80%	50%	10%	5%	2%	1%
1	0.847	$0	$0	$215	$1,174	$6,639	$22,570
3	0.624	$0	$0	$2,409	$8,354	$44,034	$67,035
5	0.467	$0	$62	$5,768	$19,204	$65,586	$67,067
10	0.247	$0	$486	$14,931	$51,930	$68,026	$77,643
20	0.057	$422	$3,490	$51,198	$69,276	$91,554	$125,000
50	0.000	$3,993	$16,170	$90,983	$134,620	$154,720	$170,010
75	0.000	$6,147	$24,626	$111,100	$135,650	$174,770	$196,550
		Normalized loss					
1	0.847	0.000	0.000	0.003	0.017	0.098	0.333
3	0.624	0.000	0.000	0.036	0.123	0.649	0.989
5	0.467	0.000	0.001	0.085	0.283	0.967	0.989
10	0.247	0.000	0.007	0.220	0.766	1.003	1.145
20	0.057	0.006	0.051	0.755	1.022	1.350	1.843
50	0.000	0.059	0.238	1.342	1.985	2.282	2.507
75	0.000	0.091	0.363	1.638	2.000	2.577	2.898

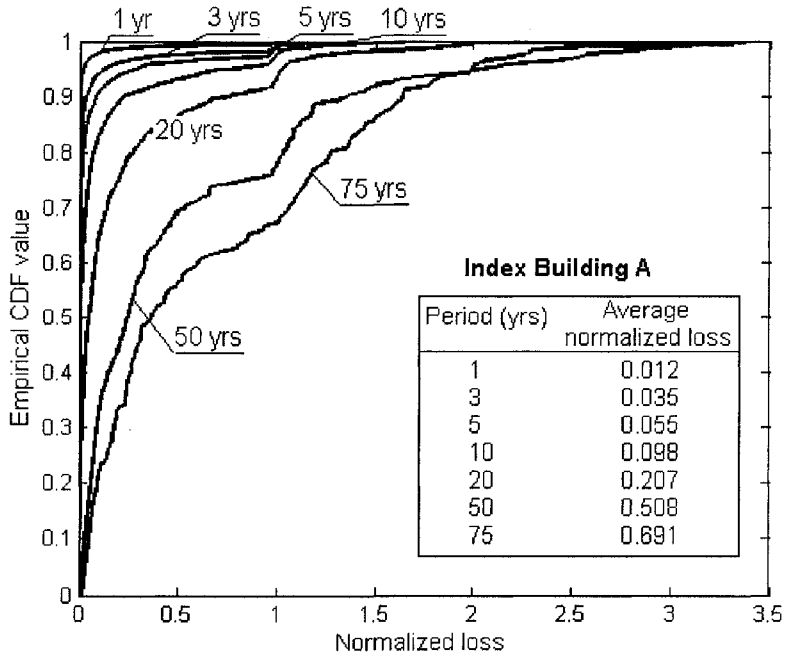

Figure 7-18: Empirical CDF curves for building A long term losses

Table 7-18: Statistics of building B long term loss samples

Time duration (year)	Zero loss probability	Probability of exceedance					
		80%	50%	10%	5%	2%	1%
1	0.797	$0	$0	$653	$2,070	$9,023	$23,506
3	0.547	$0	$0	$3,670	$10,210	$26,739	$73,561
5	0.384	$0	$241	$9,246	$22,107	$73,362	$75,132
10	0.165	$95	$1,007	$20,691	$60,508	$75,484	$79,543
20	0.031	$1,031	$5,254	$73,321	$76,378	$91,550	$104,060
50	0.000	$6,039	$21,924	$96,323	$124,010	$181,370	$200,830
75	0.000	$15,181	$35,234	$114,040	$141,150	$164,170	$217,200
		Normalized loss					
1	0.797	0.000	0.000	0.009	0.027	0.119	0.310
3	0.547	0.000	0.000	0.048	0.135	0.353	0.971
5	0.384	0.000	0.003	0.122	0.292	0.968	0.992
10	0.165	0.001	0.013	0.273	0.799	0.996	1.050
20	0.031	0.014	0.069	0.968	1.008	1.208	1.373
50	0.000	0.080	0.289	1.271	1.637	2.394	2.650
75	0.000	0.200	0.465	1.505	1.863	2.167	2.866

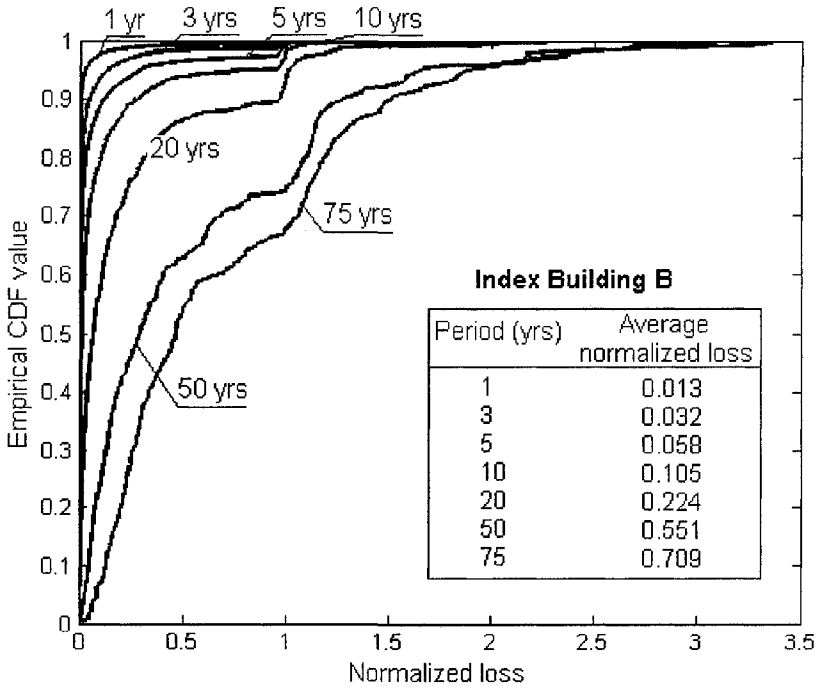

Figure 7-19: Empirical CDF curves for building B long term losses

Table 7-19: Statistics of building C long term loss samples

Time duration (year)	Zero loss probability	Probability of exceedance					
		80%	50%	10%	5%	2%	1%
1	0.902	$0	$0	$0	$77,342	$206,770	$452,480
3	0.749	$0	$0	$122,420	$294,980	$1,373,900	$1,405,900
5	0.632	$0	$0	$215,720	$500,980	$1,395,000	$1,419,000
10	0.428	$0	$36,601	$466,050	$1,378,700	$1,515,100	$1,754,800
20	0.292	$0	$97,997	$1,371,400	$1,488,000	$1,627,700	$1,779,500
50	0.057	$158,260	$409,420	$1,814,500	$2,215,900	$2,844,500	$3,128,300
75	0.005	$423,090	$994,740	$2,551,600	$3,082,900	$3,385,000	$3,478,100
		Normalized loss					
1	0.902	0.000	0.000	0.000	0.055	0.146	0.320
3	0.749	0.000	0.000	0.087	0.209	0.972	0.995
5	0.632	0.000	0.000	0.153	0.354	0.987	1.004
10	0.428	0.000	0.026	0.330	0.975	1.072	1.241
20	0.292	0.000	0.069	0.970	1.053	1.152	1.259
50	0.057	0.112	0.290	1.284	1.568	2.012	2.213
75	0.005	0.299	0.704	1.805	2.181	2.395	2.461

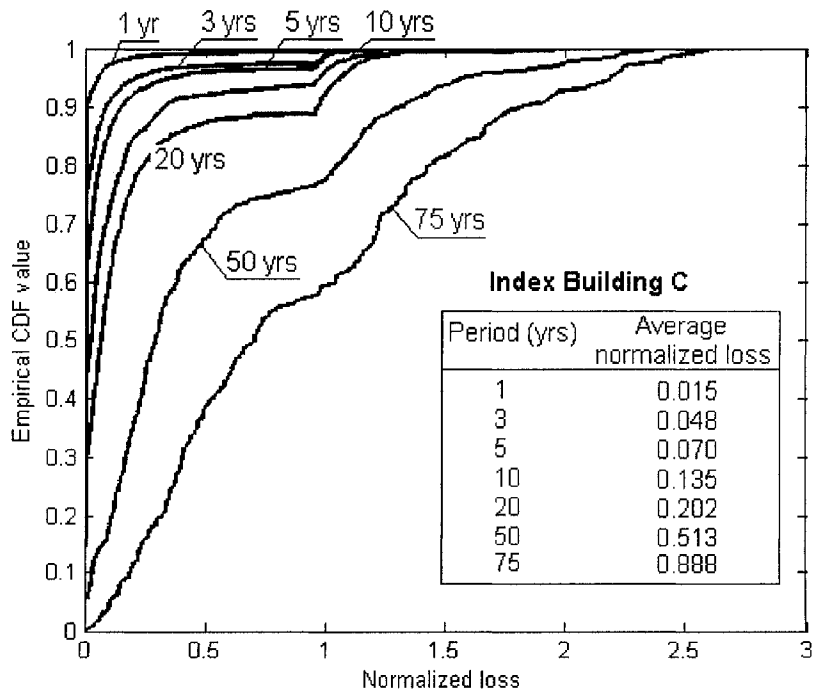

Figure 7-20: Empirical CDF curves for building C long term losses

Several conclusions can be drawn from the simulated long term loss samples. At first inspection, the behavior of the index buildings with respect to normalized loss is similar. Although the actual loss for office building is much more than single family homes, this cost is proportional to the value of the building. In a relatively short period of time (less than 5 years), it is reasonable to assume there will be no or only minor earthquakes, thus resulting in zero loss, at least in an average sense. Given the high seismic hazard near San Francisco, CA, the worst situation predicted during a home owner's lifetime (approximately 75 years) would be equivalent to the rebuild of their entire house approximately three times (only considering earthquake hazard). Apparently there are many factors contributing to the final results of the analysis. The effects of seismic hazard and structural properties will be studied in detail in the sensitivity analysis presented in Chapter 8.

7.4 Loss Based Design Examples

The loss based design procedure discussed in Chapter 5 is illustrated using index building B as an example in this section. The loss based design statements (i.e. the performance requirements) used in the example are arbitrarily assigned, but are then checked so that they will result in code-exceeding design configuration. Both type I and type II statements were designed for in the examples and the final design output was verified using the vulnerability based loss simulation.

Performance Targets

Starting from the current configuration of index building B, the loss based design example here seeks to mitigate seismic loss for the structure through the procedure introduced in Chapter 5. Initially, two loss based design cases with different performance targets were set forth as follows:

1. The structure should have loss below 75% of the collapse loss under an intensity level of Sa=1.5 g with 95% confidence level (corresponding to 5% probability of exceedance).
2. The structure should have loss below 120% of the collapse loss over 75 years with 90% confidence level in the San Francisco area.

As one compares these design statements to the current performance of the structure listed in previous sections (long term loss results and vulnerability analysis results), it is quite obvious that the current configuration failed to meet these requirements. For example, the original design of index building B has a collapse probability of 0.389 at 1.0 g spectral acceleration, which indicates that the loss corresponding to a 5% probability of exceedance will be approximately equal to the collapse loss rather than the 75% of the collapse loss as required in the design target statement above. The 75-year loss simulation results from the original index building B with San Francisco hazard data showed that the loss is about 150% of the collapse loss with a 90%

confidence level. However, this original configuration could be used as the lower boundary in the binary searching procedure.

The design target point can be directly identified from the requirement in design case 1. However, the long term loss requirement (case 2) must be represented with a target loss probability curve. Using the procedures discussed in Chapter 5, the long term loss for different collapse intensity values were calculated using San Francisco hazard data (see Figure 7-21). The target collapse intensity for the long term loss requirement is calculated to be 0.82g based on the results. Then, the loss requirements in both cases can be represented with design points and target loss probability curves as shown in Figure 7-22. It should be pointed out that the target curve for case 1 shown in the figure was just one of many curves that might satisfy the case 1 requirement. Theoretically any curve that has a loss value less than 75% collapse loss at 1.5g spectral acceleration could satisfy the loss requirement outlined in design case 1. Although the target curves correspond to different probability of exceedance values, it is quite obvious from the curves that the first design target would very likely control the design if both requirements were to be applied at the same time. However, both cases were designed for in this study for illustration and the final result for these two design targets is (and should be) different.

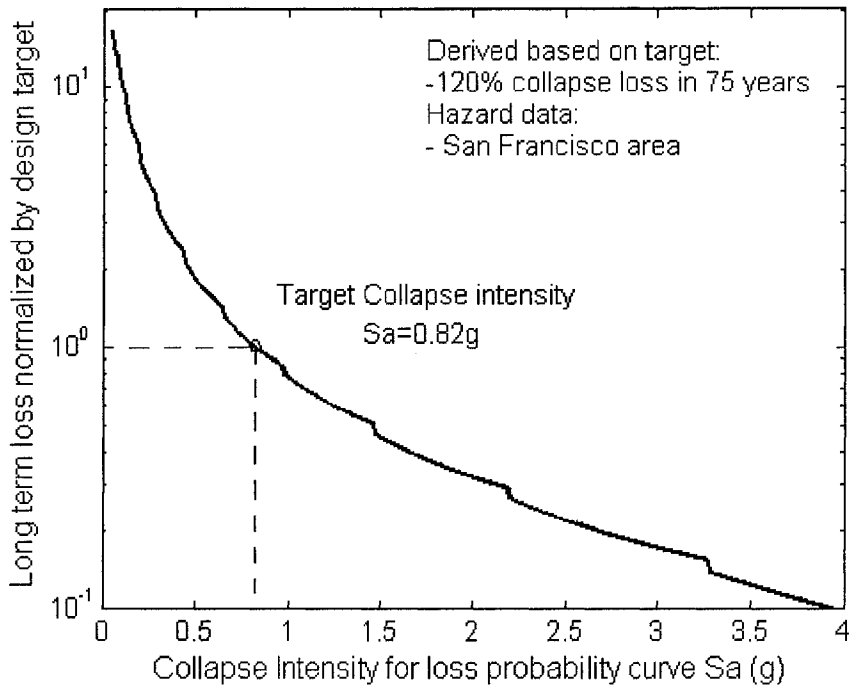

Figure 7-21: Identifying the target collapse intensity for a long term loss requirement

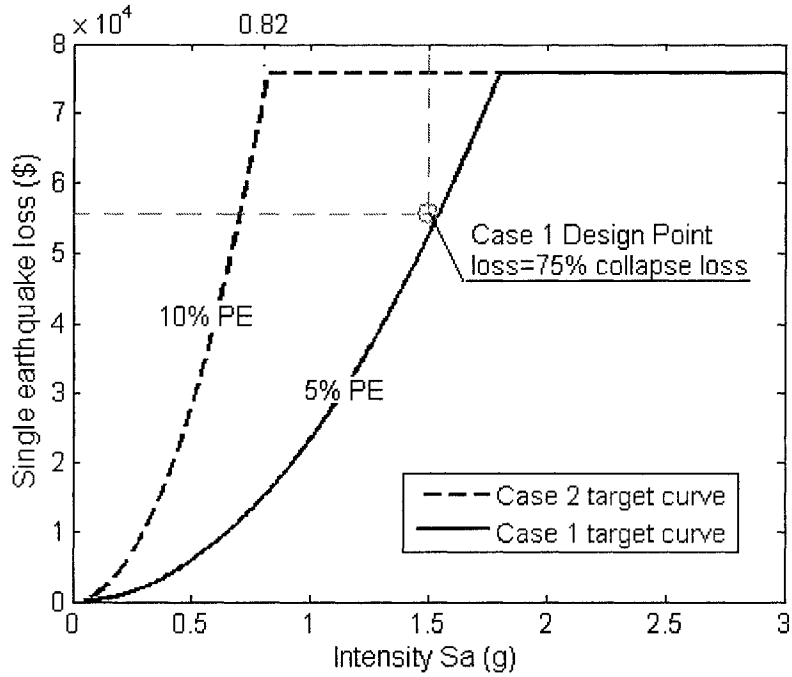

Figure 7-22: Design targets represented with loss probability curves

Structural configuration

The structure used as the design example is index building B. In order to clearly identify the modifications involved in the incremental optimization, it is necessary to assign a label and ID for each structural component so that they are easily identified and referred to during the discussion. A numbering system was introduced for the structural components (shearwalls and partition walls) of index building B for easier identification of each individual wall, as it was shown in Figure 7-23. The walls drawn with dashed lines are partition walls sheathed with GWB in the original design. If needed, partition walls could be changed to structural shearwalls to increase the strength of the building without modification of the floor plan. Other wall segments in black are the exterior shearwalls. The equivalent shearwall length could be doubled by applying sheathing panels on both sides. The nailing pattern might also be changed to provide extra strength/stiffness. Finally, if these measures fail to provide the performance desired, the windows might be removed to add in extra length of walls and a final option (not addressed in this dissertation) would be to add response modification devices such as dampers (Symans et al., 2000).

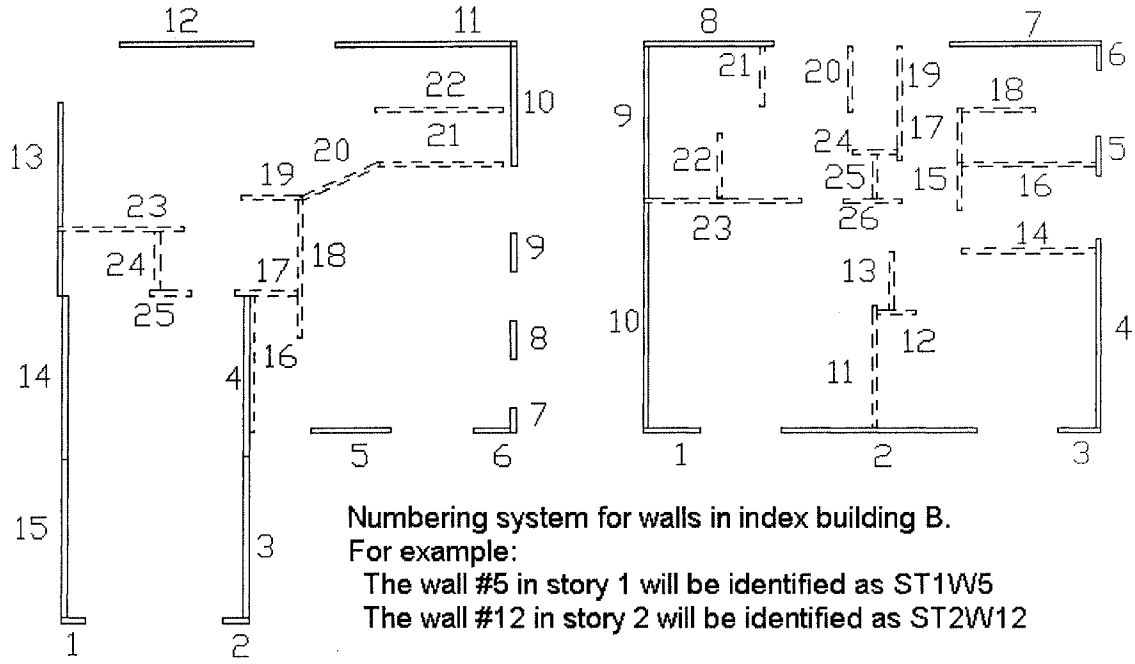

Figure 7-23: Floor plan for the design example

Binary search

A binary search procedure was introduced to the loss based design procedure to narrow down the range of incremental optimization options quickly by making modifications on a large scale, e.g. changing the nailing pattern for the entire story, etc. From the previous discussion, the "lower boundary" design for the performance target was set by using a 6/12 nailing pattern on all shearwalls. Without changing the wall length or location on the architectural floor plan, the nailing pattern for all shearwalls were modified to 2/12 as a trail case in attempt to identify a design that can exceed the performance target to serve as the "upper bound". The vulnerability analysis results from these two configurations indicates that the design using 2/12 pattern satisfied the target curve for the case 2 requirement but failed to achieve the performance in case 1. Thus one needs to continue increasing the performance of the

structure for design case 1 using additional improvement measures. Since a nail spacing less than 2 inches is not practical, the next step in trying to identify the "upper boundary" design will be to change all shearwalls into double sided walls with 2/12 nailing pattern. This design was considered first because it requires less effort in the design and construction than changing the interior walls or opening configurations. With double-sided shearwalls, the strength of the elements in the structural model was doubled. Notice this step was not necessary for design case 2 since the "upper boundary" for that case has already been identified as the structure with a 2/12 nailing schedule. The loss probability curves for 6/12, 2/12, and double-sided 2/12 configurations were plotted in Figure 7-24 and Figure 7-25 together with the design target curve/point. It is obvious from the figure that the performance target in design case 1 has been exceeded with the 2/12 double-sided design and this may serve as an upper bound in the optimization

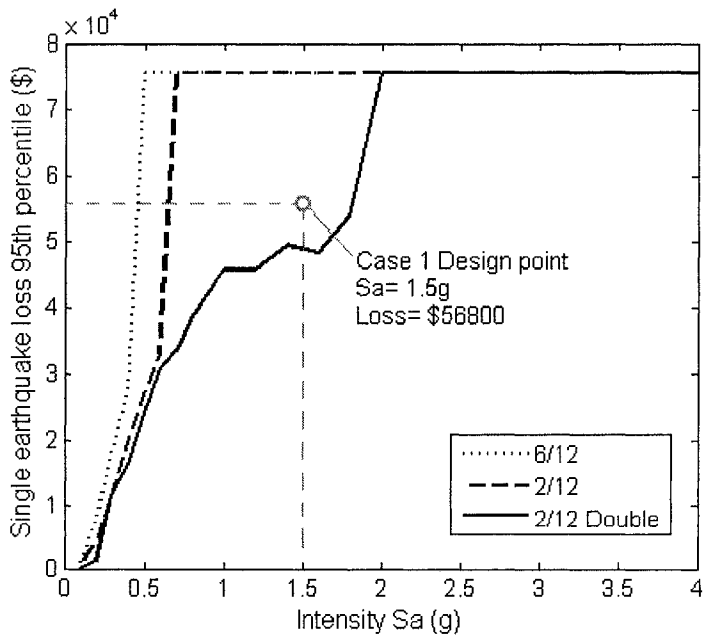

Figure 7-24: Binary search towards case 1 design target point

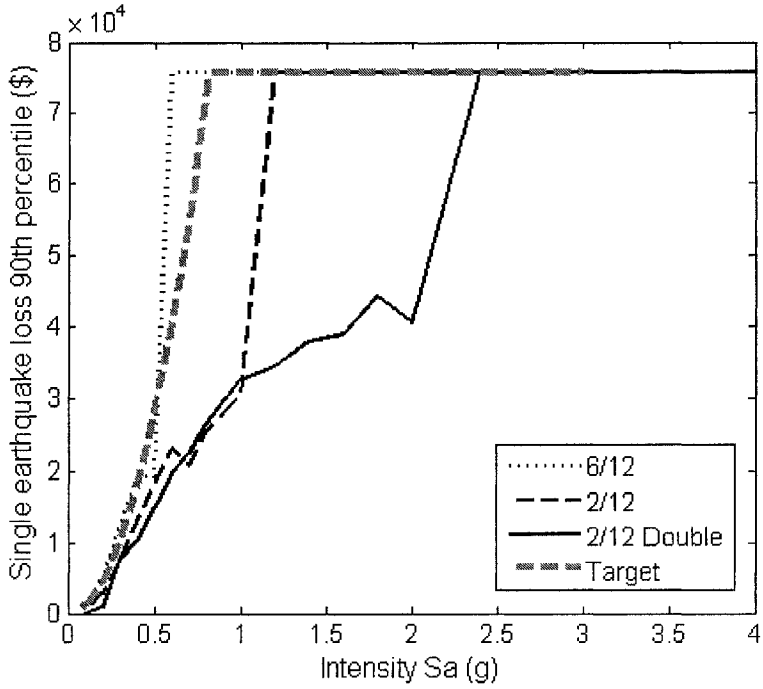

Figure 7-25: Binary search towards case 2 design target curve

The results from the first iteration of binary search indicates that the final design for case 1 will be found in between the 2/12 configuration and 2/12 double-sided configuration if only nail spacing is the design variable of interest. The configuration that satisfies the case 2 requirement should be sought between the 6/12 and 2/12 configurations. The designer may stop the binary search and choose the boundary which is closer to the design target to use as the initial design for incremental optimization. Or another trial configuration could be proposed in between the boundaries to reduce the range further. In this example, another binary search iteration for both cases was performed. For case 1, the structure with only double-sided walls in the 1st story was used as a trial configuration between the 2/12 pattern structure and

2/12 double-sided pattern structure. For case 2, the design with the 4/12 nailing pattern was investigated. The analysis results were listed in Figures 7-26 and 7-27.

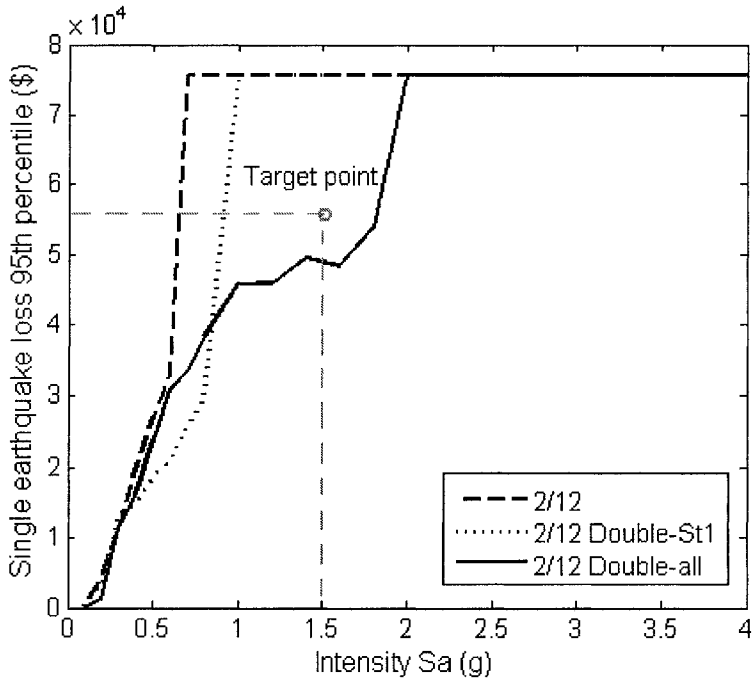

Figure 7-26: Binary search towards case 1 design target point (2nd iteration)

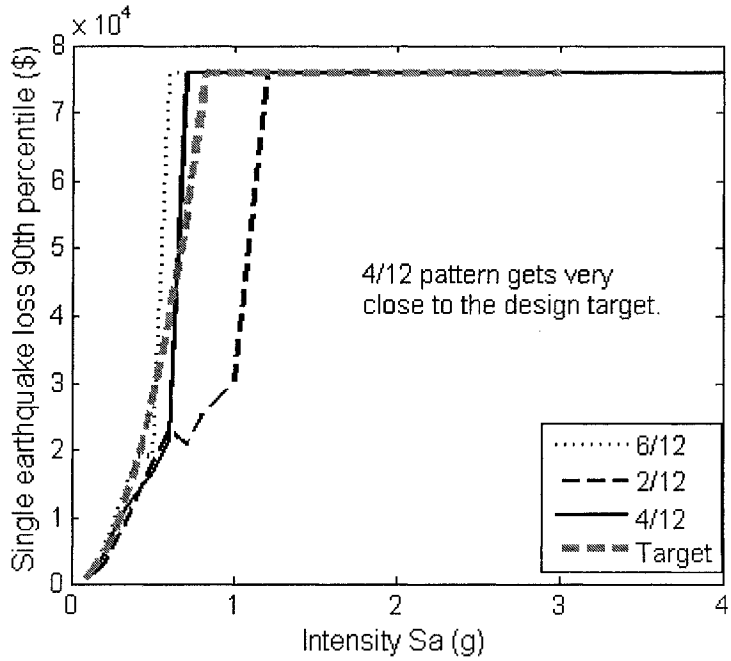

Figure 7-27: Binary search towards case 2 design target curve (2nd iteration)

The results of the second binary search iteration for case 1 and 2 were different. For case 1, although the performance of the altered design lay in between previous boundary cases, the performance at 1.5g spectral acceleration has not been improved. However, the information provided by this analysis indicates that the incremental optimization could be focused on the change of upper floor configurations for case 1. On the other hand, the structure with a 4/12 nailing pattern was so close to the target curve that it was hard to identify the relative location of the two curves by just looking at loss probability plots. Therefore, this configuration should be used as the initial trail for the incremental analysis for case 2.

Incremental optimization

Different from the binary searching procedure where the design alternatives were drastically different and the comparison was performed by looking at the difference between loss probability curve and target curve, the incremental optimization procedure makes detailed changes to individual structural components and actually compares the design target quantities with the results from loss analysis simulations. For the design cases in this example, the trial configurations were first analyzed to figure out the direction of modification, i.e. should the configurations be made "stronger" or "weaker"? Since the two design cases were obviously diverging into two different designs, the optimization for each one of them was performed separately.

Case 1

It was quite obvious for case 1 (even without further simulation) that the wall configuration on the second story should be changed, either using double-sheathed (both sides) walls or replace partition walls with shearwalls. Changing all of the walls to the double-sided configuration will of course hit the upper boundary of the binary search result, which might be a waste of both material and effort. The most reasonable option under this situation may be to change some of the partition walls in the 2nd story to shearwalls. For incremental optimization, only two partition walls were changed to 2/12 pattern shearwalls as the first trial configuration. The modified floor plan was illustrated in Figure 7-28 with the vulnerability analysis results plotted on the right.

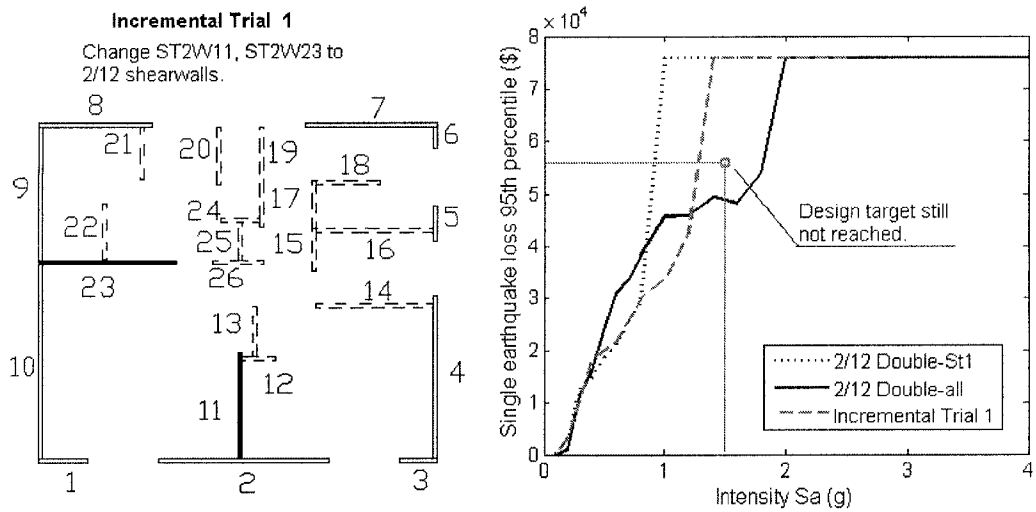

Figure 7-28: Results for incremental trail configuration 1 (Case 1)

The analysis results indicated that the 95th percentile value of the single earthquake loss at 1.5 g for the incremental trial configuration 1 still exceeded the design target value. Thus additional modification must be made to the upper level to increase its

performance, and subsequently decrease losses. Another configuration was then proposed to change another two partition walls (ST2W16 and ST2W19) to the 2/12 pattern shearwalls. The modified structure was analyzed and the results were plotted in Figure 7-29. The 95th percentile value for single earthquake loss at 1.5 g spectral acceleration was about $48,200, which was less than $56,800 (75% of collapse loss).

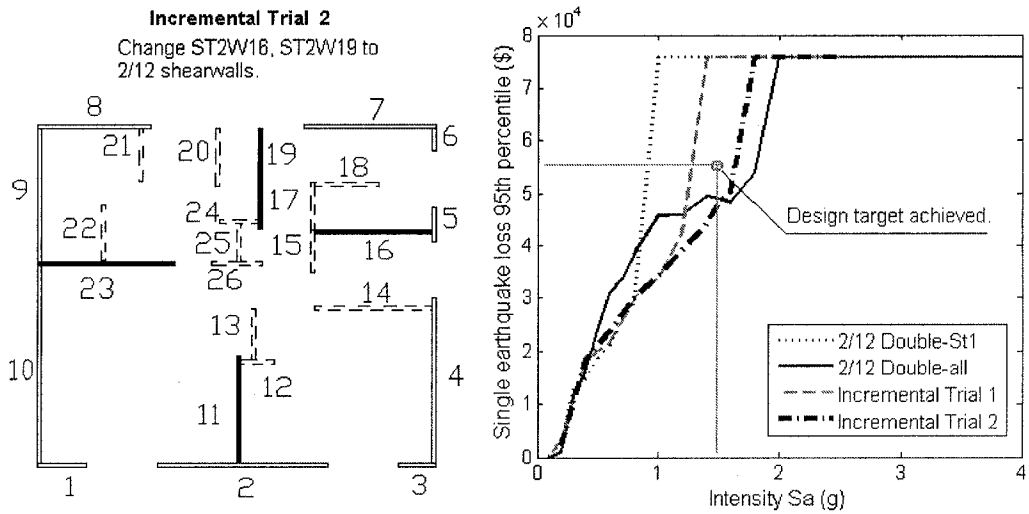

Figure 7-29: Results for incremental trial configuration 2 (Case 1)

This configuration can be used as the final design for the case 1 loss requirement. Notice that the 95th percentile loss value did not change gradually with the change of configuration. This is quite common for high percentile values since they were usually controlled by the most damaging ground motion records used in the analysis. If a change in structural configuration could prevent the structure from total collapse, it will bring significant change to the high percentile values. The sensitivity of loss to structural properties will be discussed in detail later in Chapter 8. For this example, the case 1 loss based design procedure was completed.

Case 2

As mentioned earlier, the floor plan with 4/12 nail pattern could be used as the initial trial configuration for the long term loss target. Firstly, it is important to perform long term loss simulation on this trial configuration to find out in which direction the structure should be incrementally modified. The comparison between the loss probability curve and the target curve was a good indicator in the binary search where the difference between design configurations was significant. The effect of incrementally changing the design might not be reflected easily with such an indirect indicator developed with simplified assumptions. So the long term loss simulation result will be needed in the comparison of incremental trial design performance. The long term loss simulation result for 4/12 configuration in 75 years is shown in Figure 7-30

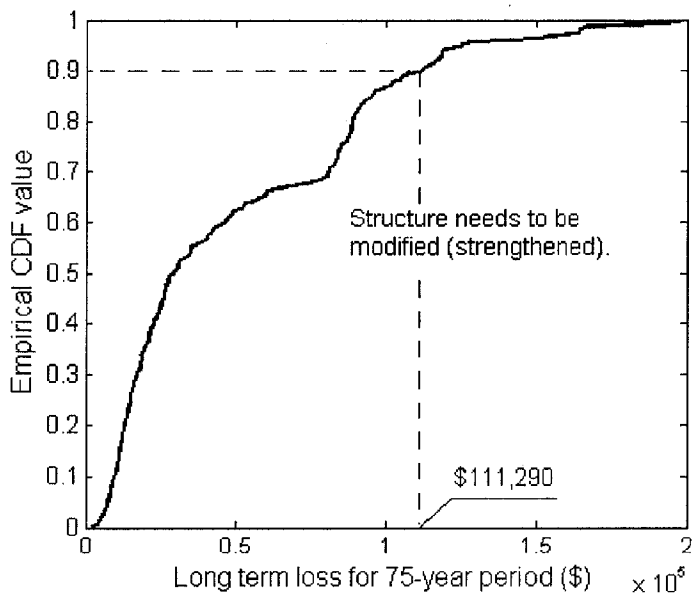

Figure 7-30: Empirical CDF curve for 75-year loss (4/12 configuration)

The 90th percentile value for the simulated data was $111,290, which is greater than the design target value $90,930 (120% of the collapse loss). So this structure should be strengthened based on the 4/12 configuration. For the ease of construction (explained earlier in design case 1), part of the partition walls were changed to shearwalls with the 4/12 nailing pattern. The incremental trial configuration is shown in Figure 7-31. The long term loss simulation results from this incremental trial configuration were shown in Figure 7-32. Some improvement can be seen based on the performance of the incremental trial design. However, the 90th percentile value ($95,740) is still greater than the design target, making another incremental modification necessary.

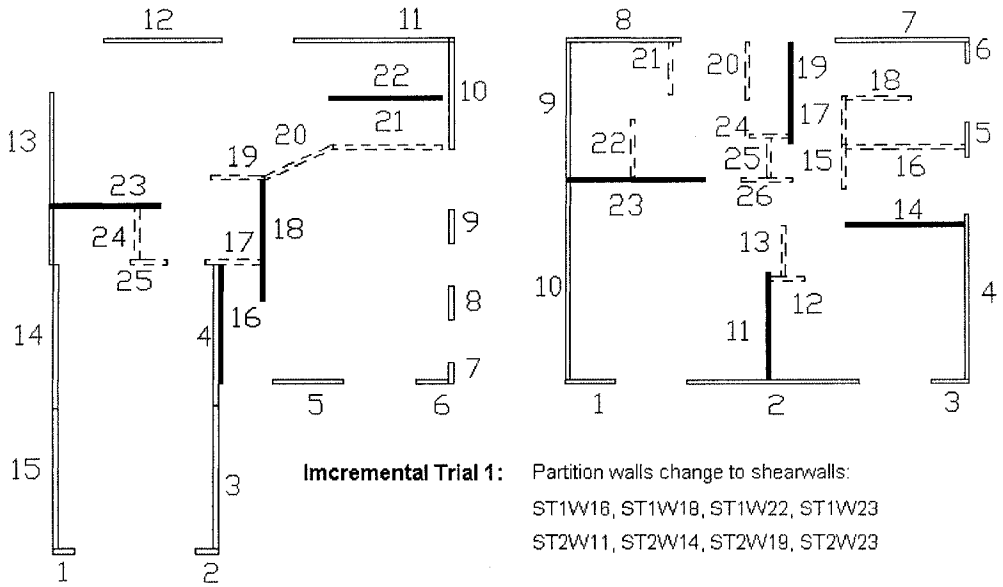

Figure 7-31: Incremental trial configuration 1 for design case 2

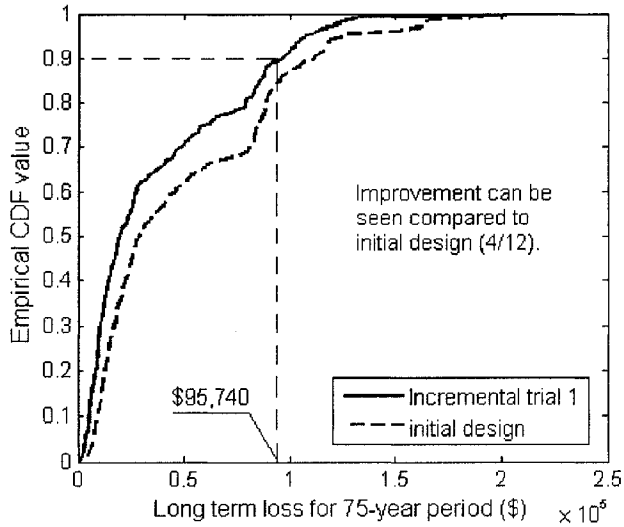

Figure 7-32: Empirical CDF curve for 75-year loss (incremental trial configuration 1)

Additional partition walls were changed to shearwalls in the modified trial design. The revised floor plan was shown in Figure 7-33. Long term loss simulation was performed and the results were presented in Figure 7-34, together with the results from previous trial analyses. It can be seen from the results that the 90^{th} percentile loss value of this design was $87,870, which satisfied the loss requirement in design case 2. Thus, this was the final design for the long term loss requirement.

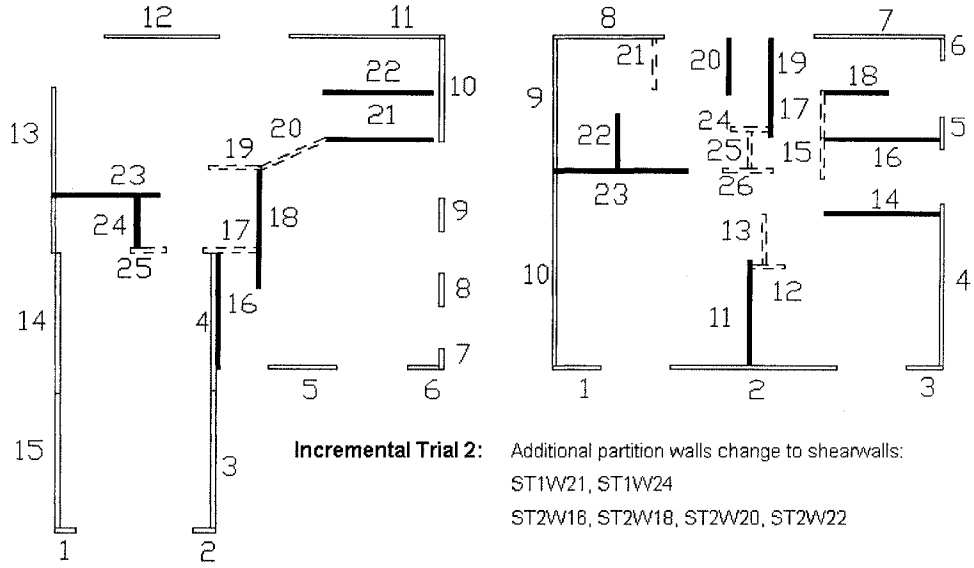

Figure 7-33: Incremental trial configuration 2 for design case 2

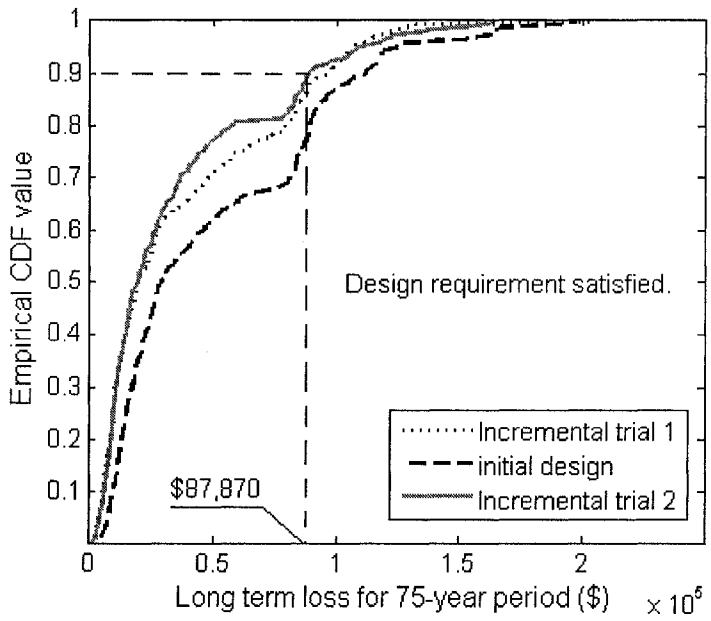

Figure 7-34: Empirical CDF curve for 75-year loss (incremental trial configuration 2)

The design results for case 1 and 2 confirmed the prediction that the long term loss requirement used in this example would result in a weaker configuration. So a simplified comparison of loss probability curves derived from the loss based design

statements might be applied to identify the controlling case without performing detailed loss simulations. On the other hand, the final design results for the examples used here were just part of the viable designs one could adopt to achieve the loss target and satisfy the loss based design requirements. Designers following other improvement strategies might attempt other configurations capable of achieving the loss requirements in this example. This type of flexibility is often viewed as a major advantage of adopting the PBSD philosophy.

Chapter Eight

Sensitivity Analysis

Introduction

As part of the loss estimation framework being proposed and illustrated in previous chapters of this dissertation, it is important to estimate the influence of different input variables within the framework, e.g. seismic hazard, structural properties, and damage accumulation assumptions. In this chapter, the procedures to perform sensitivity analysis on these inputs were illustrated and the influence of each factor to the statistics of the simulated long term loss samples will be studied. The rationality of framework results will be confirmed based on the trend in the change of long term loss. In order to represent a very typical construction style for residential structures throughout North America, index building B and its variations were used throughout the sensitivity analysis examples in this chapter. The analysis will first examine the influence of location, i.e. site, on loss estimation through an expansion to a continuous range of seismic hazard levels. Then the effects of commonly adopted construction alternatives will be discussed and expanded to the influence of structural strength/stiffness. Finally the results from the vulnerability based simulation procedure

and Virtual Hazard simulation procedure will be compared to explore the possible impact of damage accumulation.

8.1 Seismic Hazard

In this section, the comparison between the loss performances of the same structure at different locations throughout the U.S. was performed. The structural configuration remained unchanged to enable cross comparison of locations. Index building B, which has a collapse loss value of $75,775, was used for all locations to generate long term losses. The change in the cost of material and repair in different locations was not considered to isolate the effect of seismic hazard. Seismic hazard input of the loss estimation framework might affect the final simulation results through two aspects. Firstly, the single earthquake loss behavior (vulnerability model) might change if localized suites of earthquake ground motions were used in vulnerability analysis. However, the same ground motion suite was used for all locations in this study due to the lack of localized ground motion records, especially for seismically inactive locations. As a result, the vulnerability model for all the locations remains the same in this comparison. Secondly, the occurrence rate of the earthquake and the hazard curve for different locations will have impact on the long term loss estimation. Four locations (other than San Francisco, see table 8-1) across the United States including both seismically active and inactive locations were considered. The hazard curve for each location was plotted in Figure 8-1. Los Angeles was selected to represent locations with an extremely high seismic hazard level. Portland, OR represents locations with considerable but not extremely high seismic hazards. Fort Collins, CO

and Detroit, MI were representatives of locations where earthquakes rarely happen. The long term loss associated with each location was simulated and the results are shown in Table 8-2. The empirical CDF curves for different exposure periods and locations are plotted in Figure 8-2.

Table 8-1: Cities investigated in the sensitivity analysis

City	Lat.	Long.	Sa @ 0.2 sec (g)		
			IBC	PE 10%50	PE 2%50
Los Angeles, CA	33.9	118.4	1.500	0.945	1.622
Portland, OR	45.4	122.5	0.893	0.417	0.893
Fort Collins, CO	40.6	105.1	0.224	0.081	0.224
Detroit, MI	42.3	83.1	0.123	0.044	0.123

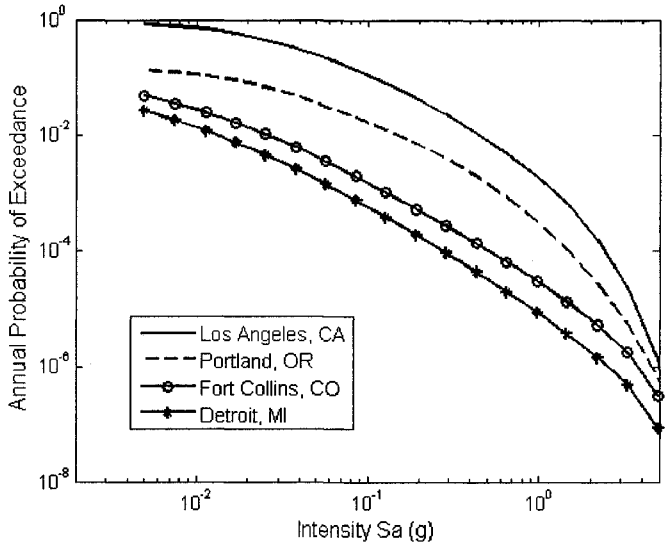

Figure 8-1: Hazard curves for different locations

Three exposure periods were inspected at each location, namely a 5-year period representing short-term, a 20-year period representing mid-term, and a 75-year period representing life-time or long-term. It can be seen from the results that the location, or the seismic hazard, greatly influences the loss results on all ranges of exposure period as one would expect. In low seismic hazard locations such as Fort Collins and Detroit,

the economical loss caused by seismic events has a very high chance to be zero in 20 years which is consistent with what has happened over almost any 20 year period in those areas; and was very minor even for a life cycle period of time. The extreme loss values (the percentile values with very low probability of exceedance) were only a friction (less than 5%) of the collapse loss, which means the damage from earthquakes to the structure in a life time was very likely to be just cracking in the drywall. However, when considering the location with considerable seismic hazard such as Portland, one would expect some chance of total collapse in 20 years (the 99th percentile loss value was close to collapse loss). The probability of collapse loss increased to 5% for a 75 year period. Finally, in Los Angeles, a place similar to San Francisco with respect to seismic hazard, home owners of structures with similar configurations to index building B will very likely (with 80% chance) experience a loss equivalent to one third of the collapse loss in 75 years. Some extreme cases (95th percentile value) indicated that the owner might experience a cumulative loss amount that is more than the cost of rebuilding the entire structure twice.

Table 8-2: Statistics of loss sample for different locations

Location	Period (year)	Probability of exceedance					
		80%	50%	10%	5%	2%	1%
DE	5	$0	$0	$0	$0	$0	$0
	20	$0	$0	$0	$0	$443	$723
	75	$0	$0	$64	$580	$1,335	$1,516
FC	5	$0	$0	$0	$0	$0	$0
	20	$0	$0	$0	$0	$22	$269
	75	$0	$0	$378	$755	$1,086	$2,206
PO	5	$0	$0	$354	$1,639	$5,553	$10,738
	20	$0	$132	$4,846	$12,613	$30,944	$72,649
	75	$664	$3,249	$30,907	$76,136	$80,811	$81,606
LA	5	$0	$438	$7,917	$16,300	$60,141	$74,337
	20	$1,915	$6,760	$31,818	$49,985	$80,237	$93,387
	75	$21,040	$41,755	$119,100	$145,890	$169,690	$181,550

In order to plot and separate the empirical CDF curves for the loss samples from low seismic hazard level locations, a log-scale axis was used for the long term loss amount (vertical) axis in Figure 8-2. Since the curves for Detroit were very similar to those for Fort Collins, they were not plotted for the clearness of the figure. One can see from the figure that the long term loss behavior of index building B for Los Angeles in 5 years was similar to that of Portland for 20 years. Similarity could also be found on the LA-20 year curve and PO-75 year curve. Such comparisons could be used to design risk-consistent earthquake insurance plans for different locations.

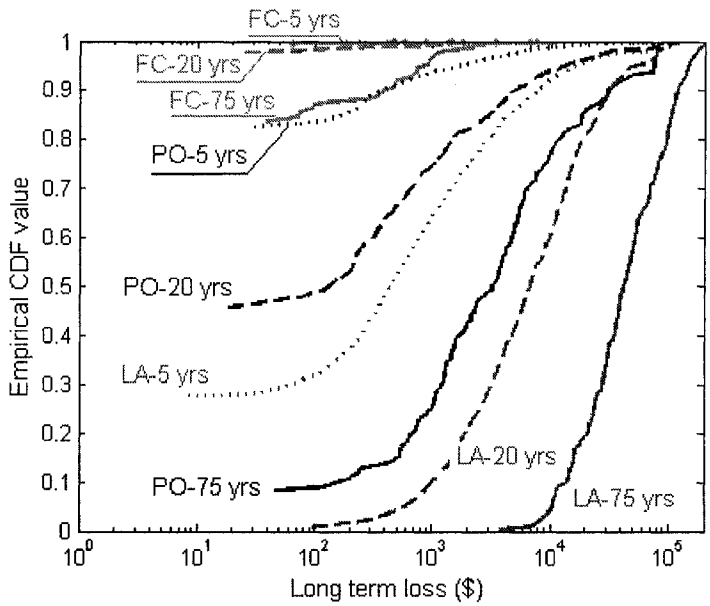

Figure 8-2: Empirical CDF curves of long term loss for different locations

Although the results obtained using different locations could qualitatively show the influence of seismic hazard input on the framework output, a continuous trend of how long term loss changes as intensity level increases cannot be fully observed from just four locations. In order to illustrate this trend, a series of artificial hazard curves were

developed based on the existing curves and used as an incrementally varying input into the loss simulation process. These artificial hazard curves were constructed based on hazard curves ranging from Detroit to San Francisco. On a log-scaled plot, the hazard curves for Detroit (very low hazard level) and San Francisco (very high hazard level) are very similar to each other in shape with only the difference in location (see Figure 8-1). By varying the location in between these two locations while keeping the shape of the curve on a log-scaled plot, a group of artificial hazard curves could be established. In this study, thirteen artificial hazard levels (from level 0 to level 12) were defined with the level 0 hazard level assigned to be equivalent to Detroit hazard curve and level 10 corresponding to San Francisco hazard. The concept of this hazard level system was illustrated in Figure 8-3 with some of the artificial hazard curves plotted. In this way, the framework behavior under a continuous incremental artificial hazard level could be studied. Notice that this hazard level defines the annual probability of exceedance of a range of earthquake intensity levels. It is different from the hazard level for a single earthquake event defined in some PBSD procedures such as the IO, LS, and CP levels set force in FEMA 356 pre-standard (2000). Since these curves were evenly distributed in a log-scaled plot, the change in annual probability of exceedance between each level is not linear.

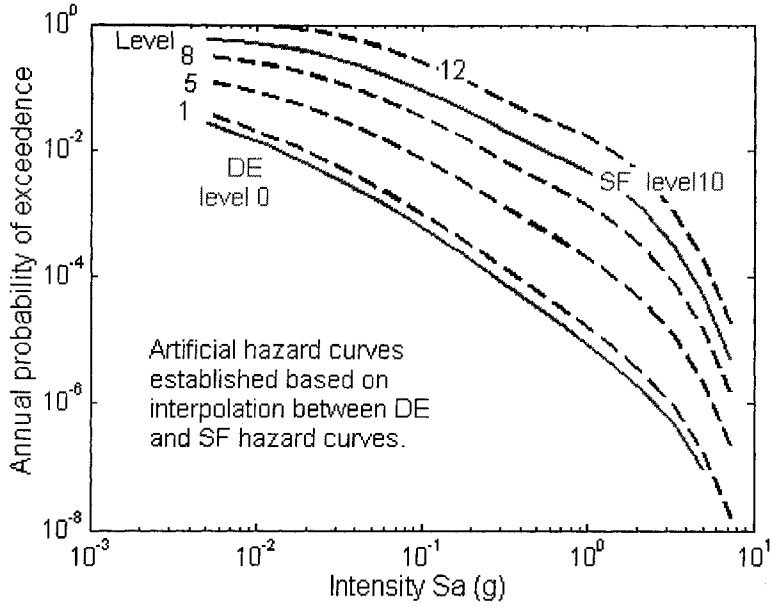

Figure 8-3: Concept of artificial hazard levels

The long term loss for index building B was also simulated with 5-year, 20-year, and 75-year periods for all the hazard levels described above. The statistics of the results were listed Table 8-3, 8-4, and 8-5.

Table 8-3: Statistics for 5-year loss simulation results for different hazard levels

Hazard Level	Pr0	Probability of exceedance					
		80%	50%	10%	5%	2%	1%
0	0.995	$0	$0	$0	$0	$0	$0
1	0.986	$0	$0	$0	$0	$0	$98
2	0.976	$0	$0	$0	$0	$111	$390
3	0.967	$0	$0	$0	$0	$311	$816
4	0.936	$0	$0	$0	$142	$1,106	$2,821
5	0.901	$0	$0	$0	$324	$1,374	$3,519
6	0.852	$0	$0	$249	$938	$3,746	$8,736
7	0.774	$0	$0	$737	$2,381	$9,245	$20,641
8	0.651	$0	$0	$2,097	$6,680	$20,874	$72,112
9	0.521	$0	$0	$3,941	$10,319	$32,968	$73,456
10	0.412	$0	$199	$7,799	$21,563	$73,477	$75,737
11	0.211	$0	$759	$16,683	$47,123	$75,456	$78,963
12	0.058	$497	$2,850	$37,314	$75,612	$85,928	$105,040

Table 8-4: Statistics for 20-year loss simulation results for different hazard levels

Hazard Level	Pr0	Probability of exceedance					
		80%	50%	10%	5%	2%	1%
0	0.949	$0	$0	$0	$0	$862	$2,778
1	0.951	$0	$0	$0	$0	$469	$788
2	0.915	$0	$0	$0	$192	$1,129	$1,881
3	0.856	$0	$0	$249	$765	$3,363	$6,870
4	0.799	$0	$0	$479	$1,521	$5,352	$10,069
5	0.716	$0	$0	$831	$1,977	$7,105	$14,046
6	0.533	$0	$0	$2,759	$7,654	$14,941	$20,439
7	0.356	$0	$240	$6,894	$21,021	$62,930	$73,228
8	0.227	$0	$763	$17,947	$39,458	$76,934	$85,543
9	0.079	$345	$1,889	$24,006	$73,470	$77,401	$84,690
10	0.041	$1,139	$4,951	$55,927	$78,355	$94,742	$106,730
11	0.000	$4,568	$14,252	$84,374	$105,090	$148,070	$160,620
12	0.000	$11,921	$34,072	$112,350	$134,100	$166,630	$202,650

Table 8-5: Statistics for 75-year loss simulation results for different hazard levels

Hazard Level	Pr0	Probability of exceedance					
		80%	50%	10%	5%	2%	1%
0	0.900	$0	$0	$0	$385	$667	$885
1	0.825	$0	$0	$221	$969	$6,437	$13,006
2	0.720	$0	$0	$493	$1,194	$2,502	$4,562
3	0.585	$0	$0	$1,024	$3,801	$9,801	$13,272
4	0.410	$0	$156	$4,443	$17,706	$27,643	$72,861
5	0.225	$0	$432	$22,202	$40,153	$73,522	$75,416
6	0.130	$226	$1,280	$21,464	$29,927	$44,685	$72,411
7	0.025	$728	$2,762	$29,677	$44,267	$77,309	$81,375
8	0.000	$1,902	$8,534	$74,564	$78,969	$90,710	$108,710
9	0.000	$5,599	$14,753	$82,458	$105,280	$127,480	$131,540
10	0.000	$12,836	$36,808	$129,740	$164,650	$179,790	$216,290
11	0.000	$43,272	$90,314	$181,490	$201,120	$255,980	$264,910
12	0.000	$112,980	$171,610	$304,410	$352,590	$379,430	$430,770

One of the most direct observations from the simulated data is that higher hazard level resulted in higher loss as one would expect. This trend could be easily identified in all types of exposure periods analyzed. Empirical CDF curves for simulated data of 75-

year loss were plotted for different hazard levels in Figure 8-4. It could be seen that the increase in the amount of loss was not linearly related to hazard level.

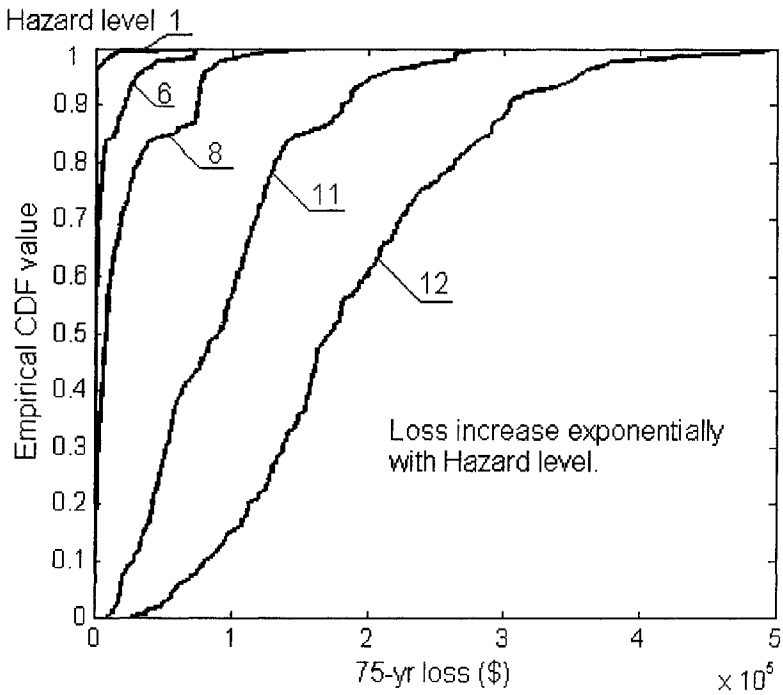

Figure 8-4: Empirical CDF curves for different hazard levels

By plotting the key statistics of the simulated long term loss against hazard level, the characteristics of interaction between seismic hazard and loss behavior could be more clearly illustrated. Since the hazard levels were defined with equal increments of annual probability of exceedance in a log-scaled axis, it is hard to determine the direct relationship between the loss statistics and annual PE levels on a linear vertical axis. So both linear and log scale were used for the vertical axis for easier observation. If the curve appears to be a straight line on the log-scaled plot, it indicates that there is a linear relationship between the plotted statistics and the annual PE value. Three key

statistics, namely zero-loss probability, the median of long term loss (50^{th} percentile value), and the 99^{th} percentile of the simulated data, were plotted in Figure 8-5, 8-6, and 8-7. The figure on the left is the plot using linear scale on vertical axis; log-scaled plot is on the right. The data used in these plots were the same except that the points with 0 values were not shown in the log-scaled figure because 0 could not be converted to a log-scale value.

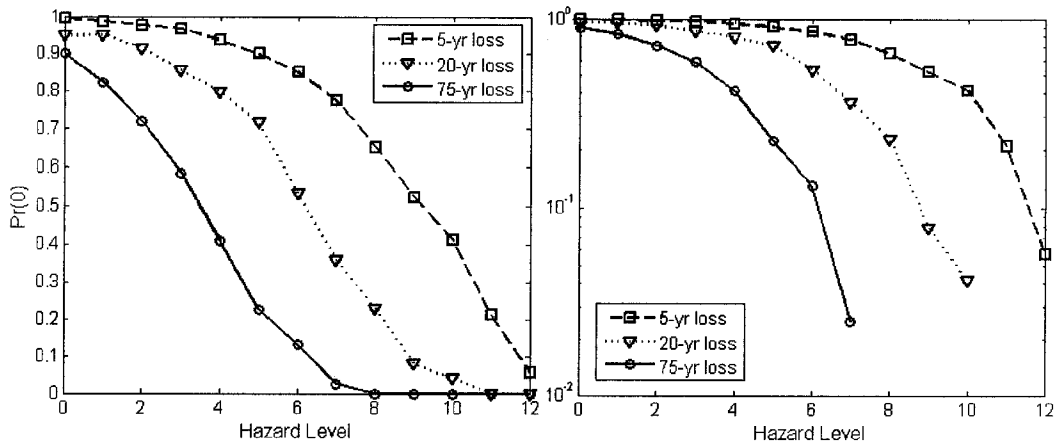

Figure 8-5: Probability of zero loss vs. hazard level

Figure 8-5 showed that the probability of zero loss at all ranges of exposure period does not have a linear relationship with hazard level or annual probability. For locations with a hazard curve lower than level 3, it was quite reasonable to expect no loss for any type of exposure period. The chance of zero loss changes greatly in the hazard level range from level 3 to 9. After the hazard level rises above level 10, the probability of having no loss drops to a very low level except for the short term exposure period.

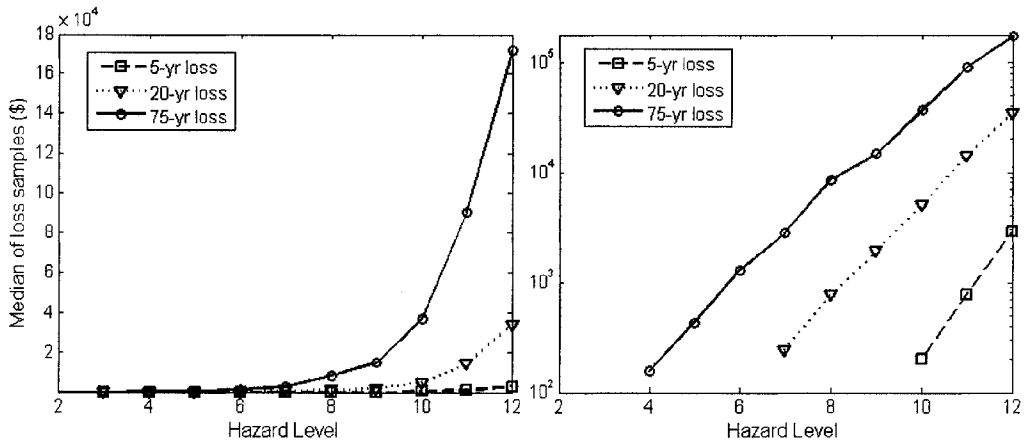

Figure 8-6: Median vs. hazard level

On the linear scaled plot, it seems that the loss median does not start to rise until the hazard level increases to above level 6. It can be seen more clearly on the log-scaled plot that the median values for different exposure periods were all zero until a certain hazard level was reached (level 4 for 75-year period, level 7 for 20-year period, and level 10 for 5 year period). After the median value became non-zero, the relationship between the sample median and annual probability of exceedance value on the hazard curve follows a linear relationship very well. This characteristic is consistent for all types of exposure time spans.

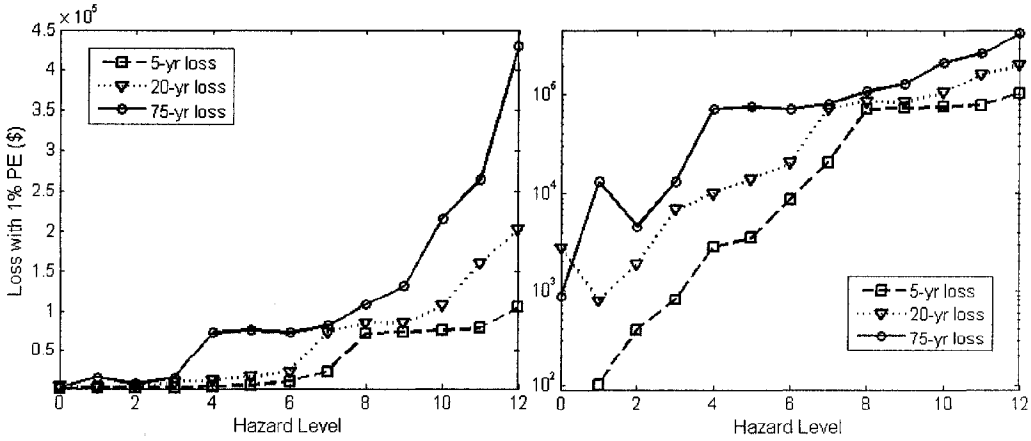

Figure 8-7: One percentile value vs. Hazard level

Similar to the median, the extreme values which have low probabilities of exceedance, e.g. the 95^{th} or 99^{th} percentile are often of special interest for design and evaluation purposes in civil engineering. It can be seen from Figure 8-7 that there exists a "step-up" pattern in the change of these extreme statistics over seismic levels. For example, in the 75-year curve the loss value suddenly stepped-up to the level close to the collapse loss value from a very low level as the hazard level increased from level 3 to level 4. Then the loss stayed at that level with only minor variation from hazard level 4 to level 7 before it began to step up again. Similar patterns can be observed for shorter time spans except the "step-up" pattern occurs at higher hazard levels (level 6 for 20-year curve and level 7 for 5-year curve). It can also be seen from the log-scale plot that the behavior of extreme statistics was quite different from the median as the hazard level changes, i.e. not close to a linear relationship anymore. These sudden changes of the curve are related to the sudden "jump" in the loss amount upon the collapse of the building. If the empirical model for extreme statistics of long term loss conditional on hazard level is to be developed, these effects and details must be taken into account. The loss estimation framework developed in this study provides a viable tool to investigate these issues.

8.2 Structural Configuration and Quality

Structural configuration, without a doubt, will affect the dynamic responses during earthquakes thus has a substantial impact on the resulting financial loss. In traditional strength based methods for light frame wood structures, shearwalls with different

nailing patterns are used to resist different levels of seismic lateral load. In this section, investigation into the loss-based "performance" of different wall configurations using the simulation methods developed in early chapters is accomplished. Firstly, the loss behavior of the three most commonly used nailing schedules, namely 2/12 pattern, 4/12 pattern, and 6/12 pattern, was investigated. By changing from one pattern to another, it is assumed in traditional strength based design that the shear capacity of the wall could increase considerably. Now the focus is on the impact of these changes on the vulnerability model and long term loss. Another subject investigated in this section is the reduction of strength and stiffness of the structure which was assumed to be related to construction quality. It has been indicated by many post-earthquake surveys, inappropriately installed structural components do not have the full design capacity and usually became the weak link in the load transfer which can led to the failure of the whole system, e.g. a weak soft first story. For a first cut in assessing the construction quality interaction with loss, a simple assumption was made in this study that quality problems could be reflected through a strength and stiffness reduction in the structural components. This is consistent with the assumptions of nails missing studs used by Rosowsky and Kim (2005). Specific quality issues, such as missing hold-downs and un-tightened anchor bolts on individual walls, could not be modeled unless the condition of the structure was specifically given in detail. So such effects were not considered in this study. To study the loss performance of the structure at different reduction levels, the parameters of the wall elements in index building B were incrementally reduced with a reduction factor from 0% to 70% from the original values (full capacity). It was believed that

this range covers a considerable amount of uncertainty in construction quality, even for some extremely poorly constructed buildings.

Different from the previous section where a range of seismic hazard levels were applied to a single vulnerability model, the changes in structural configuration results in different vulnerability models which were used as the input to the long term loss simulation. Similarly, in order to isolate the effects of structural configuration, an identical seismic hazard level was used for all long term loss simulations conducted in this section. Hazard data for San Francisco was selected for illustration because it is a highly active seismic zone in which the differences might be more identifiable. Unlike seismic hazard input which directly controls the simulation of the long term loss, structural configuration could only affect the behavior of vulnerability models. Then the vulnerability model would carry its impact to long term loss simulation. So the impact on both the vulnerability model and long term loss were investigated. The analysis was aimed at developing a basic idea of the interaction between structural properties and earthquake induced loss performance.

Commonly adopted construction options

In most residential light woodframe construction, wood shearwalls are built on site by contractors following different nailing patterns indicated by the structural design. Since the architectural floor plan is typically in place before the structural design, the length and position of walls in the building will not change unless there is critical need

to do so. The resistance was adjusted by using different nailing patterns, changing interior walls into shearwalls, or applying double sided sheathing when necessary. The construction practices were believed to be able to provide considerable improvement for the lateral load resisting capacity. Although this improvement may prevent the structure from collapse in the design intensity level, the impact of these alternative nailing patterns on the loss behavior was not clear. By changing the nailing pattern for all walls from 6/12 to 2/12, which will probably take a construction crew significant construction time, it was not clear how much would the potential saving be in the long run or when a specific earthquake occurs. The simulation results presented in this section will help shed some light on these and similar questions.

Firstly, one should look into the vulnerability model for different nailing patterns, which controls the distribution of single earthquake loss. The change in structural configuration will directly affect the vulnerability models and then interact with the long term loss simulation. The analysis for the 2/12, 4/12, and 6/12 nailing patterns was conducted on index building B by changing all of its shearwalls to these patterns while keeping the wall lengths and locations the same. The partition walls in the structure were not changed because GWB sheathing panels are typically installed in the same way even with different shearwall configurations. The vulnerability parameters for different nailing patterns are listed in Table 8-6 with the vulnerability curves shown in Figure 8-8.

Table 8-6: Vulnerability parameters for different nailing patterns

Intensity	μ_{ln}			σ_{ln}			Pr_0			Pr_c		
	6/12	4/12	2/12	6/12	4/12	2/12	6/12	4/12	2/12	6/12	4/12	2/12
0.10	5.96	5.81	5.37	1.01	0.95	1.05	0.05	0.05	0.17	0.00	0.00	0.00
0.20	7.17	6.95	6.57	1.12	1.08	1.15	0.00	0.00	0.01	0.00	0.00	0.00
0.30	8.00	7.75	7.37	1.09	1.15	1.20	0.00	0.00	0.00	0.00	0.00	0.00
0.40	8.56	8.29	7.99	1.01	1.08	1.16	0.00	0.00	0.00	0.00	0.03	0.00
0.50	8.94	8.69	8.44	0.87	0.98	1.07	0.00	0.00	0.00	0.05	0.05	0.00
0.60	9.19	9.03	8.79	0.78	0.88	0.98	0.00	0.00	0.00	0.15	0.05	0.00
0.70	9.40	9.28	9.01	0.70	0.78	0.88	0.00	0.00	0.00	0.20	0.10	0.05
0.80	9.54	9.46	9.26	0.66	0.73	0.83	0.00	0.00	0.00	0.32	0.17	0.05
1.00	9.77	9.69	9.60	0.56	0.65	0.73	0.00	0.00	0.00	0.39	0.39	0.07
1.20	9.86	9.85	9.72	0.54	0.54	0.62	0.00	0.00	0.00	0.56	0.52	0.26
1.40	9.93	9.98	9.92	0.50	0.50	0.57	0.00	0.00	0.00	0.65	0.60	0.37
1.60	10.08	10.11	10.05	0.46	0.42	0.49	0.00	0.00	0.00	0.68	0.63	0.45
1.80	10.21	10.11	10.07	0.43	0.39	0.45	0.00	0.00	0.00	0.71	0.77	0.64
2.00	10.20	10.27	10.21	0.46	0.40	0.41	0.00	0.00	0.00	0.82	0.77	0.67
2.40	10.32	10.45	10.29	0.39	0.35	0.34	0.00	0.00	0.00	0.85	0.78	0.83
2.80	10.43	10.49	10.34	0.34	0.31	0.30	0.00	0.00	0.00	0.85	0.85	0.90
3.20	10.47	10.43	10.46	0.31	0.27	0.26	0.00	0.00	0.00	0.87	0.90	0.90
4.00	10.37	10.60	10.53	0.24	0.27	0.25	0.00	0.00	0.00	0.95	0.86	0.90

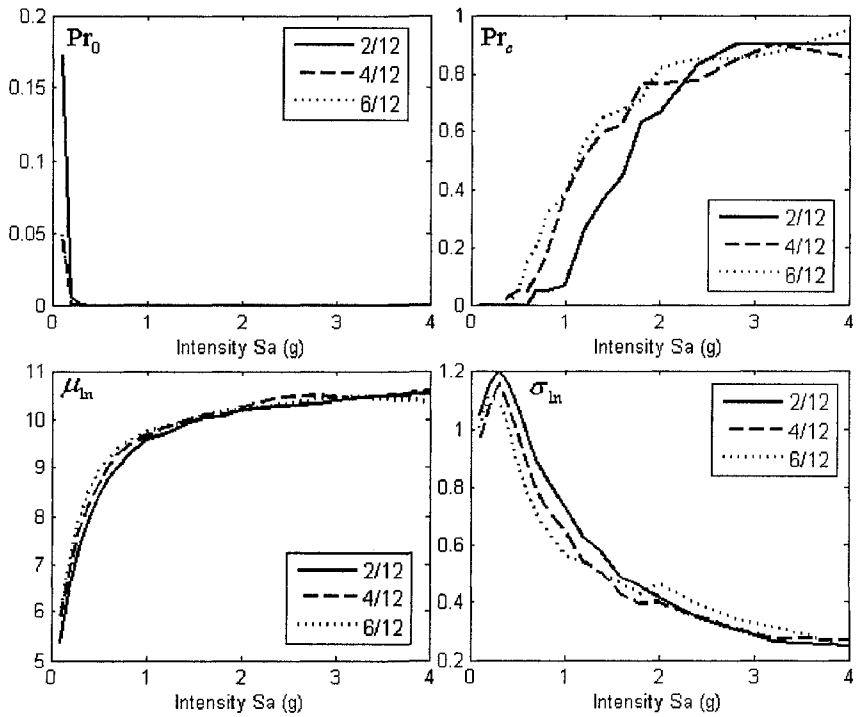

Figure 8-8: Vulnerability model for different nailing patterns

From the results listed in the table, it can be seen that the difference in vulnerability parameters for different nailing patterns does exist, but is not very significant. The stronger configuration (2/12 pattern) showed better performance in the zero loss probability at low intensity levels (this probability drops to 0 for all configurations after the seismic intensity increases to 0.3 g spectral acceleration). The collapse probability was lower for the stronger configuration than for others at the same intensity levels. As mentioned earlier, the focus of this analysis is to examine the difference in loss behavior of alternative configurations. Although some differences can be seen from the vulnerability curves, the effects of these differences on single earthquake loss result cannot be directly identified, underscoring the earthquake-specific nature of seismic design. Since the single earthquake loss distribution is controlled by all of these parameters, the trend in one of these parameters does not represent the trend in the single earthquake loss. A more useful plot can be obtained by directly comparing the difference in the key statistics of single earthquake loss samples. The mean value of the single earthquake loss for all three nailing patterns was plotted in Figure 8-9 (a). Figure 8-9 (b) showed the difference between these mean loss values from 4/12 and 6/12 pattern and that from the 2/12 pattern. This plot directly shows the additional cost of repairing the building (in an average sense) after events having different seismic intensities occurred if a 4/12 or 6/12 pattern was selected instead of the 2/12 pattern. From the plots, one can see the difference in loss was not significant in both the low and high ends of the intensity level. This simply implies that the advantage of having a stronger configuration would not be significant

if the earthquake is too small or too large, but is present for moderate seismic intensity levels. In the case of this example, when earthquake spectral acceleration is below 0.3 g, the damage to all types of structures was very minor, thus resulting in similar loss responses. After spectral acceleration exceeds 2 g (as can be seen also from Figure 8-8), the collapse probabilities for all structures were very close, thus resulting in a negligible loss difference. The intensity range between 0.3 g to 2 g was the intensity level within which the structural configuration makes a difference. This range was termed here as the *intensity sensitive region* (ISR) for structural configuration, and aligns almost directly with the seismic intensities used in current force based design. In Figure 8-10, the loss difference was divided by the loss of the 2/12 pattern to see the change in average loss relative to the strongest configuration, i.e. normalize. It can be seen from the comparison that changing from the 2/12 pattern to the 4/12 or 6/12 pattern might result in 40% or 90% more loss, respectively, on average if an earthquake with a Sa=0.7 occurs.

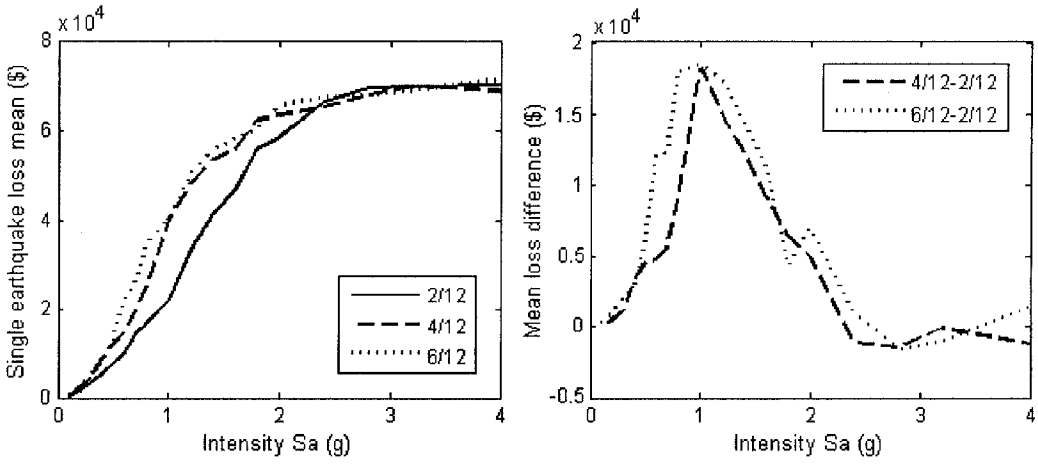

Figure 8-9: Difference in single earthquake loss mean value for different nailing patterns

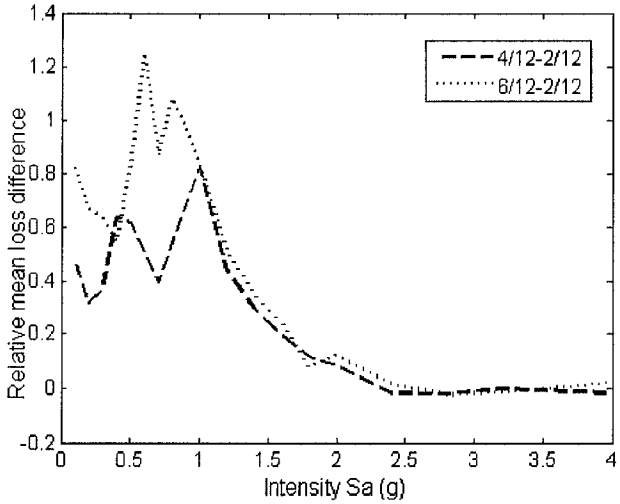

Figure 8-10: Difference in single earthquake loss mean value relative to 2/12 pattern case

Since the structural configuration can only effectively change loss behavior under earthquake intensity values within the intensity sensitive region (ISR), the impact of structural configuration will not significantly affect the long term loss if the earthquakes that occur during the exposure period do not fall in that range. For example, if a situation occurred in which only a large amount of small earthquakes and a few extremely large earthquakes occur, the total loss for a 2/12 pattern structure would not be very different than a 6/12 pattern house, given the same nominal floor plan. In other words, the improvement in structural configuration does not guarantee improvement in long term loss behavior of individual cases due to the existence of the intensity sensitive region. However, the trend in the impact of the structural configuration to long term loss value can be seen as one inspects the simulation results which reflected the average performance under different earthquake hazard combinations. The statistics of long term loss samples for 3 exposure periods were listed in Table 8-7. The empirical CDF curves were plotted in Figure 8-11.

Table 8-7: Statistics for long term loss results for different nailing patterns

Period	Pattern	Pr(0)	Probability of exceedance					
			80%	50%	10%	5%	2%	1%
5-year	2/12	0.36	$0	$196	$3,249	$7,600	$29,842	$73,542
	4/12	0.33	$0	$411	$5,431	$14,363	$72,761	$75,494
	6/12	0.33	$0	$474	$6,775	$16,309	$73,026	$75,656
20-year	2/12	0.03	$768	$2,441	$24,112	$64,580	$78,418	$83,432
	4/12	0.01	$1,303	$3,900	$42,142	$77,487	$82,221	$86,149
	6/12	0.01	$1,436	$4,898	$45,343	$76,995	$83,425	$89,872
75-year	2/12	0	$8,224	$17,370	$86,289	$99,529	$121,160	$126,960
	4/12	0	$12,757	$28,959	$111,290	$124,470	$164,360	$166,660
	6/12	0	$16,015	$33,093	$117,200	$142,200	$175,890	$199,350

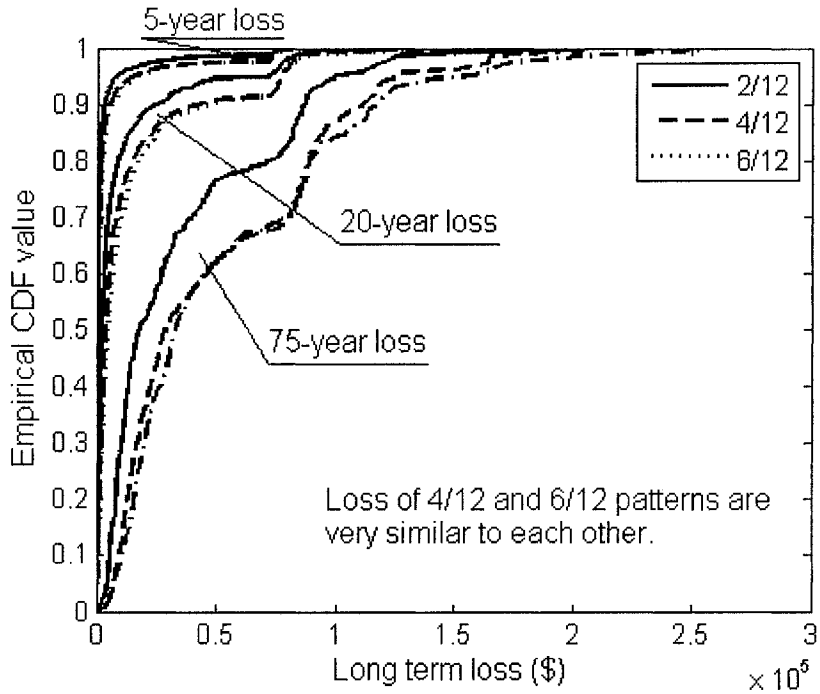

Figure 8-11: Empirical CDF curves for long term loss for different nailing patterns

It can be seen from the results that structural configuration does affect the distribution of long term loss. However, if the focus was on high percentiles (higher than 95th

percentile) of the long term loss, the difference due to the nailing patterns is negligible for short and mid-term exposure periods. Another direct observation from the CDF curves was that the loss behavior of 4/12 and 6/12 nailing patterns are very similar (although the 4/12 pattern performance is theoretically better). In 75 years, the improvement of a 2/12 nailing pattern from a 6/12 nailing pattern for index building B is significant. Comparing the median of the simulated loss data, the loss of the structure with 2/12 nailing pattern was only about 50% of the 6/12 pattern building. The 4/12 pattern option only changes the performance by about 12% considering the median value.

Incremental deduction

In this section, sensitivity analysis is aimed at determining the significance of construction quality on the loss behavior of wood frame structures. However, the model used here to reflect construction quality is quite simplified. It only considers the construction quality as a reduction factor to the strength and stiffness parameters for all the hysteretic elements in the numerical model. Thus the observations and conclusions obtained in this analysis should only be applied to construction quality problems that result in an overall strength and stiffness reduction to the structural components. Index building B with 2/12 nailing pattern was used as the full capacity prototype (0% reduction). The reduction factor was applied to K_0, F_0, F_{1m}, and F_{1r} of the EPHM elements (shearwalls) and K_0, F_0, and F_1 of the CUREE elements (GWB partition walls). Partition walls were considered because they can also be affected by

the construction quality. The uncertainty of the stiffness and strength was not considered since it is now treated as an influence factor. Thus only one structural model (rather than samples of structural models) was used for each reduction level.

The comparison of the vulnerability model (or single earthquake loss distribution) for different reduction factors was shown in Figure 8-12 where the vulnerability parameter curves were plotted. Only four different reduction levels were selected to show the trend in the comparison (with the vulnerability parameters listed in Table 8-8). The probability of zero loss for stronger structures (with less reduction) is higher than that of weaker ones. However, the probability of zero loss quickly drops to 0 after the intensity exceeds a certain value (0.3 g in case of example). The collapse probability, as always, is monotonically increasing with intensity levels until it approaches unity. It begins to increase at very low intensity levels for structures with high quality reduction factors, which indicates that these structures will collapse easier in low intensity situations than other building models with lower reduction factors, i.e. "stronger structures". In the plots of $\mu_{\ln}$ and $\sigma_{\ln}$, it can be seen that $\mu_{\ln}$ for better quality structures are lower than for low quality structures in the low intensity range, while $\sigma_{\ln}$ is bigger for higher stiffness and strength.

Table 8-8: Vulnerability parameters for different reduction factors

Intensity	$\mu_{\ln}$				$\sigma_{\ln}$			
	0%	20%	40%	70%	0%	20%	40%	70%
0.1	5.324	5.833	6.374	7.857	1.060	0.926	0.763	0.424
0.2	6.488	6.796	7.260	8.156	1.151	1.071	0.957	0.681
0.3	7.339	7.543	7.903	8.608	1.213	1.079	1.082	0.759
0.4	7.966	8.195	8.471	8.900	1.181	1.078	1.020	0.741
0.5	8.407	8.573	8.743	9.095	1.091	1.000	0.941	0.694
0.6	8.760	8.858	9.050	9.281	0.977	0.920	0.842	0.651
0.7	8.959	9.149	9.262	9.426	0.905	0.840	0.785	0.633
0.8	9.222	9.350	9.455	9.514	0.830	0.789	0.711	0.586
1	9.624	9.623	9.679	9.634	0.716	0.688	0.609	0.578
1.2	9.770	9.776	9.783	9.808	0.647	0.603	0.558	0.516
1.4	9.936	9.932	9.984	9.907	0.562	0.544	0.496	0.483
1.6	10.052	9.987	10.037	9.861	0.485	0.474	0.470	0.523
1.8	10.097	10.177	10.198	9.956	0.470	0.449	0.450	0.483
2	10.192	10.260	10.014	10.154	0.417	0.384	0.417	0.481
2.4	10.345	10.198	10.180	10.172	0.331	0.360	0.385	0.366
2.8	10.345	10.350	10.348	10.138	0.311	0.303	0.304	0.310
3.2	10.429	10.442	10.422	10.219	0.255	0.269	0.287	0.296
4	10.528	10.527	10.393	10.326	0.251	0.259	0.253	0.223

Intensity	Pr_0				Pr_c			
	0%	20%	40%	70%	0%	20%	40%	70%
0.1	0.181	0.049	0.004	0	0	0	0	0
0.2	0.007	0.001	0	0	0	0	0	0
0.3	0	0	0	0	0	0.05	0	0
0.4	0	0	0	0	0	0	0	0.05
0.5	0	0	0	0	0	0.05	0.05	0.20
0.6	0	0	0	0	0	0.05	0.05	0.20
0.7	0	0	0	0	0.05	0.05	0.10	0.30
0.8	0	0	0	0	0.05	0.05	0.15	0.40
1	0	0	0	0	0.05	0.15	0.30	0.60
1.2	0	0	0	0	0.20	0.35	0.50	0.60
1.4	0	0	0	0	0.30	0.45	0.55	0.70
1.6	0	0	0	0	0.40	0.60	0.65	0.85
1.8	0	0	0	0	0.60	0.60	0.75	0.85
2	0	0	0	0	0.65	0.65	0.90	0.85
2.4	0	0	0	0	0.75	0.90	0.90	0.90
2.8	0	0	0	0	0.90	0.90	0.90	0.95
3.2	0	0	0	0	0.90	0.90	0.90	0.95
4	0	0	0	0	0.90	0.90	0.95	0.95

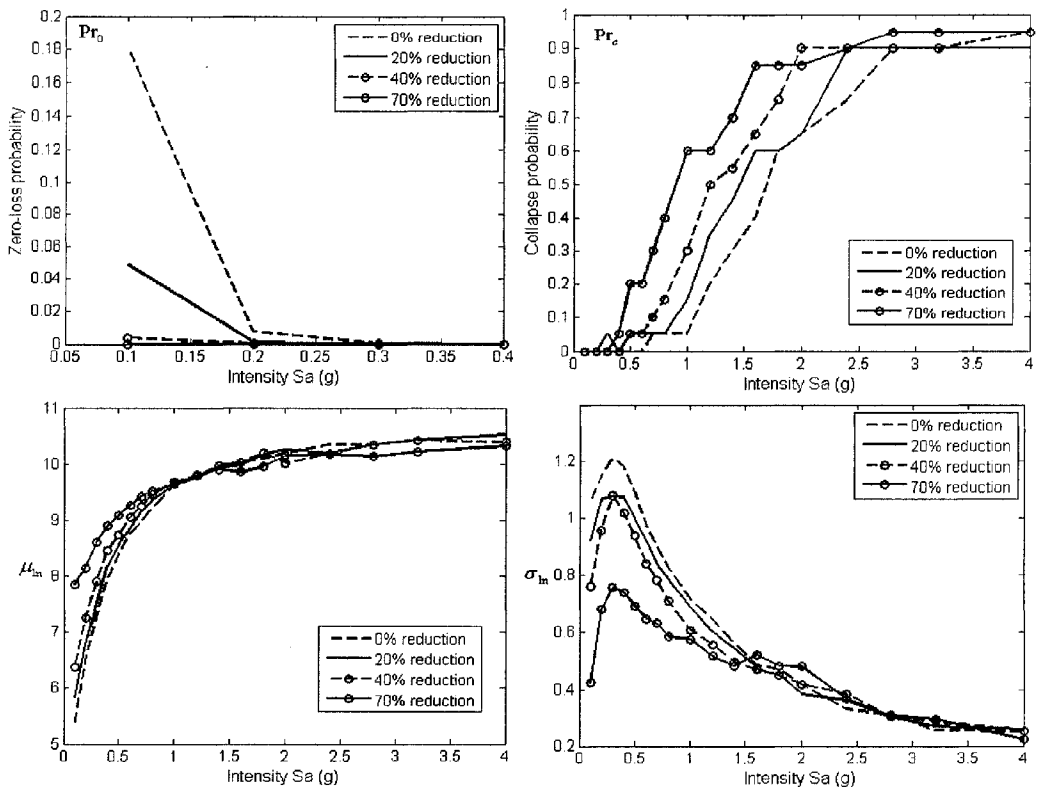

Figure 8-12: Effects of reduction factor on vulnerability parameters

Similar to the difference plots used earlier to compare different nailing patterns, a direct comparison of the single earthquake loss sample mean could be more informative when differences among reduction factors is of interest. Figure 8-13(a) shows the mean from all simulated samples plotted against intensity level. Figure 8-13(b) shows the difference between the reduced structure and the full capacity structure in the single earthquake loss mean value. Although the loss for the full capacity structure is always smaller than for the reduced quality structures, the difference is only significant for a certain range of intensity levels. This range is the intensity sensitive region (ISR) for strength/stiffness reduction. Similar to the case of nailing pattern sensitive region, the information from the comparison can be interpreted that the merits of a well constructed structure over a poorly built one will

only be exhibited when a "suitable" earthquake occurs. If the earthquake is too small, both will result in similar amounts of loss. If the earthquake is too large, both will collapse and the structure with superior construction quality might technically result in more loss due to the cost of materials. An optimized design should then extend the range of this sensitive region on both ends to help control the long term loss, since it is very likely that the earthquakes that actually occur will be numerous small ones and several large events. The advantage of construction configuration and quality will not be significant if the intensity of these earthquakes falls outside of the sensitive range.

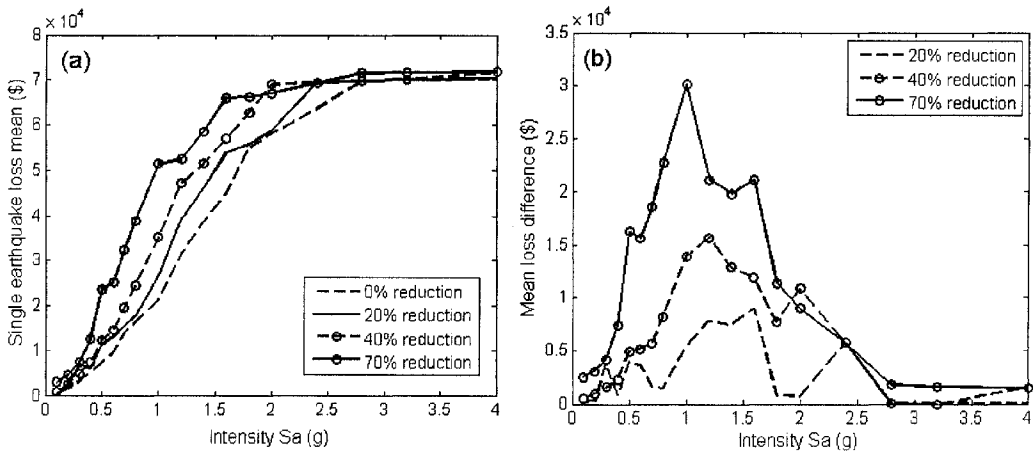

Figure 8-13: Comparison of single earthquake loss mean value for different reduction factors

With the vulnerability models obtained above, long term loss samples were generated for the vulnerability models using San Francisco hazard data. The resulting statistics for simulated data are listed in Table 8-9, 8-10, and 8-11 for 5–year, 20-year, and 75-year time periods. It can be seen from these results that the reduction in structural strength and stiffness will lead to bigger losses in most cases. The difference between different reduction cases increases as the time span becomes longer. The loss difference between the structure with 50% reduction factor and full capacity structure was about $80,000, according to the 95th percentile value of the simulated data for a

75-year period. As one looks at the high percentile values of the simulated data, a "step-up" pattern (similar to that in the seismic hazard level sensitivity analysis) can be seen as the reduction factor changes. For example, the 1% PE loss for 5 years for all reduction factors was about the same, while these values congested at three levels for the 20-year period (about $85,000, $100,000, and $150,000). The samples in these high percentile regions were mainly caused by the occurrence of collapse events which are associated with very large earthquakes during the simulation periods. The intensity of these earthquakes had exceeded the sensitive region of the structural property and loss relationship. Thus the loss values for different structural configurations become very close to each other. In other words, the high percentile values corresponding to extreme situations in which all buildings, despite the construction quality, experience a significant amount of damage or even collapse, resulting in loss values close to or equal to the collapse loss of the building.

Table 8-9: Loss statistics for different reduction factors in 5 years

DR	Pr(0)	Probability of exceedance					
		80%	50%	10%	5%	2%	1%
0	0.366	$0	$181	$3,192	$7,504	$28,098	$73,401
5%	0.339	$0	$253	$3,728	$9,064	$34,297	$73,885
10%	0.342	$0	$260	$4,369	$11,159	$38,614	$74,266
15%	0.328	$0	$327	$4,371	$10,378	$40,023	$73,845
20%	0.326	$0	$406	$4,730	$13,181	$72,655	$75,305
25%	0.308	$0	$499	$4,696	$12,254	$36,347	$74,427
30%	0.315	$0	$530	$4,979	$13,431	$72,727	$75,095
35%	0.315	$0	$576	$5,643	$13,678	$73,079	$75,382
40%	0.308	$0	$712	$6,350	$16,412	$74,166	$75,703
45%	0.300	$0	$878	$6,672	$17,124	$73,817	$75,876
50%	0.299	$0	$1,118	$7,927	$20,592	$73,837	$76,248
55%	0.307	$0	$1,456	$8,743	$18,439	$73,245	$76,613
60%	0.302	$0	$2,057	$9,368	$17,695	$74,454	$77,356
65%	0.304	$0	$2,480	$11,073	$20,748	$74,528	$77,850
70%	0.309	$0	$3,033	$12,970	$27,469	$76,877	$79,846

Table 8-10: Loss statistics for different reduction factors in 20 years

DR	Pr(0)	Probability of exceedance					
		80%	50%	10%	5%	2%	1%
0	0.035	$657	$2,273	$22,144	$46,571	$78,059	$83,503
5%	0.016	$830	$2,758	$23,152	$73,726	$78,209	$82,703
10%	0.020	$901	$3,041	$24,821	$72,900	$79,040	$88,987
15%	0.019	$998	$3,032	$26,677	$74,479	$78,025	$82,226
20%	0.013	$1,369	$3,867	$38,331	$76,150	$81,057	$89,519
25%	0.013	$1,500	$3,920	$28,242	$73,009	$78,819	$84,427
30%	0.013	$1,665	$4,175	$41,182	$77,091	$81,457	$89,327
35%	0.012	$1,792	$4,852	$48,672	$76,934	$80,497	$85,818
40%	0.008	$2,171	$5,579	$49,114	$79,449	$89,829	$107,020
45%	0.011	$2,726	$6,875	$61,016	$78,962	$84,865	$109,580
50%	0.008	$3,209	$7,442	$63,358	$82,084	$93,011	$99,663
55%	0.011	$4,280	$9,261	$50,595	$80,424	$89,195	$99,195
60%	0.004	$5,649	$11,400	$54,175	$83,566	$93,181	$116,360
65%	0.011	$6,958	$13,895	$67,573	$85,597	$95,506	$116,360
70%	0.008	$8,031	$16,554	$82,141	$92,832	$102,900	$150,380

Table 8-11: Loss statistics for different reduction factors in 75 years

DR	Pr(0)	Probability of exceedance					
		80%	50%	10%	5%	2%	1%
0	0	$7,967	$17,338	$86,340	$97,017	$129,930	$142,550
5%	0	$8,646	$17,091	$96,601	$105,460	$119,280	$166,790
10%	0	$9,661	$22,643	$92,304	$106,940	$117,430	$123,790
15%	0	$9,995	$22,279	$89,935	$99,058	$125,780	$152,210
20%	0	$12,473	$27,435	$106,700	$121,600	$148,560	$163,180
25%	0	$12,436	$25,365	$98,138	$125,410	$160,210	$169,810
30%	0	$13,865	$28,419	$100,970	$120,460	$200,210	$215,520
35%	0	$15,271	$34,967	$105,110	$150,930	$172,610	$185,630
40%	0	$17,445	$39,240	$115,170	$166,110	$185,500	$212,560
45%	0	$20,172	$40,563	$127,390	$174,080	$222,720	$229,280
50%	0	$25,205	$50,617	$121,050	$173,640	$184,400	$193,090
55%	0	$27,375	$45,275	$135,460	$159,780	$186,270	$193,070
60%	0	$34,825	$57,167	$131,770	$180,960	$195,590	$256,460
65%	0	$41,419	$65,817	$138,490	$166,410	$202,920	$261,240
70%	0	$52,159	$88,972	$186,180	$209,620	$228,750	$248,180

Part of the simulated loss data was plotted in Figure 8-14 for a visible comparison between different reduction factors. Since the 5-year curves with different reduction factors were similar and hard to distinguish on the CDF plot, only 20-year and 75-year period curves were plotted. It can be seen that the difference between the curves became more significant as the exposure period became longer. The shape of the CDF curves also changed.

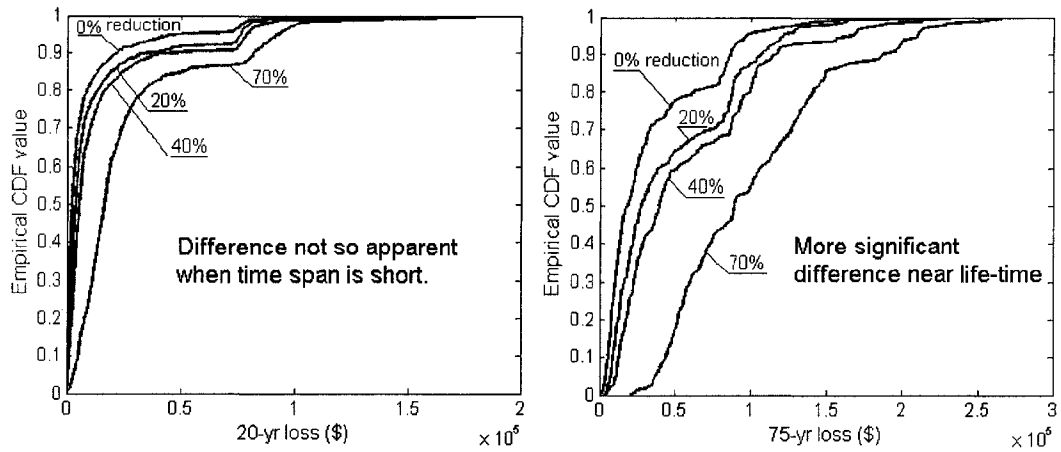

Figure 8-14: Empirical CDF curves for long term loss for different reduction factors

Similar to the sensitivity study on hazard levels, the effects of reduction factor on long term loss could be illustrated by plotting key statistics against reduction factor. From the table, one can see that this effect on the long term zero-loss probability was negligible (it was controlled by the hazard level). So only the median and 99th percentile values for long term loss samples were plotted. In Figure 8-15, it can be seen that an increasing trend of loss median exists for all exposure periods. The curves were plotted with log-scale vertical axis for a better illustration. For extreme loss values (99th percentile values, Figure 8-16), the increasing trend still exist for longer periods. But the curves were not steadily increasing (more fluctuation observed)

because these extreme values were the results of a few extreme events whose occurrence has a high level of uncertainty even for 75 years. For the short term exposure period, the extreme value did not change with reduction factor and remained very close to collapse loss (this could also be seen from the table), which indicated the occurrence of a single large earthquake in 5 years under San Francisco seismic hazard environment.

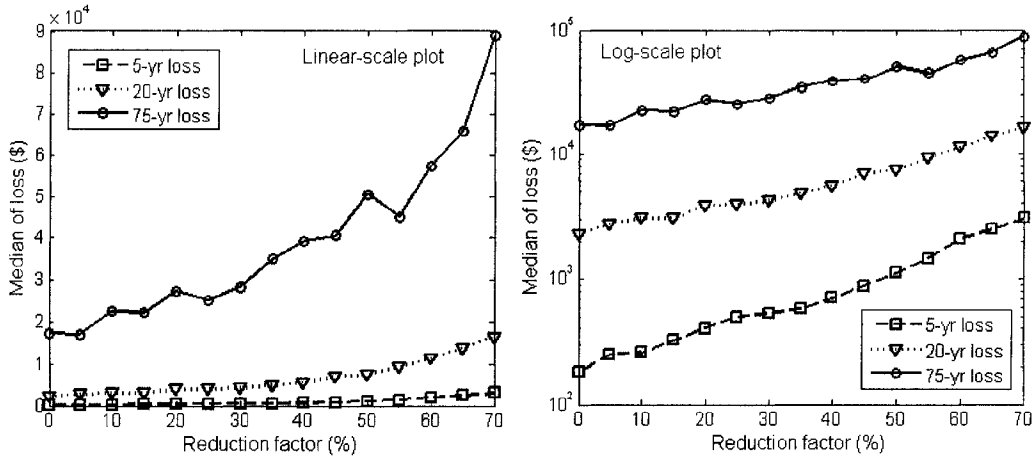

Figure 8-15: Long term loss median vs. reduction factor

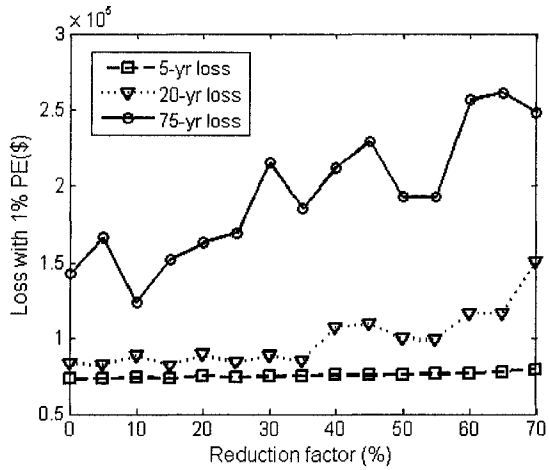

Figure 8-16: Extreme loss value vs. reduction factor

From the results for different construction qualities, it can be concluded that the influence of structural properties can influence the distribution of the long term loss

distribution. Reduction in stiffness and strength can result in considerable change in long term seismic induced loss. However, this effect might only be of practical significance in seismically active locations, such as the San Francisco area used in this study. As long as the strength and stiffness reduction caused by quality issues was kept under 20%, the influence of the reduction on long term loss will not be very significant. On the other hand, because the strength/stiffness reduction due to the variation in construction quality would very likely be below 20%, its effect to long term seismic loss is very limited.

8.3 Virtual Hazard assumptions

The concept of Virtual Hazard simulation was introduced in Chapter 4. It is a simulation procedure to generate long term losses with a more realistic set of assumptions than that of the vulnerability based method, such as accumulation of damage in the structure and the effect of after-shocks. Whether or not virtual hazard should be favored over vulnerability methods should be judged based on the difference in the final output of these simulations. However, it is not known without a sensitivity analysis how much the final output will differ from one method to the other. In this section, the output from the virtual hazard simulation was compared with the results obtained from the vulnerability based simulation in order to determine to what extent this assumption would change the final long term statistics. By adding in the occurrence of after-shocks, it was believed that the impact of cumulative damage could be reflected by the simulated loss samples, since the structure will be damaged during the main earthquake and then experiences another earthquake event (after-

shock) before repair. Since the virtual hazard simulation is very computationally intensive, limited cases for index building B were investigated using this method. The first case assumed that after-shocks have a probability of 95% to occur following any earthquake with intensity greater than 0.1 g spectral acceleration, and the intensity of the after-shock will be 70% to 80% of the main earthquake intensity. This case does not represent any realistic after-shock model but provides a chance to investigate the situation where cumulative damage effects may be significant. The other case reduced the probability of after-shock occurrence to 30% following intensities greater than 0.8 g, with the after-shock intensity set to 20% to 70% of the main earthquake, representing a much lower level (more realistic) of after-shock activity. The simulations were conducted for 5-year, 20-year, and 75-year cases and compared with the results from vulnerability based simulation. The construction quality and repair quality were set to be superior for all cases. Nailing pattern was selected to be 6/12 since it is widely used for residential construction. Table 8-12 shows some of the resulting statistics from the simulations. The actual simulated data and their empirical CDF curves are plotted in Figure 8-17

Table 8-12: Long term loss statistics from different simulation methods

Period	Simulation method*	Pr(0)	Probability of exceedance					
			80%	50%	10%	5%	2%	1%
5-year	0	0.33	$0	$474	$6,775	$16,309	$73,026	$75,656
	1	0.39	$0	$254	$6,220	$15,767	$72,526	$74,757
	2	0.41	$0	$240	$6,601	$16,219	$73,475	$75,065
20-year	0	0.01	$1,436	$4,898	$45,343	$76,995	$83,425	$89,872
	1	0.03	$1,035	$3,382	$33,130	$76,002	$87,876	$94,856
	2	0.02	$1,062	$3,204	$40,267	$77,922	$91,046	$101,100
75-year	0	0.00	$16,015	$33,093	$117,200	$142,200	$175,890	$199,350
	1	0.00	$15,561	$33,849	$107,020	$127,600	$167,080	$195,980
	2	0.00	$11,039	$32,636	$115,250	$167,720	$191,580	$213,850

* Simulation method 0: vulnerability based method; 1: Virtual Hazard method with low after-shock probability; 2: Virtual Hazard method with high after-shock probability.

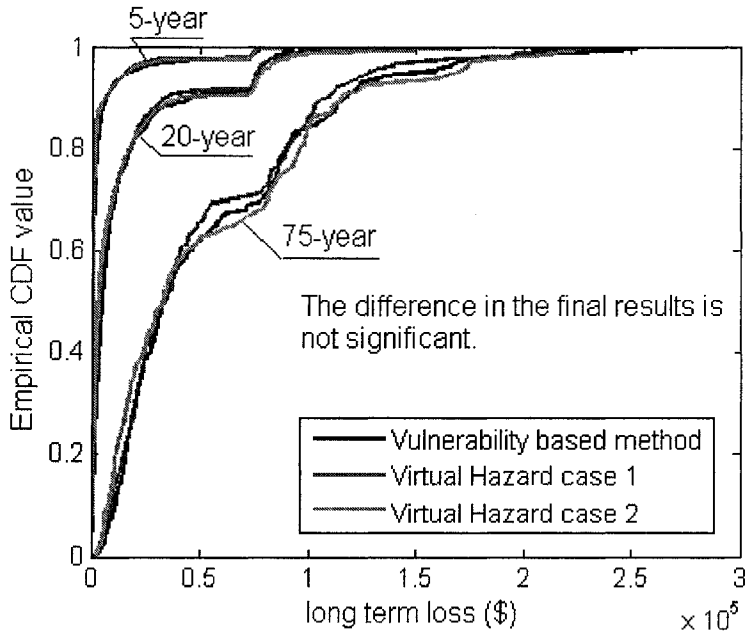

Figure 8-17: Empirical CDF curves for long term loss from different simulation methods

It can be seen from the simulation results that the difference between the different simulation methods is not significant. The fluctuation in the relative difference between the vulnerability simulation and Virtual Hazard simulation was very likely caused by the randomness in the simulation itself rather than the assumptions used in the simulation. The comparison between low and high after-shock probabilities showed that the resulting long term loss was higher for high after-shock probability case. But the difference was too minor to make any practical difference. This result can be explained with two arguments. Firstly, the structures with accumulated minor damage (recall only level I damage was accumulated during the simulation) would experience stiffness reduction while the ultimate capacity (strength) remains approximately the same with the undamaged structure (because the damage index in the EPHM will not affect the height of the backbone curve). This stiffness reduction might help control the structural response during an after-shock because the natural

period of the structure was elongated. So the responses in the after-shock were unlikely to exceed the responses in the main earthquake. Then the loss will remain the same as if there is no after-shock because the loss estimation method only considers the maximum responses. Secondly, because the relationship between damage level and structural responses was not deterministic and depend on discrete damage levels, even when the after-shock did result in a bigger response, the difference in responses might not be enough to trigger a change from one damage level to the next. Thus the resulting repair cost might not change.

However, the analysis results indicates that the vulnerability based method, although using less realistic assumptions, yields similar results to the Virtual Hazard simulation whose assumptions are more realistic. The cumulative damage in the structure, as long as it remains minor (level I), will not greatly change the loss behavior of the structure in the long run. Although there seems to be no reason to favor one method over another from the analysis results, Virtual Hazard simulation has the potential to incorporate other types of hazard loading and a wide range of repair strategies which might have significant impact to long term loss of wood frame structures.

Chapter Nine

Summary, Conclusions, and Recommendations

9.1 Summary and Conclusions

A wide scope of analyses on light frame wood structures were conducted in this study, from sub-assembly level connector behavior, assembly level quasi-static analysis, time domain analysis of whole structural systems, seismically induced loss analysis, and finally loss-based seismic design. A variety of numerical models, solution frameworks, and implementation procedures were developed during this process. These subjects and the findings during the investigation of them were summarized in this section, along with the conclusions drawn mainly based on the analysis of woodframe structures conducted in Chapter 7, Chapter 8, and partly from Chapter 2.

An accurate time domain analysis model is the basis for accurate seismic response simulation results. Numerical modeling of woodframe structures has been studied by many researchers in recent years. The models used in this research mainly fall into two categories: nonlinear finite element models and simplified shear building models. A simplified biaxial shear building model was selected for this study based on the

balance between modeling complexity and accuracy. Although the nonlinear finite element method is more flexible and powerful in the sense that virtually all kinds of physical effects can be modeled, it was not suitable for this situation due to the complexity of modeling and computational expense required. A more significant reason to use a simpler model is the fact that the level of accuracy in the input information (structural, seismic, and loss-related inputs) of loss analysis for woodframe structures is not justifiable with the accuracy of a very detailed model. A shear building model consists of floor diaphragms connected with spring elements. Its accuracy depends largely on the nonlinear spring elements used to represent lateral load resisting components. In order to improve the accuracy of the model, a new type of hysteretic model (EPHM) was developed for a flexible and robust modeling of the reverse cyclic behavior hysteretic components, including wood frame assemblies and the connectors. This new model has the ability to incorporate the effect of accumulated damage during loading by using a set of damage-driven parameters. The comparison of this model with the test data showed that the model was well suited for the modeling of cyclic behavior of degrading system with a "pinching" hysteresis loop. This new hysteresis model was first used for the modeling of connectors in the quasi-static light frame assembly analysis model developed in this study. This virtual work based model, termed herein as the Nail-Pattern (NP) model, was an improved version of the CASHEW model developed in the CUREE woodframe project.

With the individual wall component readily represented by EPHM, biaxial shear building model for wood frame structures could be built and analyzed under seismic excitation. The focus of the shear building model was to obtain reliable predictions of

the lateral drifts of each story in the structure. The damage/loss assessment procedures are a function (probabilistically) of the maximum inter-story drift prediction. In this study, a system level model was verified by comparing the prediction with full-scale shake table tests on an 1,800 square foot two-story building. The results showed that the model successfully predicted the behavior of the real structure at various seismic intensity levels with and without finishing materials, keeping the relative difference within an acceptable range.

The numerical modeling of wood frame structures is the main focus in the first phase of this dissertation work. In summary of structural modeling efforts:

- New concepts and models were developed based on existing research results. The EPHM, NP model, and biaxial shear building model together established a viable system to investigate static and dynamic responses of wood frame structures.
- Improvement in the earthquake response prediction for wood frame structures has been seen with the implementation of these new models. These results provided a solid basis for the development of the loss estimation framework and procedures in this study.
- All of the numerical models were integrated into a user friendly software package, SAPWood, which makes the results and tools of this study more available to the research community and practitioners.

The study on structural behavior of wood frame structures was then followed by the investigation on the loss behavior. Two types of loss behavior are of central interest in the PBSD framework. The first one is the loss due to an event associated with a predefined hazard level or return period; the other is the loss in a specific period of time for a location of interest. Both of these losses were studied in this dissertation work. The assembly-based vulnerability framework was adopted to predict loss after a deterministic seismic loading event. A probabilistic framework incorporating most of the important contributors to seismic induced loss was established. Since single earthquake induced loss was of PBSD importance, the framework was first targeted at establishing a model for the single earthquake loss distribution with seismic intensity as the control parameter. In this procedure termed as vulnerability analysis, simulation incorporating the uncertainties in structural components, earthquake ground motion, and response-damage-loss relationship was conducted to obtain single earthquake loss distribution given intensity level. Based on the simulated data, this distribution was characterized with four parameters (Pr_0, Pr_c, $\mu_{\ln}$, and $\sigma_{\ln}$) as functions of intensity. This vulnerability model could be directly used to assess the loss of a structure in a single event associated with a given intensity level. Or it could be combined with time-dependent earthquake event simulation to generate cumulative loss in any given period of time. The simulation that uses vulnerability analysis results (vulnerability model) to generate single earthquake losses is called the vulnerability based method. It is assumed in vulnerability based method that the structure is repaired to be equivalent to the new structure after each earthquake, since the vulnerability model only represents loss from a new structure. In reality, damage that are not detectable (i.e.

hidden) might accumulate in the structural components and affect the loss in later earthquakes; or the repair practice on damaged items might not be able to restore the structure to full initial strength. These issues gave rise to another alternative method of simulation for long term accumulated losses, termed herein as Virtual Hazard simulation, in which losses induced by each earthquake event were generated using time domain analysis with the "current" structure rather than an empirical vulnerability models. This simulation method may help with the investigation of the effects of accumulated damage and also the behavior of a structure under successive ground motions (such as after-shocks) without repairing. However, it was indicated from the comparison conducted in this study that the vulnerability based method will, in realistic circumstances (both the hazard and structure), yield results very similar to the results of Virtual Hazard simulation method. Thus the effects of accumulated damage and after-shock ground motion were not significant given the current level of accuracy of the input information and assumed repair strategy.

Based on the framework developed, loss simulations for different index buildings were conducted based on limited response-loss data. The results from the vulnerability analysis indicated that the loss estimation framework developed in this study was a viable way to conduct reasonable estimation for the loss behavior of wood frame structures. According to single earthquake loss samples generated for all index buildings, a zero loss probability and collapse probability must be used in combination of a continuous distribution model (a lognormal model in this case) in order to represent the fact that the loss will be 0 for small earthquakes and capped at the

collapse loss for extreme events. The model proposed to represent single earthquake loss distributions matched the simulated data closely and was shown to be valid for all intensity values. The zero loss probability drops to 0 very quickly once the intensity of an earthquake event exceeds a certain value (about 0.2 g spectral acceleration for the index buildings in this study). Collapse probability increases gradually to one as earthquake intensity increases. The single earthquake loss amount, on average, increases with intensity until collapse loss is reached. A cross comparison among index buildings for single earthquake loss mean values indicated that there are differences in single loss behaviors for different structures. The comparison of the normalized loss value for different types of damageable components revealed the difference in damage resistance of these components, or more specifically, resistance indicated by the component damage fragility functions. This information, once described as common sense, could now be quantitatively analyzed and compared for different structures and components.

Long term loss data for the index buildings were also simulated and compared for typical time spans that were of interest. It was quite clear from the results that it was very possible to avoid loss for a short period of time. But the losses from earthquakes became increasingly inevitable as time increased for a location like San Francisco. This zero loss probability for long term loss apparently decreases with the time span, and was shown later in the sensitivity analysis to be closely related to earthquake hazard levels. The comparison of normalized long term losses from index buildings showed that the behavior of these examples were similar to one another. The empirical

CDF curves for long term losses showed that the long term loss distributions are not like typical parametric distribution models (such as lognormal or Normal distribution) in the way that the curves became flat as the loss value approaches collapse loss or some integer times the collapse loss. This is a reflection of the influence from the occurrence probability of extreme earthquake events. Thus, it is not as accurate to represent long term cumulative earthquake loss with just simple parametric distribution models.

Loss-based design concepts and requirements were defined in this study. Two types of loss-based design requirements were expressed in term of target loss statements explicitly associated with a probability of exceedance or confidence level. The first type is directly associated with single earthquake loss given intensity level, which can be obtained from vulnerability analysis. The second type is the requirement on long term loss at a specific location. By introducing a simplified method to estimate long term loss given loss-probability curve, both statements could be represented with target points or curve on the loss-intensity plot associated with the required confidence level. The loss based design problem then became a procedure to find a realistic and acceptable configuration that would produce target loss probability curves. These target probability curves can also serve as an indicator for the comparison of the relative relationship between different loss requirements. After the definition and representation of the problem, a trial and error based procedure was introduced to perform the loss based design. This procedure includes a simple binary search and a refined incremental optimization. Vulnerability analysis must be carried out at each

search or optimization step. With the help of a series of optimization guidelines for different types of loss sources, the optimization could eventually converge at a point near the design target. These steps were shown in Chapter 7 with index building B for two different loss targets. It can be seen from the design examples that the loss-based design procedure proposed in this study was a viable and effective solution for the achievement of practical loss requirements. The loss probability curve served successfully as an indicator for the trial and error searching process. The relative comparison of different loss requirements was efficiently conducted with target loss probability curves. Strength-based and loss-based requirements for wood frame structures may influence the design configuration separately. However, the loss-based requirement needs to exceed strength based requirement (i.e. the current design code) to be of practical significance. The comparison between possible loss based requirements and current force-based design requirements was not covered in this study, but is felt to be straightforward.

Based on the results from the numerical models, the conclusions on the earthquake loss modeling and simulation could be summarized as:

- The loss estimation framework proposed in this study is a reasonable representation of the earthquake loss accumulation mechanism over time.
- The two simulation procedures introduced in this study can be applied to a variety of woodframe structures and yield realistic loss prediction results.
- Loss based design concept defined in this study is a viable option of PBSD for woodframe structures. The incremental optimization procedure used to

implement this design concept can be applied to the single family style woodframe buildings.

Sensitivity analysis on the loss estimation framework inputs was conducted in Chapter 8 for seismic hazard, structural strength/stiffness, and damage accumulation. The seismic hazard within the loss analysis is determined by the location of the construction site and/or structure. With the hazard data from USGS, loss behavior of a nominally identical structure at four different locations was investigated and compared. As expected, the result indicated that the difference between active and inactive seismic zones was dramatic. An artificial hazard level was then introduced to study the trend of long term loss statistics over a range of hazard levels. It was discovered that the zero loss probability decreases with artificial hazard level; long term loss median and extreme value (99^{th} percentile) increases with hazard level. The median of the long term loss increases linearly with the probability of exceedance on the hazard curve. A "step-up" pattern could be found in the extreme loss value as hazard level increased. Structural strength and stiffness can be affected by the design configuration of each component and construction quality. The sensitivity analysis first focused on the impact on loss behavior for the same architectural floor plan using different nailing patterns. Three commonly adopted nailing patterns were studied. The results indicated that the loss behavior for 6/12 and 4/12 nailing pattern were very similar. The structure with a 2/12 nailing pattern resulted in less loss for both single earthquake analysis and long term loss simulation. The concept of an *intensity sensitive region* was introduced for single earthquake loss results to indicate the

intensity values at with the structural configuration makes a significant difference in loss. The range, for example, covered in the study was approximately 0.3g ~ 2.0g spectral acceleration, which means the advantage of using a stronger nailing pattern will not be significant if an earthquake intensity level occurs that is outside of these bounds. The impact of structural configuration on the long term loss was not as significant as that from the seismic hazard environment. In order to investigate the interaction between structural properties (mainly strength and stiffness) and loss behavior (both single earthquake loss and long term loss) systematically, a series of reduction factors were applied to the structure with 2/12 nailing pattern to see the impact on loss statistics from reduced strength/stiffness. Such a reduction could be related to construction quality or degradation over time. Generally speaking, the seismically induced loss statistics for the higher reduction factor was higher than the lower ones as one might expect. However, this trend is not constant for high percentile values of long term loss, which again exhibits a "step-up" pattern as the reduction factor increases. This observed behavior of the loss function was similar to the situation with different nailing patterns, thus an *intensity sensitive region* for strength and stiffness also exists. This range starts from the intensity at which the weakest structure begins to experience excessive loss, and ends at the intensity where the strongest structure collapses. By only changing the stiffness and strength of wall components, the impact on the long term loss was limited. Theoretically, the maximum loss would be the number of earthquake occurrences times the collapse loss (corresponding to failure upon every earthquake event), no matter how much

reduction was applied to the structure. In this sense, the structural properties only affect the loss within the range controlled by the seismic hazard parameters.

The impact of the damage accumulation and after-shock activities was studied through the comparison between the results obtained from the Virtual Hazard simulation and vulnerability based simulation. Qualitative comparison on the frequency of after-shock events was also performed by using different after-shock generation parameters. It was found through the analysis that the impact of damage accumulation on the long term loss was very limited if the components with damage level II and above were repaired in time. The difference between the distributions of long term loss obtained from different simulation procedures was not significant. The degradation in components with damage level I does not affect the financial loss of a structure very much. The effect of after-shock frequency was identified from the simulation results. The simulation associated with higher probability of after-shocks yielded greater loss values in the long run, but the difference was not felt to significant. However, this result should not be viewed as a universal conclusion since the structure and earthquake after-shock model and repair strategies used in the analysis were very specific. More analysis could be performed following the procedures illustrated in the examples to explore structure-hazard-loss interaction in the desired perspectives.

9.2 Contributions

The contributions of this dissertation work to the woodframe research and design profession are summarized as follows:

1. Contribution to wood frame PBSD

In this study, the concept of loss-based design for wood frame structures was developed and practiced. The procedure was proven to be viable for single family dwellings. The first generation PBSD procedures for wood frame structures mainly focused on achieving specific inter-story drift requirements at a single earthquake event corresponding to a pre-defined hazard level or return period. Although these drift-related targets can be correlated with structural damage better than the traditional strength based procedures, they can not be directly used to guide the decision making process of the end-user, i.e. the building owner. On the other hand, the design target for loss-based design directly addresses the performance level of interest from an end-user (homeowners) point of view. Thus it could be viewed as a second generation PBSD procedure, which is end-user oriented PBSD. In this sense, the study in this dissertation work represents a substantial step forward for the PBSD framework of wood frame structures.

2. Contribution to loss analysis and modeling

The loss estimation framework developed in this study provided a way to analyze the impact of the major uncertainty sources in earthquake-induced loss for wood frame structures. Although long term loss modeling methods similar to the framework proposed here have been used for other types of structures such as steel and concrete, the procedures and techniques developed to implement this framework to the loss analysis of light frame wood structure were new and represent a contribution to the woodframe research community. These techniques, including the application of Bayesian models, the damage fragility system, the loss vulnerability models, and the virtual hazard simulation scheme, were proven to be well suited for the loss assessment of woodframe structures. The subjective information was quantitatively incorporated in the loss estimation through Bayesian statistics models. The accuracy of the framework was able to be improved with additional data. The damage fragility system effectively organizes the uncertainties in the response-loss relationship and could be easily constructed from test data. The behavior of structural loss from individual earthquakes could be accurately reflected through the vulnerability model developed in this work. The virtual hazard simulation provided an alternative way to estimate long term seismic loss in which damage accumulation and more realistic simulation configurations can be considered. Either as a whole system or individual component, these procedures and tools were valuable references for loss-related research on wood frame structures.

3. Contribution to Structural modeling

Based on existing models, new structural models were developed in this study to improve the accuracy and flexibility for the numerical analysis of wood frame structures. These models represent a step forward in numerical modeling of woodframe structures. The concept of an EPHM was introduced for the first time. The model was shown to be a powerful tool in the modeling of hysteretic elements, such as nail connections and light frame assemblies. The Nail Pattern model was able to represent the interaction of sub-assembly components at a more detailed level than its predecessor, the CASHEW model. The validity and accuracy of these models were verified with test data. The overall performance of time history prediction has been confirmed to be an improvement through the comparison of model results and full scale shake table tests.

4. Contribution to numerical analysis tool for wood frame structures

The software SAPWood was developed and made available to the public to facilitate the time domain analysis of woodframe structures. This software package, with a user friendly interface, includes most of models and procedures included in this dissertation work. It will benefit both researchers and practitioners by providing easy access to a powerful time domain and quasi-static analysis tool for woodframe components and structures. The loss estimation module enables the vulnerability analysis and long term loss simulation in a single click (with the model and input information ready). The incorporation of advanced dynamic models into PBSD would not be practically possible without software programs that could be used and understood by engineers.

The development of SAPWood was a timely fulfillment of the increasing need for the development of a nonlinear analysis software package for light frame wood structures.

9.3 Recommendations

The loss analysis and loss-based design for wood frame structures are new and evolving topics that will be studied thoroughly in the future along with the development of PBSD. Currently, the general framework and concept has been established which gives rise to a number of new research tasks that need to be studied for a better understanding of hazard-loss interaction and finally promote practical user-oriented PBSD. Some of the important topics that should be addressed in the future research are as follows:

Except for the total collapse situation, the loss of the structure was the sum of the repair cost of the damageable components. Inaccurate response-loss information will result in unreliable loss estimation output. As it was discussed earlier, the usable response-loss relationship data for woodframe structure components were very limited at current stage. Systematic response-loss experiments on damageable components need to be carried out to improve the accuracy of damage fragility modeling. A standard testing procedure should be developed for response-loss relationship to ensure the quality and usability of the test data. With the increasing use of pre-fabricated standard structural components in light frame wood construction, a loss-resistance standard or categorization system could be introduced to these components

as they are manufactured and sold on the market. The impact of system effects, i.e. when these components were installed together, to the component damage fragility should also be studied.

Numerical model used in the loss simulation is another important factor that controls the accuracy of the framework output. Although the framework itself is general and does not depend on any specific numerical model, improvement of the dynamic response prediction will always improve the quality of the loss prediction. Currently the structural model used in this study, as well as in the SAPWood program, is a biaxial pure-shear model. Although the accuracy of this model was suitable for this study and compatible with the accuracy of current available information, there exists a need for a more detailed model as the level of accuracy in loss prediction increases. For example, the damage of sill plate and hold-down anchorage might be associated with the maximum uplift forces or the out of plane deformations/forces during earthquake excitation. This information is not explicitly provided by the shear building type models. The next step in the improvement of numerical models will be to enable response simulation in the vertical direction and eventually the second order effects, i.e. p-delta effect.

The loss behavior of different wood frame construction styles should be studied systematically. The scope of this dissertation work was limited in that only three index buildings were analyzed. Although the number of examples was enough to illustrate the loss estimation framework and obtain reasonable conclusions, more analysis on

different building types and floor plans will be needed for a thorough understanding of the seismic loss of wood frame structures as a comprehensive category. Results from this research could be beneficial to regional loss estimation and loss-based building inventory planning against earthquake hazards.

Loss-based design using incremental optimization procedures has been shown to be a viable way to achieve loss requirements within a reasonable range. In order to transform this concept from a research result to a practical procedure, several issues must be investigated first. The first one is the validity of the loss requirements. Only loss requirements that lie in a suitable range of loss values will lead to realistic design output, thus a simplified procedure should be developed to serve as a pre-qualification of the loss-based design statements. On the other hand, the relationship between loss-based design and current design requirements must be studied to ensure the loss-based target exceeds the existing criteria of strength-based design. The incremental optimization procedure could be formulized by introducing a group of systematically organized optimization measures as guidelines. The development of such a guideline will involve detailed sensitivity study on each measure with respect to their impact on loss estimation. Advanced devices such as base-isolation and damping systems should also be included in the loss-based design scenario based on sensitivity studies of using these devices.

In order to promote the practice of PBSD and facilitate the related procedures developed in academic research, additional effort should be put into the development

of the specialized software package. Without such tools, it might take a long time for engineering practitioners to experience the benefit of newly developed research findings. Although most of the procedures and tools developed in this study have been built into SAPWood, the program itself still needs to be continuously developed to incorporate new models and methods to help practitioners perform loss-based design and assessment.

References

ANSI/AF&PA, National Design Specification for wood construction 2001 edition. American Wood Council, Washington DC.

Baber, T., and Wen, Y.K. (1981). "Random vibration of hysteretic degrading systems." J. Engrg. Mech., ASCE, 107(EM6), 1069-1089.

Baber, T., and Noori, M. N. (1985). "Random vibration of degrading, pinching systems." J. Engrg. Mech., ASCE, 111(8), 1010-1026.

Benjamin J.R. and Cornell C.A. (1970). "Probability, statistics, and decision for civil engineers." McGraw-Hill, New York.

Christopher R. et.al. (1986). "Earthquake damage and loss evaluation for California." Earthquake Spectra, 2(4). 767-782.

Christovasilis I.P., Filiatrault A., and Wanitkorkul A. (2007). "Seismic testing of a full-scale two-story wood lightframe building: NEESWood Benchmark test" Report NW-01, NEESWood research project.

Crowley H. and Bommer J.J. (2006). "Modelling seismic hazard in earthquake loss models with spatially distributed exposure." Bulletin of earthquake engineering; 4:249-273.

Dinehart, David W., Shenton III, Harry W. (2000). "Model for dynamic analysis of wood frame shear walls." J. Engrg. Mech., ASCE, 126(9), 899-908.

Dong, W. (1990). "New method for calculating expected loss of existing buildings subjected to probabilistic earthquake loading." Soil dynamics and earthquake engineering, 9(4). 166-171.

Easley, J.T., Foomani, M., and Dodds, R.H. (1982). "Formulas for wood shear walls." J. Struct. Div. ASCE, 108(11), 2460-2478

Ellingwood, B. (1998). "Reliability-based performance concept for building construction." Structural Engineering World Wide (CD-ROM), Elsevier, CA .

Ergonul, S (2005). "A probabilistic approach for earthquake loss estimation." Structural Safety, 27, 309–321.

Fajfar, P. (2000). "Nonlinear analysis method for performance-based seismic design." Earthquake Spectra, 16(3), 573-592.

FEMA (2000a). Prestandard and Commentary for Seismic Rehabilitation of Buildings, FEMA356, Federal Emergency Management Agency, Washington, DC.

Filiatrault, A. (1990). "Static and dynamic analysis of timber shear walls." Canadian J. of Civil Eng.,17, 643–651.

Filiatrault, A. and Folz, B. (2002). "Performance-Based Seismic Design of Wood Framed Buildings." J. Struct. Engrg., ASCE, 128(1), 39-47.

Foliente, G.C. (1995). "Hysteresis modeling of wood joints and structural systems." J. Struct. Engrg., ASCE, 121(6), 1013-1022.

Folz, B. and Filiatrault, A. (2001). "Cyclic Analysis of Wood Shear Walls." J. Struct. Engrg., ASCE, 127(4), 433-441.

Filiatrault, A. and Folz, B. (2002). "Performance-Based Seismic Design of Wood Framed Buildings." J. Struct. Engrg., ASCE, 128(1), 39-47.

Folz, B. and Filiatrault, A. (2004). "Blind predictions of the seismic response of a woodframe house: An international benchmark study." Earthquake Spectra, 20(3), 825-851

Folz, B. and Filiatrault, A. (2004). "Seismic analysis of woodframe structures. I: Model formulation." J. Struct. Engrg., ASCE, 130(9), 1353-1360.

Folz, B. and Filiatrault, A. (2004). "Seismic analysis of woodframe structures. II: Model implementation and verification" J. Struct. Engrg., ASCE, 130(9), 1361-1370.

Foschi, R. O. (1974). ''Load-slip characteristics of nails.'' Wood Sci., 7(1),69–74.

Gatto K., and Uang C. (2003). "Effects of Loading Protocol on the Cyclic Response of Woodframe Shearwalls." J. Struct. Engrg. ASCE, 129(10), 1384-1393.

Gelman A., Carlin J.B., Stern H.S., and Rubin D.B. (2004). "Bayesian data analysis." Chapman & Hall/CRC Press, New York.

Gupta, Ajaya K, and Kuo, George P. (1985). "Behavior of wood-framed shear walls." J. Struct. Engrg., ASCE, 111(8), 1722-1733.

He, M., Lam, F. and Prion, Helmut G.L. (1998). "Influence of cyclic test protocols on performance of wood-based shear walls." Canadian J. of Civil Eng., 25, 539-550

Judd, Johnn P., and Fonseca, Fernando S. (2005). "Analytical model for sheathing-to-framing connections in wood shear walls and diaphragms." J. Struct. Engrg., ASCE, 131(2), 345-352.

Kiremidjian, A. (1985). "Subjective probabilities for earthquake damage and loss." Structural safety, l2(4), 309-317.

Krawinkler, H., F. Parisi, L. Ibarra, A. Ayoub, and R. Medina (2000). "Development of a Testing Protocol for Woodframe Structures.", CUREE Publication No. W-02, Richmond, CA.

Langlois J.D., Gupta R., and Miller T.H. (2004). "Effects of Reference Displacement and Damage Accumulation in Wood Shear Walls.", J. Struct. Engrg., ASCE, 130(3), 470-479.

Leelataviwat, S. et. al. (1999). "Toward performance-based seismic design of structures." Earthquake Spectra, 15(3), 435-461.

Liu, M. (2005). "Seismic design of steel moment-resisting frame structures using multiobjective optimization." Earthquake Spectra, 21(2), 389-414.

Liu.S.C, and Neghabat F. (1972). "A Cost Optimization model for seismic design of structures." The bell system technical journal, 51(10).

Mario Paz, (1997). "Structural dynamics theory and computation." Chapman & Hall, New York.

Minoru, M. and Akira, A. (1982). "Bayesian calibration of embankment safety under earthquake loading." Structural Safety, 1, 53-65.

Pang W.C., and Rosowsky D.V. (2007). "Direct displacement procedure for performance-based seismic design for multistory woodframe structures." Report NW-02, NEESWood research project.

Pang, W.C., Rosowsky, D.V., Pei, S. & van de Lindt, J.W. (2007). "Evolutionary parameter hysteretic model for wood shearwalls." J. Struct. Engrg., ASCE, accepted in press.

Pei S., and van de Lindt J.W. (2007). "Methodology for earthquake-induced loss estimation in woodframe buildings" submitted to Structural Safety.

Pei S., van de Lindt J.W., Rosowsky D.V., and Pang W.C. (2006). "Next generation hysteretic models for development of a performance-based seismic design philosophy for woodframe construction." 8th National Conference on Earthquake Engineering, San Francisco.

Porter, K.A. (2000). "Assembly-based vulnerability of buildings and its uses in seismic performance evaluation and risk-management decision-making," Doctoral dissertation, Stanford CA.

Porter, K.A. et. al. (2001). "Improving loss estimation for woodframe buildings." CUREE Publication No. W-01, CUREE-Caltech Woodframe Project, Dept. of Structural Engineering, Univ. of California, San Diego.

Porter, K.A., Scawthorn, C.R., Beck, J.L. (2006). "Cost-effectiveness of stronger woodframe buildings." Earthquake Spectra. 22(1): 239-266.

Richard, N., Yasumura, M., and Davenne, L. (2003). "Prediction of seismic behavior of wood-framed shear walls with openings by pseudodynamic test and FE model." J. of wood science, 49, 145-151.

Rosowsky, D.V. (2002). "Reliability-based Seismic Design of Wood Shear Walls." J. Struct. Engrg., ASCE, 128(11), 1439-1453.

Rosowsky, D.V. and Ellingwood, B.R. (2002). "Performance-Based Engineering of Wood Framed Housing: Fragility Analysis Methodology.", J. Struct. Engrg., ASCE, 128(1), 32-38.

Rosowsky, D.V. and Kim, J.H. (2001) "Task 1.5.3 – Reliability Studies," Final Report submitted to CUREE-Caltech Woodframe Project, Element 1 (Testing and Analysis), Research Report WEM-01-02, Oregon State University, Corvallis, OR.

Schierle, G.C. (2001) "Northridge earthquake field investigations: Statistical analysis of woodframe data" CUREE-Caltech woodframe project, Report W-09, Richmond, CA.

Shenton III, Harry W., Dinehart, David W., and Elliott, Timothy E. (1998). "Stiffness and energy degradation of wood frame shear walls." Canadian J. of Civil Eng., 25, 412-423

Symans, M.D et. al. (2004). "Seismic behavior of wood-framed structures with viscous fluid dampers." Earthquake Spectra, 20(2), 451–482.

van de Lindt, J.W. (2005b). "E-proceedings of the 1st International Workshop on Performance-based Design of Woodframe structures." Fort Collins, CO, July 28-29, 2005

van de Lindt, J.W. (2005). "Damage-Based Seismic Reliability Concept for Woodframe Structures." J. Struct. Engrg., ASCE, 131(4), 668-675

van de Lindt, J.W. and R. Gupta. (2005). "Damage and Damage Prediction for Wood Shearwalls Subjected to Simulated Earthquake Loads." J. of Perf. Of Const. Focilities, In Press.

van de Lindt, J.W. (2004). "Evolution of Wood Shear Wall Testing, Modeling, and Reliability Analysis: A Bibliography." ASCE Practice Periodical on Structural Design and Construction, 9(1), 44-53.

van de Lindt, J.W., Walz, Matthew A. (2003). "Development and application of wood shear wall reliability model." J. Struct. Engrg., ASCE, 129(3), 405-413

van de Lindt, J.W., H. Liu, and S. Pei. (2006). "Performance of a Woodframe Structure During Full-Scale Shake Table Tests: Drift, Damage, and Effect of Partition Wall." Journal of Performance of Constructed Facilities, ASCE, In Press.

van de Lindt, J.W., S. Pei, and H. Liu. (2006). "Performance-Based Seismic Design of Wood Frame Buildings Using a Probabilistic System Identification Concept" J. Struct. Engrg., ASCE, In Press.

Wen, Y.K. (2001). "Minimum lifecycle cost design under multiple hazards." Reliability Engineering and System Safety, 73(3), 223-231.

Ziegler A. (1987). "Maximum loss prediction for earthquake insurance." Reliability engineering, 18 (1), 61-69.

White, Maurice W., and Dolan, J. Daniel (1995). "Nonlinear shear-wall analysis." J. Struct. Engrg., ASCE, 121(11), 1629-1635.